SURFACE COATINGS FOR MODIFYING CIRCULATING BLOOD CELL BEHAVIOR

by

Alexander D. Malkin

B.S., Mechanical Engineering, Carnegie Mellon University, 2008

Submitted to the Graduate Faculty of

Swanson School of Engineering in partial fulfillment

of the requirements for the degree of

Doctor of Philosophy in Bioengineering

University of Pittsburgh

2017

UNIVERSITY OF PITTSBURGH

SWANSON SCHOOL OF ENGINEERING

This dissertation was presented

by

Alexander D. Malkin

It was defended on

August 28th, 2017

and approved by

John A. Kellum, MD, FACP, FACM
Professor, Departments of Critical Care Medicine, Bioengineering, and Clinical & Translational Science

Gilles Clermont, MD, MSc
Professor, Departments of Critical Care Medicine, Industrial Engineering, and Mathematics

Kai Singbartl, MD, MPH, FCCM
Associate Chair, Research, Department of Critical Care Medicine, Mayo Clinic

William R. Wagner, PhD
Professor, Departments of Surgery, Bioengineering, and Chemical & Petroleum Engineering

Dissertation Director: William J. Federspiel, PhD
William Kepler Whiteford Professor, Departments of Bioengineering, Chemical & Petroleum Engineering, and Critical Care Medicine

SURFACE COATINGS FOR MODIFYING CIRCULATING BLOOD CELL BEHAVIOR

Alexander D. Malkin, PhD

University of Pittsburgh, 2017

Advances to biomaterial polymers and surface coatings have markedly improved the safety and efficacy of extracorporeal devices, but there is untapped potential to use these surfaces to modulate blood cell behavior. Sepsis, a severe inflammatory response to infection that affects nearly 1 million Americans per year, results in high levels of interleukin (IL-8) spilling into the circulatory system and diffusing into healthy tissue. Subsequently, circulating neutrophils become redirected into these healthy tissues, where they impair organ function. The focus of this work is the development of an extracorporeal device which can "reprogram" neutrophils using IL-8 immobilized within the device. Additionally, a zwitterionic thromboresistant coating was developed to reduce platelet deposition in extracorporeal devices.

A mechanistic computational model was developed to study the role of IL-8 induced CXCR-1/2 neutrophil surface receptor downregulation and its role in the progression of sepsis. The findings suggest that a device which modulates receptor expression could reduce morbidity and mortality in sepsis, but there is also potential for harm if implemented incorrectly. Scaled prototypes of an extracorporeal device, which used immobilized IL-8 to reduce neutrophil migratory response, were constructed and evaluated. While significant downregulation of CXCR-1 and CXCR-2 was achieved, this effect was insufficient to cause consistent migratory shutoff to IL-8 as measured by a Boyden chamber chemotaxis assay. Learnings from this testing were used to develop alternate device concepts which modulate leukocyte activity within an extracorporeal circuit.

A zwitterionic macromolecule surface coating was developed to reduce platelet deposition on polymethylpentene (PMP) hollow fiber membranes (HFMs). Two techniques of PMP HFM functionalization and subsequent conjugation of sulfobetaine block copolymers were evaluated within scaled PMP fiber minimodules. Both fiber configurations resulted in an 80-95% reduction in adherent platelets from whole ovine blood, stability under shear stress, and uninhibited gas exchange performance relative to unmodified HFMs. Initial testing indicates this coating is effective on polycarbonate and poly(vinyl chloride), two other materials commonly found in extracorporeal circuits, which may allow for tip to tip coating of extracorporeal circuits.

TABLE OF CONTENTS

LIST OF TABLES

LIST OF FIGURES

ACKNOWLEDGEMENTS

Above all, I would like to extend my thanks and appreciation to my advisor, Dr. William Federspiel. He has offered constant guidance and mentorship, always encouraging me to improve my skills as a scientist and researcher. His support has enabled me to work independently, knowing that my ideas will be valued. I learned the importance of continually pushing an idea forward, even in the face of unexpected results. I will continue to use the lessons he has taught as my career progresses.

I would also like to thank my thesis committee members, Dr. Gilles Clermont, Dr. John Kellum, Dr. Kai Singbartl, and Dr. William Wagner. Each member has offered a unique perspective that shaped the direction of my research and I could not have completed the work in this dissertation without their input and support. I am honored to have worked closely with such knowledgeable and influential leaders and appreciate the time they all have contributed.

I would like to express my appreciation to all the member of the Medical Devices Laboratory, who were both colleagues and friends. It was extremely valuable to be constantly surrounded by students and staff willing to brainstorm and share new ideas. Additionally, I would like to thank all the undergraduate students who contributed to the project, from teaching me at the very beginning to supporting experiments at the end.

I could not have achieved so much without access to the support programs and generous funding opportunities at University of Pittsburgh. The Gerald E. McGinnis Fellowship offered the opportunity to conduct research and education with a focus on translational medicine. The Cardiovascular Bioengineering Training Program (NIH T32-HL076124), under the guidance of Dr. Sanjeev Shroff, helped develop my knowledge in the field of bioengineering, as well as providing access to a knowledgeable group of trainees.

Finally, I would like to thank all of my friends and family who supported me throughout graduate school. My mother, father, and sister provided unwavering support, always expressing interest and excitement in my work. I could not have done it without their inspiration and guidance. All of my friends from Pittsburgh and across the country, who have provided both advice and distraction. Above all, I would like to thank Steph. She has always provided love and support. I look forward to sharing whatever is coming next.

1.0 INTRODUCTION

Sepsis is a severe inflammatory response to infection that affects nearly 1 million Americans per year [1]. Importantly, much of the mortality and morbidity in sepsis is not due directly to the causal infection, but rather is due to sepsis induced organ failure. A normal innate immune response to infection involves local inflammation at the site of infection, and neutrophils migrating from the blood stream into the infected tissues due to chemical gradients of the chemokines such as Interleukin-8 (IL-8) released by macrophages. In sepsis, high levels of IL-8 at the site of infection spill into the circulatory system and move into healthy tissue. Subsequently, neutrophils become redirected into these healthy tissues where they impair organ function [2]. Potential treatments that indiscriminately suppress neutrophil activity have proven ineffective in sepsis [3,4] because they lead to immune suppression and the inability to clear the underlying infection.

The work described in this dissertation will focus on development of an extracorporeal device that can "reprogram" neutrophils to attenuate their chemotactic response to IL-8 as a potential treatment for sepsis. Other background information, particularly pertaining to respiratory assist device, will be covered in the sixth chapter. The Neutrophil Reprogramming Device (NeRD) is essentially a hemodialyzer cartridge in which IL-8 is covalently bound to the inner lumens of the dialyzer fibers. Similar to hemodialysis, blood is perfused through the NeRD and neutrophils, which naturally marginate toward the fiber inner lumens, interact with the

immobilized IL-8 through CXCR-1 and CXCR-2 surface receptors, the same interaction that causes chemotaxis. As a result of the interaction, CXCR-1/2 surface expression on neutrophils is down-regulated, thus reducing the neutrophils chemotactic response to IL-8 as blood is perfused back into the patient.

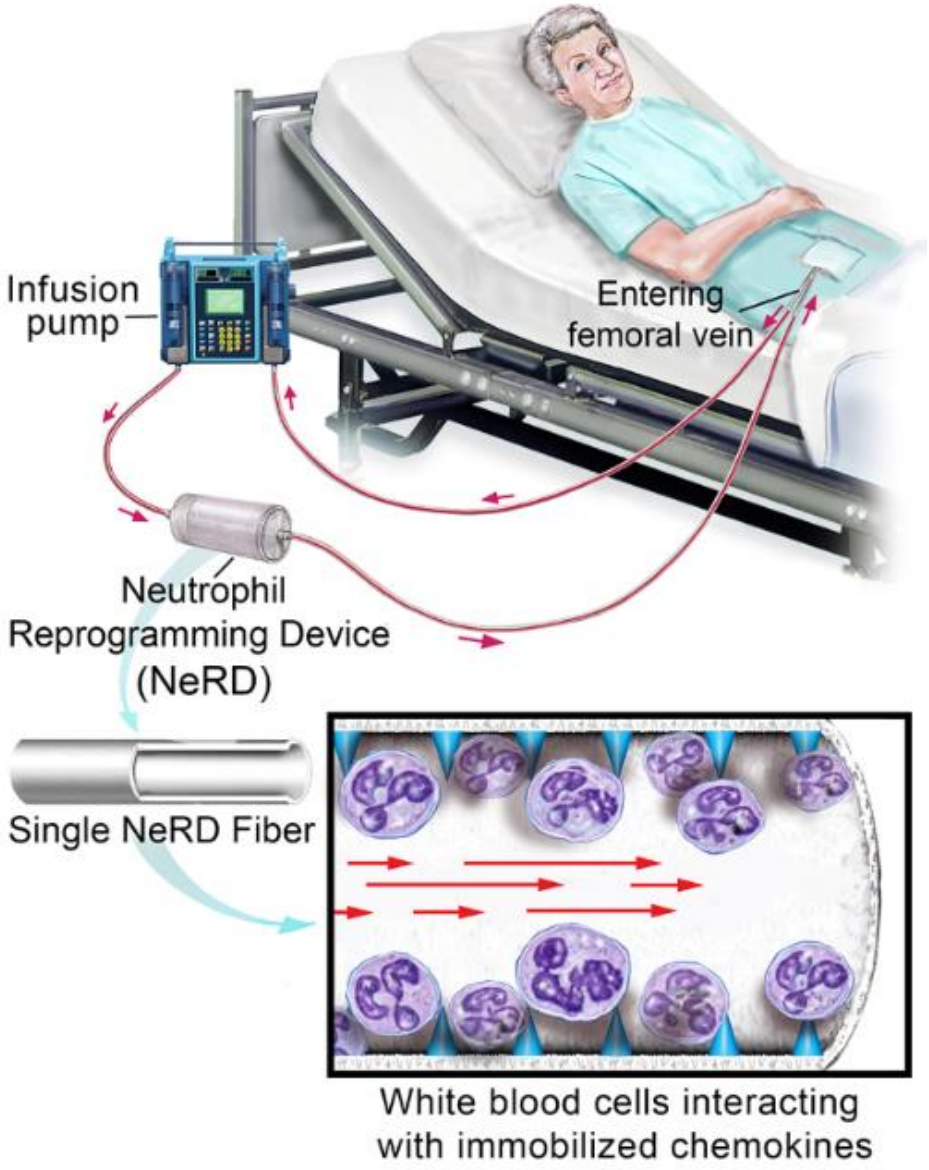

Figure 1. Schematic of Neutrophil Reprogramming Device (NeRD).

The neutrophils maintain the ability to target and eliminate bacteria in infected tissue through secondary CXCR-1/2 independent cell signaling pathways involving N-formyl-metyl-leucyl-phenyl (fMLP), a byproduct of bacterial destruction. It is hypothesized that the reduced chemotactic response to IL-8 will reduce the redirection of neutrophils into healthy tissue and reduce sepsis induced organ failure.

In addition to development and evaluation of the NeRD, a mechanistic computational model was developed to study the role of CXCR-1/2 neutrophil surface receptors and neutrophil phenotype in the progression of sepsis. This model was used for *in silico* evaluation of an extracorporeal treatment that modulates these surface receptors. This information helps support the underlying mechanism of the NeRD and guide intervention timing. Findings from development of the NeRD device were also be used to establish future directions of extracorporeal devices for treatment of sepsis. In particular, approaches that modulate neutrophil activity within an extracorporeal circuit were explored. The final element of this dissertation focusses on implementation of zwitterionic macromolecule conjugation to functionalized polymethylpentene (PMP) hollow fiber membranes. Different fiber functionalization configurations, including amine and hydroxyl fiber functionalization were evaluated. Macromolecular coatings may be integrated into the NeRD to improve device hemocompatibility at a later stage of development.

2.0 BACKGROUND

2.1 SEPSIS

The incidence of sepsis is expected to increase over the next 10-20 years as the population ages [1]. Despite improvements in care, the hospital mortality rate associated with sepsis has remained persistently high and is nearly 20% [1,5,6]. Recent studies have shown that at one year, survival is less than 60% for patients with septic shock [7]. Sepsis is now the leading cause of in-hospital death in the United States [1,8], yet there are currently no FDA approved specific treatments for sepsis. Intensivists are limited to managing the symptoms of sepsis until the patient's immune system naturally recovers, if it does so. The current standard of care for sepsis is treatment of the causal infection with source control and antibiotics, while providing necessary organ support using drugs (e.g. vasoactive medication) or devices (e.g. hemodialysis, mechanical ventilation, etc.) [9].

2.1.1 Clinical definition

There has been much debate about how to define sepsis, leading to inconsistency amongst reported results and treatments prior to the early 1990s. The wide range of symptoms and presentations of sepsis makes it particularly challenging to identify and define. To help address this challenge, the first consensus definition of sepsis was established as a systemic inflammatory response to an infection. Additionally, severe sepsis was defined as sepsis with complications related to organ dysfunction and septic shock was identified as sepsis with symptoms associated with hypotension [10]. Additional clarity was added during the surviving sepsis campaign [5,11], which defined

sepsis and established guidelines for treatment. A clear diagnostic criteria was established, which included infection, general variables such as temperature and heart rate, inflammatory variables such has white blood cell count, hemodynamic variables, organ dysfunction observations, and tissue perfusion variables (see Table 1). Additionally, severe sepsis was defined as sepsis with sepsis induced hypoperfusion or organ dysfunction. These new standards improved consistency.

Table 1. Diagnostic criteria for sepsis. Adapted from Dellinger, et al[11].

Suspected or documented infection and some of the following:				
General	**Inflammatory**	**Hemodynamic**	**Organ-dysfunction**	**Tissue-perfusion**
Fever	Leukocytosis	Arterial hypotension	Arterial hypoxemia	Hyperlactatemia
Hypothermia	Leukopenia		Acute oliguria	Decreased capillary refill
Elevated heart rate	>10% immature WBC		Creatinine increase	
Tachypnea	Elevated plasma C-reactive protein		Coagulation abnormalities	
Altered mental status	Elevated procalcitonin		Ileus	
Significant edema			Thrombocytopenia	
Hyperglycemia			Hyperbilirubinemia	

2.1.2 Contributions of innate and adaptive immunity to sepsis progression

Many theories have been presented to help understand the progression and root cause of sepsis. Early hypotheses were based on the presence of an infection in the bloodstream. Researchers determined that infection alone could not be solely responsible for sepsis, because use of antibiotics did not eliminate symptoms. In last thirty years, as our understanding of host immunity expanded, it became clear that the patient's immune response was key to the progression of sepsis. Initially, innate immune response was determined to play a key role. Particularly elevated levels

of both pro and anti-inflammatory cytokines which were observed in circulation of septic patients [12,13]. These cytokines led to an overwhelming immune response, leading neutrophil activation and organ dysfunction. If the patient survives the hyperinflammatory phase of sepsis, a strong anti-inflammatory response will follow. This is a result of the anti-inflammatory cytokines which were released in parallel and response to pro-inflammatory cytokines. This response leads to immune suppression and inability of the patient to fight the underlying or additional infections.

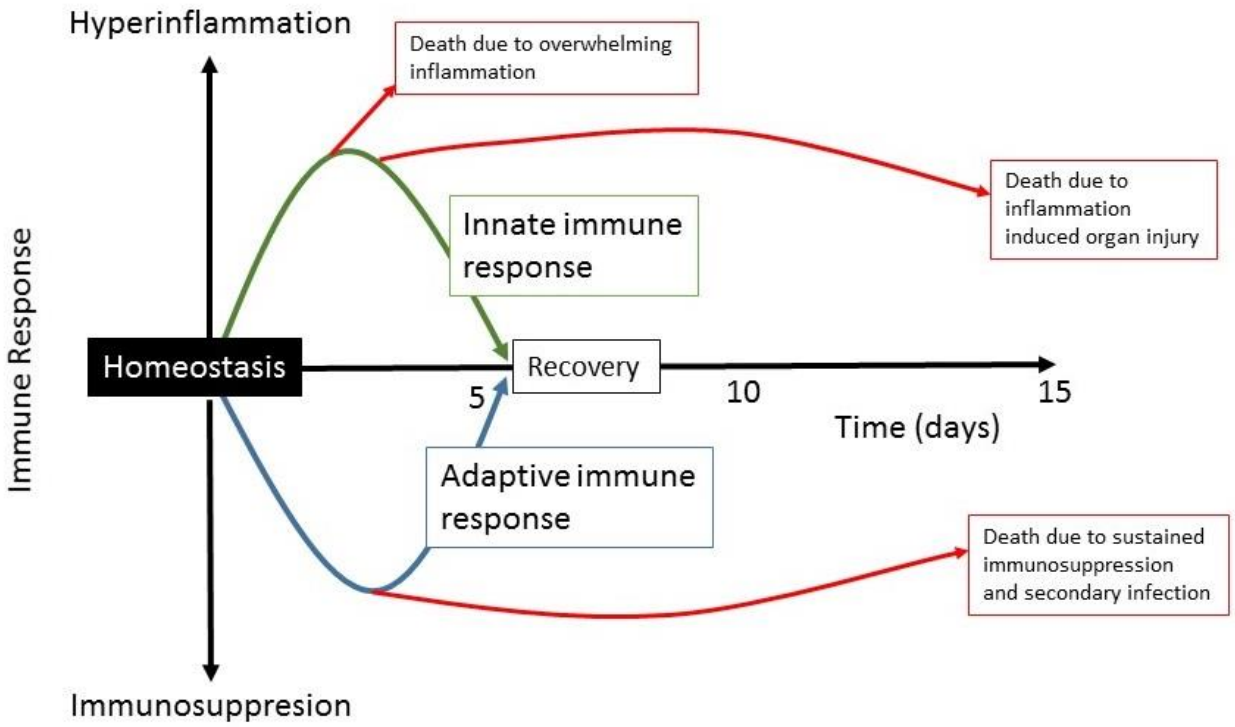

Figure 2. Possible sepsis progressions. Patients can die from either overwhelming inflammation, sustained inflammation, or immunosuppression. Adapted from Hotchkiss, et al [14].

More recently, the host-response hypothesis has been expanded to also include the role of adaptive immunity. This is particularly relevant in the development of the anti-inflammatory response [14,15]. This concept does not ignore the importance of innate immunity, but presents

the possibility of targeting adaptive immune processes to minimize immune dysfunction, particularly for patients who survive the initial hyperinflammatory stage. These hypothesis are shown in Figure 2. This also highlights the importance of establishing immune homeostasis to encourage patient's recovery. Treatments which alter immune response to drastically are likely to lead to patient morbidity and mortality. The importance of treatment timing is also critical, as immune response is clearly time dependent and perturbations to either innate or adaptive immunity may only be possible at a single stage of sepsis development.

2.1.3 Role of neutrophils in the progression of sepsis

Neutrophils are the first responders to sites of inflammation and play critical roles in the innate immune response. Neutrophils are short lived (less than a week) granulocytes, which are the most common type of white blood cell. They typically enter the blood stream as mature cells, without the ability to proliferate [16]. Cytokine signals prime and active neutrophils [17–19], stimulating extravasation. Neutrophils migrate through the endothelial cell wall, following chemokine gradients to the source of infection. At the site of infection neutrophils are able to help eliminate pathogens through granule production, phagocytosis, and generation of neutrophil extracellular traps (NETs) [20–22]. Additionally, neutrophils can release cytokines, leading to continued inflammation and leukocyte infiltration. Recent studies have also linked neutrophils to adaptive immune functions, increasing the importance of their role in the later hypoinflammatory stage of sepsis [23,24]. While neutrophils are critical to eliminating infections, they are a double edged sword, capable of damaging healthy tissue [25]. The same mechanisms used to eliminate pathogen will just as easily damage healthy tissue.

Normally, neutrophils migrate from the bloodstream into the infected tissues due to inflammation there by sensing chemical gradients of the chemokine IL-8, which is released by macrophages in response to foreign invaders like bacteria. The IL-8 chemokine binds to the expressed neutrophil cell surface receptors CXCR-1 and CXCR-2 and induces chemotaxis to the site of infection [2]. The increased neutrophil activity in sepsis, however, results in undesirable systemic-level inflammation and elevated IL-8 levels in healthy tissues and organs [26,27]. Activated neutrophils then infiltrate these tissues/organs where they can damage cells and lead to multiple organ dysfunction [2,28]. This process is illustrated in Figure 3. The lung is especially susceptible to sepsis induced organ failure. Again, potential treatments that indiscriminately suppress the activity of neutrophils can cause immune suppression and the inability to clear the causal infection [15,29,30].

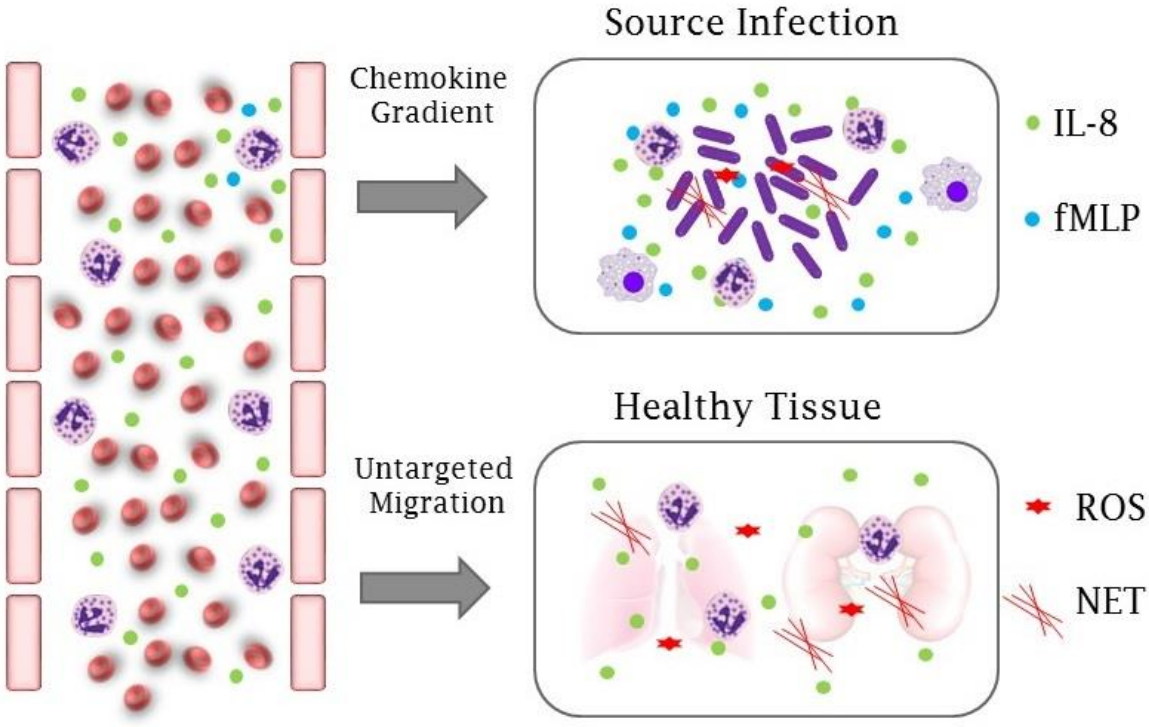

Figure 3. Neutrophil induced organ damage occurs when cytokines enter systemic circulation.

2.1.4 Current treatments

There is a long history of potential treatments targeting sepsis. While many approaches have shown promise early in development, no specific treatments have been FDA approved [31]. The lack of substantial advancements comes even with advancements in understanding the underlying pathogenesis of sepsis. This lack of progression highlights the complexity and challenges of sepsis treatment. The current standard of care is management of symptoms, source control, and supportive care. Although new treatments have not been reaching patients, recent clinical studies have shown a gradual improvement in mortality among patients suffering sepsis, with current 60 day mortality sitting at approximately 18% [6,7].

2.1.4.1 Protocolized treatment and supportive care

Physicians have long been searching for ways to improve outcomes for patients suffering from sepsis. One previously promising approach, called early goal-directed therapy (EGDT) [32] followed a 6-hour protocol which quickly and aggressively used central venous catheterization intravenous fluids, vasopressors, blood transfusions, and dobutamine to meet target physiologic parameters. Initial single-center clinical trials indicated this approach provided a significant improvement in short term mortality of patients. These studies encouraged physicians to move towards protocolized treatments, but there were arguments over which elements of the protocol were responsible for improvements in mortality (or whether the outcomes could be repeated in a large scale clinical study) [33,34].

In 2014 a multicenter clinical study (the ProCESS trial), was completed which specifically set out to address this question. Protocol based resuscitation was compared to both usual care and an EGDT based protocol which used central hemodynamic monitoring to guide treatments [7].

This study found that protocol-based resuscitation on septic shock patients diagnosed in the emergency department did not improve outcomes based on usual care. These show that required central hemodynamic monitoring is not critical to reducing mortality in septic patients. Additionally, the lack of difference between mortality in treatment groups may be because physicians had already adjusted their treatment approach to reflect the advantages of EGDT, with a focus on early diagnosis and treatment.

Currently the focus of sepsis management is early diagnosis, source control, and treatment of symptoms. These steps have been shown to improve patient outcomes [35] Initial treatment guidelines are to be completed within 6 hours of sepsis presentation. These are intended to provide cardiorespiratory resuscitation and address the underlying infection. Use of intravenous fluids, vasopressors, and respiratory support are suggested when necessary. After being transferred to the ICU patients begin a new set of therapies which focus on organ function and de-escalation of treatment. While these treatment guidelines have gradually improved patient outcomes, there is still a need for therapies that address the underlying mechanisms of sepsis and provide physicians with more treatment options.

2.1.4.2 Pharmaceuticals

Many experimental pharmaceutical treatments have been tested in animals and early stage human clinical trials. However, currently none of these treatments are FDA approved specifically for use in sepsis. Many of these treatments target the inflammatory response, attempting to suppress the hyper immune response and associated organ damage. The only immunosuppressive treatment currently recommended for certain patients is a short low dose of hydrocortisone [11,36], but even this is controversial due to the possibility of unintended immune suppression and other complications.

Activated protein C (APC) therapy showed promise early in its development. This therapy is intended to limit coagulation complications observed during sepsis. During sepsis endothelial cell expression of thrombomodulin is typically impaired, limiting APC generation from circulating protein C. Administration of APC is thought to facilitate controlled fibrinolysis and inactivation of factor Va and VIIa, limiting coagulation complications [37]. Additionally, APC is thought to modulate the inflammatory response in sepsis, inhibiting IL-1, IL-6, and TNF-α production [38]. Initially trials with recombinant APC indicated an improvement in mortality [39] and the drug gained FDA approval. However, these clinical results could not be replicated [40] and FDA approval was withdrawn and the drug was removed from all markets due to lack of clinical evidence and possibility of severe complications.

Pharmaceuticals have also directly targeted inflammatory response to encourage either pro or anti-inflammatory responses. Experimental drug therapies to attenuate pro-inflammatory cytokines such as tumor necrosis factor (TNF) and interleukin-1 (IL-1) have had little success [4]. Use of interferon-γ and GM-CSF have attempted to stimulate immune response in immunosuppressed patient, but clinical results have been mixed [41–43]. While these might have potential benefits for certain patients, clinical data does not appear to support their widespread use.

Other pharmaceutical treatments target elements of sepsis ranging from coagulation to immune response. High-mobility group box 1 (HMBG1) has been targeted for therapy in sepsis. Studies have shown that HMGB1 plays a key role in sepsis progression and inflammation [44–47]. However, these studies have not progressed beyond pre-clinical testing and full therapeutic implications are not understood.

2.1.4.3 Blood filtration

Extracorporeal devices addressing sepsis have primarily focused on removing components from whole blood. Specifically, they target cytokines or endotoxin and pathogens, intending to disrupt the progression of sepsis. These device, which include hemofiltration and hemoadsorption, broadly modulate cytokine levels [48,49]. It is hypothesized that widespread removal of cytokines will be beneficial in two ways. First, broad removal of cytokines will dampen both pro and anti-inflammatory immune response, allowing the patient to return to homeostasis [50]. Second, it is believed that cytokine removal from blood may decrease cytokine concentrations in tissue by changing the concentration gradient, potentially reducing organ damage [51]. However, clinical results have not yet supported the widespread use of blood filtration. These techniques are more commonly utilized in Japan than the United States and Europe [52]. Further clinical testing may determine which subset of patients would benefit from use of these devices.

Cytokine removal from whole blood is typically completed using either hemofiltration or hemoadsorption. Hemofiltration utilizes semi-permeable membranes to remove components of a specific size range from blood. Pore size on these membranes prevent large solutes such as albumin from being removed, but can remove smaller cytokines. High volume hemofiltration (HVHF) is a potential approach to quickly remove a substantial amount of cytokines from plasma. High flow rates and convective transfer lead to faster removal than relying on diffusion alone. Use of HVHF has shown encouraging results in animal studies and smaller clinical studies [53–55], particularly regarding improvement of hemodynamic parameters. However, additional large studies are likely required to achieve widespread use. Other lower flow hemofiltration techniques, such as continuous renal replacement therapy and conventional continuous venovenous hemofiltration, have not shown advantages compared to standard care for septic patients [56,57]. High cutoff

membranes (HCO) have increased pore size, allowing more efficient removal of a wider range of cytokines [58]. The downside of this increased pore size is increased albumin loss. Hemodialysis using HCO relies on diffusion to remove solutes and appears to allow for greater removal of cytokines while minimizing albumin loss [59,60].

Hemoadsorption removes components from blood using a sorbent surface which comes in direct contact with blood in an extracorporeal circuit. Unlike hemofiltration there are no limitations on target molecule size. Additionally, certain solutes can be removed preferentially by carefully selecting sorbent properties such charge, hydrophobicity, and chemical composition. Polymyxin B, which is approved for use in Japan, is an example of a hemoadsorption device which preferentially removes endotoxin from the blood [61,62]. Recently, a multi-center clinical study examining use of Polymyxin B outside of Japan concluded that there are some benefits associated with endotoxin removal [63]. However, there is some argument over the relevance of these results, and a data from US and Canadian patients did not appear to meet its primary endpoint [64]. While some results and case studies have been encouraging, it is clear more research is required to improve device deployment.

The Cytosorb filter has been approved in the European Union for extracorporeal cytokine removal. Porous polymer beads are used to specifically remove hydrophobic middle molecular weight proteins such as cytokines. This approach leads to rapid removal of multiple cytokines associated with negative outcomes in sepsis [65]. This approach has showed success in animal models and case studies [49,66,67], but larger clinical studies have either not been completed or have not shown significant reductions in pro-inflammatory response [68]. Coupled plasma filtration adsorption works in a similar manner to the Cytosorb filter, but plasma is separated from whole blood prior to cytokine removal. Removing the cytokines from plasma minimizes

complications related to coagulation, platelet activation, and red blood cell damage. Clinical data is still lacking, but this approach appears to be fairly safe and has shown the ability to remove cytokines from circulation [69–72]. Like many therapies that target the immune response in sepsis, early treatment may be required to obtain benefits from this approach. High-adsorption hemofiltration combines hemofiltration and hemoadsorption to effectively remove endotoxin and/or cytokines [54,73].

Many blood filtration therapies are challenged by their tendency to remove antibiotics from circulation in addition to targeted solutes. Antibiotics play a critical role in the treatment of sepsis and it is important for clinicians to understand how antibiotic regimens must change with use of these devices. An early stage technology being developed at the Wyss Institute is constructed from modified hemodialysis fibers coated with genetically modified form of the human opsonin Mannose Binding Lectin linked to an Fc domain [74]. This coating efficiently removes a range of pathogens and endotoxin. Additionally, research in rats has shown a synergistic effect when this treatment is combined with antibiotics, due to the device's ability to adsorb pathogen-associated molecular patterns released after antibiotic treatment. This technology is still extremely early stage, but shows some promise of extracorporeal devices in treatment of sepsis.

Another approach, being developed by David Humes at University of Michigan, directly targets activated neutrophils that cause organ damage. The Cytopherx device utilized a selective cytopheretic device, which binds activated neutrophils within an extracorporeal circuit [75]. Pre-clinical studies have shown promise using this approach for sepsis and other inflammatory diseases [76,77]. A small clinical study using the Cytopherx device on patients suffering from acute kidney injury showed no, significant difference in 60 day mortality, but there were issues with maintain correct levels of calcium in the circuit, limiting he devices efficacy. There was some potential

improvement when only patients who were within recommended protocol parameters were considered [78]. This study illustrated challenges of implementing a device which relies on citrate anticoagulation, which is not widely used and requires a well trained staff. Another downside of this approach is removal of activated neutrophils from circulation, potentially limiting the patient's ability to fight the underlying infection. However, with further data and clinical training to take full advantage of the device's ability to modulate neutrophil activity, this approach may prove beneficial? Additionally, this device shows that there is promise in targeting neutrophil's role in sepsis and other acute inflammatory conditions.

Overall, extracorporeal devices have made much progress in sepsis treatment over the last decade, with many options showing promise. However, none of these approaches have established sufficient clinical data to be utilized worldwide, limiting their impact. While more clinical data may open the doors for increased usage, sepsis treatments in general must adjust target clinical endpoints and better select target patients. While a theranostic approach did not appear effective in Spectral Diagnostics North American Polymyxin B trial, improved patient diagnostics may help limit patient heterogeneity and improve device deployment. This may be particularly critical for therapies that are time sensitive such as immunomodulatory treatments. For these therapies late deployment may prove to be ineffective or even detrimental. An important takeaway from the plethora of experimental extracorporeal treatments is their improving safety. Typically complications related to extracorporeal devices have been limited, showing that an extracorporeal devices are a safe approach which physicians are likely to be comfortable using.

3.0 COMPUTATIONAL MODELING OF CXCR-1/2 SURFACE RECEPTORS, NEUTROPHIL PHENOTYPE, AND EXTRACORPOREAL TREATMENTS WHICH MODULATE THESE FACTORS IN THE PROGRESSION OF SEPSIS

The following chapter includes work from the manuscript titled *A Neutrophil Phenotype Model for Extracorporeal Treatment of Sepsis* [79], which was published in PLOS Computational Biology.

While understanding of the underlying mechanisms in sepsis has been rapidly improving, translation to clinically effective treatments has proven very challenging [9,80]. Much of this difficulty translating treatments may be due to the diversity and complexity of individual immune response and patient population [81,82]. These complexities lend themselves well to computational modeling, which can help integrate these complexities into a unified pathophysiological framework and optimize potential treatments [83]. This chapter discuss the construction of a computational model used to predict neutrophil induced organ damage in sepsis then estimate efficacy of a proof of concept extracorporeal device which modulates CXCR-1/2 activation. These results are used to support device proof of concept and better understand how to deploy device clinical use.

3.1 INTRODUCTION

Sepsis, a systemic inflammatory response due to an infection, affects 900,000 Americans per year and its incidence is expected to increase over the next 10-20 years as the population ages [84]. While it is acknowledged that sepsis is a growing problem, its associated mortality rate has remained persistently high for the last 20 years and is currently near 20% [84–87]. Sepsis is now the leading cause of in-hospital death in the United States, yet there are no FDA approved specific treatments [88]. While understanding of the underlying mechanisms in sepsis has been rapidly improving, translation to clinically effective treatments has proven very challenging [89,90]. Much of this difficulty translating treatments may be the diversity and complexity of individual immune response and patient population [91,92]. These complexities lend themselves well to computational modeling, which can help integrate these complexities into a unified pathophysiological framework and optimize potential treatments [83].

Neutrophils are one of the first responders to sites of inflammation and play a critical role in the innate immune response. When effective, neutrophils migrate from the bloodstream through endothelial walls to the site of inflammation by sensing gradients of chemokines, which bind to neutrophil cell surface receptors. In early stages of sepsis neutrophils potentially play a duplicitous role, both actively fighting the invading pathogen but also contributing to undesirable systemic inflammation, which often leads to multiple organ dysfunction, immune paralysis, or death [20,93]. Neutrophils' roles in sepsis are well recognized but the dynamics of multiple phenotypes and their impact on treatments is not fully understood. A key chemokine impacting neutrophil behavior and phenotype is interleukin-8 (IL-8). IL-8 signals through functionally distinct surface receptors CXCR-1/2, which are primarily expressed on neutrophils. CXCR-1 is primarily

responsible for activating phospholipase D [94], which mediates respiratory burst and other pathogen killing functions. CXCR-2 has been shown to stimulate migratory functions such as chemotaxis and diapedesis [95,96].

The motivation of this work is to use computational modeling of CXCR-1/2 signaling, and the associated dynamics in neutrophil phenotype composition, to explore whether modifying this dynamic could be exploited to favorably impact outcome in sepsis. A population based mechanistic computational model, which incorporates both receptor level dynamics and neutrophil response to pathogen, was developed to explore the mechanisms involved in sepsis progression and calibrated in septic baboons. Furthermore, an experimental extracorporeal treatment which modulates CXCR-1/2 receptor levels was evaluated *in silico* using the model framework. The computational model described in this manuscript provides a physiologic rationale for neutrophil's CXCR-1/2 mediated activity in sepsis, delivers insight into the overriding mechanisms involved, and suggests that interventions aiming to modulate phenotypic composition are time sensitive.

3.2 METHODS

3.2.1 Experimental Data Set Protocol

After general anesthesia, instrumentation and a 30 minute stabilization period, sixteen baboons (*Papio ursinus*) weighing between 19 and 32 kg were infused with 2 x 10^9 CFU *Escherichia coli* per kg over a two-hour period as described previously [97]. Thereafter, antibiotic therapy was delivered (gentamycin 4mg/kg twice a day). Eight animals were placed in an acute study lasting 6 days, while another eight were placed in the chronic study intended to last 28 days.

All animals were observed for a 4-hour period after bacteria infusion then 11, 23, 35, 47, 72 hour and 6 days after infusion. Pathogen counts in blood, IL-8, creatinine, white blood cell, neutrophil elastase / α1-PI complex, and other physiologic parameters and biomarkers were gathered at multiple time point. For animals in the chronic study an additional time point was collected at 28 days. At the end of the study period, the baboons were again anesthetized for measurements and thereafter sacrificed with an overdose of pentobarbital. This study was approved by the Institutional Animal Care and Use Committee at Biocon Research Institute and animals were treated according to NIH guidelines.

3.2.2 Model Framework and Description

A simplified mechanistic model of IL-8 mediated activation of CXCR-1/2 receptors and neutrophil response to a pathogen was developed based on available literature information and general knowledge of acute inflammatory response. Receptor level dynamics and systemic parameters were coupled with multiple neutrophil phenotypes to generate dynamic populations of activated neutrophils which reduce pathogen load, and/or primed neutrophils which cause adverse tissue damage when misdirected. Mathematical representation of the interactions detailed in Figure 4 were generated using ordinary differential equation (ODE) framework with the rate of interactions described by mass action kinetics or Hill type kinetics [98,99]. The interactions included in the model gives rise to 16 ODE state variables and 43 rate parameters.

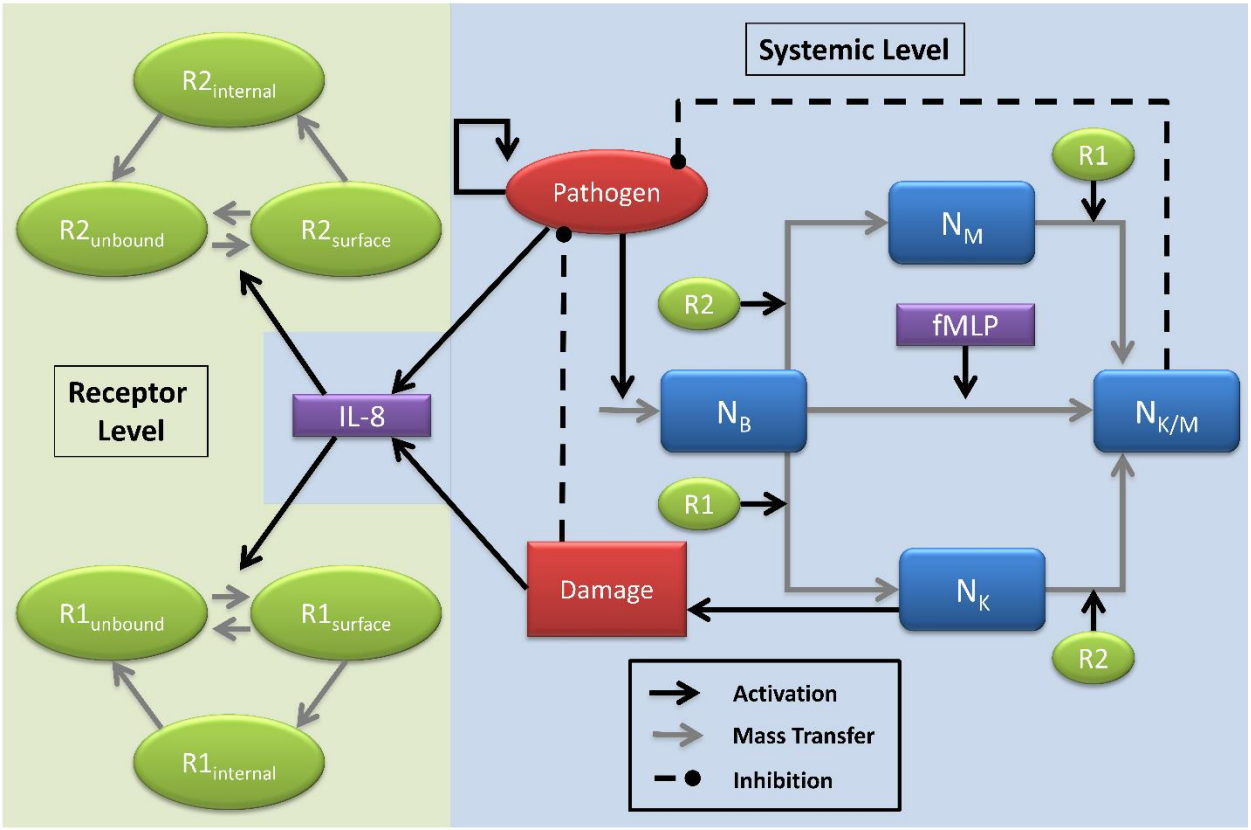

Figure 4. Model diagram detailing neutrophil phenotypes and critical feedback loops.

In brief, the model is initiated by a pathogen load, which represents a bacterial inoculation. Presence of pathogen leads to continued growth as well as IL-8 and fMLP cytokine production. IL-8 is generated indirectly from pathogen generation from responding phagocytic mononuclear cells [100]. IL-8 initiates CXCR-1/2 activation in the receptor level, which in turn generates neutrophil phenotype change. Depending on phenotype, neutrophils may cause either pathogen elimination or misdirected tissue damage. A systemic damage indicator represents overall patient health. Increased systemic damage results in further IL-8 generation [101,102], resulting in a positive feedback loop. This simplified system captures the basic functionality of acute IL-8 mediated immune response to pathogen and is capable providing valuable feedback on potential therapeutic treatments modulating these mechanisms. A more detailed description of model equations follows.

Pathogen: Equation (1) describes the population of foreign pathogen. Base pathogen growth rate increases linearly with pathogen until approaching a carrying capacity at elevated pathogen loads. In addition to basal pathogen death, the Neutrophil kill/migrate phenotype is capable of decreasing pathogen population through diapedesis, followed by targeted phagocytosis [20,103,104].

$$\frac{dP}{dt} = k_{PG}P - k_{P-N_{K/M}}N_{K/M}P - \frac{k_p P}{k_p^d + P} - k_{pL}P^2 \quad (1)$$

Ligands: Interleukin-8 (IL-8) and fMLP: In the model, neutrophils progress through multiple phenotypes which dictate neutrophil migratory, phagocytic, and antibiotic activity. The association of chemokine IL-8 with the surface CXCR-1/2 triggers the transition of basal

neutrophils to functional phenotypes. Previously characterized receptor surface activation, internalization, and recycling rates of CXCR-1/2 are utilized to predict receptor levels and neutrophil phenotypes in response to systemic IL-8 stimulation [95,105]. IL-8 production rate is a function of elevated pathogen and tissue damage [106,107]. Both terms are represented as Hill Equations in equation (2). While IL-8 is not directly linked to pathogen levels, this simplified representation captures IL-8 release from macrophages and endothelial cells in response to infection.

$$\frac{dC_{IL8}}{dt} = \frac{k_{IL8-P}P}{k_{IL8-P}^{d} + P} + \frac{k_{IL8-D}D^{2}}{k_{IL8-D}^{d} + D^{2}} - k_{IL8}C_{IL8} \tag{2}$$

Equation (3) characterizes a general pro-inflammatory pathway, which is independent of CXCR-1/2 activation has been added to represent alternate means of neutrophil induced pathogen activation. This generic pathway is not modeled using receptor level dynamics and directly transitions the N_{Basal} (N_B) population to $N_{Killing/Migratory}$ ($N_{K/M}$).The generic proinflammatory ligand growth is dictated by pathogen level.

$$\frac{dC_{fMLP}}{dt} = \frac{k_{fMLP}P}{k_{fMLP}^{d} + P} - k_{fMLP-D}C_{fMLP} \tag{3}$$

Neutrophil Surface Receptors CXCR-1 & CXCR-2: Receptor level dynamics dictate neutrophils advancement into one of four phenotypes depending on CXCR-1/2 surface activation. Each receptor can occupy one of the three states, namely free surface receptor, surface receptor

bound to IL-8 and internalized receptor bound to IL-8 [108]. Equation (4) and Equation (5) describe CXCR-1 surface and internalized populations, which have been non-dimensionalized to remove the free receptor state. Equivalent equations are present for CXCR-2. The active surface state was modeled as the dynamic condition which drives neutrophil population phenotype change [109]. This model makes the assumption that CXCR-1/2 receptors are conserved.

$$\frac{dC_{R1s}}{dt} = k_{f1}C_{IL8}\left(1 - C_{R1s} - C_{R1i}\right) - k_{r1}C_{R1s} - k_{i1}C_{R1s} \tag{4}$$

$$\frac{dC_{R1i}}{dt} = k_{i1}C_{R1s} - k_{i1'}C_{R1i} \tag{5}$$

Neutrophil Phenotype: Equation (6) represents the resting state (N_B) represents basal neutrophils which have not been stimulated by IL-8 or other proinflammatory stimuli. These neutrophils are mobile in blood, but not capable of causing systemic damage or utilizing their anti-pathogen capacity without transitioning to another phenotype. All neutrophils begin in this basal state prior to activation and priming. Without stimulation, neutrophil growth and death rates are in equilibrium, however growth rate increases with the introduction of pathogen, which has been expressed through a filter equation to produce a physiologic time delay [20,110]. CXCR-1/2 surface complex levels dictate the transition rates of N_B to the $N_{Migratory}$ (N_M) or $N_{killing}$ (N_K) phenotypes. Additionally, there is a direct pathway to transition N_B to $N_{K/M}$. This mechanism represents a general proinflammatory process independent of CXCR-1/2 signaling. A filter equation was generated in Equation (7). This function fits the physiologic delay between pathogen generation and increased neutrophils entering circulation.

$$\frac{dN_B}{dt} = k_{NG}\left(1 + \frac{k_{N_B-G}F}{k^d_{N_B-G} + F}\right) - k_{N_{K-IL8}}N_B C_{R1s} - k_{N_{M-IL8}}N_B C_{R2s} - k_{N_B}N_B - k_{fMLP-N_B}N_B \quad (6)$$

$$\frac{dF}{dt} = k_{filter\_on}P - k_{filter\_off}F \quad (7)$$

Equation (8) contains neutrophils which have been activated via IL-8 mediated CXCR-2 stimulation.

$$\frac{dN_M}{dt} = k_{N_M-IL8}N_B C_{R2s} - k_{N_M-N_K-IL8}N_M C_{R1s} - k_{N_M}N_M \quad (8)$$

Equation (9) characterizes the killing phenotype (N_K), representing neutrophils which have been activated via IL-8 mediated CXCR-1 stimulation. N_K neutrophils are capable of untargeted cytotoxic activity, resulting in systemic organ damage. The CXCR-1/2 surface population dictates transition rates into phenotypes. Neutrophil elastase / α1-PI complex was utilized in the model to fit N_K neutrophil population. As shown in Equation (10) levels of neutrophil elastase / α1-PI complex equate to levels of circulating N_K phenotypes.

$$\frac{dN_K}{dt} = k_{N_K-IL8}N_B C_{R1s} - k_{N_K-N_M-IL8}N_K C_{R2s} - k_{N_K}N_K \quad (9)$$

$$\frac{dC_{elas}}{dt} = k_{NE}\frac{dN_K}{dt} \tag{10}$$

Both N_M and N_K phenotypes are capable of progressing to the $N_{K/M}$ phenotype through CXCR-1/2 surface receptor activation. This neutrophil state ($N_{K/M}$), shown in Equation (11), represents neutrophils which have been activated through both CXCR-1 and CXCR-2 and are capable of target pathogen removal, effectively fighting infection. The pathogen equation (Equation (1)) contains a term which dictates pathogen death in response to $N_{K/M}$ levels. Once activated through CXCR-1/2 neutrophils are not capable of returning to the basal N_B phenotype.

$$\frac{dN_{K/M}}{dt} = k_{N_K - N_M - IL8}N_K C_{R2s} + k_{N_M - N_K - IL8}N_M C_{R1s} - k_{N_{K/M}}N_{K/M} + k_{fMLP-N_B}N_B \tag{11}$$

Damage: A systemic damage indicator (Equation (12)) was developed to represent overall animal health. Damage is increased by the population of N_K and decays gradually as tissue and organs recover. Creatinine, a biomarker for kidney function, was utilized in Equation (13) as an indicator for the damage term ensemble computation. Creatinine is maintained at a constant level in the absence of damage, but systemic levels increase with damage as body's ability to clear creatinine decreases [111].

$$\frac{dD}{dt} = k_{D-N_K}N_K\left(1-D\right) - k_D D \tag{12}$$

$$\frac{dC_{creat}}{dt} = k_{creat-P} - k_{creat}\left(1-D\right)C_{creat} \tag{13}$$

The model uses empirical time series of Pathogen (CFU), IL-8 (nM), creatinine (mM), White Blood Cell count (10^3 cells/µl), and neutrophil elastase / α1-PI complex (ng/ml) for computation of the ensemble. State variables and their initial conditions are listed in Table 2.

Table 2. Initial Conditions.

No.	Symbol	Description	Initial Condition – Survivors	Initial Condition – Non-Survivors	Units
1	P	Pathogen	1000	1000	CFU
2	N_B	Basal neutrophils	4.4	5.06	10^3 cells/µl
3	N_K	Neutrophils with killer phenotype	0.0	0.0	10^3 cells/µl
4	N_M	Neutrophils with migratory phenotype	0.0	0.0	10^3 cells/µl
5	$N_{K/M}$	Neutrophils with dual phenotype	0.0	0.0	10^3 cells/µl
6	C_{IL8}	Systemic IL-8 concentration	0.0	0.0	nM
7	D	Global tissue damage	0.0	0.0	unitless
8	C_{R1s}	Surface CXCR1 population	0.0	0.0	unitless
9	C_{R1i}	Internalized CXCR1 population	0.0	0.0	unitless
10	C_{R2s}	Surface CXCR2 population	0.0	0.0	unitless
11	C_{R2i}	Internalized CXCR2 population	0.0	0.0	unitless
12	C_{creat}	Creatinine	91.5455	102.4	nM
13	F	Filter term	0.0	0.0	unitless
14	C_{R1t}	CXCR1 trapped	0.0	0.0	unitless
15	C_{fMLP}	fMLP	0.0	0.0	nM
16	C_{elas}	Neutrophil elastase / α1-PI complex	0.0	0.0	ng/ml
17	WBC	Total white blood cells	4.4	5.06	10^3 cells/µl

3.2.3 Parameter estimation

The model contains 38 parameters, 13 of which are fixed based on literature data (Table 2). Parameter values were inferred using a Bayesian parallel tempering approach [112,113], which utilizes traditional Markov Chain Monte Carlo (MCMC) methods to sample the Bayesian posterior distribution P(**p**|**y**), the probability of parameter set **p** given data **y**, given by the Bayes formula

$$P(\boldsymbol{p}\,|\,\boldsymbol{y}) = \frac{L(\boldsymbol{y}\,|\,\boldsymbol{p})\theta(\boldsymbol{p})}{\int L(Y\,|\,\boldsymbol{p})\theta(\boldsymbol{p})}$$

where L(**y**|**p**) is the likelihood of observing **y** for a model with parameters **p**, θ(**p**) is the prior distribution, and $\int L(Y\,|\,\boldsymbol{p})\theta(\boldsymbol{p})$ is the normalizing constant. Additional sampling efficiency is gained by running multiple parallel chains evolving at different temperatures. Higher temperature increases the likelihood of acceptance of proposed steps. This allows the high temperature chains to move more freely through the parameter space, avoiding getting stuck in local minima. This results in more efficient exploration of parameter space [114,115] a method we have applied extensively in parameter estimation of practically unidentifiable complex non-linear models [83,116,117]. This resulted in the creation of parameter ensembles, where each parameter is represented by a posterior distribution, rather than a single value. Free parameters were fit separately to the survivor and non-survivor experimental data sets, resulting in two parameter ensembles representing surviving and non-surviving animals.

3.2.3.1 Bayesian Priors

Prior distributions were selected for each parameter. In each case uniform priors were used, with a suitably large range so as to encompass all reasonable parameter values. This was ideal due to the limited prior knowledge and phenomenological nature of many of the parameters. Tighter ranges were enforced on select parameters as required to avoid non-physiologic model behavior. All candidate parameter values were selected from these pre-defined priors.

3.2.3.2 Parameter Set Fitness

Fitness (log likelihood) of candidate parameters sets was determined by the difference between model simulations and experimental data, as determined by the sum of squared residuals cost function,

$$Fitness = \sum_{i,j,k} w_{i,j,k} * \frac{\left(y_{i,j,k} - \hat{y}_{i,j,k}\right)^2}{2\sigma_{i,j,k}^{\ 2}}$$

Where $w_{i,j,k}$ is a weighting function, $y_{i,j,k}$ is the output for a simulation with a single set of parameters, $\hat{y}_{i,j,k}$ is the experimental mean, and $\sigma_{i,j,k}$ $\sigma_{i,j,k}$ is the experimental standard deviation at time point *i*, observable *j*, and data set *k*. No additional penalties or constraints were added to parameter selection. To ensure proper fitting of the pathogen observable a threshold was added to change all values below the experimental limit of detection (4.4 CFU) to 0.

3.2.3.3 Parallel tempering

To efficiently sample the posterior distribution, six separate Markov chains were run, initiated with parameter values randomly selected from the supplied prior distributions which met a maximum energy criterion. Each chain was initiated with a temperature and step size parameter which controlled the chain's ability to fully explore the parameters space. Chains were allowed to swap from a higher temperature to a lower temperature every 25 steps to allow for local sampling of newly found local minima. Step size and temperature parameters dynamically changed every 6,250 and 2,500 steps respectively to attempt to reach an ideal step acceptance rate of 23% [118], and swap rates of 15%-30%. Once these targets were reached, the temperature schedule and step sizes were fixed. Parameter sets were saved every 25 steps. Full exploration of parameter space was confirmed by examining, for each parameter, the frequency histogram of its full marginal posterior distribution, confirming that it spanned the prior domain.

We measured convergence and chain stationarity using the Gelman-Rubin criteria [119,120]. All parameters had converged with a potential scale reduction factor (PSRF) < 1.1 following 200,000 (x25) MCMC steps. Another 100,000 steps were taken to build a posterior distribution for each parameter that would be used for all model analysis and simulation. This ensured that all samples from the burn-in time for each chain were discarded, and only samples from the correct stationary distribution were used. The ensemble of all parameter sets from the lowest chain comprised the computed ensemble (posterior distribution).

3.2.4 Selection of key parameters

In order to better capture the underlying biological differences between animals that survive and those that die following the same challenge we attempted to identify the most important parameters in determining animal fate. After computing ensembles for survivors and non-survivors, we performed regularized logistic regression, forward conditional stepwise logistic regression, and backward conditional logistic regression to identify a subset of parameters that are most indicative of outcome. Predictors consisted of all estimated parameters of both ensembles, and the indicator variable was the source (survivor or non-survivor) of the ensemble. Parameters were selected that were considered significant by all three methods, leaving a set of seven key parameters.

3.2.5 Model fitting

A second round of model fitting was then performed. In this round, 18 of the 25 parameters were fit simultaneously to both data sets, resulting in identical parameter values in the two ensembles. The seven parameters identified as being significant were fit twice, once against the survivor data set and once against the non-survivor data set, resulting in different parameter values across the two ensembles. This resulted in a smaller and more focused difference between the final ensembles.

3.2.6 Global sensitivity analysis

Global Sensitivity analysis was done to determine the independent and correlated contributions of rate parameters on cumulative damage. Area under the damage curve was chosen as the system output. To reduce the computational cost of GSA, Random Sampling High Dimensional Model Representation (RS-HDMR) approach was used [121]. Here, a multivariate output function (eg. AUC_D) was approximately represented by weighted optimal expansion functions (called as component functions). The expansion coefficients of these functions were determined by least-squares regression simultaneously from one set of Monte Carlo samples. In general, for input vector, $\bar{x} = [x_1, x_2, ..., x_n]$ of rate parameters, in an n–dimensional space, a multivariate output function, $f(\bar{x})$, is approximated by a sum of terms including the mean (f_0) and the component functions (g_l). Mathematically,

$$f(\bar{x}) = f_0 + \sum_{l=1}^{2^n-1} g_l$$

Here, the index l indicates all possible combinations of the input parameters. In practice, not all component functions are significant and an F-test can be used to determine which component function should be excluded from the expansion [122]. For our work, we evaluated the variance based Sobol' indices using these component functions. The workflow adopted here starts with generation of Monte Carlo samples of the rate parameters from the ensembles obtained by the parallel tempering approach. Since they come from the ensemble, information on the covariance between the parameter distributions for the population of survivors and non-survivors is retained. Next, a detailed procedure is followed which includes simultaneous construction of all the

component functions, removal of non-significant component functions using an F-test ratio score, re-evaluation of component functions and finally evaluation of the Sobol' sensitivity indices. The first order Sobol' sensitivity indices which capture the influence of a single parameter (but averaged over the other parameters) are defined as:

$$S_l = \frac{Cov(f(\bar{x}), g_l(\bar{x}))}{s^2}, \quad l = 1, 2, 3, ..., n$$

Here, s^2 is the total variance in the output and $Cov(\cdot)$ is the covariance between the output function and each of the first order component functions. For clarity, the component function, g_l, is written as a function of $\bar{x}$ but in reality it is only a function of the input parameter for which it is defined (for example, x_l) and not the entire vector. Further, this sensitivity index is a sum of two terms that capture independent (S_l^a) and correlated contributions (S_l^b) of the input, which are defined as:

$$S_l^a = \frac{\langle g_l(\bar{x}), g_l(\bar{x}) \rangle}{s^2} \text{ and}$$

$$S_l^b = \frac{\sum_{k=1, k \neq l}^{n} \langle g_l(\bar{x}), g_k(\bar{x}) \rangle}{s^2}$$. The inner products, $\langle \cdot \rangle$, are defined as:

$$\langle g_k(\bar{x}), g_l(\bar{x}) \rangle = \int_{x_1} .. \int_{x_n} w(\bar{x}) g_k(\bar{x}) g_l(\bar{x}) dx_1 ... dx_n$$ and $w(\bar{x})$ is the probability density function of the inputs informed by the parameter ensembles. Similar equations can be written for

the higher order component functions and sensitivity indices. Further details on the evaluation of the component function for various types of models are given in [121,123,124]. To determine the importance of a given parameter, it is necessary to combine all the important sensitivity indices (all orders) into a total sensitivity index, which for a parameter i can be defined as:

$$S_{T_i} = S_i + \sum_{\substack{j=1 \\ j \neq i}}^{n} S_{ij} + \sum_{\substack{j<k=1 \\ j,k \neq i}}^{n} S_{ijk} + \ldots\ldots$$

For most systems, very high order interactions are negligible and therefore, indices until the third order are sufficient, with most systems requiring only until the second order terms [121]. In this work, we constructed a third order RS-HDMR. All GSA computations were performed using the ExploreHD software (Aerodyne Research Inc., MA, USA).

3.2.7 Treatment framework

3.2.7.1 Treatment implementation

After model fitting and analysis, a potential extracorporeal treatment was introduced (See Figure 5). The extracorporeal treatment directly modulates CXCR-1/2 levels of circulating neutrophils, limiting passage of N_B to N_K and N_M. This mechanism of limiting CXCR-1/2 surface levels is modeled solely in the receptor level equations of the model.

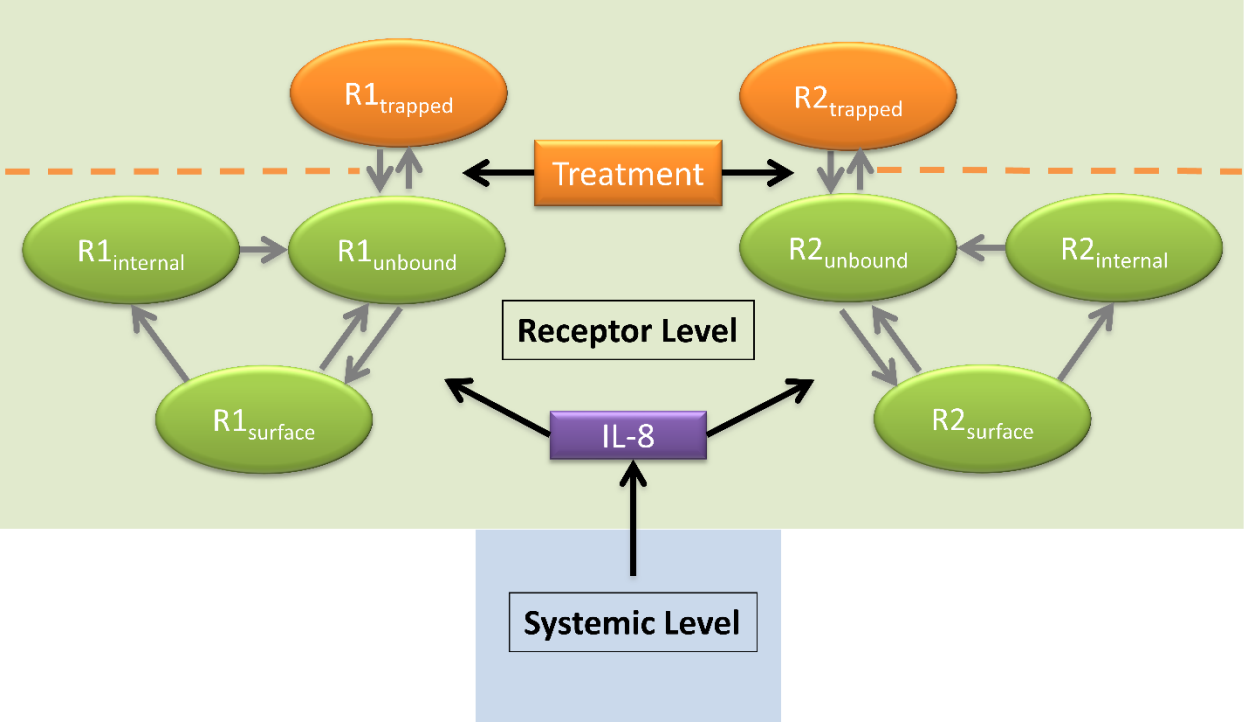

Figure 5. Model diagram showing receptor level treatment implementation.

A heaviside function is used to turn treatment on and off at various treatment times. The k_{ft1} parameter represents treatment effectiveness, which combines device size, efficacy, efficiency, and flow rate. Equation (14) is the modified CXCR-1 surface receptor equation which includes the Heaviside function. Equation (15) characterizes the trapped receptor state of CXCR-1. Similarly Equation (16) and Equation (17) are constructed for CXCR-2 and its associated trapped receptor state.

$$\frac{dC_{R1s}}{dt} = k_{f1}C_{IL8}\left(1-C_{R1s}-C_{R1i}-C_{R1t}\right)-k_{r1}C_{R1s}-k_{i1}C_{R1s}+k_{ft1'}C_{R1t} \\ -Heaviside\left(t,k_{treat-on},k_{treat-off}\right)k_{ft1}\left(1-C_{R1s}-C_{R1i}-C_{R1t}\right) \tag{14}$$

$$\frac{dC_{R1t}}{dt} = \text{Heaviside}\left(t, k_{treat-on}, k_{treat-off}\right) k_{ft1}\left(1 - C_{R1s} - C_{R1i} - C_{R1t}\right) - k_{ft1'} C_{R1t} \quad (15)$$

$$\begin{aligned}\frac{dC_{R2s}}{dt} = {} & k_{f2} C_{IL8}\left(1 - C_{R2s} - C_{R2i} - C_{R2t}\right) - k_{r2} C_{R2s} - k_{i2} C_{R2s} + k_{ft2'} C_{R2t} \\ & - Heaviside\left(t, k_{treat-on}, k_{treat-off}\right) k_{ft2}\left(1 - C_{R2s} - C_{R2i} - C_{R2t}\right)\end{aligned} \quad (16)$$

$$\frac{dC_{R2t}}{dt} = \text{Heaviside}\left(t, k_{treat-on}, k_{treat-off}\right) k_{ft2}\left(1 - C_{R2s} - C_{R2i} - C_{R2t}\right) - k_{ft2'} C_{R2t} \quad (17)$$

3.2.7.2 Classification of Patient Outcome

In order to implement and evaluate treatment frameworks, simulated patient survivorship needed to be explicitly labeled. This was accomplished using a logistic regression classifier as specified by the machine learning software Weka [125]. The estimated parameter ensemble was partitioned into a training set and test set to build the classifier, using 20% of the ensemble as training data. Two features were used for training, total accumulated damage measured by area under the curve of the damage time course for each patient, as well as the peak damage experienced by the patient. Training with these features resulted in a classifier that could label a patient as surviving or dying after being exposed to a specific infection and possible treatment.

3.3 RESULTS

3.3.1 Computation of parameter ensembles explaining survivor and non-survivor dynamics

Of the 16 baboons subjected to bacterial infusion, 11 (69%) died and 5 (31%) survived, with death occurring within 6 days of bacterial. Based on these two systemic outcomes, a thorough investigation of the model (see Methods section & Figure 4) was completed to identify parameter regimes that explain the dynamics of each group of the responders.

The initial conditions for the state variables of the ODE were fixed to simulate experimental stimulation (Table 2). Among the rate parameters, some were fixed to literature values. These included pathogen growth and decay rates, basal decay rates of naïve neutrophils, CXCR-1/2 internalization and recycling rates and creatinine decay rate (See fixed parameters in Table 3 and Table 4). Remaining parameters were estimated by generating parameter ensembles using a Bayesian parallel tempering approach that fit our model to the survivor and non-survivor experimental data sets (see Methods). We conducted the parameter estimation process in two rounds. In round one, the model was fitted to the two data sets separately. By fitting to the two data sets separately, we were able to effectively show that the model was capable of replicating both lethal and non-lethal outcomes through only a change in few parameters. In an attempt to classify the underlying differences, we identified the parameters that were most influential in determining the outcome (survivor or non-survivor) of an individual using stepwise logistic regression. This resulted in a list of seven key parameters. These parameters tend to control the

rate at which neutrophils grow and how quickly they can change phenotypes, which play a critical role in determining how quickly and severely the animal will respond to the infection.

Table 3. Shared Parameter Values

o.	Symbol	Description	Fixed/ Fitted	Mean	Std. Dev.	Units
	k_{PG}	Pathogen growth	Fixed	1	0	$Hour^{-1}$
	$k_{PG-N_{K/M}}$	Neutrophil induced pathogen death	Fitted	145.5391	0.040553	$(Hour * 10^3 cells/\mu l)^{-1}$
	k_{PL}	Pathogen population limit	Fitted	1.6533E-7	2.3409E-7	$(Hour*CFU)^{-2}$
	k_p	Pathogen decay	Fitted	271.9904	352.4858	CFU/Hour
	k_p^d	Pathogen decay	Fixed	1000	0	CFU
	k_{N_B}	Basal neutrophil natural	Fixed	0.1	0	$Hour^{-1}$
	k_{N_K}	Killer neutrophil decay	Fitted	0.0330	0.0275	$Hour^{-1}$
	k_{N_M}	Migratory neutrophil decay	Fitted	0.1244	0.1936	$Hour^{-1}$
	$k_{N_{K/M}}$	Migratory-Killer neutrophil decay	Fitted	0.1176	0.1772	$Hour^{-1}$
0	$k_{N_M-N_K-IL8}$	IL-8 induced migratory neutrophil to neutrophil migratory-killer transition	Fitted	168.7708	260.7247	$Hour^{-1}$
1	k_{IL8-P}	Pathogen induced IL-8 production	Fitted	2.7810E-6	2.0441E-6	$Hour^{-1}$
2	k_{IL8-D}	Tissue damage induced IL-8 production	Fitted	5.7938E-9	7.9615E-9	$nM*Hour^{-1}$
3	k_{IL8}	IL-8 decay	Fitted	0.3352	0.0261	$Hour^{-1}$
4	k_{D-N_K}	Tissue damage induced by killer neutrophils	Fitted	0.0319	0.0285	$(Hour * 10^3 cells/\mu l)^{-1}$

Table 3 (continued)

5	k_D	Damage recovery rate	Fitted	7.0147	8.8870	$Hour^{-1}$
6	k_{filter_on}	Filter production rate	Fitted	6.1698E-4	8.2047E-4	$(CFU*Hour)^{-1}$
7	k_{r1}	Dissociation constant for R1 receptors	Fixed	79.2	0	$Hour^{-1}$
8	k_{r2}	Dissociation constant for R2 receptors	Fixed	79.2	0	$Hour^{-1}$
9	k_D	Affinity constant for IL-8 to the receptors	Fixed	2.5E-3	0	$Hour^{-1}$
0	k_{i1}	Internalization rate for IL-8-R1 complex	Fixed	5.196	0	$Hour^{-1}$
1	$k_{i1'}$	Recycle rate for R1	Fixed	0.612	0	$Hour^{-1}$
2	k_{i2}	Internalization rate for IL-8-R2 complex	Fixed	20.796	0	$Hour^{-1}$
3	$k_{i2'}$	Recycle rate for R2	Fixed	0.144	0	$Hour^{-1}$
4	k_{fMLP}	Pathogen induced fMLP production	Fitted	5.9866E-7	1.3864E-6	$nM*Hour^{-1}$
5	k_{fMLP}^{d}	Pathogen induced fMLP production	Fitted	622.9280	1.6952E3	CFU
6	k_{fMLP-D}	Pathogen induced fMLP decay	Fitted	9.8425E4	1.7303E5	$Hour^{-1}$
7	k_{fMLP-N_B}	fMLP induced basal neutrophil to migratory-killer phenotype transition	Fitted	0.0021	0.0025	$Hour^{-1}$
8	k_{ne}	Scaling of Nk cells to neutrophil elastase / α1-PI complex levels	Fitted	0.0351	0.0209	ng/cell

Table 4. Unique Parameter Values.

o.	Symbol	Description	Fixed/ Fitted	Mean - Survivor	Std. Dev. –survivor	Mean – Non-survivor	Std. Dev. – Non-survivor	Units
1	k_{NG}	Neutrophil baseline growth rate, based on 12 h life	Fixed	0.506	0	0.54417	0	10^3 cells/ (µl *Hour)
2	k_{creat}	Creatinine decay rate	Fixed	0.1591	0	0.1792	0	$Hour^{-1}$
3	k_{N_B-G}	Pathogen influenced neutrophil growth	Fitted	6.6447E5	1.5092E6	6.4953E5	1.0063E6	unitless
4	$k^d_{N_B-G}$	Pathogen influenced neutrophil growth (denominator)	Fitted	8.8322E4	1.7149E5	5.5590E4	9.0741E4	unitless
5	k_{N_K-IL8}	IL-8 induced neutrophil basal to killer phenotype transition	Fitted	8.9617E3	4.9596E3	4.5302E4	2.6386E4	$Hour^{-1}$
6	k_{N_M-IL8}	IL-8 induced neutrophil basal to migratory phenotype transition	Fitted	4.8740E3	6.5289E3	2.9804E3	6.6655E3	$Hour^{-1}$
7	$k_{N_K-N_M-IL8}$	IL-8 induced killer neutrophil to neutrophil migratory-killer transition	Fitted	3.9436	12.6137	5.9631	16.7691	$Hour^{-1}$
8	k^d_{IL8-P}	Pathogen induced IL-8 production	Fitted	1.2814E4	1.2646E4	1.2841E4	1.4198E4	CFU
9	k_{filter_off}	Filter decay rate	Fitted	0.0813	0.0145	0.1407	0.0328	$Hour^{-1}$

Once these differentiating parameters were identified, we put the model through a second round of estimation. In the second round, the model was fit to both data sets simultaneously; allowing only the seven previously identified key parameters to vary between the survivor and non-survivor subpopulations (see Table 4). Additionally, two fixed parameters were allowed to take different values across the two populations to maintain the appropriate initial conditions in creatinine and white blood cell count. This step resulted in two new parameter ensembles that

were identical in 28 parameters but varied in nine parameters. This second step enabled us to better crystallize the differences between animals that survived and those that died. These ensembles are biologically more relevant as we expect the animals' immune responses to be highly similar, with small but important differences indicating susceptibility to a septic insult. Resulting full marginal distributions for each of the 7 parameters were statistically different across survivor and non-survivor populations (Figure 6– Box Plot). The final mean values and the standard deviation of all the estimated parameters are summarized in Table 3 and Table 4.

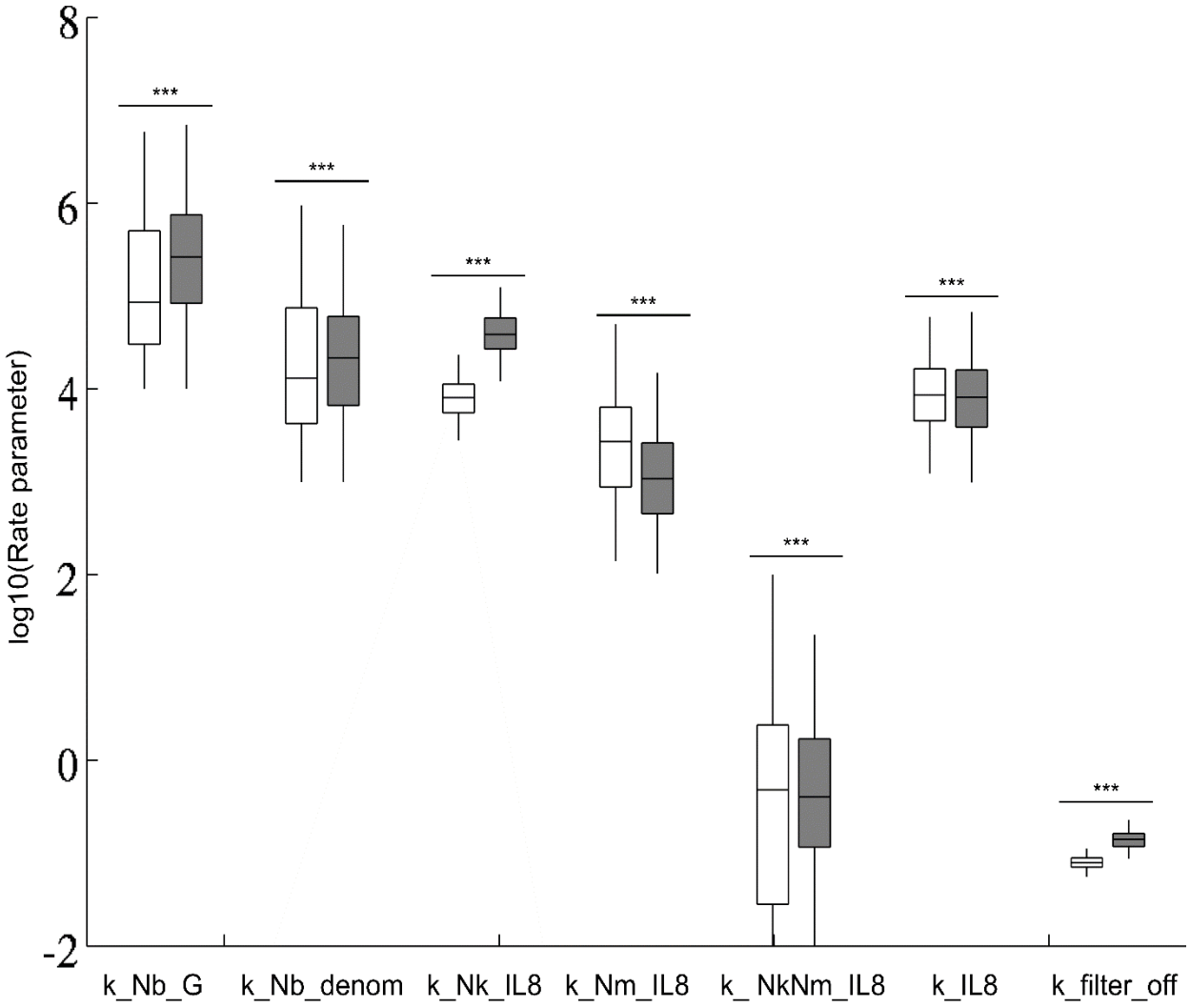

Figure 6. Posterior distributions of parameters allowed to vary across ensembles.

3.3.2 Features of survivor and non-survivor dynamics

3.3.2.1 Trained model outcomes

The two ensembles resulted in model fits that faithfully recreate the key features of the surviving and non-surviving data sets (Figure 7– experimental fits). Pathogen dynamics showed a transient behavior, with the model predicting a slightly higher peak for non-survivors. The ensembles captured the transient peak in IL-8 that occurs early after infection, with the non-surviving

population exhibiting a higher maximum peak. The predicted neutrophil populations also tracked well with the experimental results, with circulating basal neutrophils exhibiting a strong initial decline in abundance as the cells are activated and migrate to the site of infection, followed by a growth phase as the body compensates for the infection, and finally a return to baseline levels. While both surviving and non-surviving populations exhibited this trend, the surviving populations had a noticeably higher peak in basal neutrophils during the growth phase. Levels of neutrophil elastase / α1-PI complex in the blood, indicative of the killing and damage causing function of activated neutrophils, peaks around 15 hours post-infection. The non-surviving population showed a stronger and longer lasting peak, which is captured by the model. Creatinine, a measure of kidney health, increased to higher and more sustained levels in non-surviving animals, as kidney health decreases and creatinine was not as efficiently cleared.

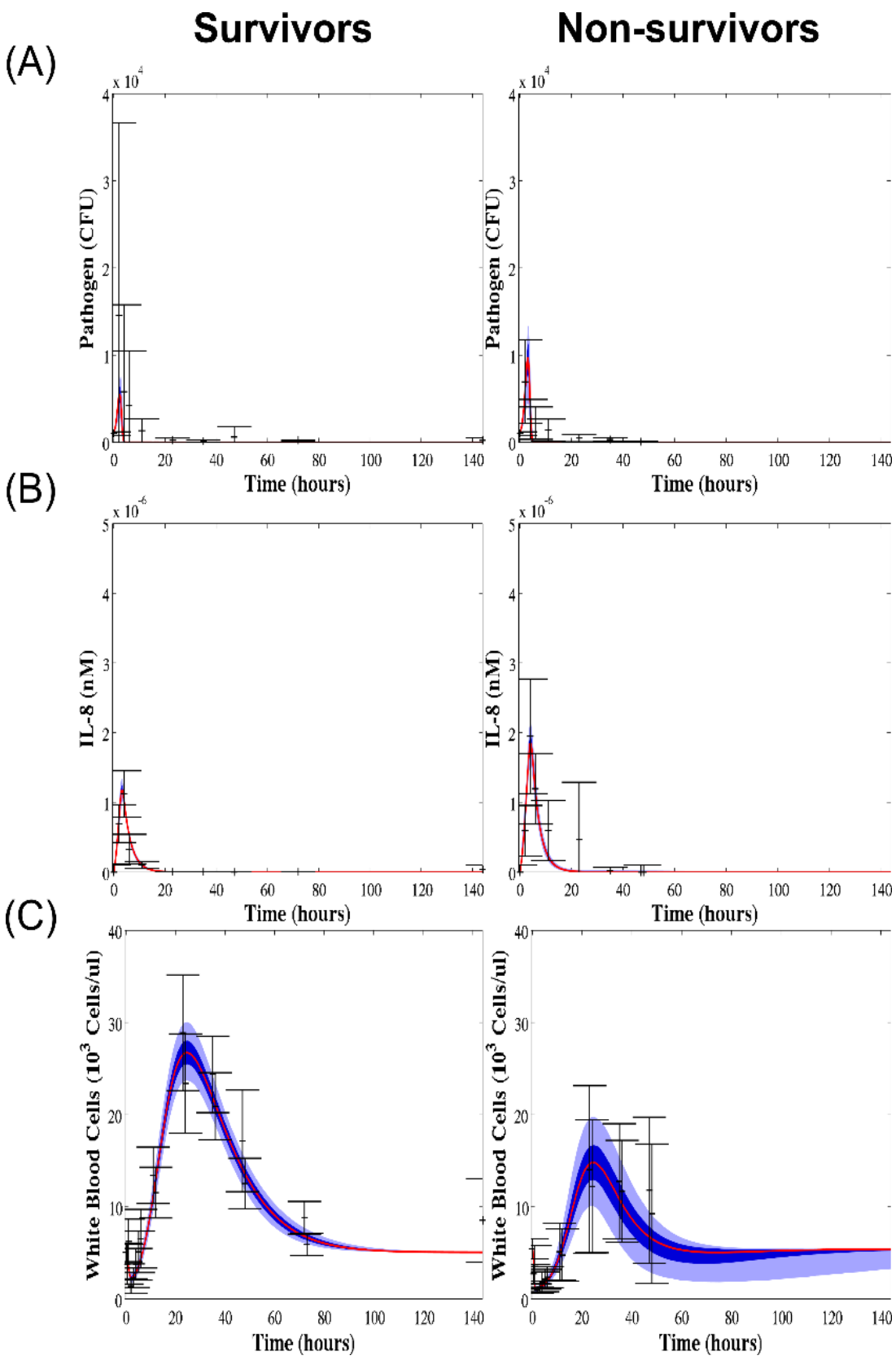
Survivors
Non-survivors
(A)
(B)
(C)
Pathogen (CFU)
IL-8 (nM)
White Blood Cells (10^3 Cells/ul)
Time (hours)
x 10^4
x 10^{-6}

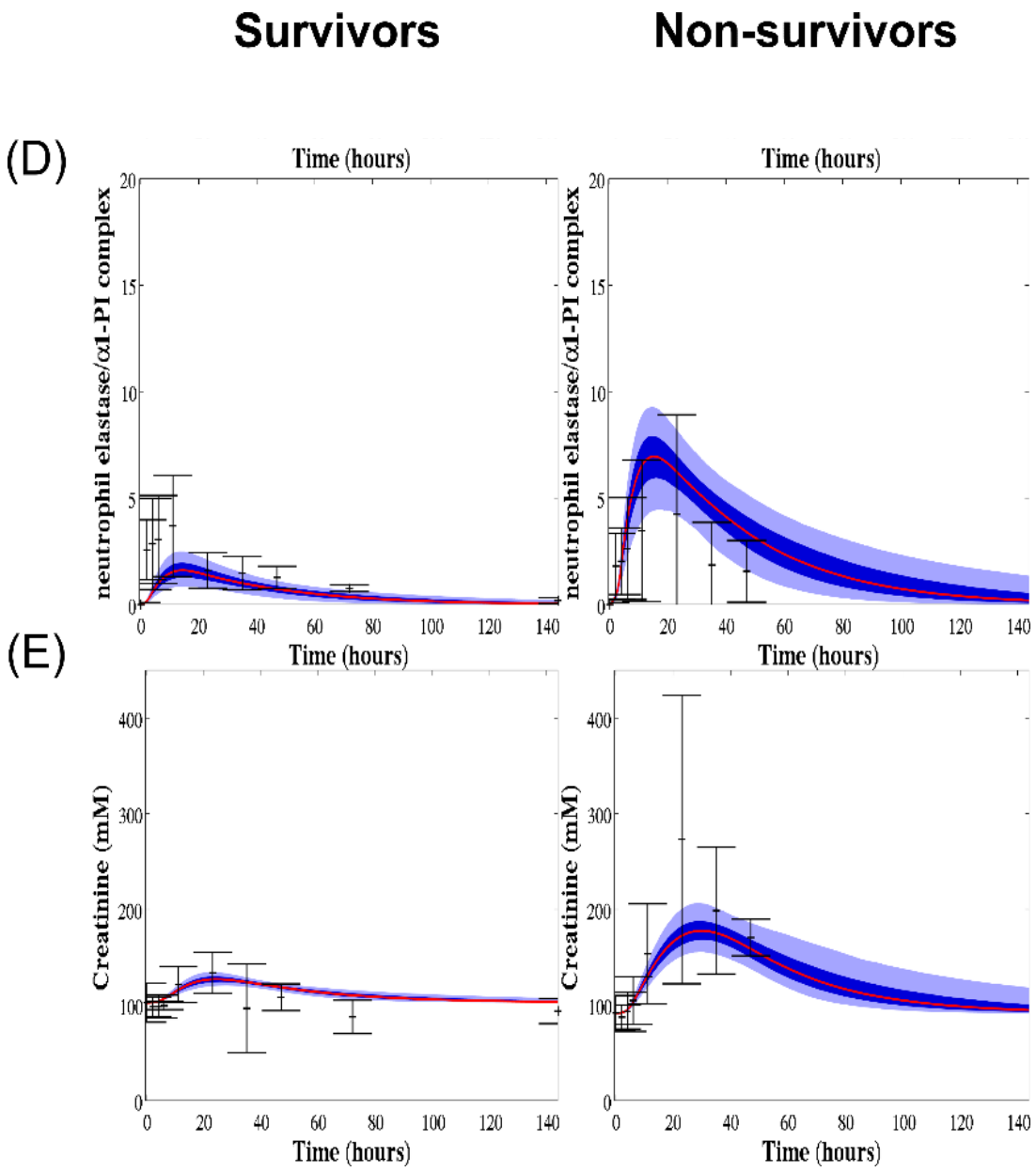

Figure 7. Simulated model fits with their experimental training data Mean (red), 25th-75th percentile (dark blue), and 5th-95th percentile trajectories of the simulated ensemble are shown.

3.3.2.2 Model Predictions

The model also made predictions in the absence of observable data on the dynamics of neutrophil phenotypes (Figure 8–Neutrophil dynamics, Figure 9- Neutrophil phenotype box plot). Although both populations had similar peaks in fully activated neutrophils, allowing them both to fight off the infection on similar time scales as predicted experimentally, they showed strong differences in other populations. Non-survivors showed a significantly stronger spike in damage-causing killer neutrophils, while survivors showed a stronger spike in migratory neutrophils.

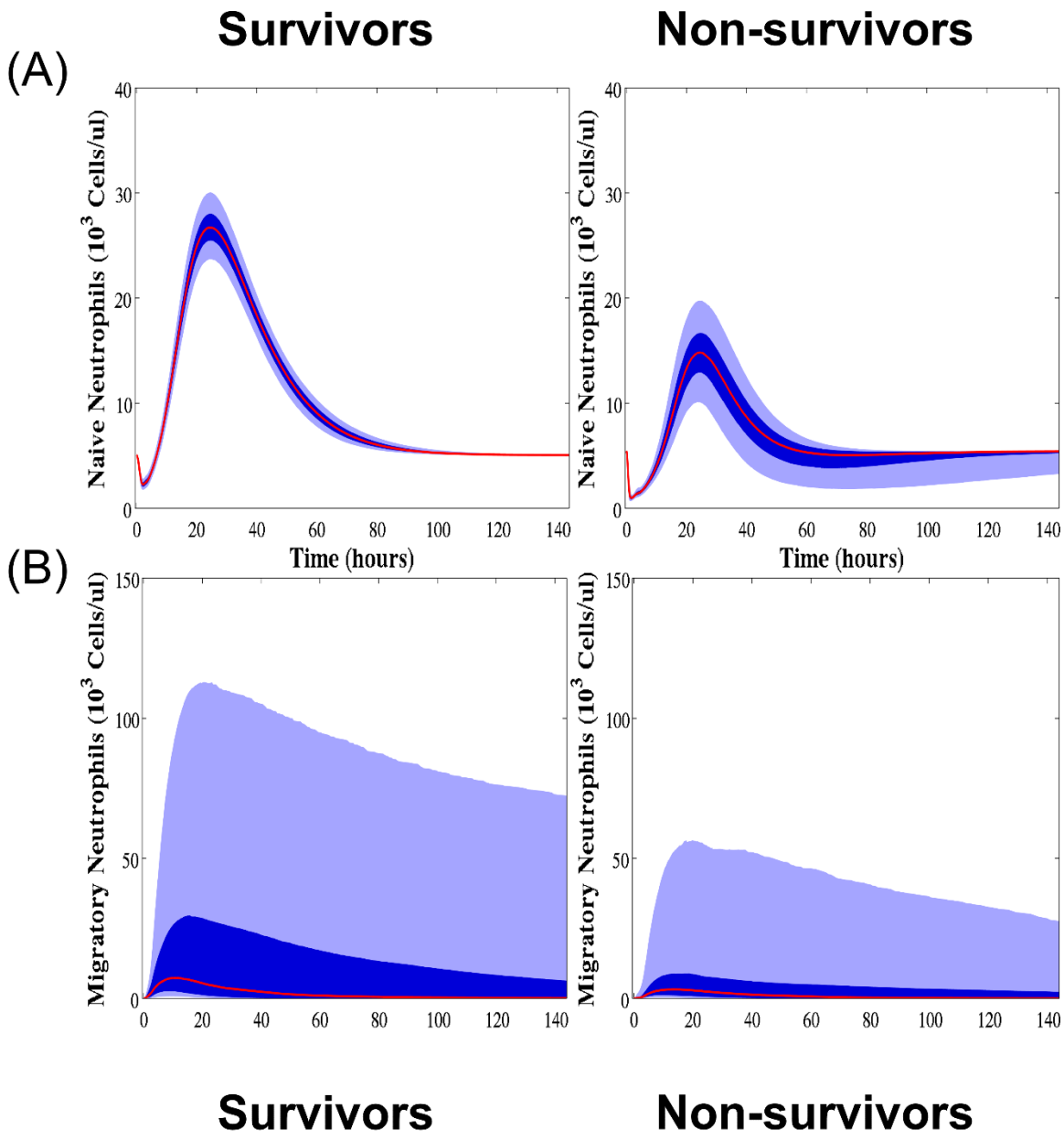
Survivors
Non-survivors
(A)
Naive Neutrophils (10^3 Cells/ul)
Time (hours)
(B)
Migratory Neutrophils (10^3 Cells/ul)
Survivors
Non-survivors

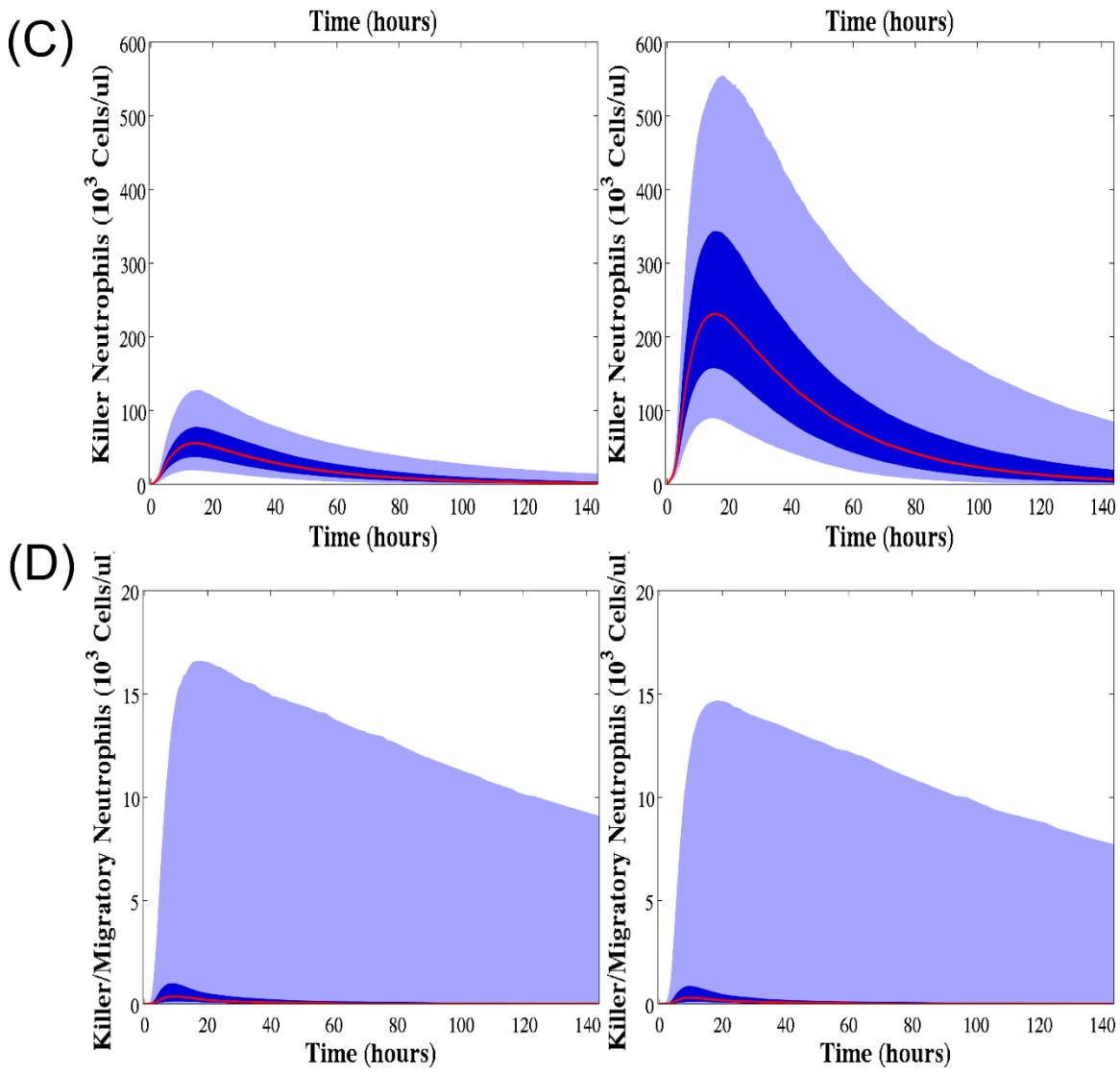

Figure 8. Model predictions for neutrophil phenotype dynamics following infection.

This can also be seen in the parameter ensembles, as neutrophils in non-survivors had an increased proclivity to activate their killing function in response to IL-8, while neutrophils in survivors were faster to activate their migratory functions (Figure 6– Box plot). Generating similar numbers of fully activated neutrophils, but through differing intermediate activation populations, could be an explanation for how these two animal populations controlled infection with similar dynamics, while still experiencing differing fates.

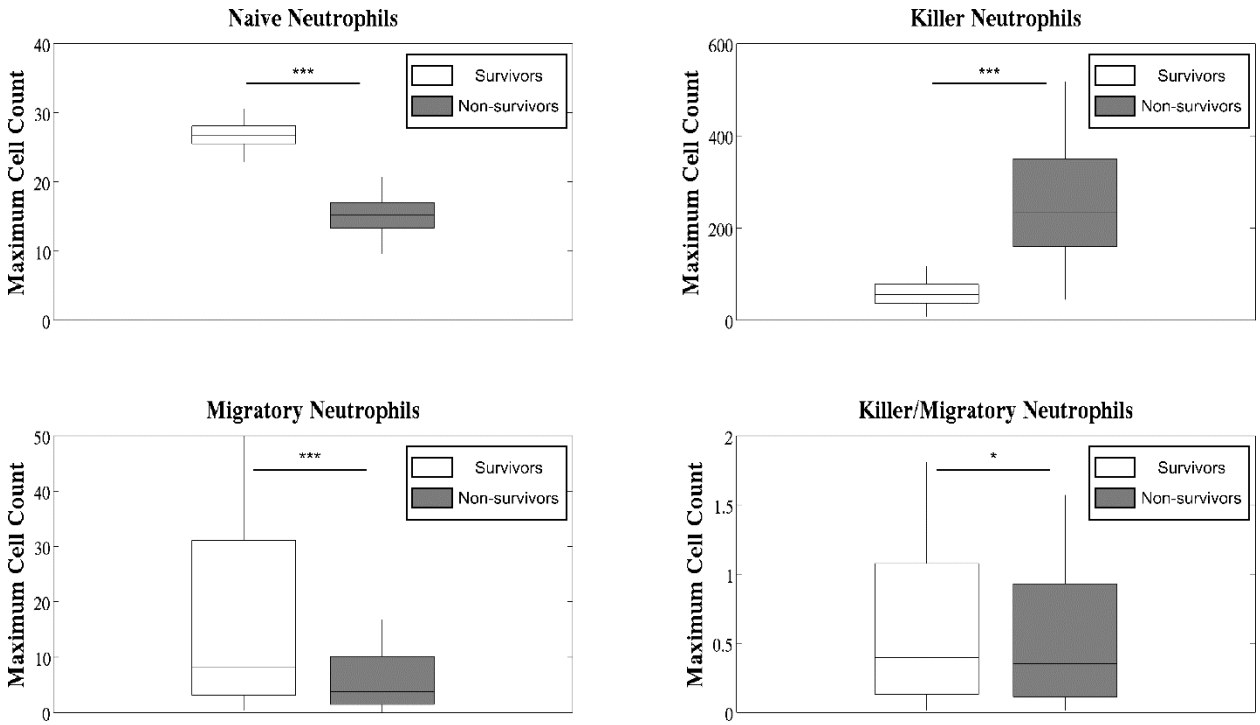

Figure 9. Model predictions for maximal levels of each neutrophil phenotype compared across ensembles

Maximal values for each neutrophil phenotype from each trajectory in both ensembles were recorded.

At the receptor level, underlying activation of CXCR-1/2 was transient in both the survivors and non-survivors (Figure 10). Compared to the neutrophil dynamics which was slow and spread across few hours, receptor dynamics was very fast. Most of the receptors were in the free state, and internalized CXCR-1 is recycled faster than CXCR-2. Among the active receptors, there was one order of magnitude higher level of internalized CXCR-1 receptors than the surface bound CXCR-1 receptors, while this difference is two orders of magnitude for CXCR-2. Non-survivors had higher levels of the surface and internalized active receptors. This can be explained by the higher peak in IL-8 levels for the non-survivors than the survivors (Figure 3 – Experimental fits). But, survivors had very close levels of CXCR-1 and -2 bound receptors and non-survivors had slightly higher levels of bound CXCR-1 than bound CXCR-2. These small differences in the peak levels of the receptors coupled with differences in the transition rates were sufficient to result in different neutrophil phenotype levels in the two populations, a key prediction from the ensemble modeling process.

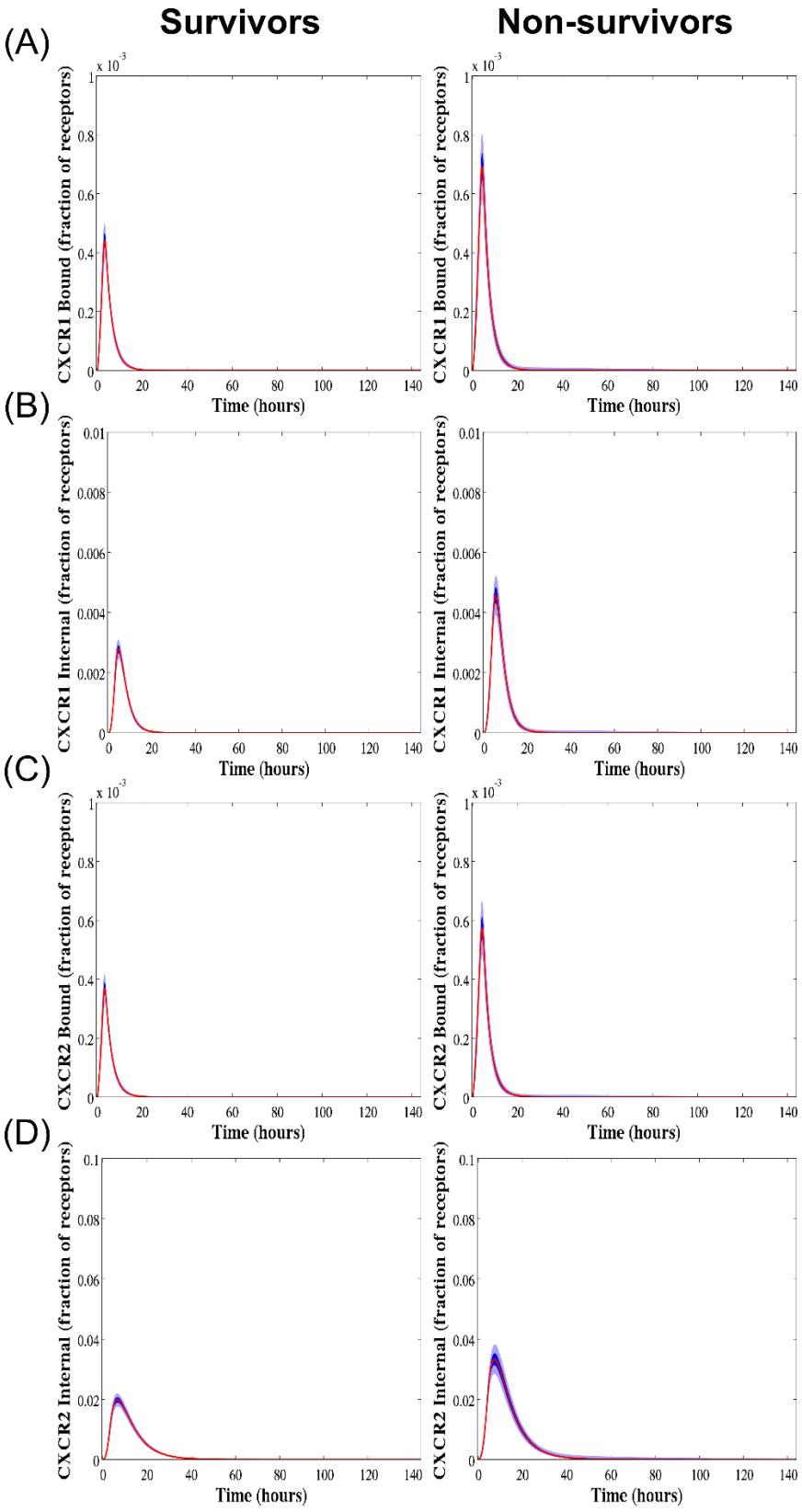

Figure 10. Model predictions of receptor dynamics following infection.

3.3.3 Factors modulating cumulative damage in the two populations

Until now, the focus was on deriving parametric ensembles explaining the mechanism of sepsis progression in each population. In this section, the sensitivity of sepsis-mediated damage to different model parameters (and hence different processes in the network) was evaluated for each population. Area under the damage curve (AUC_D) was used as an output metric of cumulative damage from sepsis. The analysis was done in two steps. First the sensitive parameters affecting damage in each population was identified to check if similar parameters were responsible for modulating damage within each population. Next, the two populations were combined to identify the parameters primarily responsible a switch from a low to a high damage region. Since the model is highly nonlinear, a global sensitivity analysis (GSA) based on variance decomposition was chosen. This method decomposes the total variance in the output into variance and co-variance contributions from each rate parameter and its higher order combinations. To reduce computational cost, a meta-model based approximation was done (See Materials and Methods). The meta-model method called Random Sampling High Dimensional Model Representation (or RS-HDMR), decomposes the output function (AUC_D) into a set of component functions that includes the mean followed by first order effects of each parameter and other higher order effects resulting from parameter combinations. The degree of sensitivity of a parameter or its combination with other parameters (as a set) is captured by Sobol' index which by definition is the fraction of the total output variance attributed to the selected parameter set. To perform GSA, 4000 samples were generated from the parameter distributions of the two ensembles and the dynamics of the damage term was simulated for the survivors and the non-survivors. Figure 11A shows the AUC_D distributions for each ensemble. As expected, the survivors show lower levels of cumulative damage than the non-survivors. The coefficient of variation was higher for the

non-survivors (CV = 1.98) as compared to the survivors (CV = 0.32). When GSA was performed on the survivor and non-survivor samples separately and in combination, it was found that a third order RS-HDMR contributed close to 95% of the variance for both the populations. However, most of the important contributions were from the parameters constituting highly ranked first order indices. Figure 11B-C shows the first order and total Sobol' indices for the first five most sensitive parameters of each population and Figure 11E shows the results when both populations are combined. Note that the total Sobol' index for each parameter, is the sum of first order index and all higher order indices involving that parameter.

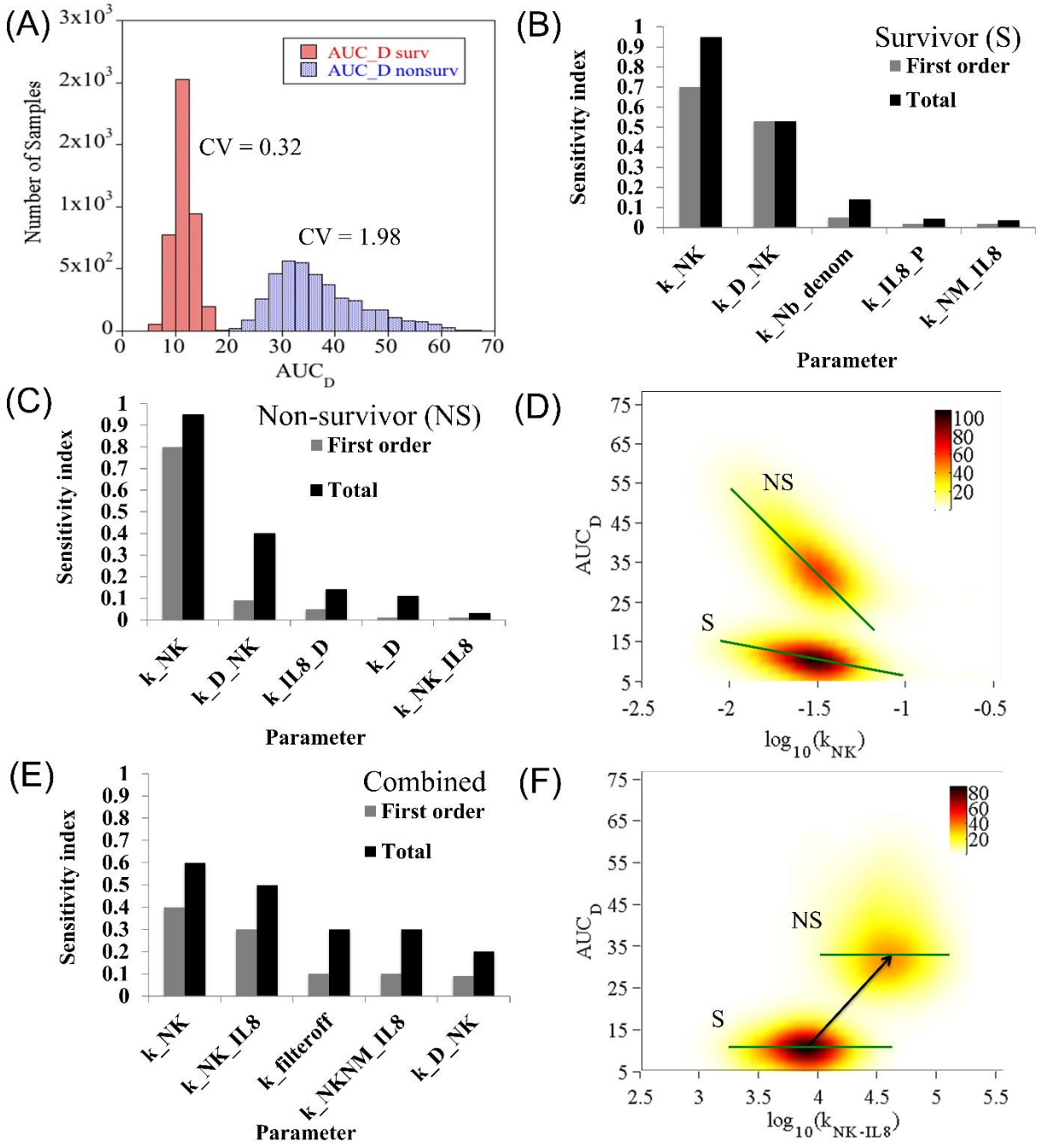

Figure 11. Factors affecting cumulative systemic damage.

For GSA conducted separately on the survivor and non-survivor ensembles, it is found that damage is mainly determined by the decay rate of the killer neutrophils, k_{N_K} (direction of influence shown in Figure 11D). The decay rate of the killer neutrophil controls the rate at which killer neutrophils are removed from the system, and the faster these neutrophils are removed, the lesser the damage. The next important term is the direct damaging effect of the killer neutrophils and this parameter has significant second order interactions with other parameters of the model as seen from the total sensitivity index. The next set of parameters has secondary importance and these parameters are different for the two populations (variance contributions of each parameter in this set is in the range, 1-10%). In survivors, damage is more influenced by the production rate of basal neutrophils and IL-8 in presence of the pathogen. In non-survivors, the effect is more pronounced for damage mediated IL-8 production (a positive feedback component), damage recovery term and killer neutrophil production rate. This indicates that overall damage in non-survivors is more sensitive to the parameters associated with killer cells, IL-8 and damage.

For GSA conducted on the combined population, the decay rate of killer neutrophils remains the most important parameter. Interestingly, the sensitivity value and ranking of three parameters increase relative to the case where the populations are analyzed separately. Among these, the transition rate of naïve neutrophils to the killer phenotype via CXCR1 ($k_{N_K\text{-}IL8}$) is the most important parameter. The next two parameters include the decay rate in filter equation (7) (which determines the delay between pathogen generation and resulting neutrophil entry into circulation during sepsis) followed by the parameter controlling transition rate of killer neutrophil to the dual phenotype by CXCR2. Functional dependence of damage on these three parameters shows that they could be responsible for shift in the population from a low to a high

damage region. For example, Figure 11F shows the dependence of AUC_D on parameter $k_{N_K\text{-}IL8}$. Within each population, no particular trend is visible, but relative increase in the transition rate in the non-survivors correlates well with increased damage. Results in Figure 6 showed that the ranges of two of the parameters, $k_{N_K\text{-}IL8}$ and k_{filter_off} were significantly different for the survivors and non-survivors. Results from sensitivity analysis support this prediction and further show that the parameter values correlate well with the transition in observed damage.

3.3.4 Treatment Implementation

Extracorporeal devices are emerging as promising therapies for treatment of sepsis [50,66,75,76]. In this instance we propose extracorporeal treatment which directly modulates CXCR-1/2 levels using a bioactive surface which interacts with unbound neutrophil surface receptors upon contact. Such a device, which is currently under development at the University of Pittsburgh, generates targeted and controlled downregulation of neutrophil surface receptors. The dynamics of this device can be analyzed within the framework of the generated computational model to determine its proof of principle *in silico* and help optimize treatment parameters. The proposed treatment implementation is shown in Figure 5. Specifically, the receptors are allowed to go to a trapped state and become unavailable for activation by IL-8 for the indicated time of treatment. To evaluate the potential of such an immunomodulatory treatment, we next performed an *in silico* trial by varying (1) the time when the treatment is introduced and removed and (2) the strength of interaction between the trapping device and the unbound neutrophil surface receptors.

For the analysis, the treatment initiation time was varied between 0 and 12 hours after the initial infection and the treatment discontinuation time was varied between 0 and 100 hours after infection. To modulate the treatment intensity, the device-receptor K_d was varied between the $1x10^{-2}$ M and $1x10^{-5}$ M, with 2.5e-3 M representing the K_d of IL-8 and the receptors. The treatment was tested on a simulated population constructed by randomly selecting 69% of parameter sets from the non-survivor ensemble and 31% of parameter sets from the survivor ensemble, as observed in the experimental population. Survivor rate was measured for each set of proposed treatment parameters, as determined by the logistic regression classifier trained on the parameter ensembles with no treatment. A survivor rate above 31% was considered an improvement over baseline, and below 31% indicated the treatment causing overall harm.

Figure 12 shows the survival rate following different treatment strengths and start-end times. In general, the optimal time for beginning treatment was between 3 and 6 hours after the original infection, resulting 40-80% survival rates depending on treatment strength. Starting the treatment after six hours was typically too late to have a strong effect on survival. Starting treatment within 3 hours of infection would often have neutral or deleterious effects, as it would dampen the initial inflammatory response that is critical to fighting off the infection. This led to an increase in pathogen growth and an increased late inflammatory response once treatment was removed. In the worst case scenarios following early treatment of a short duration, survival rates dipped as low as 13.2%, and this trend could be seen across all treatment strengths.

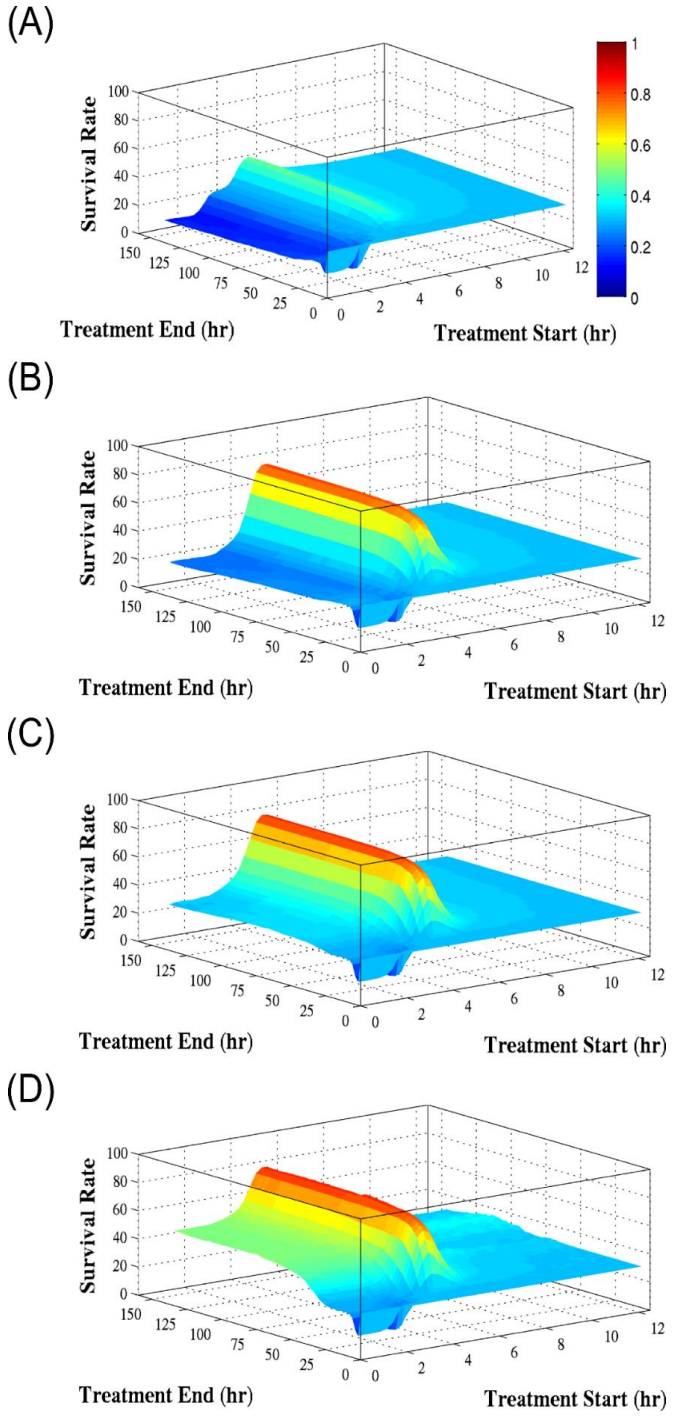

Figure 12. Effects of simulated treatment on animal survival rates Survival rates of a simulated population of animals following treatment with the proposed extracorporeal device considering a device-receptor affinity of (A) $1x10^{-2}$ M, (B) $1x10^{-3}$ M, (C) $1x10^{-4}$ M, (D) $1x10^{-5}$ M. In all cases the time of treatment was varied between 0 and 12 hours post infection and ended between 0 and 100 hours post infection.

When treated at the optimal time, survival rates increased from the 31% baseline to greater than 80% with sufficient device-receptor affinity. Using a K_d of 1e-2 M results in a maximum survival rate of 47%, and decreasing the K_d to 1e-3 M further increases this rate to 80.3%. Further decreases in the K_d to 1e-4 M and 1e-5 M results in increases in survival rate to 83.1% and 84.4%, showing there is a diminishing return to continuously increasing the device affinity. As the affinity increases, we see a new trend emerge in the simulation results, where treatment that begins as early as the onset of infection and is significantly long lasting leads to increased survival rates, and a less strictly defined optimal treatment time (Figure 12D). In this case, the treatment is so strong and long-lasting that the inflammatory response is very strongly suppressed, implying that overwhelming pathogen growth leading to death cannot be reached within the bounds of this. However, this suppression of the immune system allows for significant pathogen growth and could leave the subject vulnerable to secondary infections which are not considered in this model.

Trends in response to treatment also appear to be robust to individual parameter values. The two most sensitive parameters k_{N_K} and $k_{N_K\text{-}IL8}$ were varied, increasing and decreasing each by 10% and 50% and recalculated the simulated population response to treatment (Figure 13 and Figure 14). In general response trends remained the same, with a defined peak in survivorship when treatment is administered 2-4 hours after infection. The magnitude of responses varied predictably, as strongly increasing k_{N_K}, the death rate of damage-causing neutrophils, resulted in a higher peak of survival. Conversely, increasing $k_{N_K\text{-}IL8}$, which corresponds to a faster induction of damaging-causing cells, leads to a slight decrease in survivorship. Varying k_{N_K} had a larger effect on these results, as expected following its identification as the model's most sensitive parameter affecting damage (Figure 11).

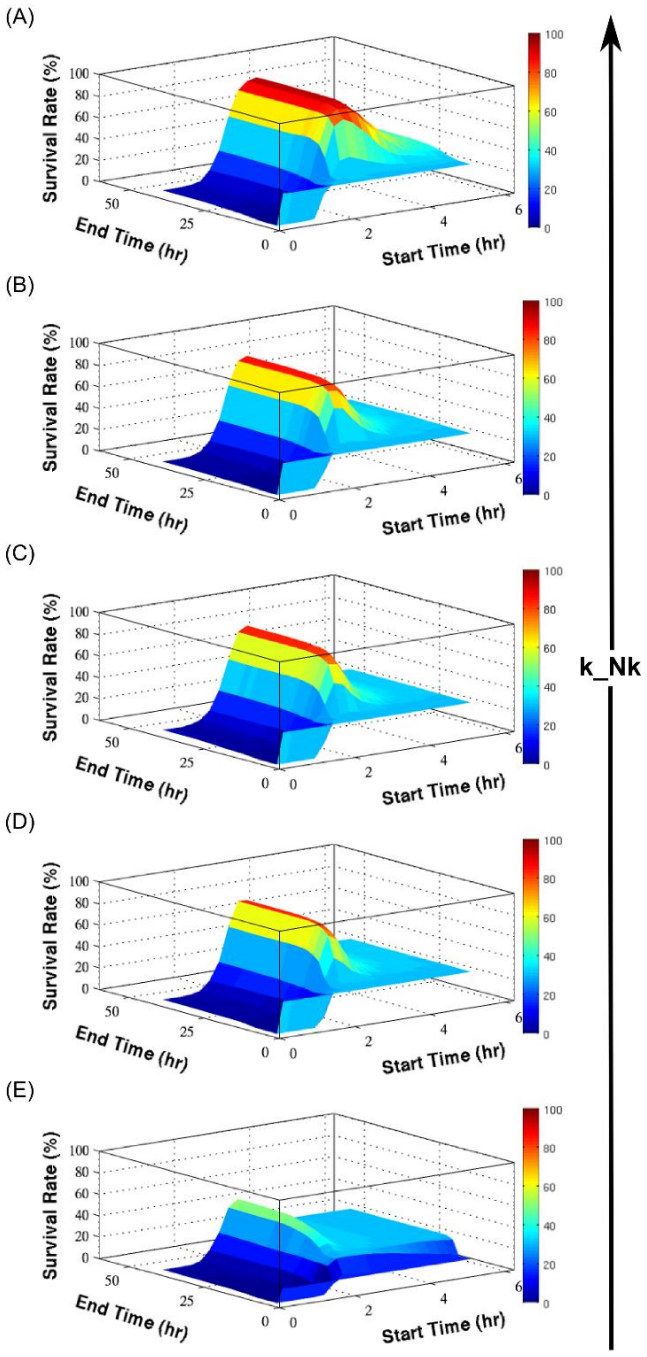

Figure 13. Effects of varying Nk decay rates on simulated treatment. Survival rates of a simulated population of animals following treatment with the proposed extracorporeal device considering a device-receptor affinity of 1x10-3 M for k_Nk values of (A) 50% above, (B) 10% above, (D) 10% below, and (E) 50% below the baseline vale (C). In all cases the time of treatment was varied between 0 and 10 hours post infection and ended between 0 and 100 hours post infection.

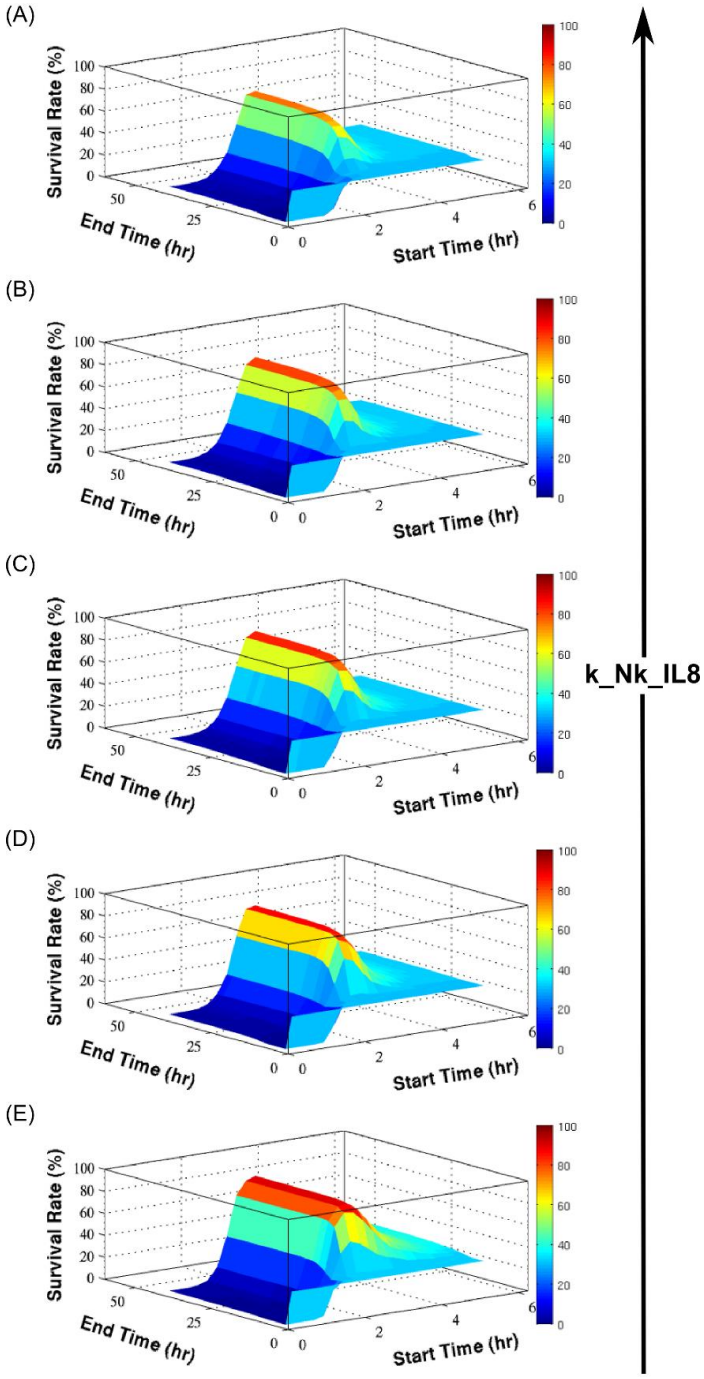

Figure 14. Effects of varying Nk induction rates on simulated treatment. Survival rates of a simulated population of animals following treatment with the proposed extracorporeal device considering a device-receptor affinity of 1x10-3 M for k_Nk_IL8 values of (A) 50% above, (B) 10% above, (D) 10% below, and (E) 50% below the baseline estimated value (C). In all cases the time of treatment was varied between 0 and 10 hours post infection and ended between 0 and 100 hours post infection.

3.4 DISCUSSION

This manuscript discusses the development of a mechanistic computational model of IL-8 mediated activation of CXCR-1/2 receptors in baboons which were administered intravenous *E. coli*. Neutrophil phenotypes, which dictate neutrophil functional response, were generated *in silico* based on CXCR-1/2 surface receptor levels, linking receptor level dynamics with neutrophil functional response. Parameter ensembles were generated for survivor and non-survivor populations, allowing for *in silico* observation of sepsis progression. Additionally, an extracorporeal treatment which modulates CXCR-1/2 levels on neutrophils was introduced *in silico*. This proof of concept evaluation allowed for preliminary device evaluation and optimization of treatment parameters.

To our knowledge, this is the first model describing dynamic interactions of neutrophils which specifically takes into account information sharing between the systemic variables and the receptor levels. The receptor level dynamics of the model function on a rapid time scale, adjusting to systemic IL-8 levels in a matter of minutes. These changes in receptor signaling dictate changes in neutrophil phenotype, which dictates neutrophil function and hence mortality. This link thus provides a valuable mechanistic framework that can be subjected to clinically relevant treatment scenarios. For example, the experimental treatment could be implemented purely on the receptor level. Alternatively, systemic variables such as IL-8 levels or neutrophil phenotype could be modulated to evaluate performance of hemoadsorption or neutrophil sequestration extracorporeal devices.

Application of parallel tempering approach for parameter estimation allowed for the efficient generation of ensembles of parameters and resulted in a model that could fit experimental data well [115], allowing reasonably accurate simulations of the system without making strong claims about the values of single parameters which are notoriously difficult to measure and are likely to vary between individuals. This allows for robust, population-level predictions rather than point predictions of model parameters and model behavior. However, the computed multi-dimensional posterior distribution in parameter space reflects constraints imposed by empirical data, as well as data sparsity and uncertainty. These constraints impose a covariance structure in the posterior distribution such that there is robustness in model behavior, despite large uncertainties in individual parameter values. Learning this structure is likely crucial in building predictive model [113,126]. Yet, the method is making no claim that individual parameter sets in the ensemble represent individuals in a population. At best, an individual could be represented by a smaller ensemble, reflecting uncertainty relating to this particular individual. Yet, it is fair to say that the ensemble is meant to represent uncertainly about a population of individuals, so that simulating the ensemble will provide expected behaviors across a population of individuals, as long as such behaviors are compatible with the empirical data used to generate the ensemble.

One trend that arose in the estimated parameter ensembles was a large difference in the magnitudes of different rate constants, sometimes spanning many orders of magnitude. This is not surprising, due to the inclusion of biological events spanning many time scales, ranging from fast molecular events to cell phenotype transitions and finally to the full duration of infections lasting for days. This suggests that future iterations of the model would benefit from a multiscale approach optimized towards handling these different time scales. Previous efforts [127–129] have worked out approaches that allow for efficient deterministic simulation of fast-scale molecular events, combined with more accurate stochastic simulation of slow-scale or rare events, and such techniques have resulted in impressive results [130,131].

Sensitivity analysis on the parametric ensembles enabled identification of the relative importance of the model parameters to state variables of the model. In general, sensitivity analysis is an important step in systems biology workflows and provides valuable information on model characteristics [132,133]. Most models in the literature resort to a local analysis which is sufficient if the parameters are well defined. For nonlinear dynamic models based on sparse experimental data and for systems which have inherently high parametric uncertainty, a global analysis needs to be done. Global techniques perform combinatorial perturbations of the parameters utilizing samples from the high-dimensional space. Application of meta-modeling approximations via RS-HDMR as was done in this work can significantly reduce the computational cost of sampling requirements for global methods. Additionally, if the sampling process takes into account parameter covariance computed from an ensemble model, biologically relevant sensitivity indices can be obtained. The systematic integration of ensemble modeling and global sensitivity analysis in this work allowed for identification of the parameters that control biological outcomes like sepsis induced tissue damage.

In addition to parameter fits, the behavior of the non-fitted state variables were inspected to check for features relevant to a clinical prognosis. Sepsis progression was analyzed by comparing differences between survivor and non-survivor populations. Neutrophil phenotypes in particular give insight into the differences between survivors and non-survivors. Of importance is the killer neutrophil population, which is highly elevated in the non-survivor population (see Figure 8 and Figure 9). This neutrophil phenotype is associated with neutrophil induced tissue damage in the model. With support from sensitivity analysis, killer neutrophil decay rate, which sets the levels and dynamics of N_K, was found to be the most important contributor to total damage in both the populations. Multiple studies support this finding, indicating that non-survivors or those with more severe sepsis experience increased levels of neutrophil induced tissue damage and MPO generation [20,134–137] . Furthermore, the importance of this term is supported by studies on neutrophil apoptosis and lifespan. Research by Taneja [138] and Fialkow [139] determined that neutrophil apoptosis was reduced in cases of severe sepsis, leading to increased lifespan of primed and activated neutrophils. Damage caused by these neutrophils was partially responsible for the progression of sepsis in these severe cases. Upon completion of the combined GSA, $k_{N_K\text{-}IL8}$ was also found to be a significant contributor to total damage. Increase of this term leads to preferential generation of the N_K neutrophil phenotype, which directly contributes to tissue damage.

On the other hand neutrophils in the migratory phenotype were similar in survivor and non-survivor populations. These findings agree with the data from Cummings *et al* [136] which found neutrophil's harvested from septic and non-septic patients migrated to IL-8 at similar levels. Interestingly, survivors and non-survivors had similar levels of neutrophil kill/migrate phenotype, indicating that both ensembles had adequate neutrophil populations to eliminate the source pathogen. Therefore, the additional damage in non-survivors was neutrophil induced resulting

from elevated neutrophil killer phenotype levels. The IL-8 mediated killing functions of neutrophils are primarily triggered through CXCR-1 rather than CXCR-2. Modulation of CXCR-1 levels in particular may reduce the killing neutrophil phenotype and reduce neutrophil induced organ damage.

A number of experimental treatments for sepsis and other acute inflammatory diseases have targeted the CXCR-1 receptor with success in animal models [140–142]. However, translation to humans has been difficult for two main reasons [89]. First are inherent species dependent differences between human and animal immune systems that must be recognized and accounted for in pre-clinical studies. Second is the misuse of animal models and misinterpretation of pre-clinical data [143]. The recent debate on the translational fidelity of critical disease mouse models is a prime example where two separate comparisons of the human versus mouse genomic leukocyte responses using the same database resulted in two contradictory conclusions [144,145]. In the case of IL-8 signaling, which is not present in murine models, homologous cytokines and their associated surface receptors must be examined in IL-8's place [146]. In this context, in silico modeling is an attractive alternative given that it allows preliminary evaluation of experimental human treatments at minimal costs.

Multiple extracorporeal sepsis treatments are currently under investigation with promising results. Blood purification techniques such as hemoadsorption [50,66,147–149] allow for cytokines and other detrimental proteins to be removed directly from the blood during the cytokine storm, curbing the patient's immune response. Another approach called activated neutrophil sequestration [75,150], selectively removes harmful neutrophil phenotypes from circulation. In this instance we propose extracorporeal treatment which directly modulates CXCR-1/2 levels using a bioactive surface which interacts with unbound neutrophil surface receptors upon contact,

resulting in CXCR-1/2 downregulation. This approach is advantageous because no components of blood are removed from circulation, allowing for a healthy immune response after appropriate modulation of neutrophil surface receptors. In addition, all necessary cell-cell interactions are allowed to occur within well-controlled microcirculation of the device. Such a setup also allows treatment to be easily titrated or halted by adjusting blood flow through the device. The dynamics of such a device were analyzed within the framework of the generated ensemble model to determine its proof of principle *in silico* and to evaluate its benefits in rescuing individuals marked as non-survivors by the parameter ensembles.

When evaluated *in silico* the proposed extracorporeal CXCR-1/2 modulation device improved mortality from 31% to above 80% when deployed under certain ranges of conditions. This substantial improvement in survival supports the hypothesis that a CXCR-1/2 modulatory device may improve patient outcomes. However, time and length of treatment implementation are critical parameters tied to this success. The importance of quickly beginning sepsis treatment has been well established [151], particularly for antibiotic administration. Our simulations showed a well-defined optimal time for the initiation of treatment, between 3 and 6 hours after the onset of severe infection. Treatment, if started within this time frame, had a high degree of success over a large range of treatment durations and strengths. This window is specific to the animal model under study and will not directly translate to a clinical setting for two main reasons. First, the model was calibrated with experimental data obtained from baboons, and differences between the baboon and human immune systems must be considered. Second, the baboons were exposed to a well-controlled bacterial infusion at a known time point, followed by a predictably quick and strong immune response. In this instance the pathogen load is well controlled and a large portion of the ensemble can therefore be addressed by a single treatment setting. In clinical practice, patients

present with varied pathogen loads and they may be in different stages of infection and immune response. So, future experiments will need to combine clinical knowledge with additional data gathering and simulation to obtain treatment timing relevant for human patients.

Clinicians are actively searching for biomarkers to track sepsis disease progression and prescribe treatment [152–154]. Neutrophil phenotype may be a valuable indicator of disease state and individual patient response, but this information is difficult to collect in the clinic. Currently neutrophil phenotype can be evaluated either through functional testing or flow cytometry analysis of critical neutrophil surface receptors. In addition to CXCR-1/2 which are the focus of this model, CD11b, CD88, and CD62L all have roles in dictating neutrophil phenotype [155] and surface receptor expressions vary depending on severity of the inflammatory response. To more readily exploit phenotype data it may be possible to map neutrophil function to easily measurable biomarkers. Using these indirect measures of neutrophil phenotype can guide clinicians to ideal treatment regimens.

In conclusion, the ensemble model presented in this report provided key insights into the progression and mechanisms involved in progression of sepsis. We underline the role of relative abundance of killer, migratory and dual neutrophil phenotypes in deciding survivorship in an animal model. In addition, an *in silico* extracorporeal treatment which modulates CXCR-1/2 neutrophil surface receptors showed promising results. Further study and collection of experimental data will help further refine both the model and experimental device. Incorporation of data from a diverse patient population and expansion of current ensembles would increase the model's generalizability, improving the potential for translation. Additional model parameters related to the device such as flow rate, surface area, and form factor could be included, allowing the model to streamline device development.

4.0 CONSTRUCTION AND EVALUATION OF AN EXTRACORPOREAL DEVICE TO MODULATE CXCR-1 AND CXCR-2 NEUTROPHIL SURFACE RECEPTOR EXPRESSION

This chapter discusses the development of an extracorporeal device that can "reprogram" neutrophils to attenuate their chemotactic response to IL-8 as a potential treatment for sepsis. The Neutrophil Reprogramming Device (NeRD) is essentially a hemodialyzer cartridge in which IL-8 is covalently bound to the inner lumens of the dialyzer fibers. Similar to hemodialysis, blood is perfused through the NeRD and neutrophils, which naturally marginate toward the fiber inner lumens, interact with the immobilized IL-8 through CXCR-1 and CXCR-2 surface receptors, the same interaction that causes chemotaxis. As a result of the interaction, the CXCR-1/2 receptors internalize and CXCR-1/2 surface expression on neutrophils is down-regulated, thus reducing the neutrophils chemotactic response to IL-8 as blood is perfused back into the patient. The neutrophils maintain the ability to target and eliminate bacteria in infected tissue through secondary CXCR-1/2 independent cell signaling pathways involving N-formyl-metyl-leucyl-phenyl (fMLP), a byproduct of bacterial destruction. We hypothesize that the reduced chemotactic response to IL-8 will reduce the redirection of neutrophils into healthy tissue and reduce sepsis induced organ failure. Multiple device configurations are presented in this chapter, presenting the progression of results and testing. Each subsequent configuration built of the past, eventually leading to some of the concepts presented in the next chapter.

4.1 INTRODUCTION

Sepsis is a severe systemic inflammatory response due to an infection and affects 900,000 Americans per year. The incidence of sepsis is expected to increase over the next 10-20 years as the population ages [1]. Despite improvements in care, the hospital mortality rate associated with sepsis has remained persistently high and is nearly 20% [1,5,6]. We've recently shown that at one year survival is less than 60% for patients with septic shock [156]. Sepsis is now the leading cause of in-hospital death in the United States [1,8], yet there are currently no FDA approved specific treatments for sepsis. Intensivists essentially can only manage the symptoms of sepsis until the patient's immune system naturally recovers, if it does so. The current standard of care for sepsis is treatment of the causal infection with source control and antibiotics, while providing necessary organ support using drugs (e.g. vasoactive medication) or devices (e.g. hemodialysis, mechanical ventilation, etc.) [9]. Drug therapies to suppress the immune response such a corticosteroids [3] are occasionally used but run the risk of immune suppression and an inability to eliminate the causal infection. Experimental drug therapies to attenuate pro-inflammatory cytokines such as tumor necrosis factor (TNF) and interleukin-1 (IL-1) have had little success [4]. Device therapies including hemofiltration and hemoadsorption broadly modulate cytokine levels [48,49], but neutrophils do not deactivate once systemic cytokine concentrations fall. Instead, cytokines such as IL-8 that spilled into the bloodstream from inflammation at the site of infection diffuse into healthy tissues and organs [157,158]. Activated neutrophils sense these elevated cytokine levels and infiltrate into healthy tissues and organs, where they can cause severe organ damage and eventually sepsis induced organ failure [159].

Neutrophils are the first responders to sites of inflammation and play critical roles in the innate immune response. Normally, neutrophils migrate from the bloodstream into the infected tissues due to inflammation there by sensing chemical gradients of the chemokine IL-8, which is released by macrophages in response to foreign invaders like bacteria. The IL-8 chemokine binds to the expressed neutrophil cell surface receptors CXCR-1 and CXCR-2 and induces chemotaxis to the site of infection [2]. The increased neutrophil activity in sepsis, however, results in undesirable systemic-level inflammation and elevated IL-8 levels in healthy tissues and organs [26,27]. Activated neutrophils then infiltrate these tissues/organs where they can damage cells and lead to multiple organ dysfunction [2,28]. The lung is especially susceptible to sepsis induced organ failure. Again, potential treatments that indiscriminately suppress the activity of neutrophils can cause immune suppression and the inability to clear the causal infection [15,29,30].

4.2 MATERIALS AND METHODS

4.2.1 Module construction

Scaled down prototype modules were constructed from loose dialyzer fibers and in a polycarbonate housing. Housing bodies were constructed from 0.250” outer diameter, 0.125” inner diameter polycarbonate tubing (see **Error! Reference source not found.**). The ends of each housing were odified to accept standard luer connecters for tubing connections and blood flow. Luer tubing connectors were also placed in the outer dialysate compartment to facilitate shell side washing. Twenty-five loose dialyzer fibers were loaded into housings and potted in place using UV cure adhesive (Dymax). Aminated dialyzer fibers were provided by Fresenius or Gambro for

evaluation. The fibers provided by both companies were modified versions of off the shelf commercial devices. Fresenius fibers were PS base material, while Gambro fibers were AN-69 acrylonitrile and sodium methallylsulfonate copolymer based.

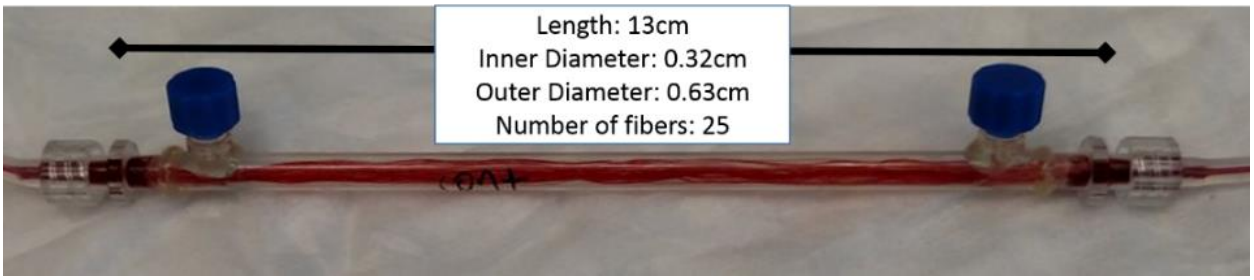

Figure 15. Scaled down leukocyte reprogramming test module.

4.2.2 Cytokine immobilization

Alternately, polymethylpentene (PMP) oxygenator fibers (Oxyplus™; OD: 380 μm, ID: 200 μm) were obtained from Membrana GmbH (Wuppertal, Germany) were evaluated in the same module housing. The shell side luer attachments were utilized for blood flow in this configuration. All module construction methods are variations of previous mini-modules constructed in the Medical Devices Laboratory for gas exchange [160–162].

4.2.3 Recirculation loop setup

Setup and evaluation of modified modules requires recirculation of buffer or blood through the module. The setup includes a buffer/blood reservoir. A 10ml beaker is typically used for this purpose. This reservoir is typically placed in a larger beaker to for stability. This reservoir is placed on a shaker plate (Hedolph Titramax 101) at 300 rpm to agitate the reservoir contents. 32”

Masterflex L/S 13 tubing leads from the reservoir through a pre-calibrated Masterflex L/S peristaltic with easy-load pump head. The tubing connects to the scaled-module then returns to the reservoir by a 16” length of tubing. An example flow loop is shown in **Error! Reference source ot found.**. Unless otherwise noted a flow rate of 1 ml/min is utilized for buffer or blood recirculation.

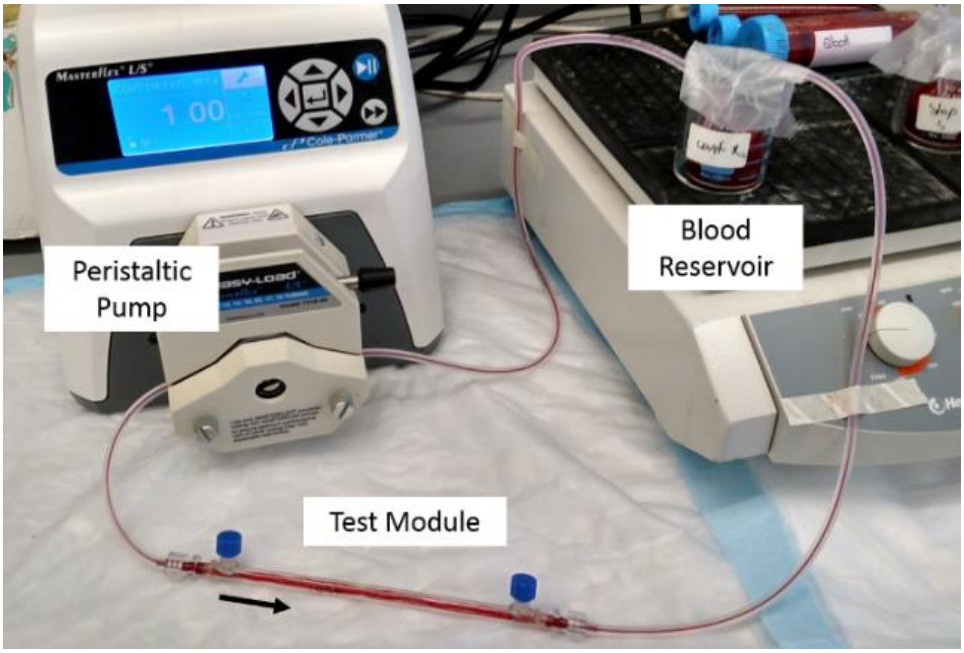

Figure 16. Standard blood recirculation loop.

A stop-flow configuration was tested with different module and immobilization setups. In this configuration, the pump was programmed to flow at 1ml/min for 45 seconds, followed by a 45 second incubation period. This flow configuration allows for neutrophil margination during flow, and complete clearance of the module, followed by a period of no flow to allow neutrophil interaction with the modified surface.

4.2.4 IL-8 immobilization

Protein immobilization procedures were completed using buffers circulated in the configuration explained above and shown in **Error! Reference source not found.**. Each procedure is described n detail below.

4.2.4.1 Chitosan spacer immobilization

A chitosan spacer approach has previously been utilized for enzyme immobilization in the Medical Devices Laboratory [160,161]. The entire method is represented schematically in Figure 16. This process requires an aminated surface to facilitate further conjugation steps. Chitosan (MW 50-190kD), glutaraldehyde, acetic acid, and other reagents were obtained from Sigma-Aldrich. Commercially available polymethylpentene hollow fibers (Oxyplus™; OD: 380 μm, ID: 200 μm) were obtained from Membrana GmbH (Wuppertal, Germany). These fibers were cut into 27 fiber wide fiber mats and washed three times in 0.5% Tween-20 in 100mM Sodium Phosphate buffer pH 8.5 then rinsed thoroughly with distilled deionized water. After washing, PMP fibers were amine functionalized using plasma enhanced chemical vapor deposition (PECVD) with a PVA TePla Ion 40 system according to a technique established by Arazawa et al [163]. Briefly, the pre-cut hollow fiber membrane samples were added to the vacuum chamber in a single layer. Upon adding samples, the chamber was evacuated to 50 mTorr. Allylamine was introduced to the chamber at a rate of 180 mL/min and 300 W of power at 150 Hz and a 20% duty cycle was introduced for 5 min. Samples were removed and immediately rinsed three times with 0.5% Tween-20 in 100 mM phosphate buffer pH 8.5 then thoroughly rinsed with deionized water.

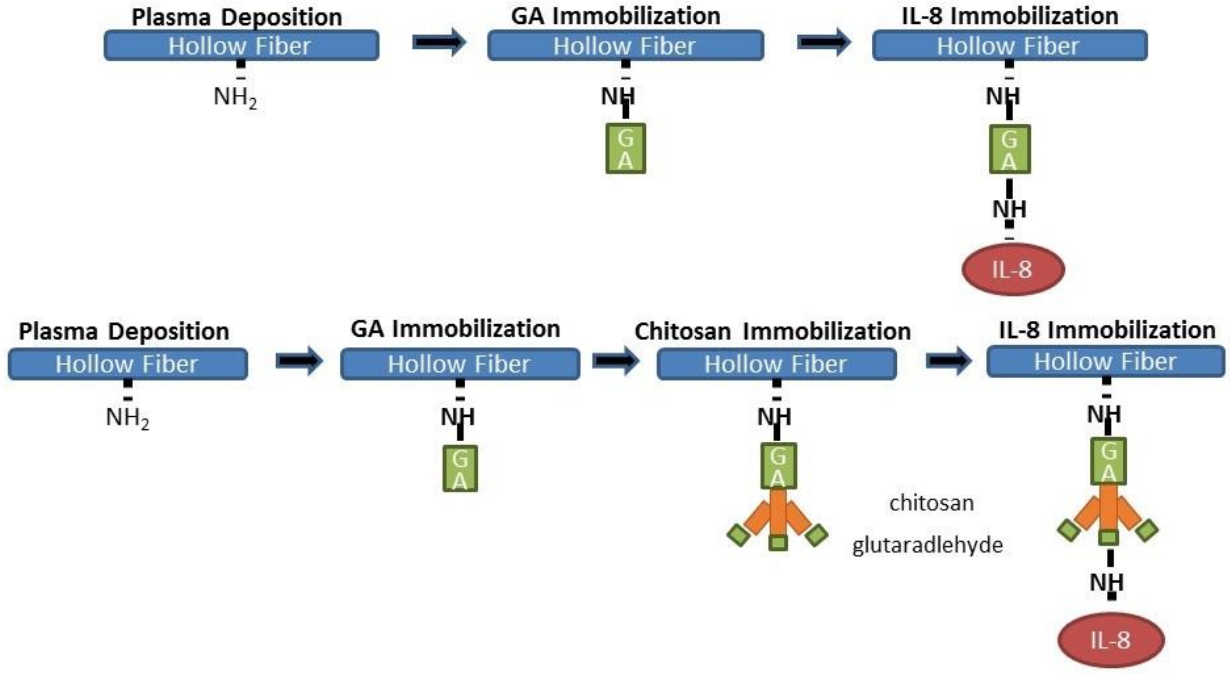

Figure 17. Chitosan immobilization process

Functionalized fiber mats were placed into 60ml glass culture tubes. 50ml 5% glutaraldehyde with 0.33 g sodium cyanoborohydride was added to the tube and placed on a rotary mixed for 15 minutes at 15rpm. The fibers were then rinsed two times with 100mM phosphate buffer pH 8.5 for 10 minutes, followed by a final rinse with 1% acetic acid to change fiber surface pH to reduce potential non-specific chitosan deposition. 1% low viscosity chitosan with sodium cyanoborohydride reducing agent was dissolved in 1% acetic acid and filtered with 60µm MILLIPORE filter and added to each fiber mat for 15 minutes on a rotary mixer. The fiber mat was then rinsed one time with distilled deionized water, then 3x with phosphate buffer. Addition of 5% glutaraldehyde solution and washing was repeated to facilitate conjugation of the chitosan

spacer. Finally, 50μg of IL-8 or the molar equivalent of BSA was added to the fibers in 10mL phosphate buffer and recirculated for 1 hour. 3x washing with phosphate buffer was completed to remove non-specifically bound protein.

4.2.4.2 PMP Fiber Scanning Electron Microscopy

Fibers were imaged using Scanning Electron Microscopy (SEM) to observe the presence and uniformity of the immobilized chitosan layer. A JSM 6335F SEM at the Center for Biological Imaging at University of Pittsburgh was utilized. PMP fiber samples were immobilized using the procedure described above. Samples were washed in distilled deionized water to remove residual salts. After drying under vacuum samples were cut into 1cm x 1cm fiber mat squares and attached to ferrules using double sided tape. Samples were sputter coated with gold/palladium then visualized under SEM at 300-10000x magnification. Three images of each magnification were randomly selected to be representative of the entire fiber surface.

4.2.4.3 PEG Immobilization

PEG immobilization was utilized with Fresenius aminated fibers, Membrana PMP fibers, and Gambro AN-69 aminated dialyzer fibers. This approach utilized a heterobifunctional PEG spacer to crosslink surface amines to a protein [164]. The flexibility of the PEG chain and increased distance from the fiber surface is hypothesized to decrease steric hindrance and increase protein activity [165,166]. This immobilization approach is detailed in Figure 18.

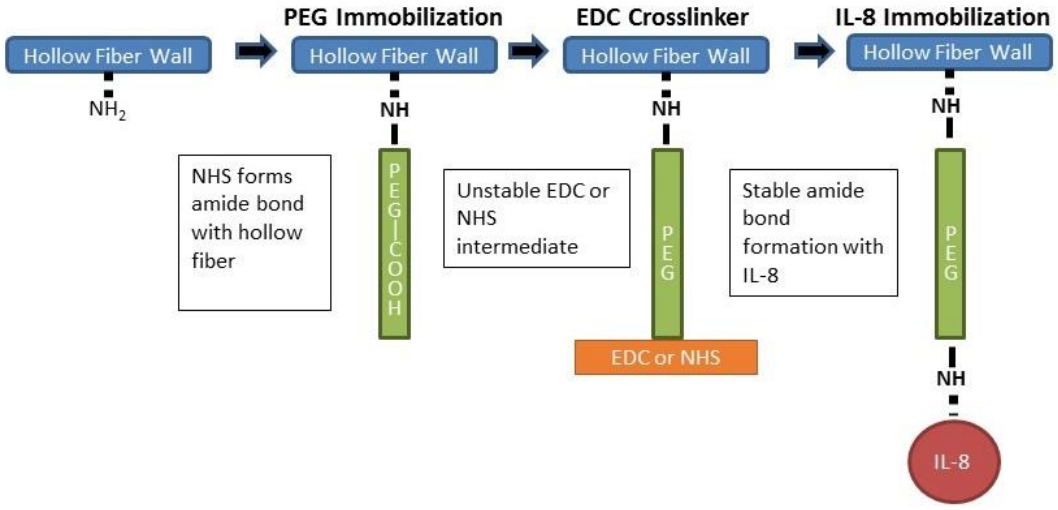

Figure 18. PEG spacer immobilization schematic.

For Fresenius and Gambro dialyzer fibers the following procedure was used by recirculating reagents through prepared minimodules. First complete single pass wash of 100mM sodium phosphate buffer pH 7.5 through the inner lumen of fibers for 15 minutes at 1.0 mL/min and flush shell side with 50ml phosphate buffer to clean fibers. Prepare beaker with 15ml with 100mM phosphate buffer pH 7.5. Working quickly under nitrogen flush add 40ul of 50mM NHS-PEG-COOH in DMF and recirculate through module at 1mL/min for 60 minutes. Remove excess reagent then complete single pass was with sodium phosphate buffer pH7.5 for 20 minutes at 1ml/min and flush shell side with 50ml of buffer. Switch wash buffer to 50mM MES pH 6.0 solution with 0.5M NaCl. Run single pass wash for 10 minutes and rinse shell side with 50 mL MES buffer. To prepare EDC/NHS solution for 2 modules, add 9.2mg EDC and 26.1mg sulfo-NHS to 24mL 50mM MES pH 6.0 + 0.5M NaCl immediately before use. Aliquot 12mL solution for each module and recirculate for 15 minutes at 1 mL/min. Discard solution and quickly rinse inner lumen with phosphate buffer pH 7.5 for 5 minutes and shell side with 50mL phosphate buffer.

Add 10mL phosphate buffer for each module. Add 50ul IL-8 or molar equivalent of control protein to solution. Recirculate protein solution for 1 hour at 1mL/min. After immobilization, complete planned was protocol as described below.

For PMP oxygenator fibers a similar procedure was followed, but immobilization was completed in test tubes prior to potting of fibers inside minimodules.

4.2.5 IL-8 ELISA and wash protocols

IL-8 ELISAs (Invitrogen KHC0084 or KHC0081) were utilized to determine the effectiveness of multiple wash protocols. After completion of the wash protocol, 5% bovine serum albumin in 1x DPBS was recirculated through modules at 1mL/min for 60 minutes. Sample from this buffer recirculation was used in ELISA testing to determine IL-8 concentration in the effluent. In conjunction with neutrophil recirculation buffer (NERB) testing, which is described below, these results are used to determine what degree of washing is necessary to eliminate functional levels of soluble IL-8 leaching during device testing. Testing followed Invitrogen directions, described briefly below. Both ultrasensitive and standard ELISAs were used for testing. First, a standard curve was prepared using the provided IL-8 standard which was serially diluted to cover the entire test range. In addition to undiluted samples, effluent was diluted 10x or 100x to cover a larger range of IL-8 concentrations. Effluent was diluted in the standard effluent buffer. 100ul of each sample was loaded into the ELISA strips, leaving 2 blank for chromogen blank controls. The plate was covered and left at room temperature for 2 hours. Washing was completed using the provided wash buffer and a plate washer. Each wash step was comprised of 4x wash and aspiration of each well. Next a biotin conjugate was added and incubated for 1 hour at room temperature. After wash and aspiration, the streptavidin working solution was diluted and added to each well for 30

minutes. Washing and aspiration was completed again, followed by addition of stabilized chromogen. Samples were incubated in the dark for 20 minutes then stop solution was added to each well. A plate reader was used to read absorbance at 450nm and effluent samples were compared to the standard curve to calculate IL-8 concentration. Finally, high salt concentrations and increased pH were also evaluated.

Standard wash protocols use the same recirculation setup as immobilization. Early wash protocols include only recirculation of 100mM phosphate buffer to remove unbound IL-8. Additional washing includes a 1-2 hour single pass wash of 100mM phosphate buffer pH7.5 + 0.5% Tween-20 with and without 5% BSA. Other washes include use of 5% BSA in 1x PBS for 1-16 hours. Other protein solutions including fetal calf serum of casein solutions were also tested. 3M NaCl with 100mM sodium phosphate buffer pH 8.5 were tested to remove unbound IL-8.

Shell side washing in a cross flow configuration to inner lumen flow was also utilized for some tests. A flow rate of 2mL/min with the same wash solutions as the inner lumen was completed to encourage transport across membranes and remove unbound protein and reagents from the shell side.

4.2.6 Neutrophil buffer recirculation (NERB) assay

A neutrophil buffer recirculation (NERB) assay is utilized to determine if the level of IL-8 leaching from modified fibers in high enough to cause a functional change in neutrophil receptor expression. Using the standard recirculation setup, 10mL of 5% BSA in DPBS is recirculated through both IL-8 modified and BSA modified modules for 60 minutes. Additionally unmodified 5% BSA is used a negative control and 5% BSA spiked with 1 ug/ml IL-8 is used as a positive control. 200ul

samples from the recirculation reservoirs or control beakers were taken at 60 minutes. An additional time point is potentially collected at 30 minutes if time course data is desired.

After collection of all samples, 200ul of whole blood is added to each sample and vortexed briefly at low speed. The samples are placed on a shaker plate for 20 minutes. After the incubation, each sample is split into 2 200ul samples (isotype and non-isotype) for flow cytometry testing. All antibodies were purchased from BD. For isotype testing 20ul of APC isotype control, 20ul PE isotype control, and 20ul CD15 FitC stain are added to each sample. For non-isotype sample 20ul CD182 APC, 5ul CD181 PE, and 20ul CD15 FitC antibodies were added to each sample. These sample were mixed then incubated for 30 minutes in the dark. After incubation, 1.5mL FACS Lyse was added to each sample, then thoroughly mixed and incubated for 10 minutes on a mixer in the dark. Samples were centrifuged for 5minutes and 500g then the supernatants were aspirated. 1% BSA in DPBS washing was completed two times to remove lysed erythrocytes and stains. After washing 300ul 4% formaldehyde in PBS was added for storage until flow cytometry could be completed.

Flow cytometry was completed using a MACSQuant Analyzer 10. Analysis was completed using Winlist software. Neutrophils gated using SSC vs FSC plots and verified for CD15+ staining. Mean fluorescent intensity (MFI) was calculated in non-isotype samples for both CD181 and CD182 after subtraction of isotype sample MFI. Compensations were applied using single stained cell samples. Analysis was completed by comparing test samples to baseline blood to generate relative receptor express of CXCR-1/2 (CD181/CD182).

4.2.7 Blood recirculation and receptor characterization

After completion of the NERB assay, blood recirculation is completed to determine *ex vivo* device performance with freshly drawn human blood from healthy volunteers. The protocol was approved by the University of Pittsburgh Instructional Review Board to protect volunteers. A loop is established as in **Error! Reference source not found.** to facilitate blood recirculation. Before lood, DPBS heparin solution is perfused through the circuit for 10 minutes. For each module, 10mL of freshly drawn whole blood is placed in a beaker. For controls 10mL whole blood is placed in a falcon tube. All containers are placed on a mixer plate to ensure blood is well mixed and does not settle. Pre-calibrated pumps are started with a flow rate of 1mL/min as the loop is de-primed of the DPBS heparin solution. Once blood enters the modules, the free IL-8 positive control is spiked with 1ug/ml IL-8 and 0 minute time point samples are taken from baseline blood (negative control). For each sample, two 100ul aliquots (isotype and non-isotype) are taken from the beaker or falcon tube. Samples are stained using the same protocol as the NERB assay.

After addition of stains, samples are incubated for 30 minutes in the dark. FACS lyse is added to samples and incubated for 10 minutes prior to centrifugation at 5min 500g. Samples are then washed 2x times with 1% BSA. After the final wash 300ul of 4% formaldehyde solution in PBS. In addition to the baseline 0 time point, samples for all modules and controls was gathered at 60 minutes. Additional time points were occasionally added to collect additional time course data. Often a sample was taken of isolated neutrophils immediately before initiating the Boyden chamber chemotaxis assay. Staining of isolated neutrophils followed the same protocol as whole blood, except initial sample volume was only 50ul of final neutrophil solution. Analysis of CXCR-1/2 receptor expression was completed using the same protocol as for the NERB assay, gating for neutrophils then comparing relative change in mean fluorescent intensity.

4.2.8 Boyden chamber chemotaxis assay

A Boyden chamber based chemotaxis assay is used to determine if *ex vivo* recirculation tests have a functional impact on neutrophil migration [167,168]. The assay works by quantifying the number of neutrophils which migrate through a polycarbonate membrane towards a chemoattractant in the bottom chamber.

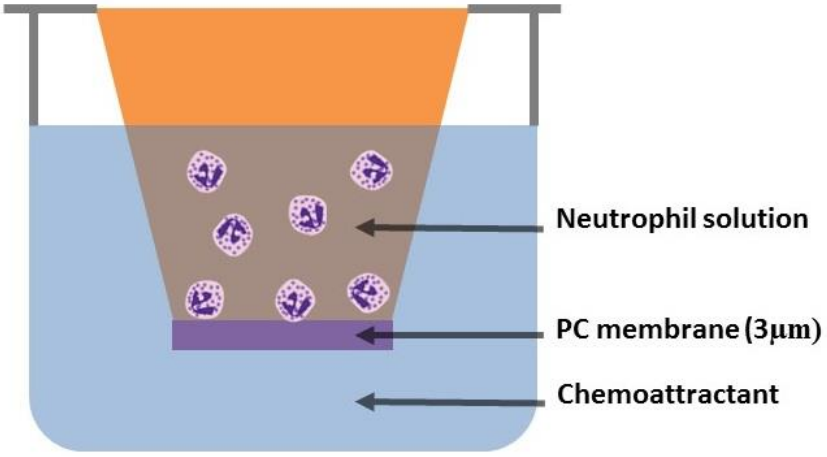

Figure 19. Boyden chamber chemotaxis assay.

Corning HTS Transwell 96 well plates are utilized for testing. Membranes and wells are incubated with a 2.5mg/mL fibrinogen solution then washed 3x times with DPBS. Plates are left to dry in a hood prior to loading with neutrophils.

After recirculation, neutrophils must be isolated from whole blood to prevent clogging of the membrane filter. Magnetic separation was completed using MACSxpress neutrophil isolation kit (Miltenyi Biotec 130-104-434). Non-target white blood cells are removed using antibody tagged magnetic beads and red blood cells are separated by sedimentation and a secondary

magnetic bead isolation step. First magnetic particles are suspended according to manufacturer's instructions. These beads are added to whole blood samples immediately after recirculation testing. After a 5 minute incubation, samples are placed in the magnetic separator for 15 minutes. The supernatant, which includes neutrophils and residual erythrocytes, is harvested and placed in a clean tube. Reconstituted beads with antibodies targeted erythrocytes are then added and allowed to incubate for 5 minutes. After 10 minutes of separation the supernatant, which contains isolated neutrophils, is collected. Samples are centrifuged for 5 minutes at 250g then suspended in 2.5ml DPBS. 50ul samples are collected for flow cytometry receptor analysis and cell counting to determine neutrophil concentration.

To prepare the assay chemoattractants must be added to the bottom well. The chemoattractants are diluted to predetermined concentrations in DPBS. Typically, unmodified DPBS, 5nM IL-8, 100nM IL-8, 100nM fMLP, and 100nM GRO-α are tested in quadruplicate for each assay. Next, pre-isolated neutrophils are loaded into the top well of the plate. A typical plate configuration is shown in Figure 19. After the entire plate is loaded it is placed in a 37˚C incubator with 5% CO_2 for 40 minutes. The plate is then removed from the incubator and 20ul of 0.5M EDTA is added to each well. The plate is placed in a 4˚C refrigerator for 10 minutes to facilitate neutrophil release from the membrane. 200ul samples from each well are then placed in labelled flow cytometry culture tubes. 300ul 4% formaldehyde is added to each sample in preparation for flow cytometry counting the following day.

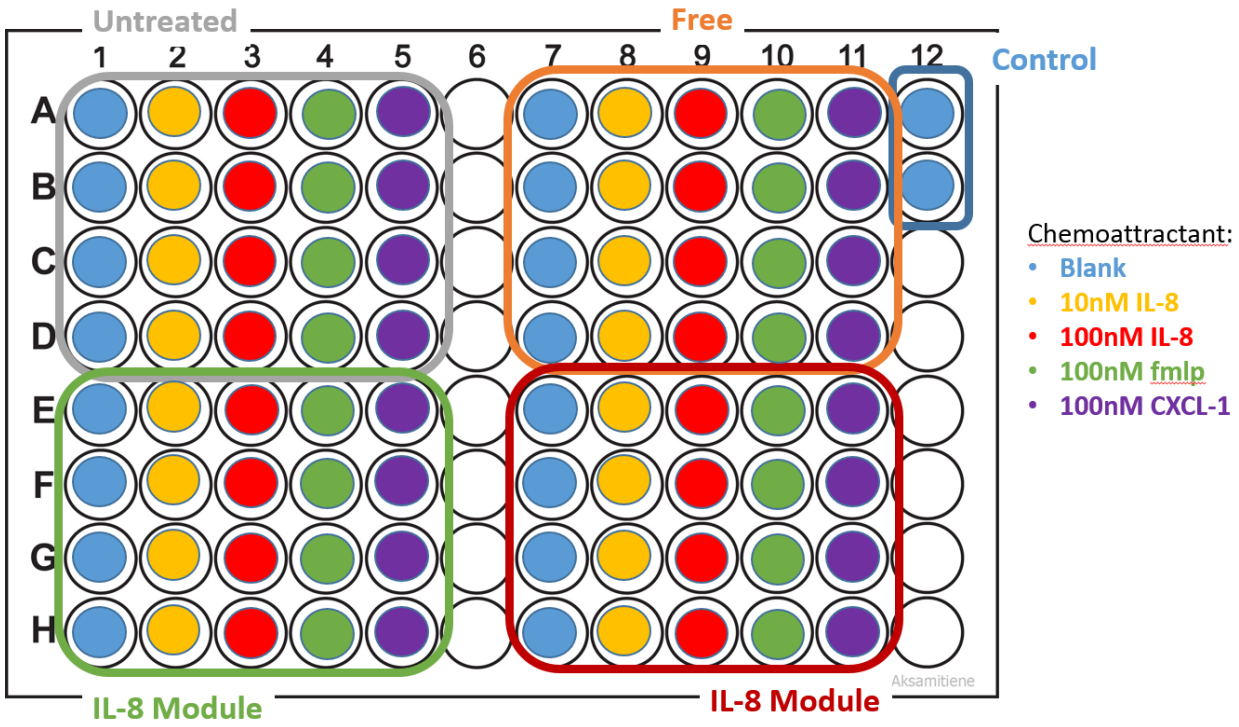

Figure 20. Typical Boyden chamber 96-well plate layout.

Flow cytometric counting of neutrophils was completed using a MACSQuant Analyzer 10. Analysis was completed using Winlist software. Neutrophils were gated using SSC vs FSC plots and counted to estimate total number of migrated cells. Mean number of neutrophils were calculated from the four duplicates. Occasionally samples were omitted if air bubbles were visible in the well after membrane removal. These were reloaded if possible. Percentage of migrated neutrophils was calculated by dividing the average number of migrated neutrophils by average number of loaded neutrophils for each test iteration.

4.3 RESULTS

4.3.1 PMP oxygenator fibers with chitosan spacer

Initial testing of PMP oxygenators utilized a branched chitosan spacer. The chitosan layer was covalently bound to aminated fibers using glutaraldehyde. A secondary glutaraldehyde step was used to immobilize the target protein. The high viscosity of chitosan prevented use of this technique with dialyzer fibers. Blood recirculation testing resulted in 34% and 29% downregulation of CXCR-1 and CXCR-2 respectively at 60 minutes relative to baseline blood. The BSA modified module showed similar levels of downregulation to the IL-8 module. The free IL-8 positive control exhibited 75% and 89% reduction in CXCR-1/2 expression. Results are shown in Figure 21 and Figure 22.

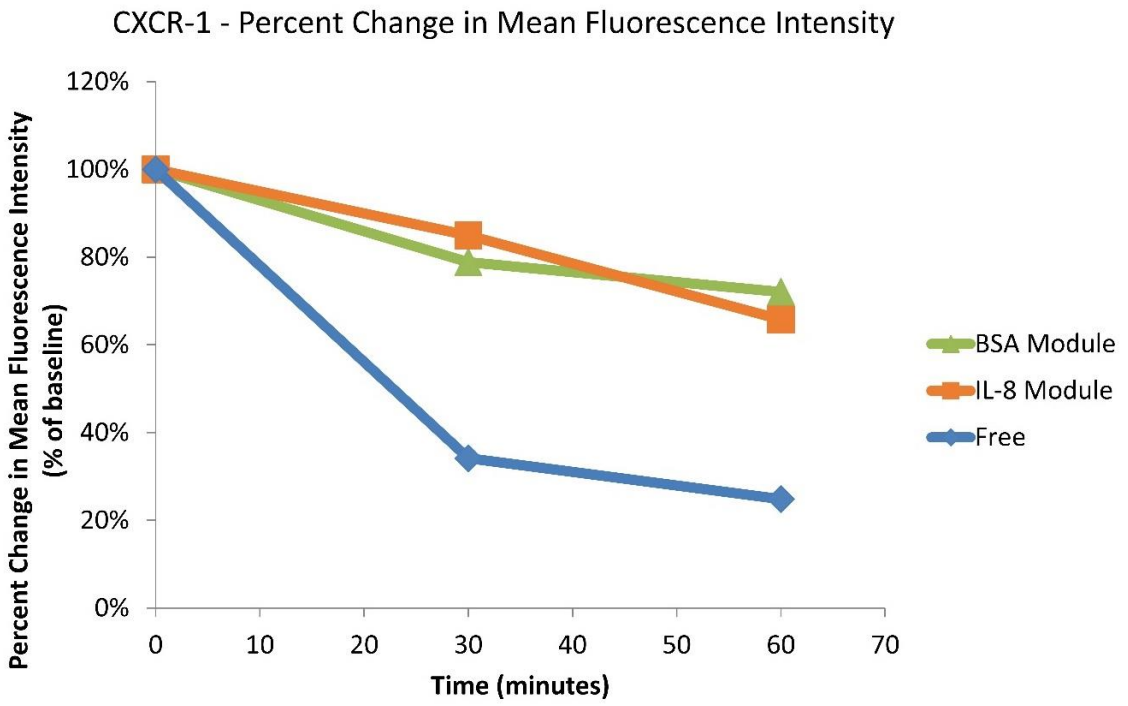

Figure 21. CXCR-1 expression after recirculation through PMP fiber modules with chitosan spacer.

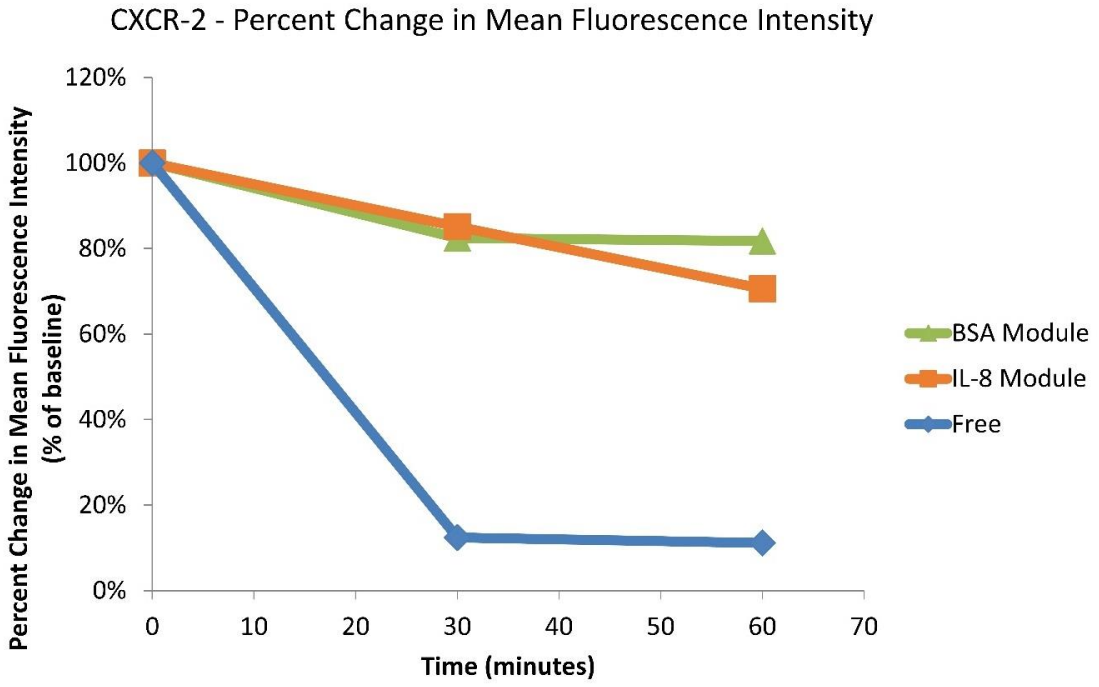

Figure 22. CXCR-2 expression after recirculation through PMP fiber modules with chitosan spacer.

Boyden chamber chemotaxis testing results are shown in Figure 23. Low chemokenesis was observed in all samples, with less than 5% of cells migrating through the filter. Baseline blood exhibited a strong migratory response toward 100nM IL-8, with 87% of neutrophils migrating through the filter. Baseline migration towards 100nM fMLP was lower than IL-8 but still significantly higher than baseline. The free IL-8 positive control neutrophils exhibited reduced migration towards IL-8, with only 24% of cell migrating. Chemotaxis towards fMLP was equivalent to baseline blood samples. Both IL-8 and BSA modules experienced increased chemotaxis to IL-8 and fMLP relative to baseline.

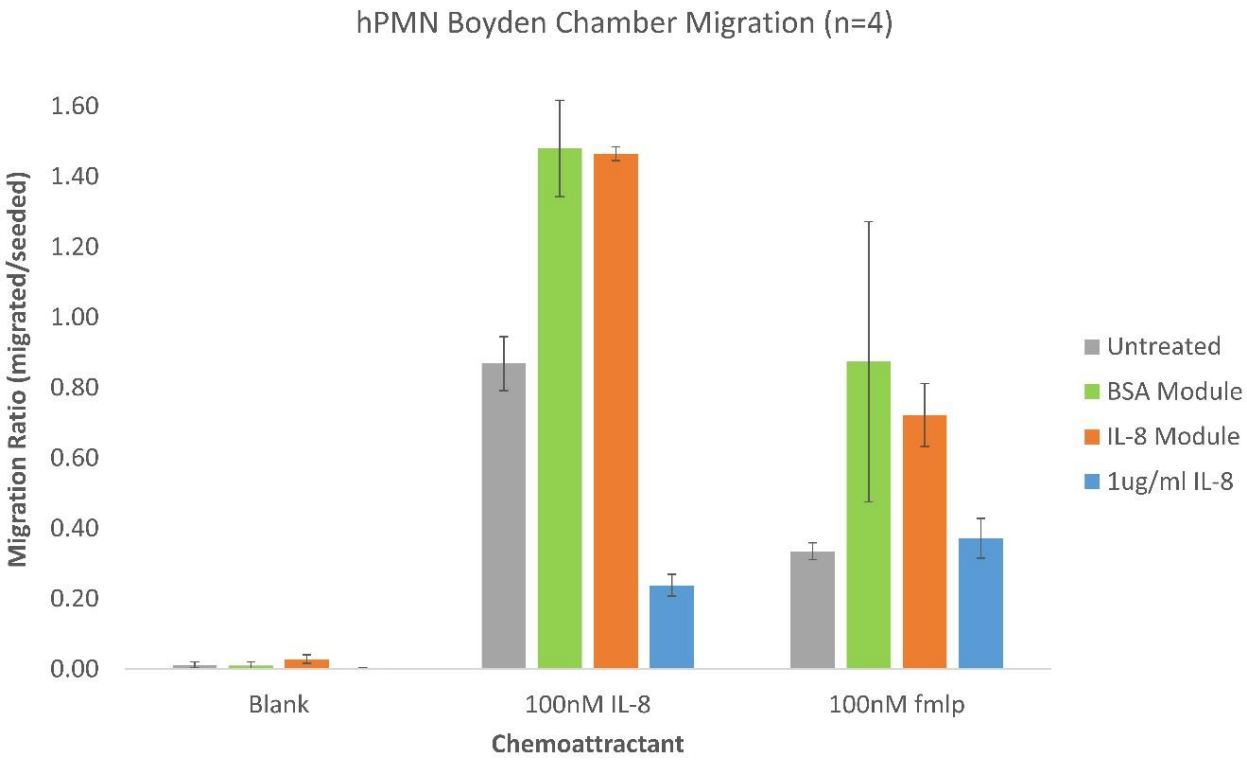

Figure 23. Neutrophil migration in Boyden chamber chemotaxis assay after recirculation through PMP fiber modules with chitosan spacer.

4.3.2 PEG spacer

An updated immobilization approach utilized a heterobifunctional PEG spacer in place of chitosan. This eliminated the use of glutaraldehyde from the procedure. The testing results are shown in Figure 24 and Figure 25. Free IL-8 positive control induced substantial CXCR-1/2 downregulation, particularly in CXCR-2 which was reduced 98% relative to baseline blood. After 60 minutes of recirculation, CXCR-1 expression was reduced 28% in the IL-8 control module and 23% in the BSA modified module. CXCR-2 downregulation was more substantial for the IL-8 module, resulting in 59% downregulation. The BSA modified module induced 41% downregulation.

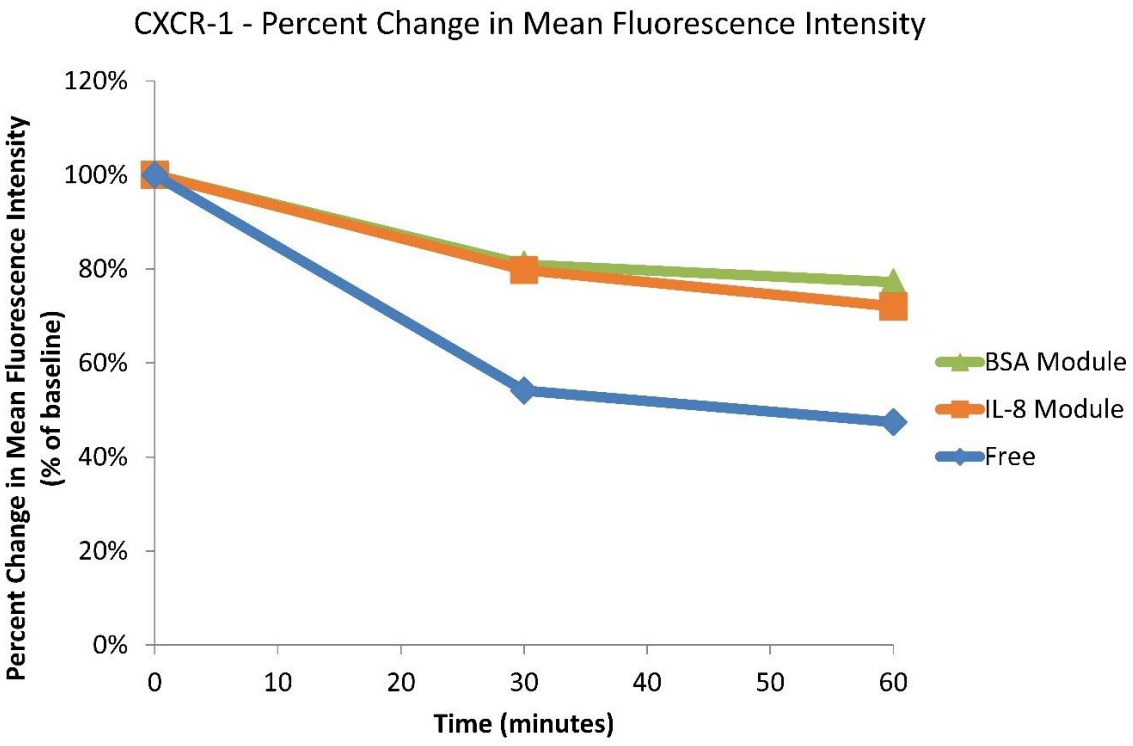

Figure 24. CXCR-1 expression after recirculation through PMP fiber modules with PEG spacer.

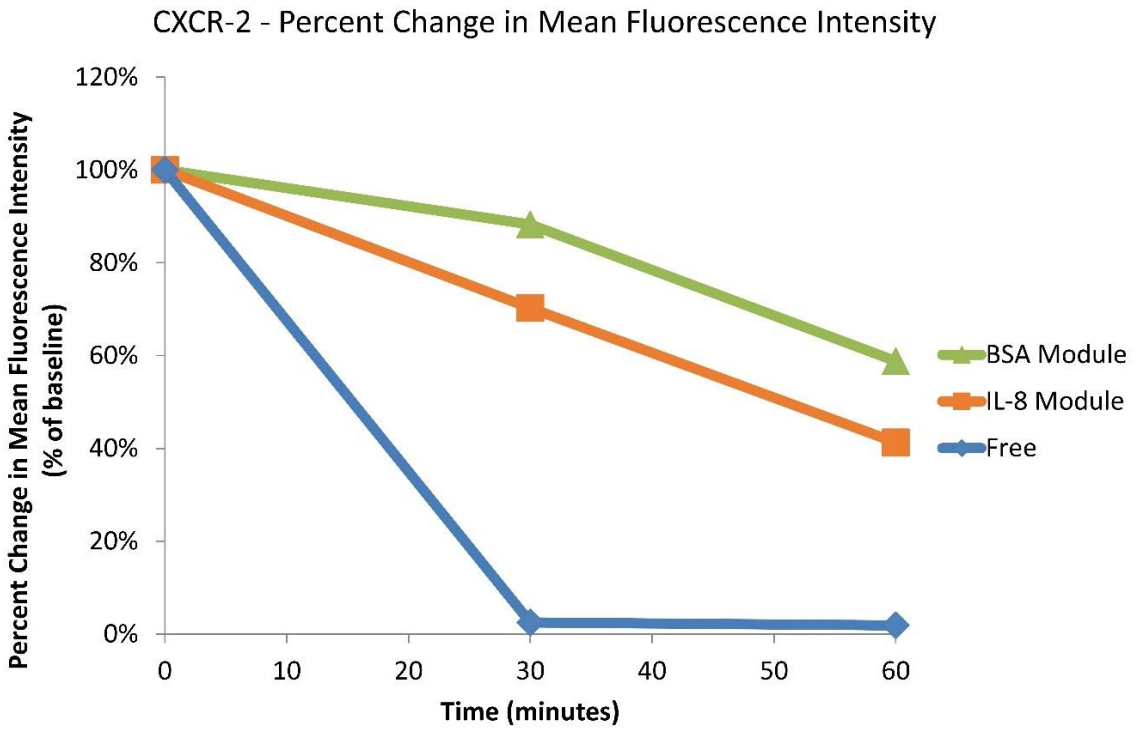

Figure 25. CXCR-2 expression after recirculation through PMP fiber modules with PEG spacer.

Chemotaxis testing results are shown in Figure 26. Low chemokenesis was observed in all samples. The free IL-8 (1 ug/mL) positive control showed migratory shutoff towards 100nM IL-8, but maintained migratory activity towards fMLP. The BSA control module and IL-8 both experienced minimal change in migratory activity compared to the untreated baseline control. A small reduction in mean migration between untreated and IL-8 module neutrophils towards 100nM IL-8 is not statistically significant.

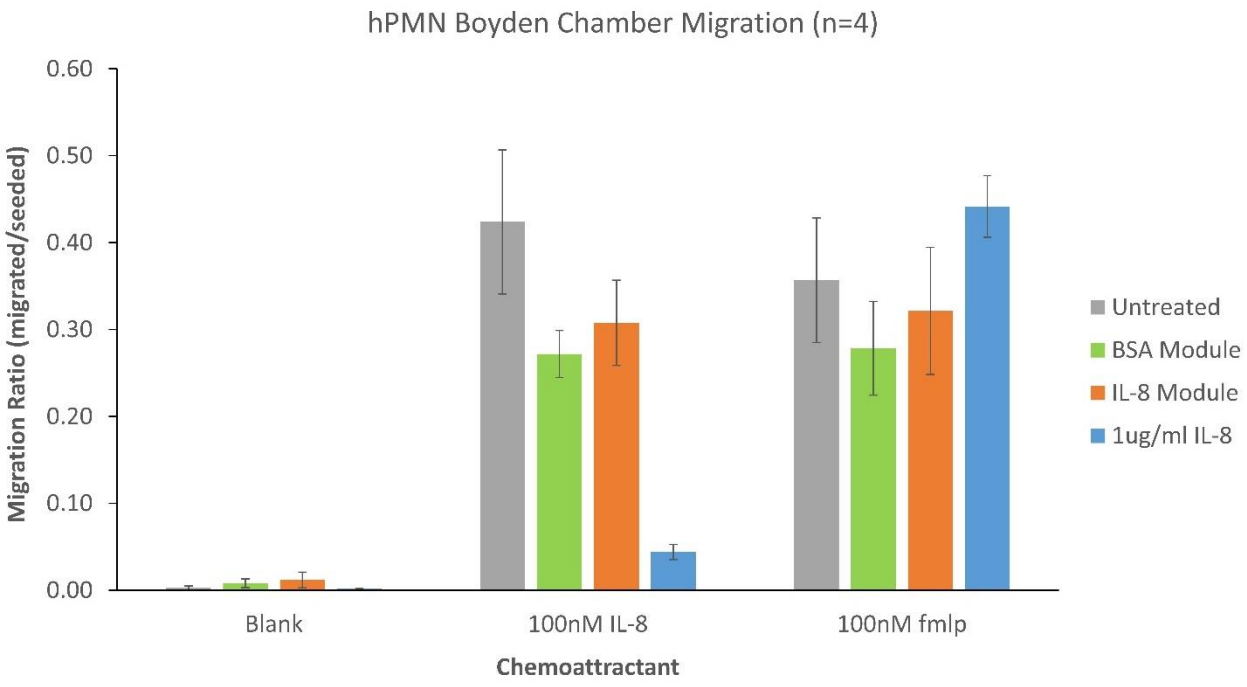

Figure 26. Neutrophil migration in Boyden chamber chemotaxis assay after recirculation through PMP fiber modules with PEG spacer.

4.3.2.1 Fresenius fibers

Aminated polysulfone dialyzer fibers, provided Fresenius, were conjugated using the PEG spacer protocol discussed above. The modules and flow loop were configured for flow and modification on the fiber inner lumen. A NERB buffer recirculation test was completed to determine if leaching was at a functionally relevant level. The free IL-8 positive control induced downregulation in both CXCR-1/2. Neither the hAlbumin nor IL-8 modules induced significant CXCR-1/2 downregulation. Results are presented in Figure 27 and Figure 28.

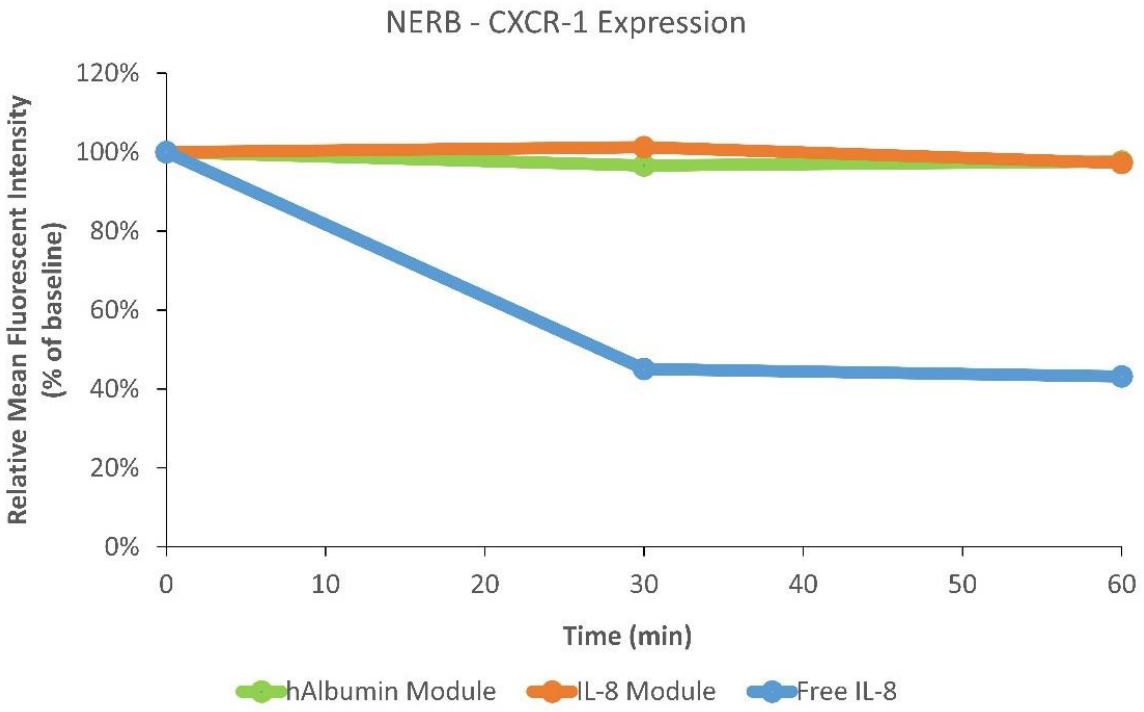

Figure 27. NERB buffer recirculation results showing neutrophil CXCR-1 expression after exposure to buffer circulated through modified aminated polysulfone fibers.

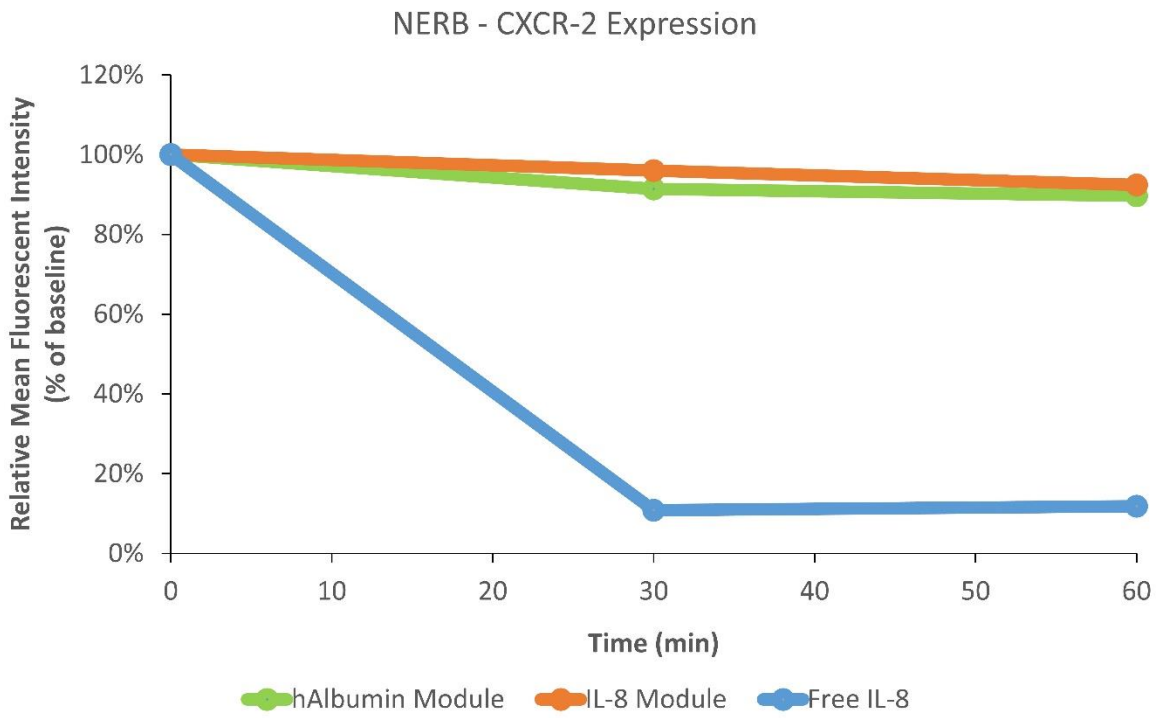

Figure 28. NERB buffer recirculation results showing neutrophil CXCR-2 expression after exposure to buffer circulated through modified aminated polysulfone fibers.

Whole blood recirculation was completed to determine the test module's impact on CXCR-1/2 expression. These results are shown in Figure 29 and Figure 30. At 60 minutes the free IL-8 positive control induced significant downregulation relative to baseline blood. Both the IL-8 and hAlbumin module induced downregulation in both CXCR-1 and CXCR-2. hAlbumin control downregulation was greater than the IL-8 module for CXCR-1, but less substantial in CXCR-2, where the IL-8 module induced greater levels of downregulation. The 150 minute time point measured CXCR-1/2 expression after the 90 minute neutrophil isolation procedure. Only minor changes in CXCR-1/2 expression relative to the 60 minute time point were observed.

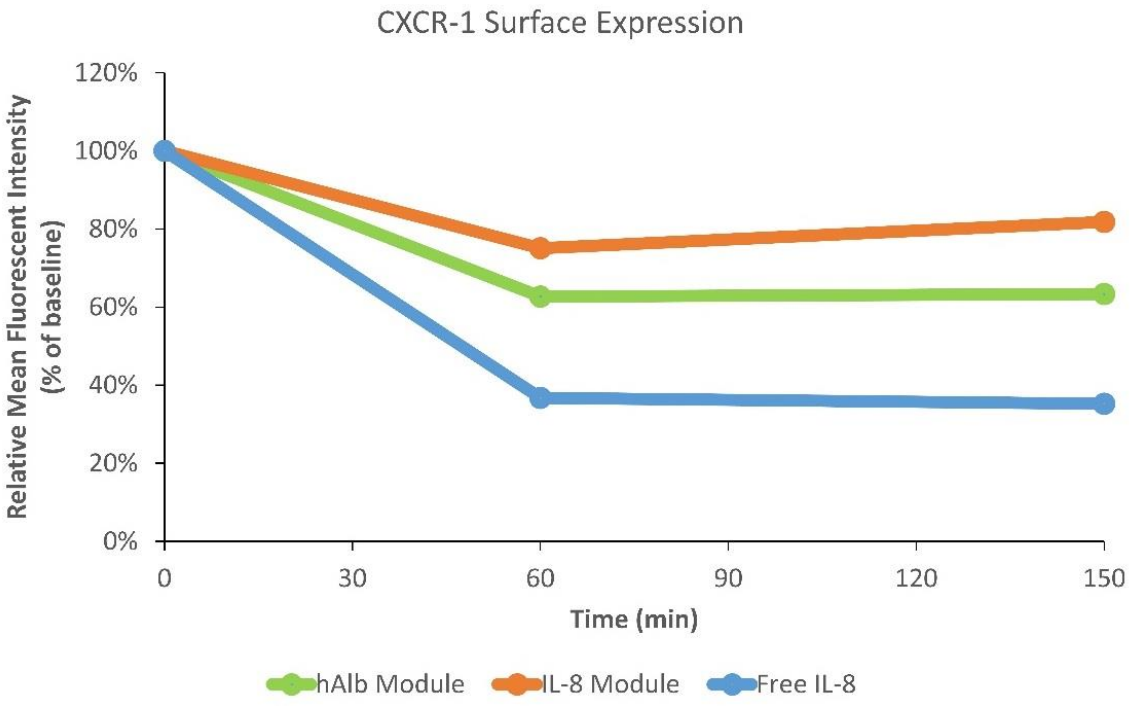

Figure 29. Neutrophil CXCR-1 expression after recirculation through modified aminated polysulfone fibers.

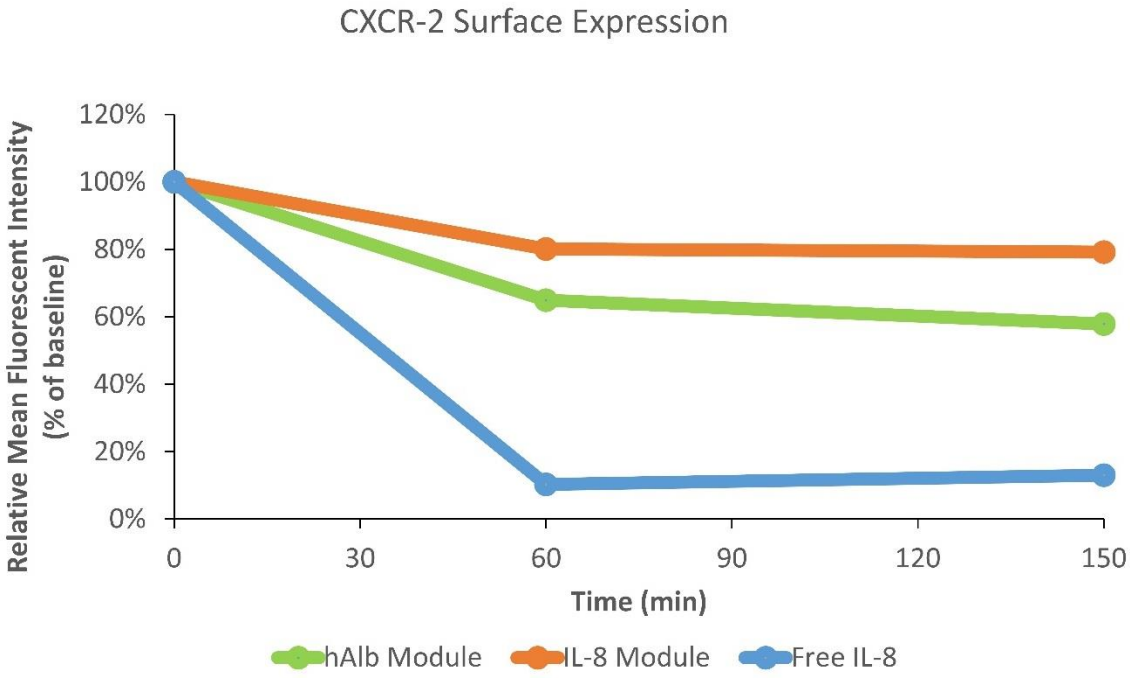

Figure 30. Neutrophil CXCR-2 expression after recirculation through modified aminated polysulfone fibers.

Boyden chamber chemotaxis results are shown in Figure 31. Chemotaxis results show slightly elevated chemokenesis for all but baseline blood samples. Baseline blood, hAlbumin control module, and the IL-8 test module all exhibited strong migration towards all chemokines. The free IL-8 positive control showed migratory shutoff towards 5nM IL-8 and GRO-α, but maintained migratory response towards 100nM IL-8 and fMLP.

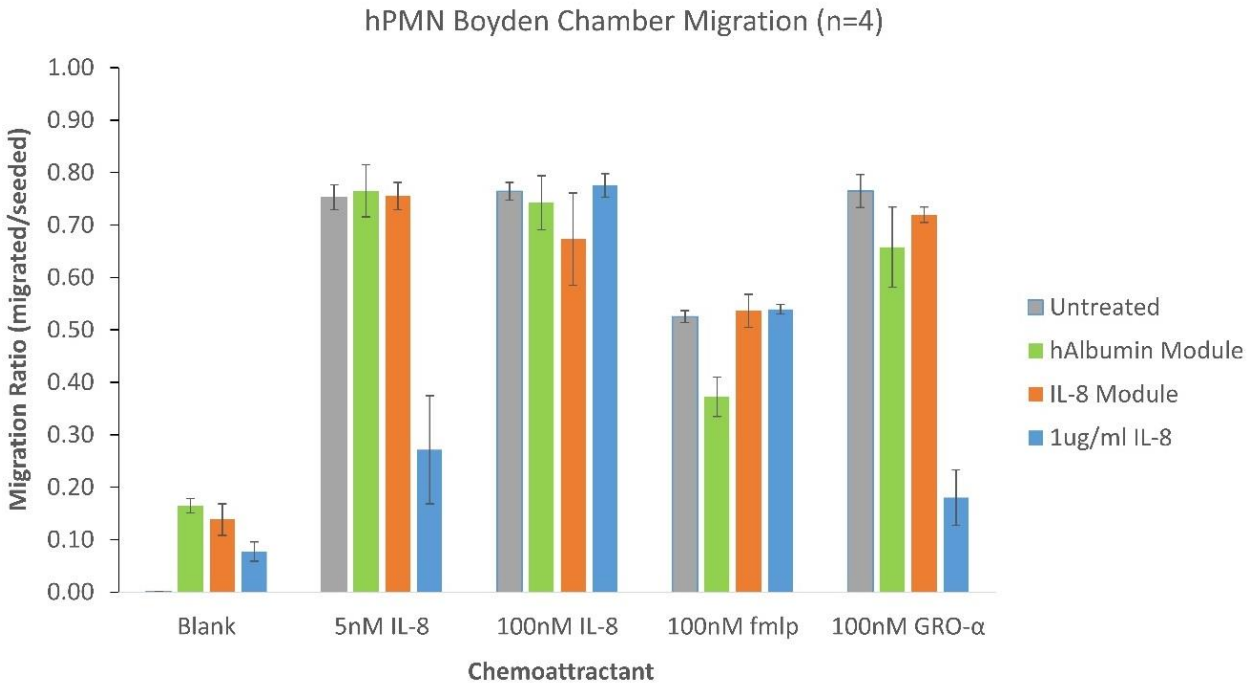

Figure 31. Neutrophil migration in Boyden chamber chemotaxis assay after recirculation through modified aminated polysulfone fiber modules with PEG spacer.

4.3.2.2 Gambro fibers

Aminated AN69 fibers were provided by Gambro for evaluation with the PEG immobilization. These fibers were modified using the same module, immobilization, and test procedure as the Fresenius-PEG fibers. Multiple donor tests were completed with the same immobilization procedures, with minor changes to the wash protocol, to better understand donor variability. Test 1 did not include a NERB assay, but additional tests included the buffer recirculation.

After whole blood recirculation, CXCR-1 and CXCR-2 downregulation was significant for the free IL-8 positive control, registering 68% and 92% respectfully. These results are shown in Figure 32 and Figure 33. The hAlbumin test module closely tracked baseline blood samples. The IL-8 module induced significant downregulation of both CXCR-1 and CXCR-2. At 60 minutes the modules reached 52% CXCR-1 and 88% CXCR-2 downregulation. CXCR-2 downregulation after recirculation through the IL-8 module nearly reached the levels achieved in the free IL-8 control. All CXCR-1 and CXCR-2 expression levels were fairly consistent at both 60 and 150 minutes.

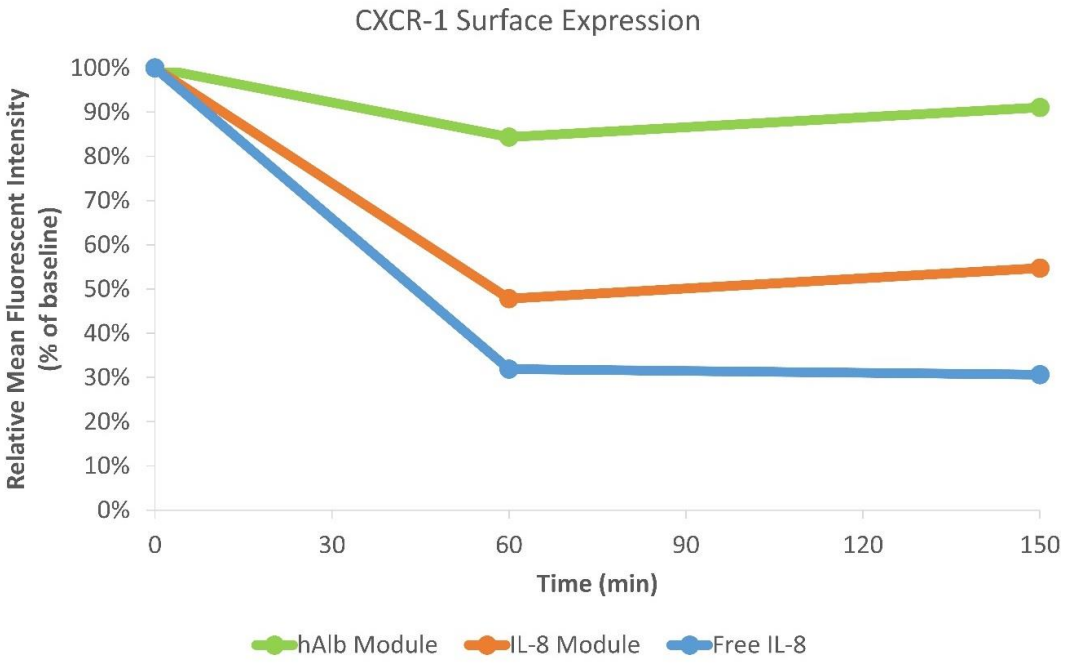

Figure 32. Neutrophil CXCR-1 expression after recirculation through modified aminated Gambro AN69 fibers.

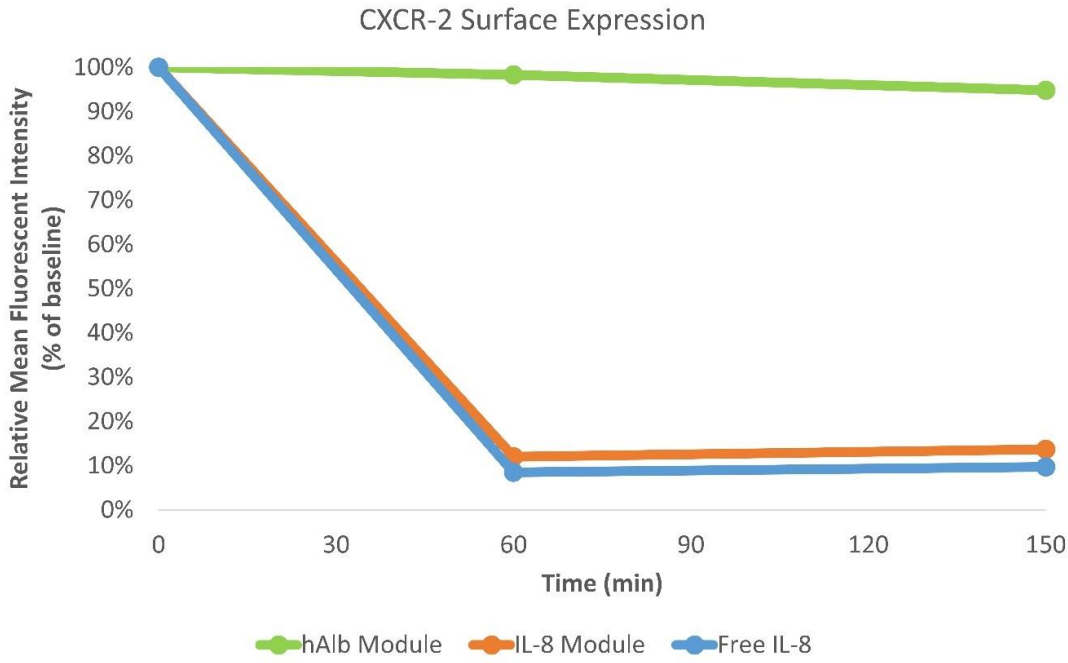

Figure 33. Neutrophil CXCR-2 expression after recirculation through modified aminated Gambro AN69 fibers.

Boyden chamber chemotaxis testing results are shown in Figure 34. Analysis of the results show high levels of migration towards all chemoattractants in the baseline neutrophil samples. Free IL-8 neutrophils exhibited slightly increased chemokenesis and migratory reduction relative to baseline in 5nM IL-8 and GRO-α chemoattractants. Migration remained consistent with baseline neutrophils towards 100nM IL-8 and fMLP. HAlbumin module treated neutrophil migration was equivalent to baseline blood migration. IL-8 module treated neutrophils experienced a similar reduction in migration as the free IL-8 control. With reduced migration towards 5nM IL-8 and GRO-α chemoattractants.

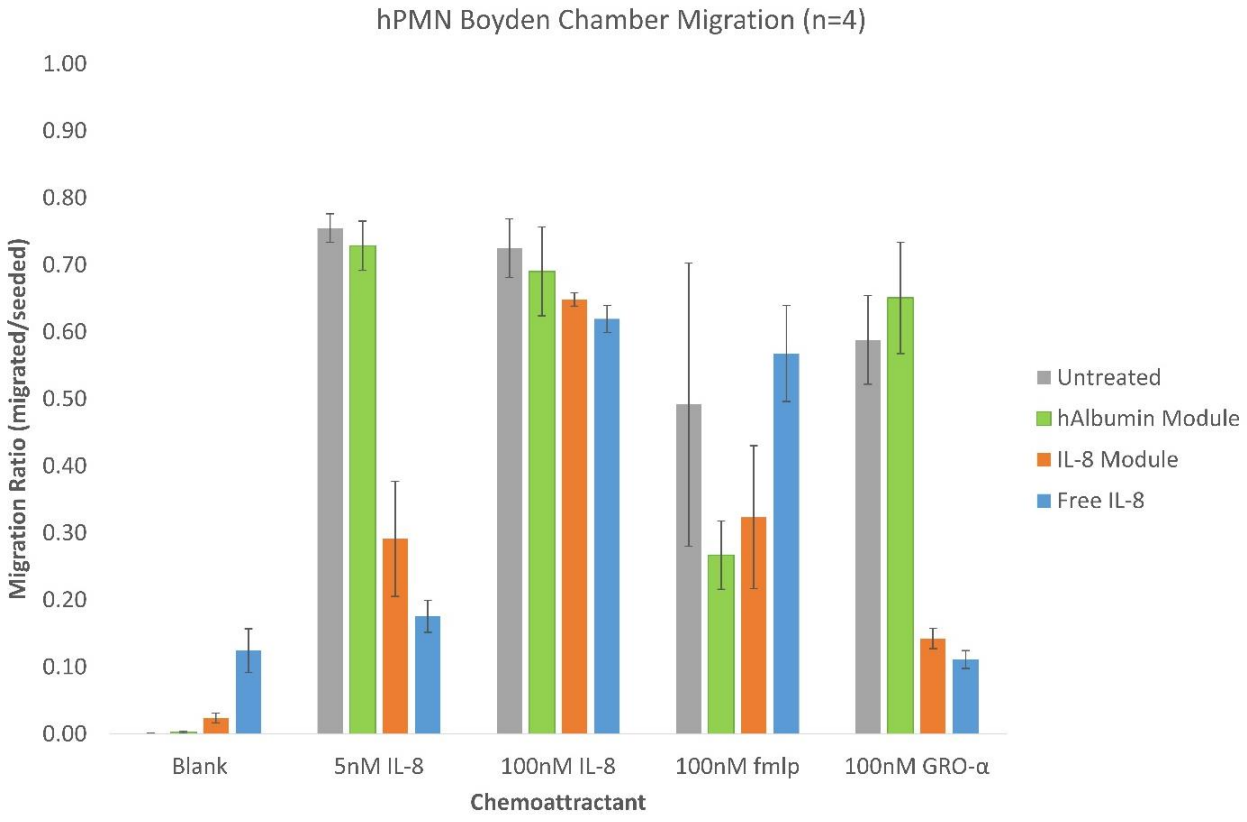

Figure 34. Neutrophil migration in Boyden chamber chemotaxis assay after recirculation through modified aminated Gambro AN69 fiber modules with PEG spacer.

NERB testing was completed in the second Gambro-PEG fiber recirculation test. The free IL-8 positive control induced downregulation in both CXCR-1/2, while hAlbumin control module closely tracked the baseline. The IL-8 module did not induce significant downregulation in CXCR-1 (Figure 35). However, there was substantial downregulation compared to baseline in CXCR-2, which led to a 39% reduction in CXCR-2 expression at 60 minutes (Figure 36).

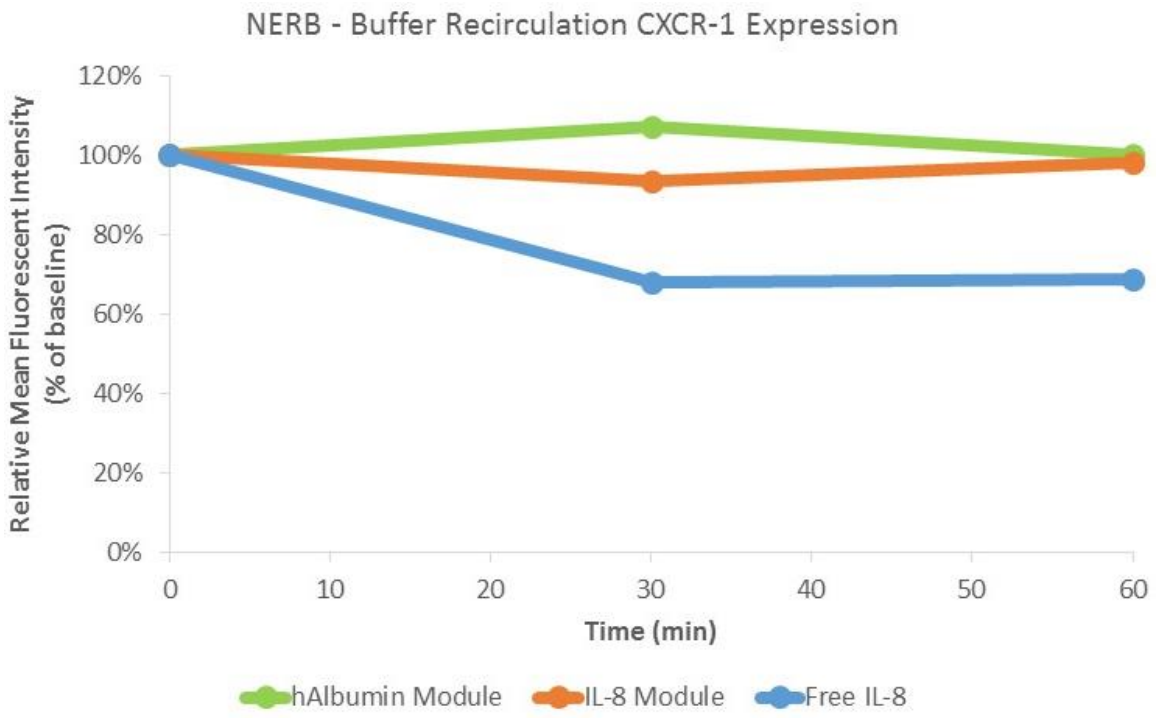

Figure 35. NERB buffer recirculation results showing neutrophil CXCR-1 expression after exposure to buffer circulated through modified aminated Gambro AN69 fibers.

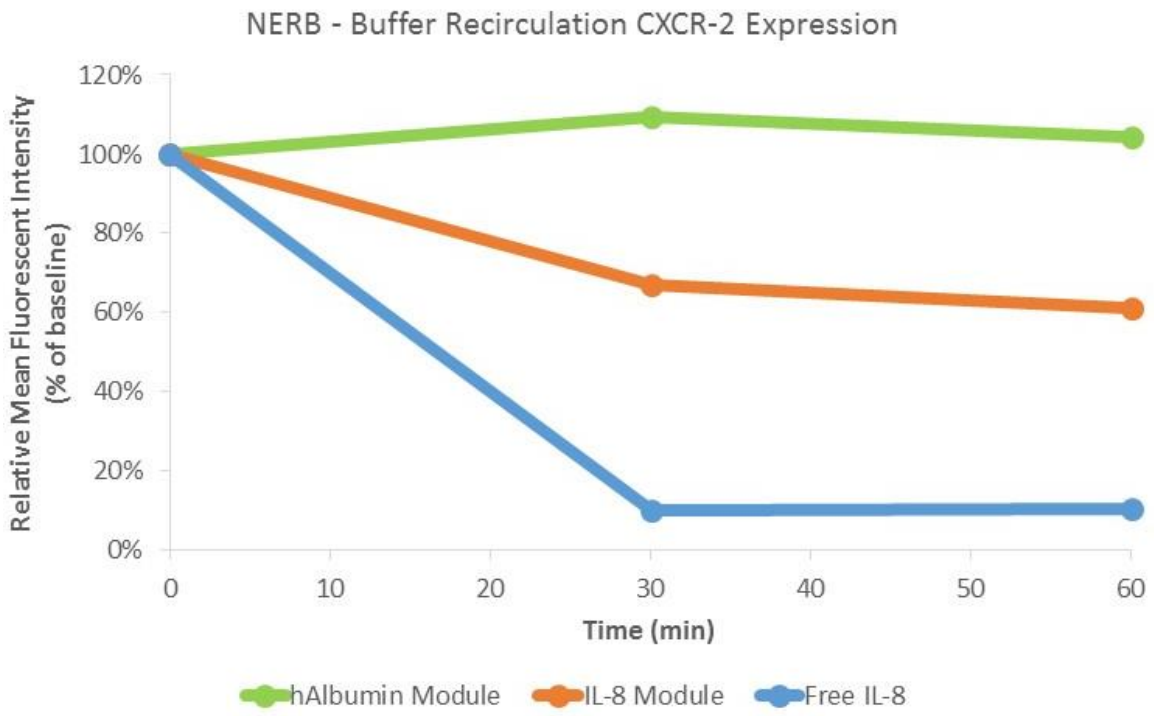

Figure 36. NERB buffer recirculation results showing neutrophil CXCR-2 expression after exposure to buffer circulated through modified aminated Gambro AN69 fibers.

Whole blood recirculation was only collected at the extended time point after neutrophil isolation due to errors in the staining procedure. After neutrophil isolation, free IL-8 downregulation was present in both CXCR-1 and CXCR-2, with hAlbumin control module treated neutrophils closely matching baseline blood. IL-8 module treated neutrophils experienced significant downregulation in CXCR-1 and CXCR-2, both approaching but not achieving the downregulation levels of free IL-8. CXCR-1/2 downregulation is shown in Figure 37 and Figure 38.

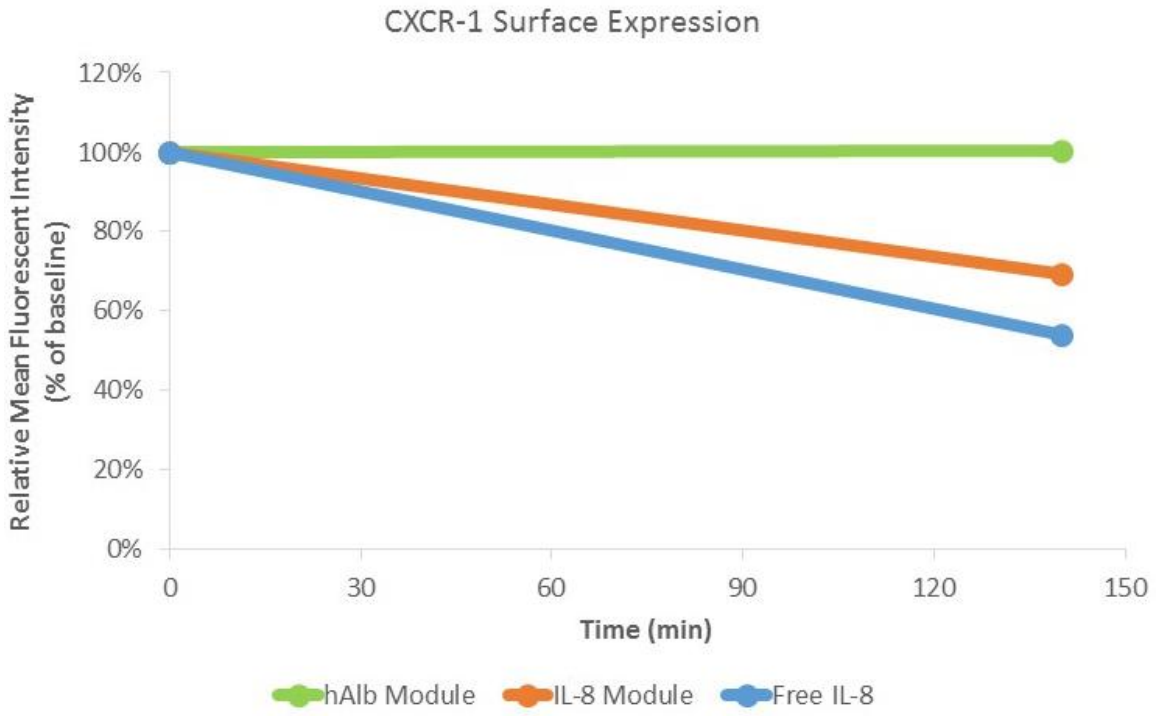

Figure 37. Neutrophil CXCR-1 expression after recirculation through modified aminated Gambro AN69 fibers.

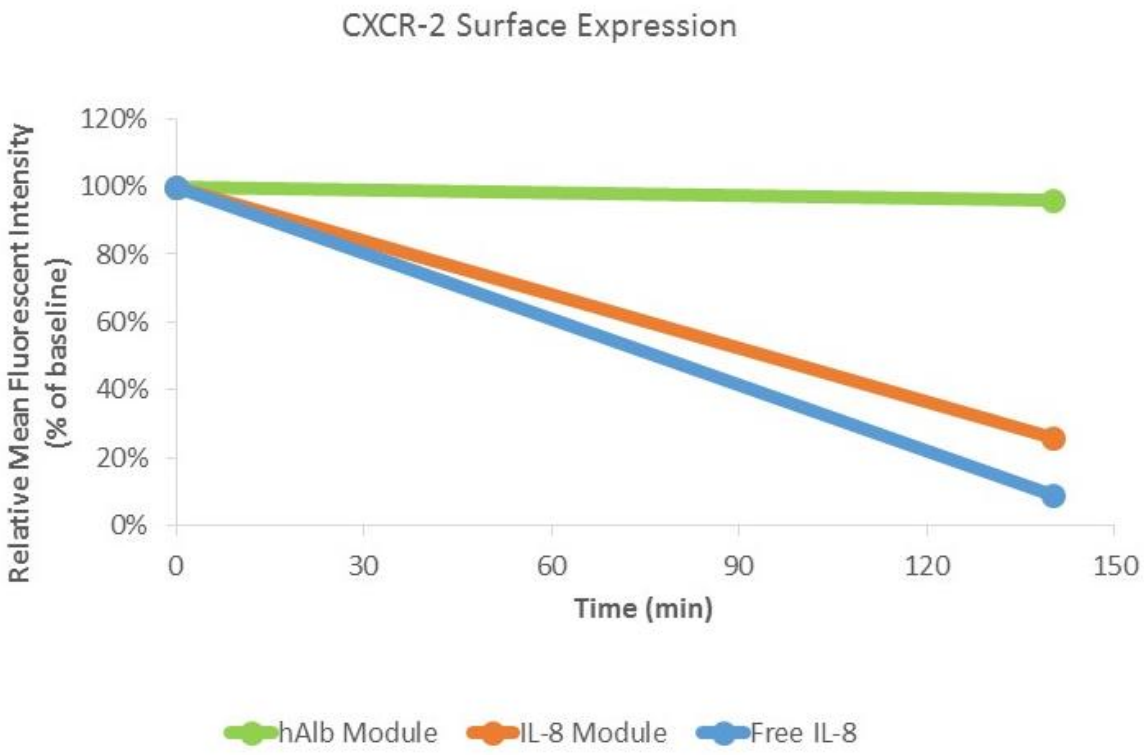

Figure 38. Neutrophil CXCR-2 expression after recirculation through modified aminated Gambro AN69 fibers.

Boyden chamber chemotaxis testing was completed with isolated neutrophils after recirculation. These results are shown in Figure 39. Baseline untreated blood and free IL-8 controls were comparable to previous testing, with strong migration towards all chemoattractants in untreated blood and migratory shutoff towards 5nM IL-8 and GRO-α in the free IL-8 control. Neutrophils treated by both the hAlbumin control module and IL-8 test module exhibited similar migratory behavior to untreated blood.

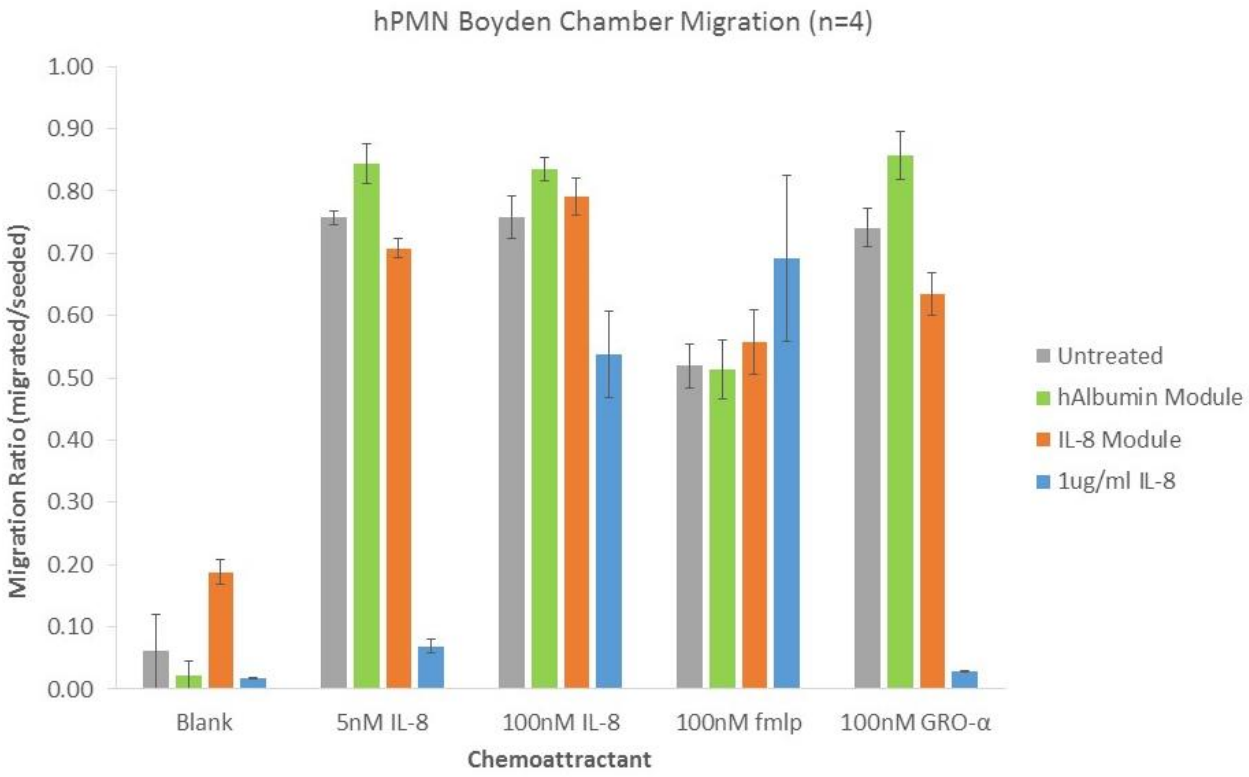

Figure 39. Neutrophil migration in Boyden chamber chemotaxis assay after recirculation through modified aminated Gambro AN69 fiber modules with PEG spacer.

The third test with Gambro-PEG fibers included some additional washing. An overnight 5% single pass BSA wash, in addition to shell side wash solution to purge unbound IL-8. However, additional washing did not eliminate leached IL-8 induced downregulation in the NERB assay. Results in Figure 40 and Figure 41 show the IL-8 test module induced both CXCR-1 and CXCR-2 downregulation compared to baseline blood and the hAlbumin control. Free IL-8 induced downregulation exceeded the test module and was comparable to past NERB tests.

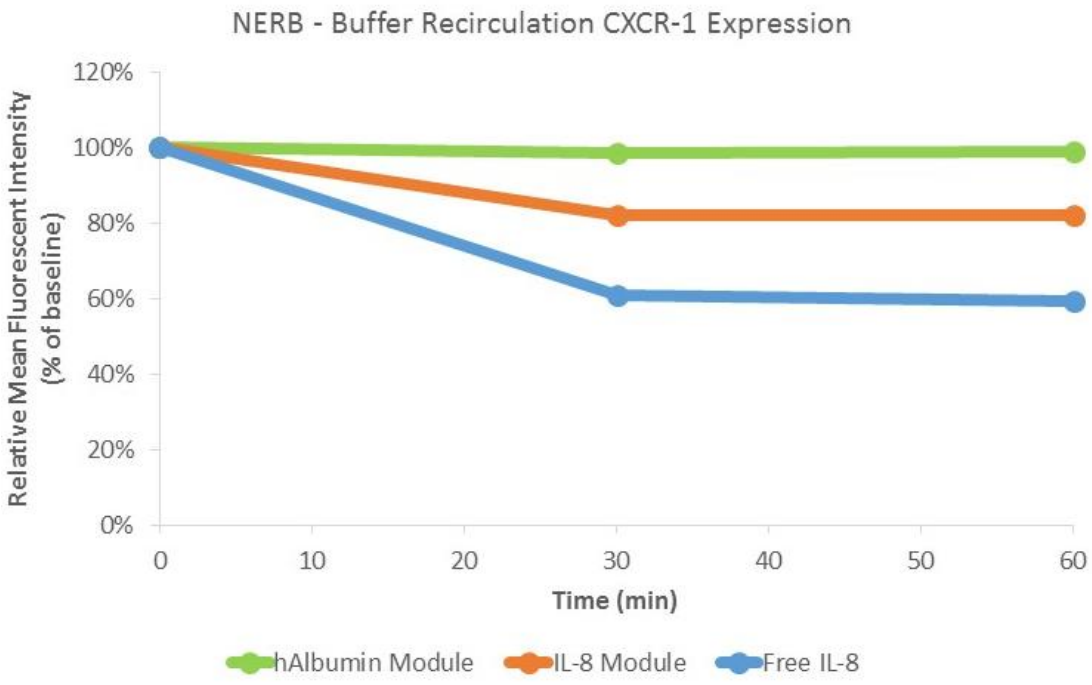

Figure 40. NERB buffer recirculation results showing neutrophil CXCR-1 expression after exposure to buffer circulated through modified aminated Gambro AN69 fibers.

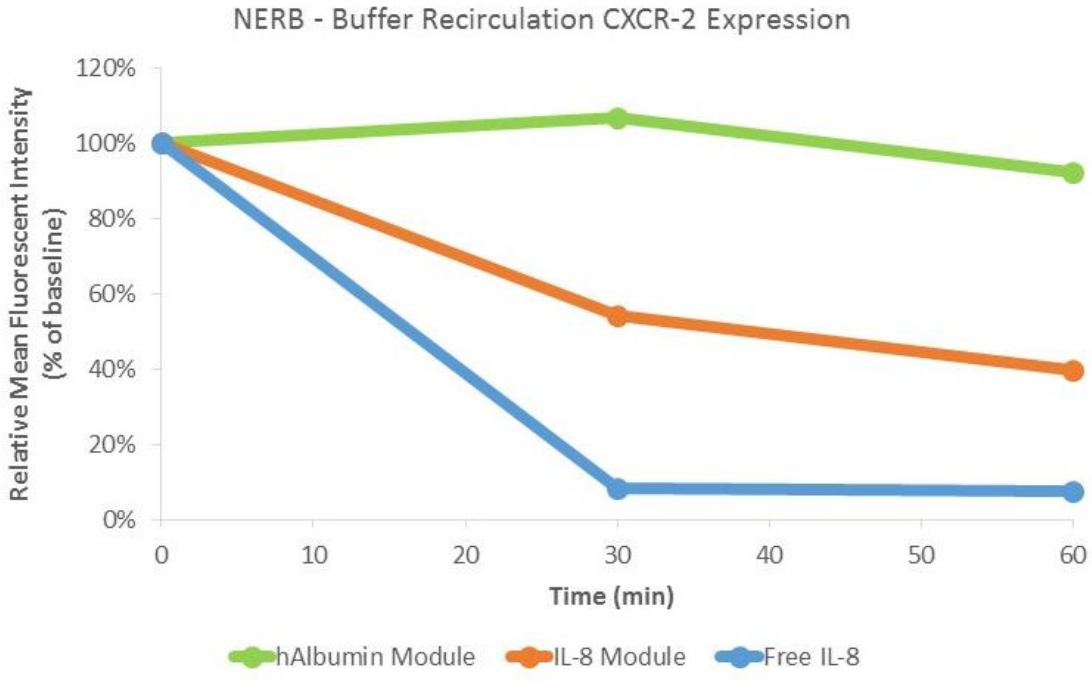

Figure 41. NERB buffer recirculation results showing neutrophil CXCR-2 expression after exposure to buffer circulated through modified aminated Gambro AN69 fibers.

Whole blood recirculation results are shown in Figure 42 and Figure 43. These results indicate that the IL-8 module treated neutrophils has reduced CXCR-1/2 expression compared to baseline blood and hAlbumin control module treated neutrophils. The free IL-8 positive control had the anticipated high levels of both CXCR-1 and CXCR-2 downregulation. The IL-8 module treated neutrophil downregulation levels approached, but did not match free IL-8 positive control samples.

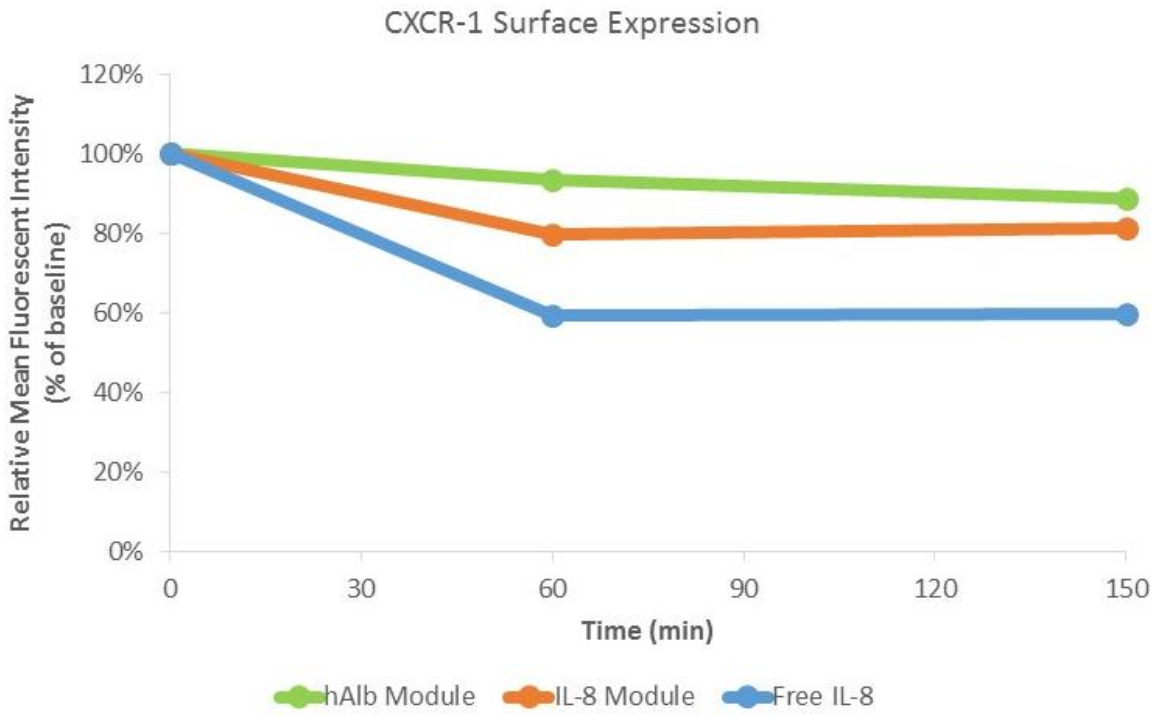

Figure 42. Neutrophil CXCR-1 expression after recirculation through modified aminated Gambro AN69 fibers.

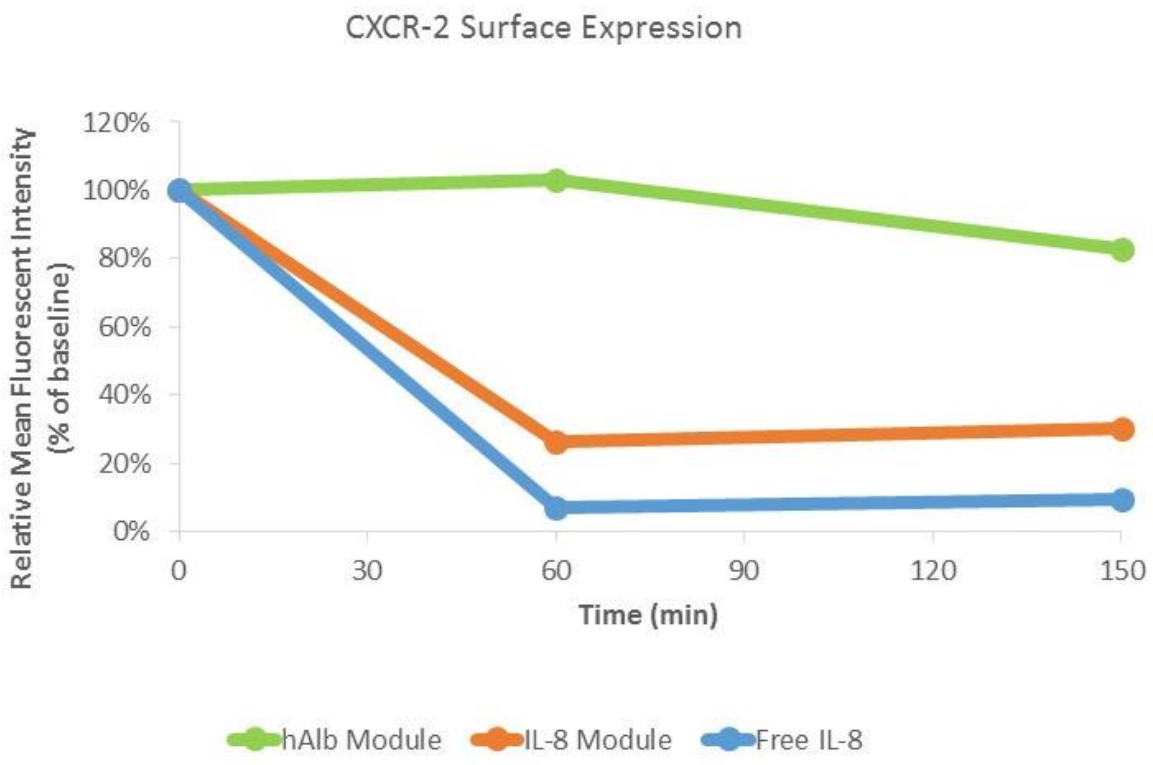

Figure 43. Neutrophil CXCR-2 expression after recirculation through modified aminated Gambro AN69 fibers.

Boyden chamber chemotaxis testing was completed after whole blood perfusion and neutrophil isolation. The results of this test are shown in Figure 44. Unmodified baseline blood showed minimal chemokenesis and strong migration towards all chemoattractants. Free IL-8 positive control showed reduced migration towards 5nM IL-8 and GRO-α, but maintained migratory behavior towards other chemoattractants, including fMLP. Both the IL-8 module and hAlbumin control showed minimal changes from untreated baseline blood. However, the hAlbumin module treated neutrophils exhibited increased chemokenesis and a reduction in migration towards fMLP.

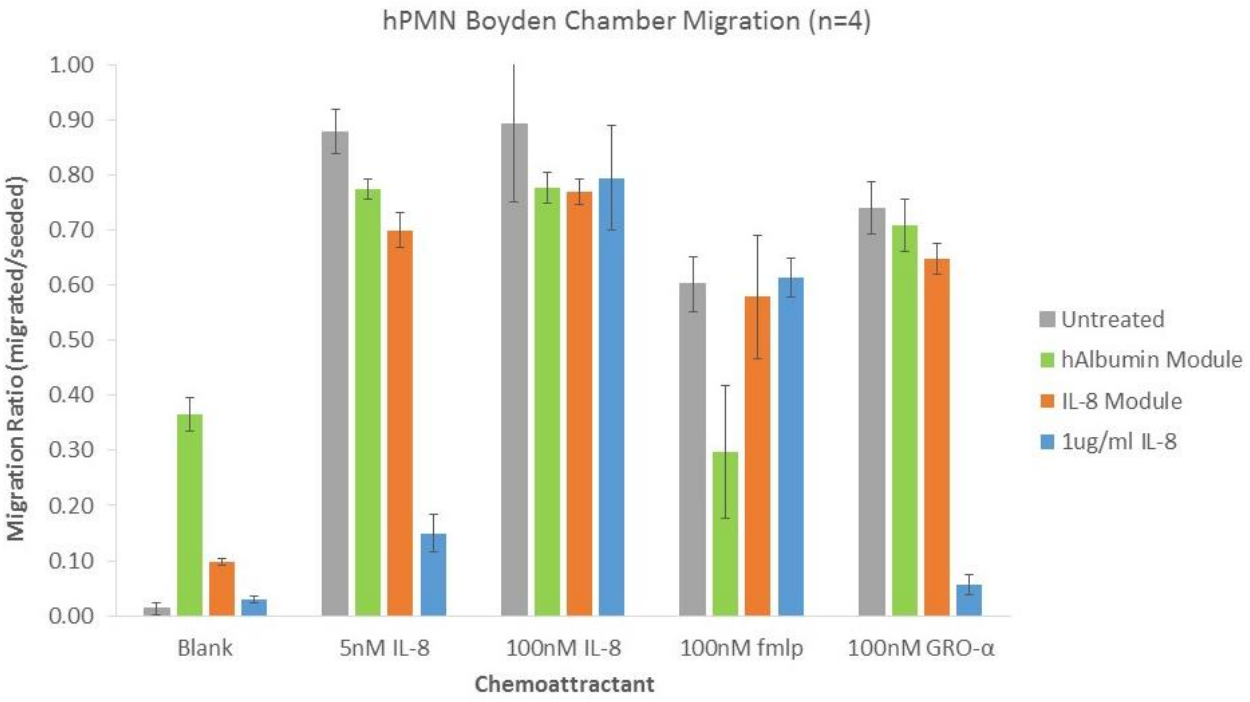

Figure 44. Neutrophil migration in Boyden chamber chemotaxis assay after recirculation through modified aminated Gambro AN69 fiber modules with PEG spacer.

4.3.2.3 Stop flow configuration

A stop flow experiment was completed to determine whether high shear rate was preventing neutrophils for interacting with immobilized IL-8 on the fiber surface. This experiment only analyzed CXCR-1/2 surface expression, not NERB or chemotaxis. Fibers were tested with Gambro-PEG immobilization and standard washing. Whole blood recirculation samples were collected every 15 minutes to get a better understanding of receptor expression over time.

Whole blood recirculation results show significant CXCR-1 and CXCR-2 downregulation at 60 minutes (Figure 45 and Figure 46). CXCR-1 downregulation begins at the first, 15 minute, time point but continues to increase through 60 minutes. It appears as if increased recirculation time may lead to a small amount of additional downregulation. CXCR-2 downregulation remained

stable from 15 through 60 minutes and appears to have reached a maximum. CXCR-1 and CXCR-2 downregulation are equivalent for both continuous and stop flow conditions. Downregulation of the modules appears to lag behind free IL-8 due to the nature of recirculation versus soluble IL-8.

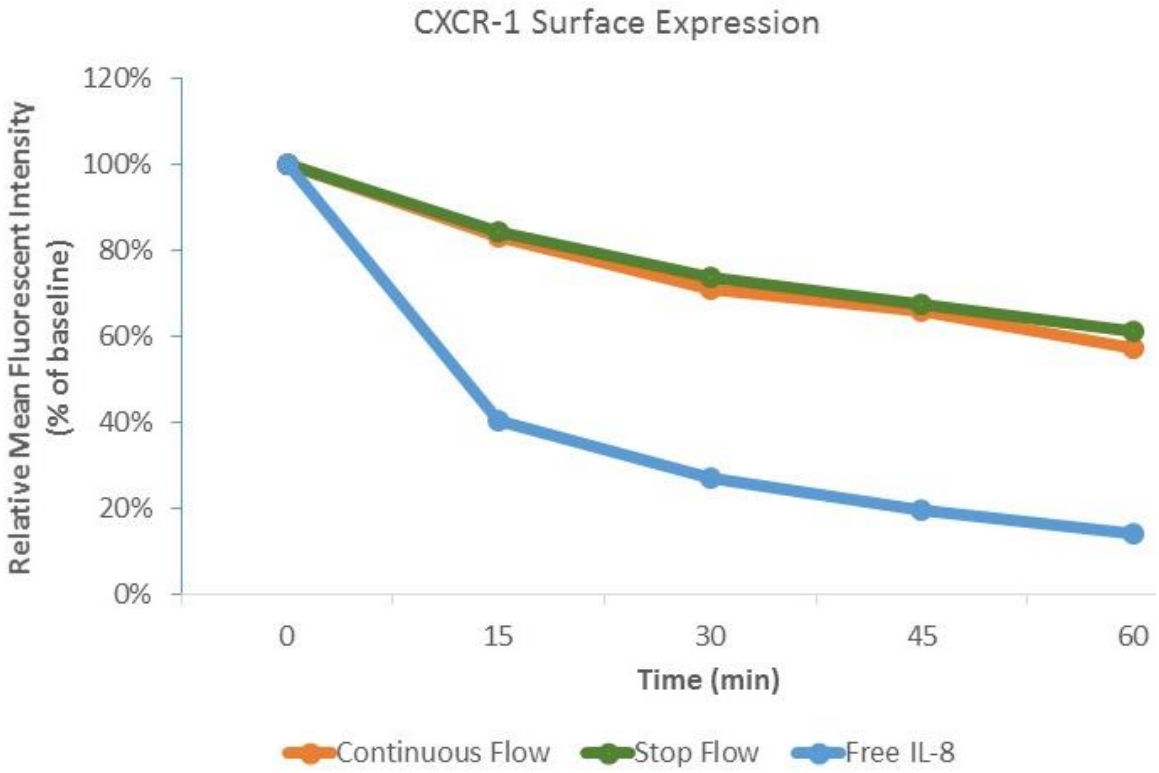

Figure 45. Neutrophil CXCR-1 expression after recirculation through IL-8 modified aminated Gambro AN69 fibers with different flow conditions.

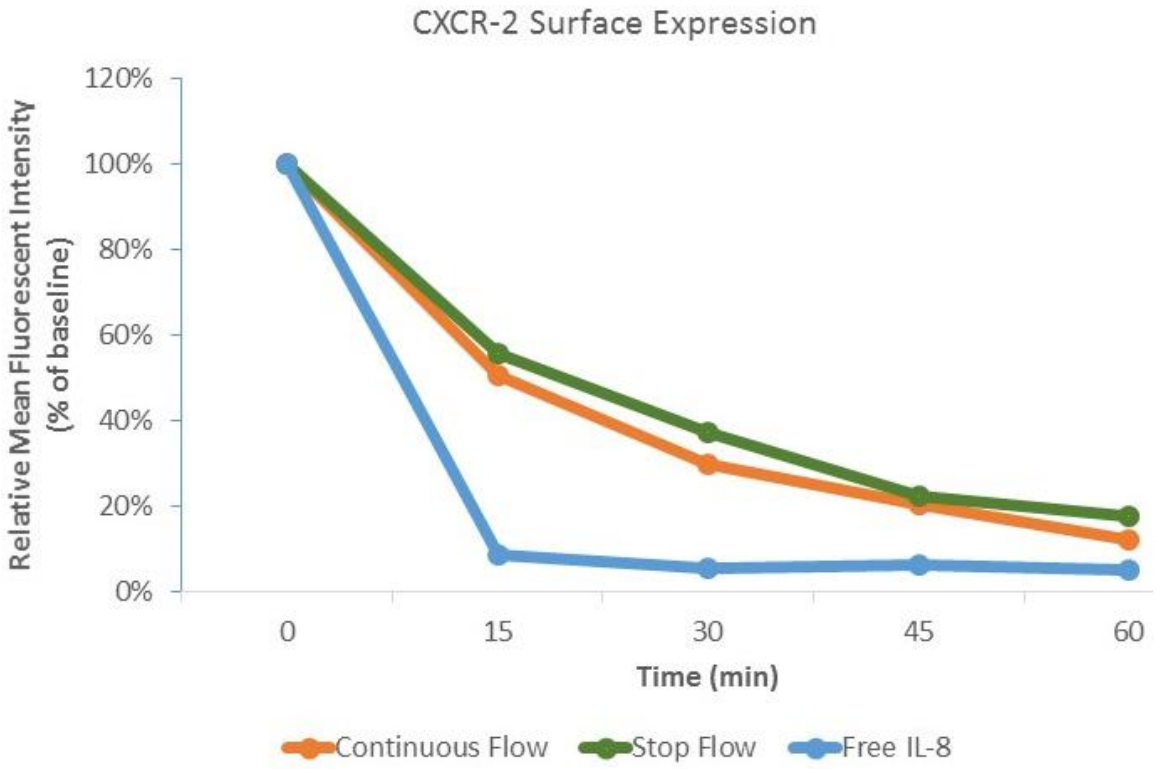

Figure 46. Neutrophil CXCR-2 expression after recirculation through IL-8 modified aminated Gambro AN69 fibers with different flow conditions.

4.3.3 Additional washing protocols and leaching evaluation

An IL-8 ELISA was used to quantify IL-8 leaching from fibers. A 5% BSA buffer was recirculated in place of whole blood then effluent was measured to determine the quantity of soluble IL-8 being released from the fibers after washing. These leaching values provide guidance to quickly iterate wash protocols without blood testing. Results of ELISA testing with multiple wash configurations is shown in Figure 47. Initial whole blood recirculation tests utilized a Tween-20 wash with overnight 5% BSA wash to remove non-covalently bound IL-8. In Gambro AN69 fibers, this wash configuration led to 1820 pg/mL IL-8 concentration. Fresenius fibers led to only 45 pg/mL. The

rate of IL-8 leaching from Gambro fibers led to receptor downregulation in the NERB assay, while Fresenius fibers had no downregulation. High salt washing was evaluated with Gambro fibers, with and without the overnight 5% BSA wash. Washing was conducted both inside and outside of the dialyzer fibers. This wash led to a reduction in IL-8 leaching, but the leaching rate was still significantly higher than the Fresenius rate.

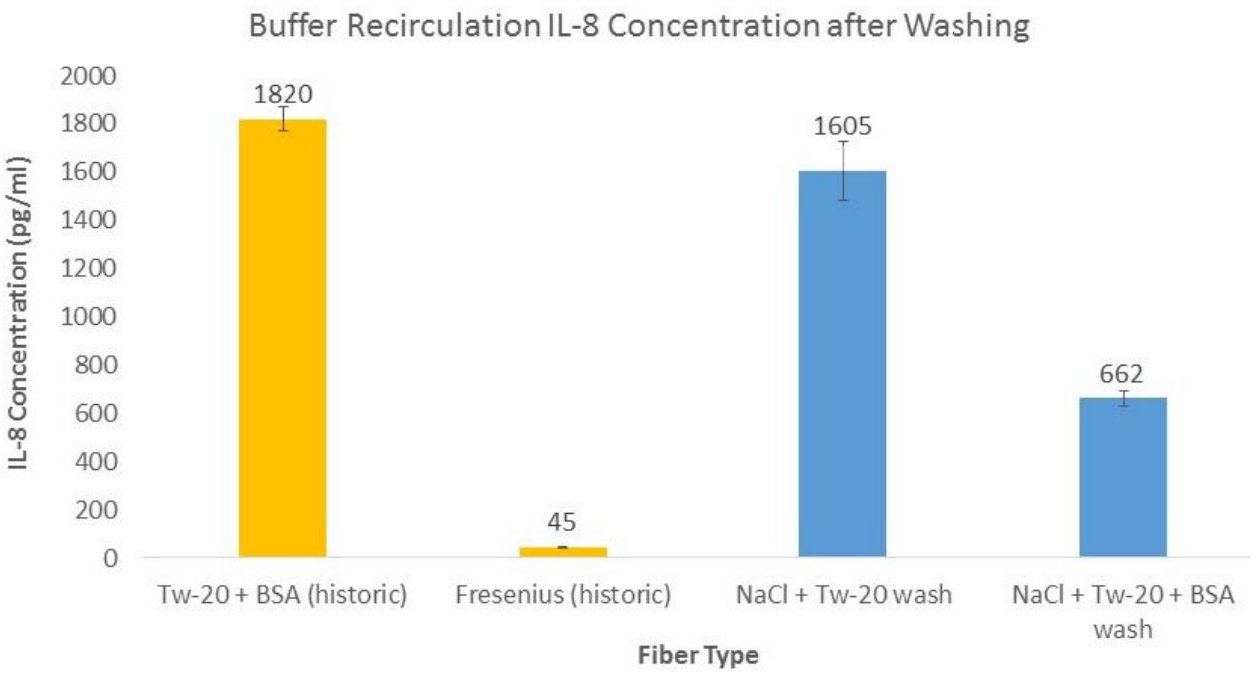

Figure 47. IL-8 concentration in buffered solution after 60 minute recirculation with various wash protocols.

4.4 DISCUSSION

This chapter discusses development of the NeRD module. Multiple device configurations were evaluated and tested using a progression of techniques used to analyze and track device performance. PMP oxygenator fibers and aminated dialyzer fibers provided by Fresenius and

Gambro were each evaluated. Flow cytometry was used to measure CXCR-1 and CXCR-2 downregulation after whole blood recirculation through devices. Additionally, a modified Boyden chamber test was developed to quantify neutrophil chemotaxis after isolation. IL-8 leaching was evaluated using a NERB buffer recirculation assay and IL-8 ELISAs. While advances were made in device performance, no configuration was capable of inducing functionally relevant levels of CXCR-1 and CXCR-2 downregulation while limiting soluble IL-8 leaching.

Early testing attempted to leverage PMP oxygenator fibers with a chitosan spacer, which has been previously used for enzyme immobilization [160]. Testing of monolayer IL-8 immobilizations with a direct glutaraldehyde cross linker showed no IL-8 activity and limited IL-8 loading capacity. Addition of a chitosan crosslinker has the advantage of increasing amine density, offering some flexibility to reduce steric hindrance, and generating a three dimensional structure to facilitate greater IL-8 loading capacity. This approach was only possible on oxygenator fibers, where blood flow is outside the fibers, due to chitosan's high viscosity which would occlude dialyzer fibers. Whole blood recirculation testing of these samples showed CXCR-1/2 downregulation compared to baseline blood in IL-8 module samples. However, the downregulation was present in the albumin control module as well, indicating the immobilized IL-8 was not fully responsible for the downregulation. Chemotaxis testing showed that the observed level of downregulation was unable to cause the intended reduction in migration towards IL-8, actually an increase in migration was observed, potentially due to priming of the neutrophils. As new immobilization techniques were established, development moved towards dialyzer fibers. The dialyzer fibers were hypothesized to leverage neutrophil margination, which potentially increases neutrophil interaction with immobilized IL-8. Dialyzer fibers, with reduced priming volume, also present a higher effective IL-8 presentation due to a higher surface area to volume ratio.

Use of a PEG spacer was adopted in place of chitosan to increased immobilized protein flexibility as well as address potential protein denaturation that can occur with use of glutaraldehyde. The PEG immobilization occurs in aqueous conditions as close to physiological pH, increasing the chances of maintaining protein activity after immobilization. Testing of this immobilization was completed on PMP hollow fibers and dialysis fibers provided by both Fresenius and Gambro. PMP-PEG fibers experienced CXCR-1/2 downregulation in both the IL-8 and albumin control modules. However, unlike the glutaraldehyde immobilization, there was a significant increase in CXCR-2 downregulation in the IL-8 module compared to control (Figure 25). This indicates IL-8 is at least partially responsible for the downregulation. However, chemotaxis testing showed no functional change resulting from this downregulation (Figure 26). These results indicated more protein activity or interaction was required to achieve a functional benefit from the device.

Both Gambro and Fresenius fibers were evaluated with the PEG immobilization. Both fibers are aminated versions of widely used dialysis fibers. Fresenius fibers, with standard Tween-20 and BSA wash protocol, did not register CXCR-1/2 downregulation in the NERB assay. This result was supported by a relatively low IL-8 buffer leach rate of 45pg/ml. These indicate that IL-8 leaching is not an issue with these fibers as the small amount of IL-8 coming off the fibers does not cause significant IL-8 downregulation. These Fresenius fibers generated significantly more CXCR-1 and CXCR-2 downregulation than baseline, with downregulation of 37% and 35% respectively (Figure 29 and Figure 30). However, the hAlbumin control, also induces downregulation compared to baseline, indicating flow conditions, contaminants, or material characteristics of the fiber are also contributing to CXCR-1/2 downregulation. While downregulation is greater than control, the levels do not match the IL-8 positive control, and

Boyden chamber chemotaxis assay results indicate the surface receptor changes did not result in functional changes to neutrophil migration (Figure 31). It is hypothesized that while IL-8 was immobilized on the surface, the quantity and activity were insufficient to achieve migratory shutoff.

Gambro fibers are manufacturing from an acrylonitrile and sodium methallylsulfonate copolymer. These formulation leads to high binding and retention of charged proteins [169]. With the same washing protocol as Fresenius fibers the NERB assay registered significant levels of CXCR-2 downregulation (Figure 36), indicating IL-8 leaching was occurring. ELISA data supported the occurrence of leaching, with an IL-8 concentration of 1820 pg/mL, more than 40 times greater than Fresenius fibers. With leaching, this configuration did induce significant CXCR-1/2 downregulation with whole blood recirculation. One chemotaxis assay registered a pronounced migratory shutoff effect (Figure 34), but a second donor did not replicate this finding (Figure 39), indicating the result is not consistent. Increased washing, with shell side rinsing, extended times, and use of high salt concentration washing could not reduce the leaching rate to a level comparable to the Fresenius fibers which would not register on the NERB assay.

The stop-flow conditions were tested to determine if the flow conditions were limiting neutrophil's ability to interact with immobilized IL-8. Flow of whole blood with shear rates that are similar to physiological post-capillary venules are hypothesized to generate leukocyte margination. With this phenomena, neutrophils and other white blood cells are forced towards the lumen walls by red blood cells. This margination is intended preferentially increase the neutrophil interaction with the wall as well as decreasing cell velocity, allowing more time for neutrophils to interact with immobilized IL-8. However, it is possible that, without integrins co-immobilized on the fiber surface, neutrophils will have difficulty interacting with immobilized IL-8. Intermittently

stopping flow allows for margination to be established, followed by a period of time for neutrophils to intimately interact with the immobilized IL-8. CXCR-1/2 expression results shown in Figure 45 and Figure 46 indicate there is no significant difference between continual and stop-flow. It is possible stop-flow offered a small increase in receptor downregulation due to increased interaction, but this affect would be counteracted by the decrease in whole blood throughput. Further optimization may offer a small increase in total downregulation, but overall the continuous flow condition appears ideal and would be easier to implement in the clinic.

Use of IL-8 to modulate neutrophil behavior is challenging. Low levels of IL-8 exposure (below 50 ng/mL) will activate neutrophils and increase chemotaxis towards IL-8, while high concentrations (100 ng/mL) result in migratory shutoff [170]. The values required for migratory shutoff are three to four orders of magnitude higher than what is expected *in* vivo, even for septic patients [157]. This indicates even low levels of CXCR-1/2 expression on receptors may be enough to result in migration towards IL-8. Achieving such high effective levels of IL-8 concentrations without any IL-8 leaching is challenging, particularly due to decreases in IL-8 activity after immobilization. The following chapter, on alternate approaches attempts to address these limitations with alternate device concepts.

In conclusion, a variety of potential configurations were evaluated to construct a neutrophil reprogramming device. This device is hypothesized to cause CXCR-1/2 downregulation and desensitization to reduce neutrophil migration towards IL-8 using immobilized IL-8 within the extracorporeal device. Fiber material, immobilization chemistry, wash protocol, and flow parameters were all adjusted in an attempt to find a combination with sufficient IL-8 activity to cause the desired results. However, no configurations were able to generate sufficient IL-8 activity to cause the desired effects. In the next chapter alternate device configurations which attempt to address the shortcomings of the current approach will be discussed.

5.0 ALTERNATIVE CONCEPTS FOR EXTRACORPOREAL TREATMENTS OF SEPSIS

Testing and evaluation of the NeRD device, described in the previous chapter, provided information about the advantages and limitations of an extracorporeal system to modulate leukocyte behavior. Among the advantages highlighted in the previous chapter, such a system potentially offers the ability to alter white blood cell behavior in a well control-microenvironment, preventing side effects associated with systemic delivery of pharmaceuticals. However, while evaluating the system with IL-8 immobilization, it became clear that achieving high levels of activity with an immobilized ligand would be challenging. This chapter describes some alternative approaches which may leverage the systems advantages and address the limitations. Only preliminary testing of these approaches has been completed and the discussion will focus on potential future testing and device concepts.

5.1 METHODS

5.1.1 Adsorptive column

A recirculation flow loop was constructed as described in 4.2.3. An additional unaminated control minimodule with 25 AN69 fibers was added immediately downstream of the protein modified module. The portion of the loop with modules in series is shown in **Error! Reference source not ound.**. ELISA testing (Section 4.2.5) as well as buffer and whole blood recirculation testing (4.2.7 and 4.2.8) were completed to evaluate this setup for IL-8 leaching and ability to modulate neutrophil behavior.

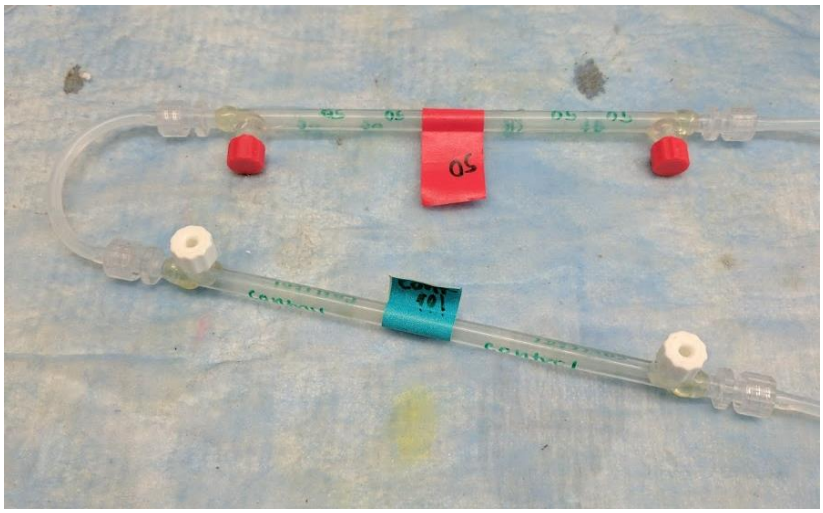

Figure 48. Adsorptive AN69 column in series with protein modified module.

5.1.2 Adsorptive column construction

Packed bead columns were evaluated in place of the AN69 fiber columns to remove leaching IL-8. Columns with 1ml volume were packed with Cytosorb adsorbent beads (Cytosorbents, Monmouth Junction, NJ). A fine mesh was secured on the inlet and outlet to prevent beads from leaving the column. As shown in **Error! Reference source not found.**, luer connectors on either nd of the column allow for the column to be incorporated into the recirculation loop.

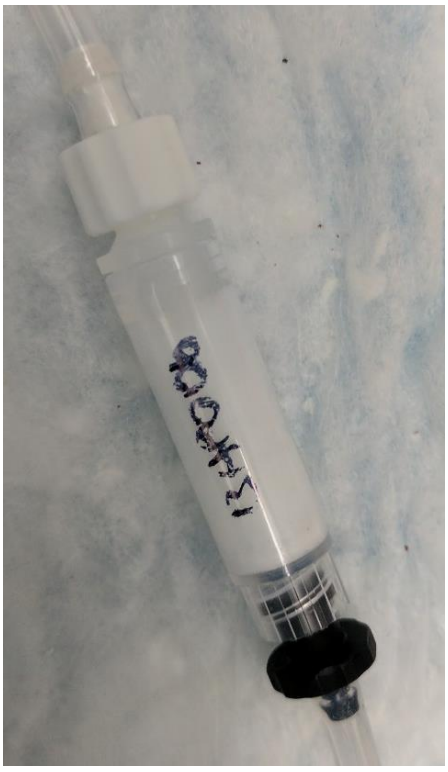

Figure 49. Packed bead column filled with adsorptive beads.

5.1.3 Infusion / Adsorption device configuration

An alternative device configuration relies on a constant infusion of IL-8 into a secondary reservoir, where IL-8 interacts with neutrophils within the extracorporeal circulation, before being removed by an adsorptive column. This loop configuration is shown in Figure 50. After the recirculated fluid is removed from the primary reservoir, a T-junction facilitates infusion of IL-8. An infusion pump with 1 mL syringe slowly infuses IL-8 solution at a rate of 20ng/ml/hr. The secondary reservoir consists of a tube with 1 mL volume which contains a static mixer. A packed bed column is at the outlet of the secondary reservoir to remove infused IL-8 before returning to the primary reservoir. This configuration is evaluated using ELISAs, NERB buffer recirculation, and recirculation with pre-isolated neutrophils resuspended in DPBS.

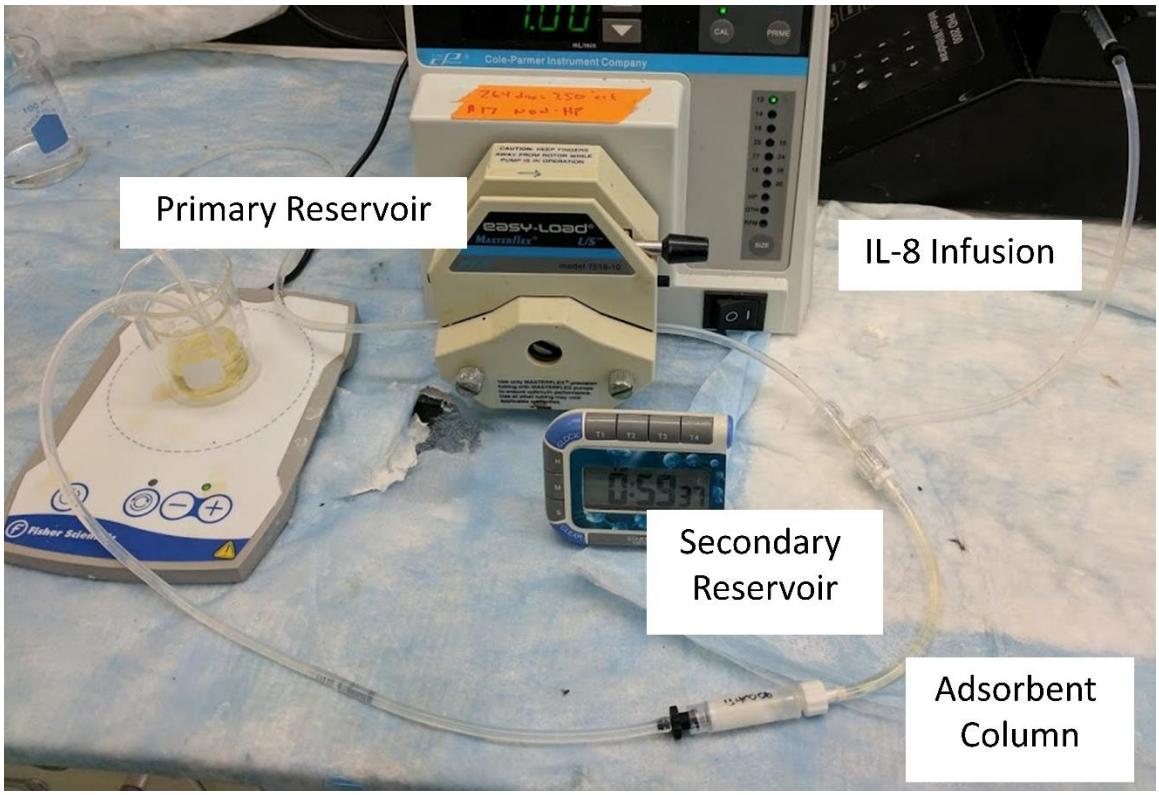

Figure 50. Infusion adsorption recirculation test loop.

5.2 RESULTS

5.2.1 Adsorptive column

Addition of an adsorptive scavenging module, in series with an IL-8 immobilized Gambro-PEG fiber module, significantly reduced effective IL-8 leaching. An IL-8 ELISA with this configuration showed that the leaching rate dropped from 1820 to 32 pg/mL after a 60 minute recirculation. This value is equivalent to the IL-8 leaching rate present in the Fresenius-PEG IL-8 immobilized fibers. These results are shown in Figure 51.

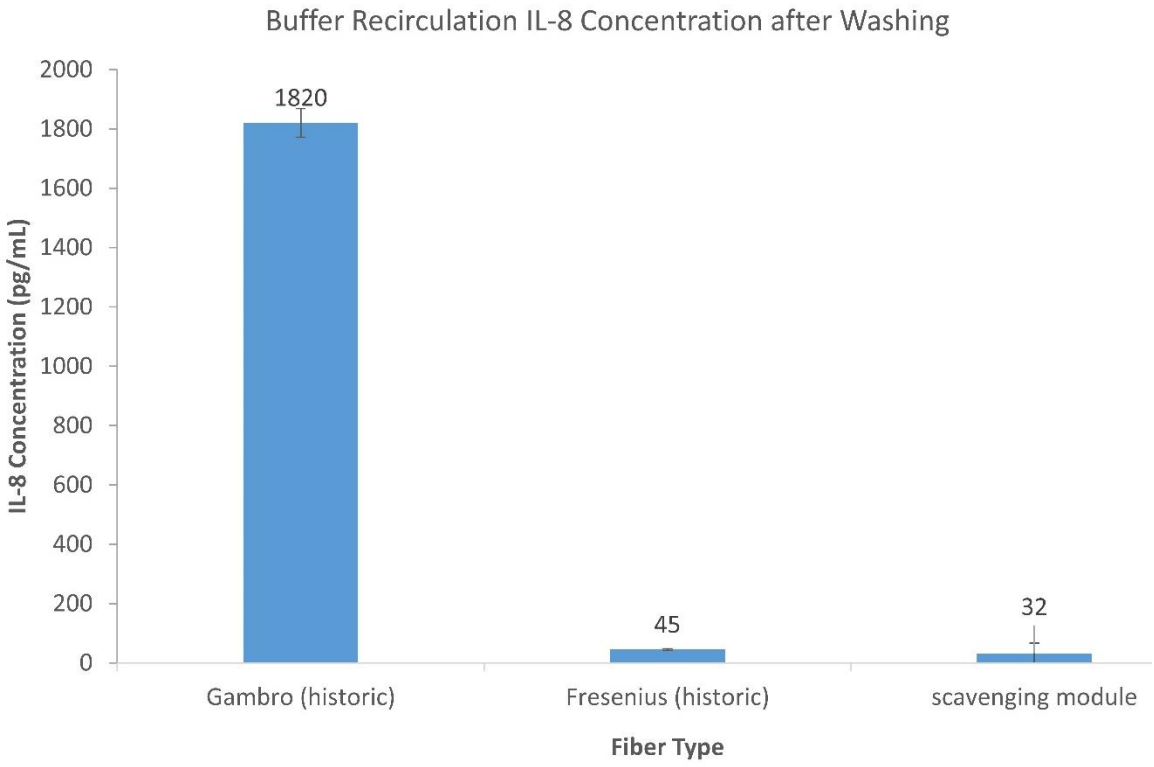

Figure 51. IL-8 leaching with inline scavenging module.

NERB buffer recirculation testing supported the low IL-8 leaching rate measured using the ELISA assay. As shown in Figure 52 and Figure 53, CXCR-1 and CXCR-2 downregulation was minimal in neutrophils combined with buffer from IL-8 and hAlbumin modified devices when scavenging modules were used in series.

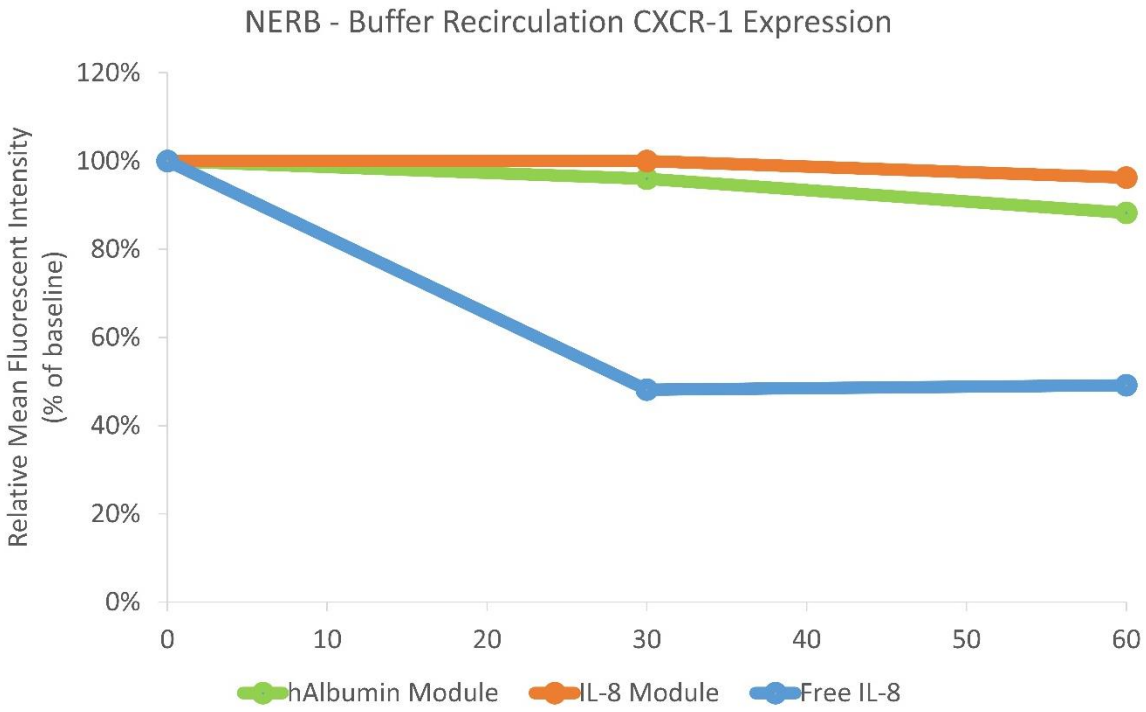

Figure 52. NERB buffer recirculation results showing neutrophil CXCR-1 expression after exposure to buffer circulated through modified aminated Gambro AN69 fibers with inline scavenging module.

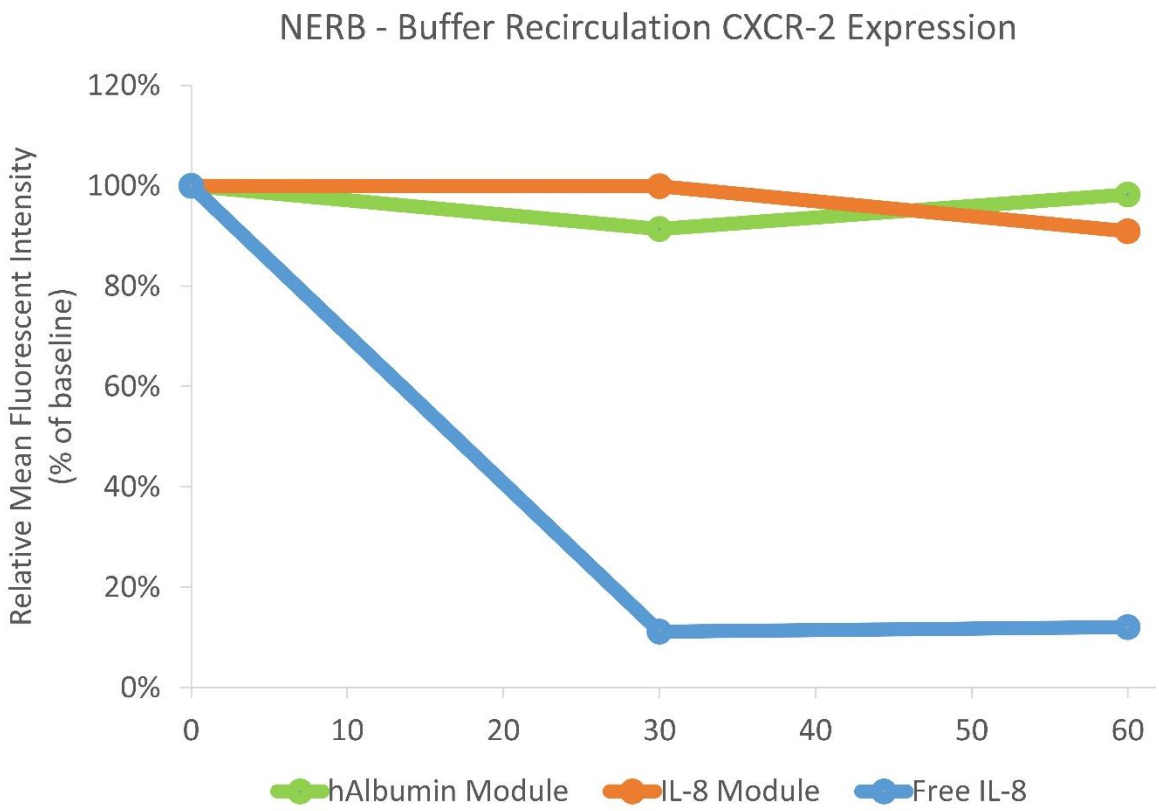

Figure 53. NERB buffer recirculation results showing neutrophil CXCR-2 expression after exposure to buffer circulated through modified aminated Gambro AN69 fibers with inline scavenging module.

Whole blood recirculation CXCR-1/2 receptor expression are shown in Figure 54 and Figure 55. The free IL-8 positive control induces substantial CXCR-1/2 downregulation, which remains consistent from 60 minutes through the neutrophil isolation process. The hAlbumin module CXCR-1/2 expression remains comparable to baseline blood throughout the entire experiment. The IL-8 module induced 42% and 44% CXCR-1 and CXCR-2 downregulation respectively at 60 minutes. However, these values returned to near baseline blood during neutrophil isolation.

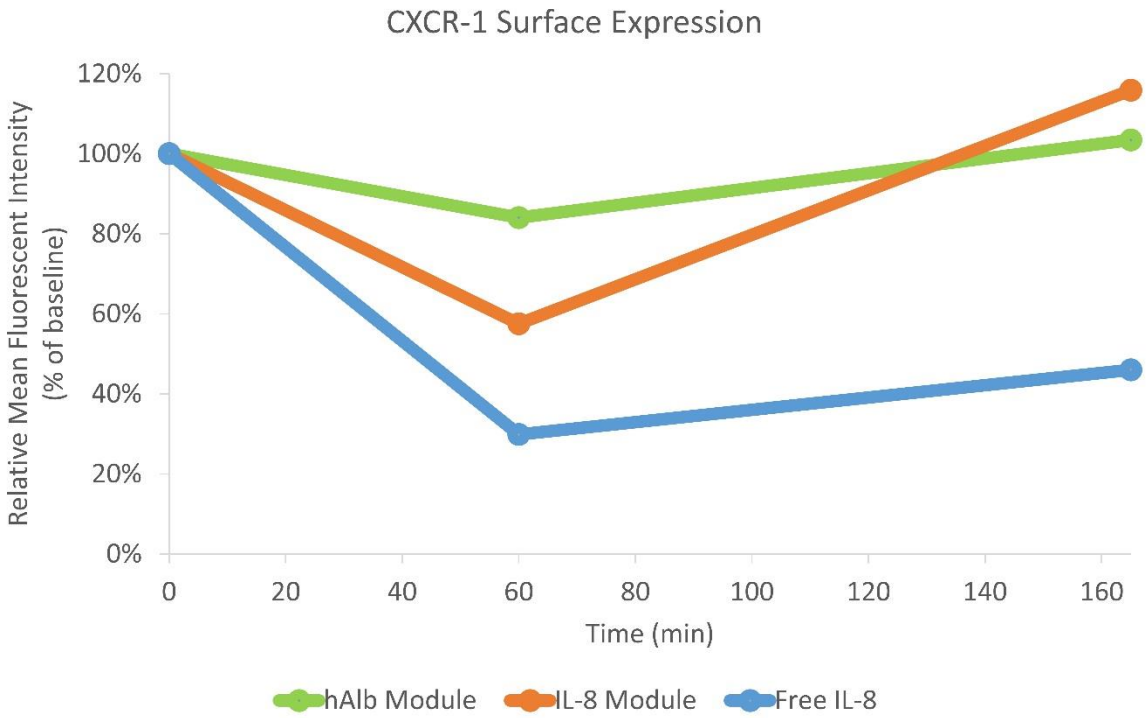

Figure 54. Neutrophil CXCR-1 expression after whole blood recirculation through modified aminated Gambro AN69 fibers with inline scavenging module.

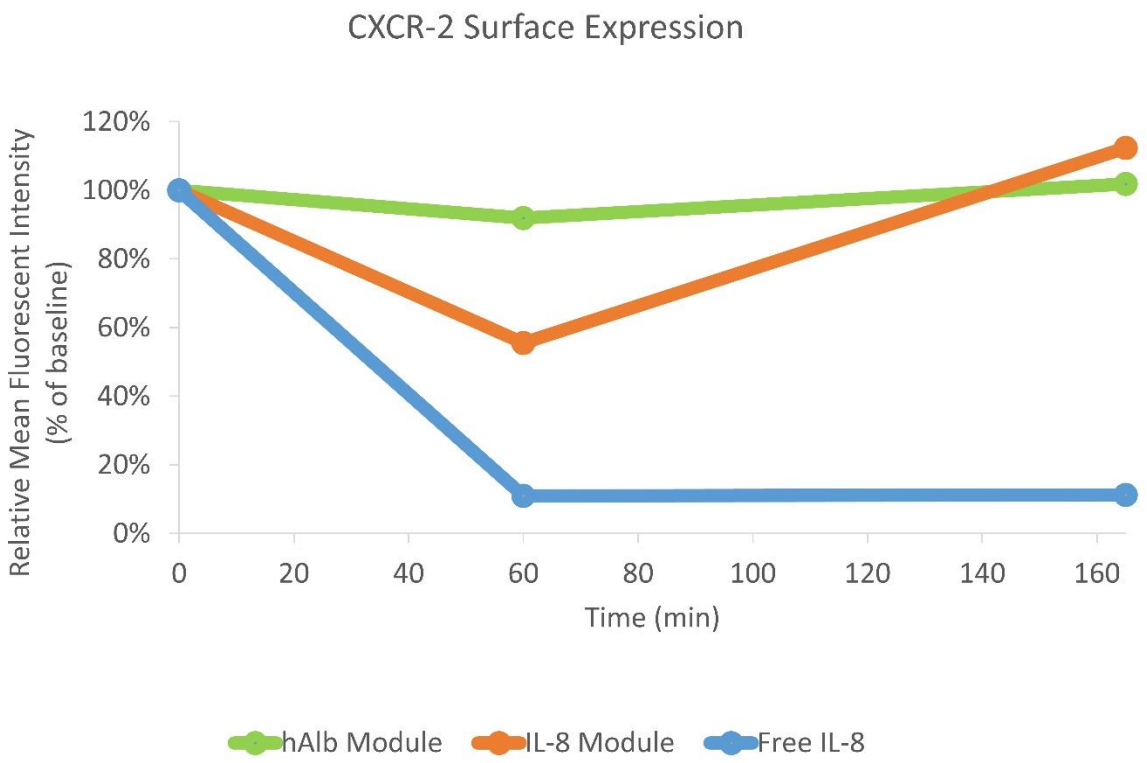

Figure 55. Neutrophil CXCR-2 expression after whole blood recirculation through modified aminated Gambro AN69 fibers with inline scavenging module.

Boyden chamber chemotaxis assay results (show free IL-8 treated neutrophils exhibit reduced migration towards 5nM IL-8 and GRO-α, but maintained migration to other chemoattractants compared to baseline. hAlbumin and IL-8 module treated samples exhibited migration comparable to baseline blood.

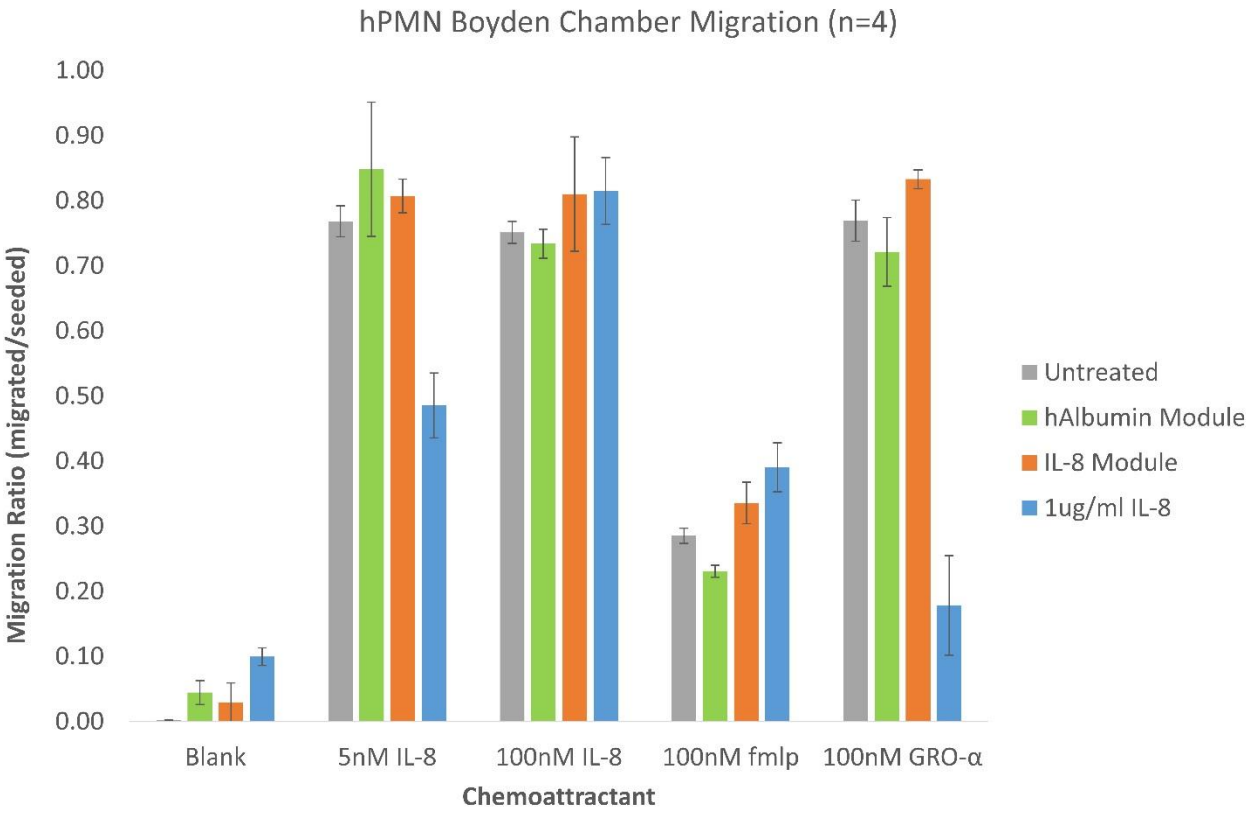

Figure 56. Neutrophil migration in Boyden chamber chemotaxis assay after recirculation through modified Gambro AN69 fibers in series with a scavenging module.

5.2.2 Infusion/Adsorption

The infusion adsorption testing replaced the IL-8 modified module with an infusion of soluble IL-8 which is removed from by either an unmodified AN69 fiber module or column of packed Cytosorb beads. IL-8 ELISA testing was used to determine which removal technique was most effective. Data indicated both the AN69 and Cytosorb columns removed large amounts of infused IL-8, but the Cytosorb column more effectively removed IL-8 at 30 minutes, with undetectable levels of IL-8 in solution compared to 236 pg/mL in the AN69 column. At 60 minutes AN69 column IL-8 levels decreased to 111 pg/mL and the Cytosorb column increased to 150 pg/ml, as shown in Figure 57.

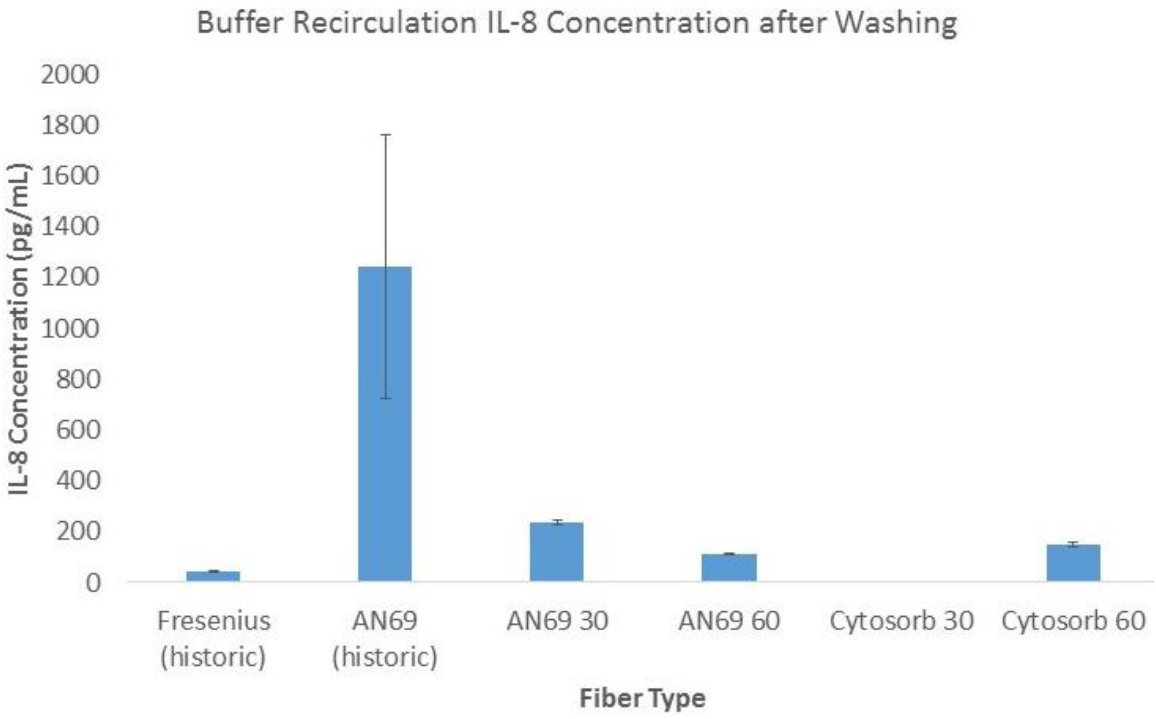

Figure 57. ELISA results of IL-8 infusion adsorption loops with either AN69 or Cytosorb bead columns for IL-8 removal. Historic results of IL-8 leaching in immobilized columns is also included.

Infusion adsorption recirculation testing was completed with a 20 ng/ml/hr IL-8 infusion rate and Cytosorb adsorptive columns. NERB data, shown in Figure 58 and Figure 59, indicated CXCR-1/2 downregulation was occurring in both IL-8 infusion and control infusion loops. IL-8 infusion CXCR-1/2 downregulation was greater than the infusion control at 30 minutes, but the two samples were reached equivalent levels of downregulation at 60 minutes.

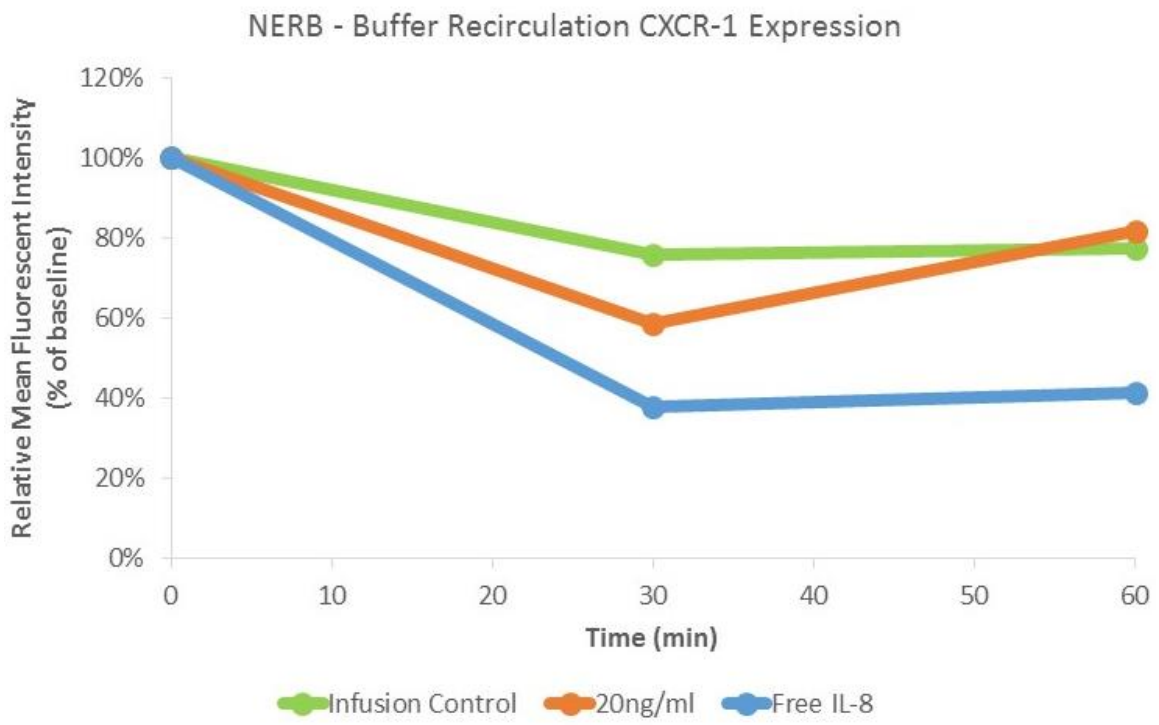

Figure 58. NERB buffer recirculation results showing neutrophil CXCR-1 expression after exposure to buffer circulated through IL-8 infusion or control infusion loops with Cytosorb columns.

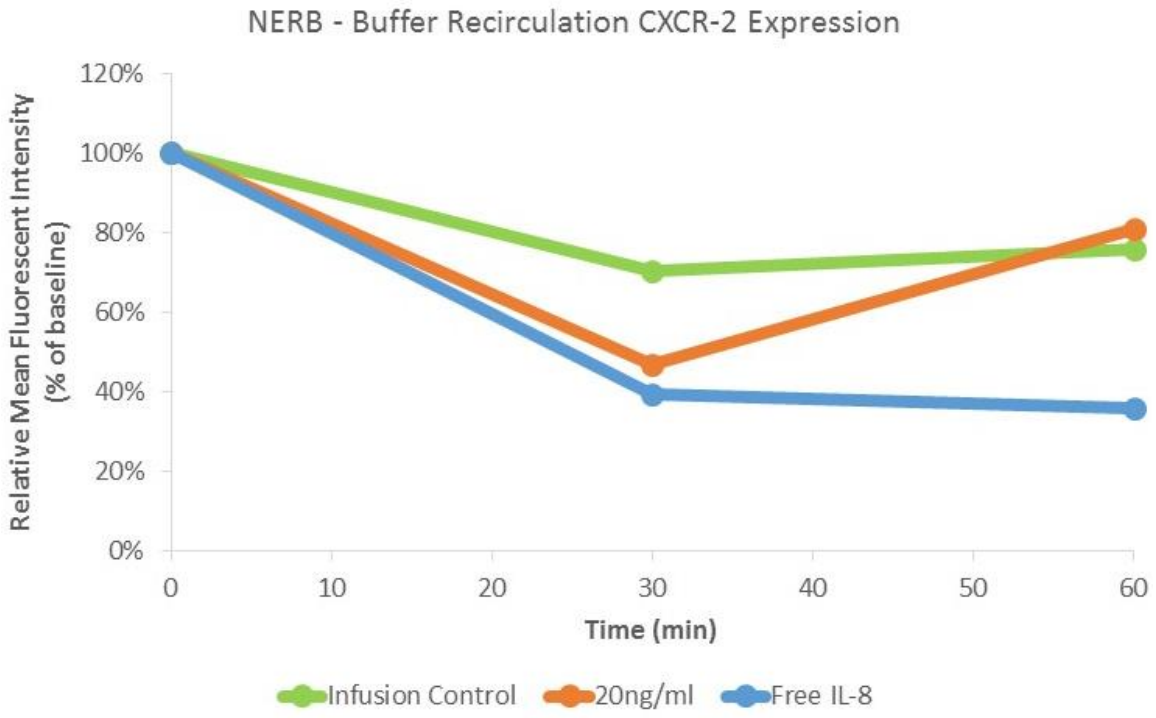

Figure 59. NERB buffer recirculation results showing neutrophil CXCR-2 expression after exposure to buffer circulated through IL-8 infusion or control infusion loops with Cytosorb columns.

Isolated neutrophils were circulated through infusion adsorption loops for 60 minutes. No CXCR-1/2 downregulation was observed in these samples compared to control. A small increase in CXCR-1/2 expression was present in these samples at 60 minutes, potentially indicating neutrophil priming or activation. These findings are shown in Figure 60 and Figure 61.

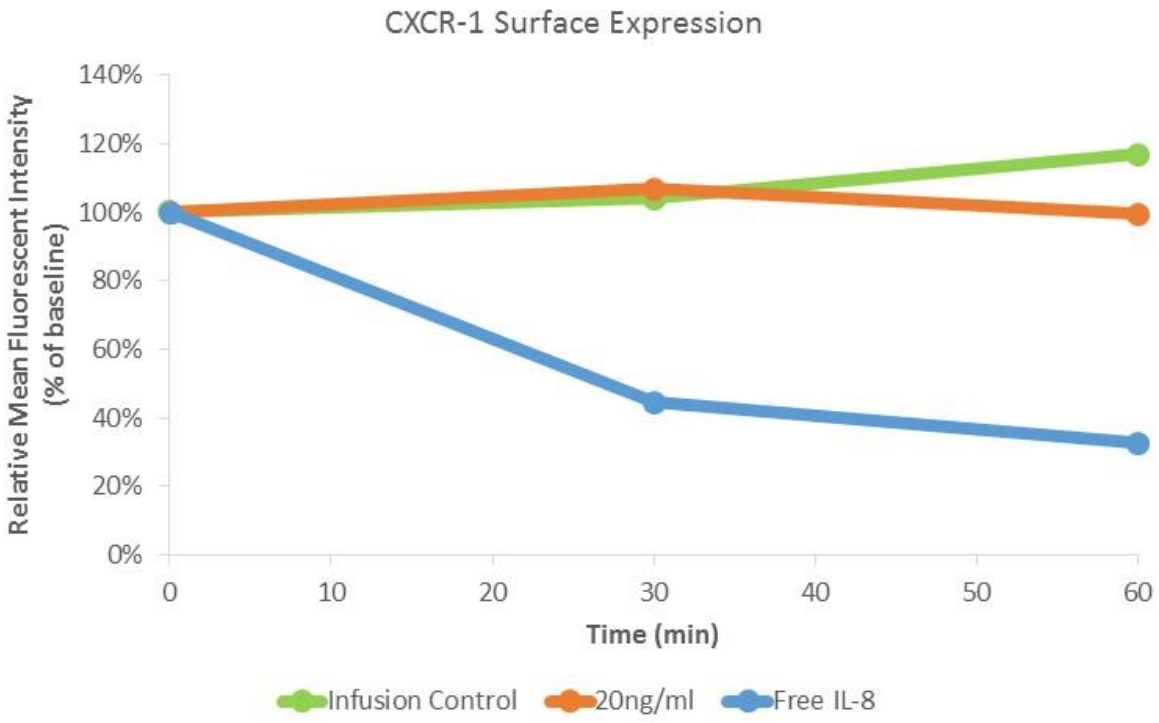

Figure 60. Neutrophil CXCR-1 expression after whole blood recirculation through recirculation loops with IL-8 infusion and Cytosorb adsorptive columns.

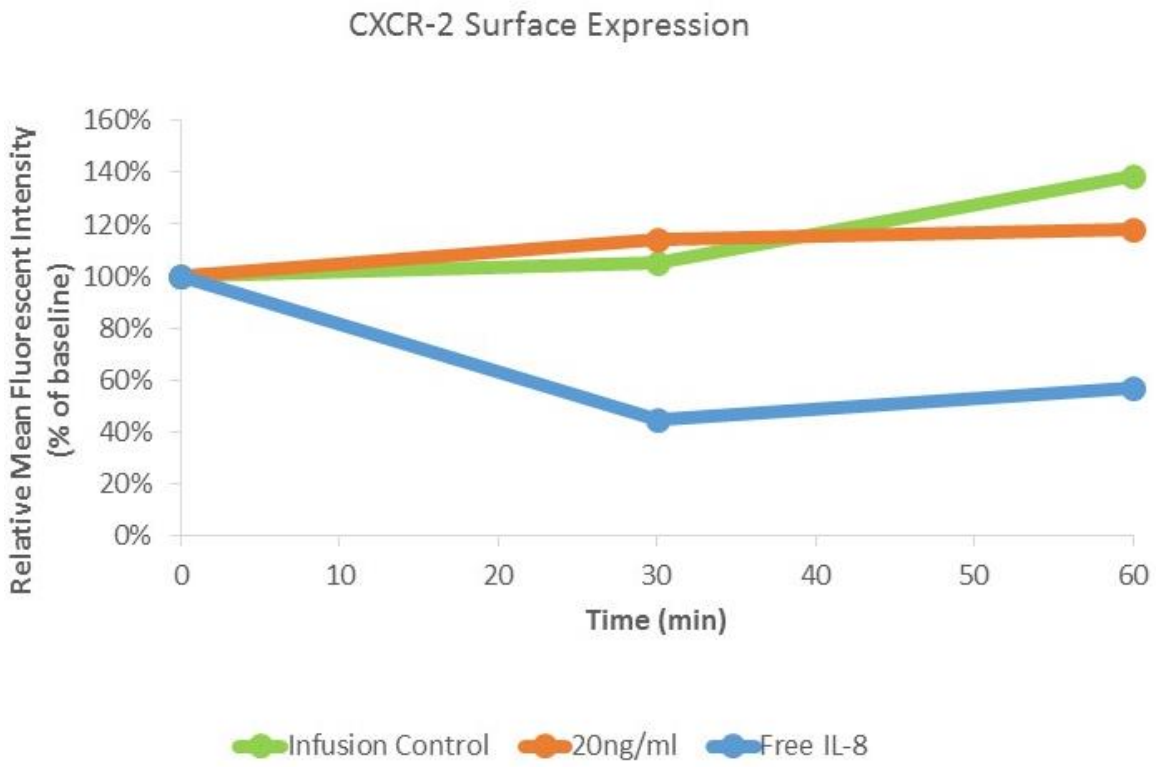

Figure 61. Neutrophil CXCR-2 expression after whole blood recirculation through recirculation loops with IL-8 infusion and Cytosorb adsorptive columns.

Boyden chamber chemotaxis results (Figure 62) indicate the expected neutrophil behavior in untreated baseline blood and free IL-8 positive control. However the infusion control and IL-8 infusion samples show increased chemotaxis. This is particularly evident in infusion control samples, which show increased chemotaxis towards all chemoattractants.

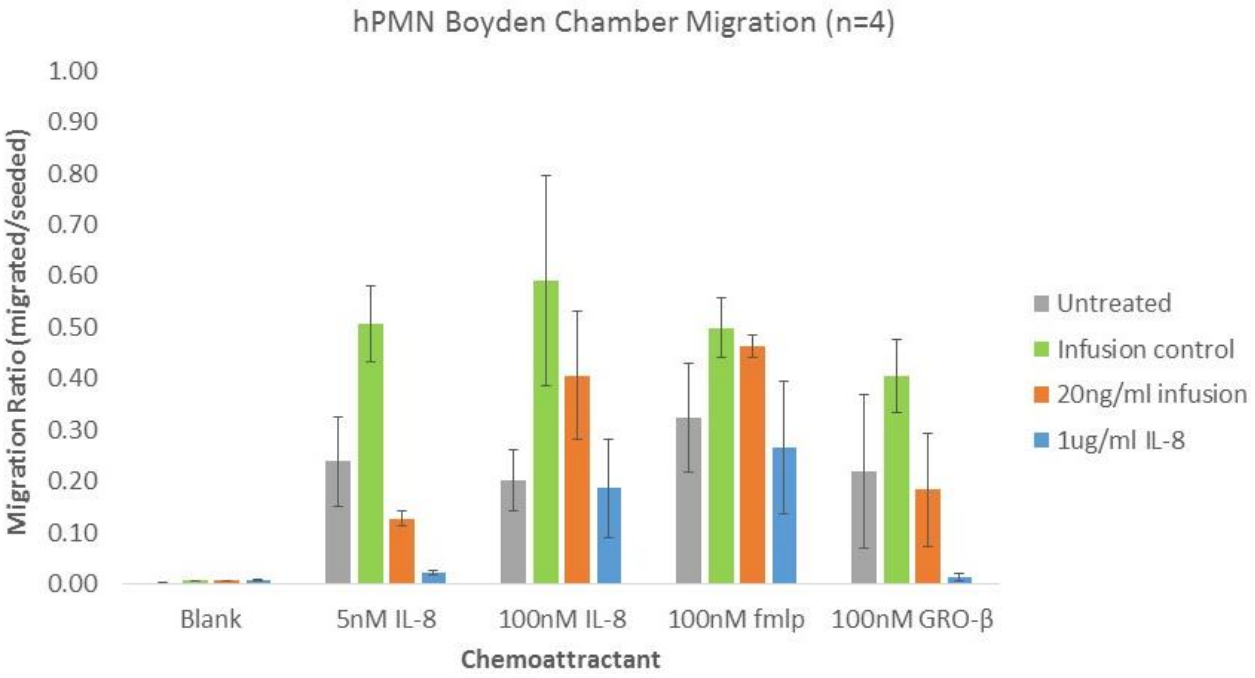

Figure 62. Neutrophil migration in Boyden chamber chemotaxis assay after recirculation through recirculation loops with IL-8 infusion and Cytosorb adsorptive columns.

5.3 DISCUSSION

This chapter discusses alternate approaches and future steps to modulate neutrophil behavior within an extracorporeal circuit. These techniques intend to build off the findings of the previous studies. Preliminary testing was completed for the techniques which relied on an absorptive column to remove unbound IL-8. Other concepts, which do not include preliminary data, will be discussed below. The preliminary data shows that it is possible to generate CXCR-1/2 downregulation using a combination of immobilized IL-8 column in series with an absorptive column, but Boyden chamber chemotaxis results indicate the level of downregulation is not significant enough to generate migratory shutoff. Further studies are required to optimize the

infusion/adsorption test setup, but preliminary results indicate that the required infusion rate of IL-8 would be higher than the adsorptive column capacity. Use of alternate ligands to generate different neutrophil behaviors should be explored to address some of the current device's limitations.

Testing in the previous chapter showed that PEG-IL-8 immobilization on Gambro AN69 fibers exhibited significant CXCR-1/2 downregulation, but IL-8 leaching could not be completely eliminated. Removal of all unbound IL-8 is extremely difficult due to charged sulfonate groups designed to bind highly charged middle molecular weight proteins such as IL-8. Due to leaching, it was difficult to differentiate downregulation induced by immobilized IL-8 from leached soluble IL-8. Testing in this chapter, with addition of a scavenging module in series is able to differentiate the source of this downregulation by leveraging the charged protein binding characteristics of AN69 fibers. ELISA results show more than 20x reduction in leached IL-8; reducing leaching to a level that does not induce CXCR-1/2 downregulation. Whole blood recirculation with this configuration results in measurable CXCR-1/2 downregulation at 60 minutes, but the neutrophils fully recovered during the neutrophil isolation process. Unsurprisingly, these fully recovered neutrophils did not show any change in migratory behavior. This is the first instance where CXCR-1/2 recovery of such magnitude was observed. It is possible that other instances, where downregulation remained constant through isolation, were able to maintain receptor levels due to low levels of leached IL-8 which were in solution during isolation. During the isolation process, neutrophils remain in their initial solution until near the end of the process, meaning any soluble IL-8 remain in solution until the final resuspension. While neutrophil surface receptor recovery makes functional testing difficult, fast recovery may be beneficial in a potential device due to its rapid reversibility.

Both unmodified AN69 fiber modules and Cytosorb bead columns were evaluated for IL-8 removal. Both established their ability to remove significant amounts of infused IL-8 through ELISA testing with the IL-8 infusion setup. Infusion adsorption testing was completed using Cytosorb bead columns because of their higher theoretical loading capacity. Not only does a packed bead column have a higher overall surface area than fiber module of similar priming volume, but Cytosorb beads have a porous structure, allowing proteins like IL-8 to penetrate the beads. AN69 fibers may have similar a similar microstructure within their pores, but the fiber's primary purpose is solute transport, not adsorption. Either column has limitations to total protein loading capacity, limiting IL-8 infusion rate. Testing with elevated IL-8 infusion rates led to IL-8 levels in solution above the leaching rate of AN69 fibers, which is known to trigger CXCR-1/2 downregulation in the NERB assay. The Cytosorb beads used for evaluation were taken from samples previously provided to the lab at an unknown time, and may have degraded over time. NERB results from the infusion control (Figure 58 and Figure 59), which induce downregulation, indicate the beads may have had a contaminant or pathogen which caused neutrophil activation. This contaminant may have counteracted effects of the IL-8 infusion. This testing should be repeated once fresh Cytosorb columns are obtained.

Many of the challenges of this approach are a result of the elevated IL-8 levels necessary to achieve receptor downregulation and desensitization. While these levels are much easier to obtain in free solution than immobilized on a surface, removing all soluble IL-8 difficult, particularly if a simple, single pass, system is desired. The infusion adsorption system can be altered in a number of way to improve efficacy. First infusion rate can be increased, requiring a larger adsorption column. The current infusion rate of 20 ng/ml/hr or 200 ng/mL over the hour long recirculation, are significantly lower than the 1 ug/mL IL-8 which is added to the free IL-8

positive control. Increased IL-8 infusion will require a scaled increase in adsorptive column surface area. The adsorptive column size in addition to cost of infused IL-8 provide commercialization challenges if this approach were scaled up. Another approach to increasing performance is increasing secondary reservoir volume, modulating flow rate, or introducing periods of no flow to increase dwell time. The 1 mL secondary reservoir leads to an average dwell time of only 1 minute. A larger reservoir may increase IL-8 interaction with neutrophils, increasing device performance.

Considering many of the device issues are related to use of IL-8, it is worth considering use of alternate ligands in its place. While desensitization generally requires high concentrations of the target ligand, which would lead to similar challenges, the systems designed in this dissertation would apply to direct receptor signaling. Generally cytokine signaling functions at pico to nano-molar concentrations, rather than micro molar concentrations required for desensitization. The approaches discussed can be used to prevent delivery of the ligands to systemic circulation, preventing adverse effects and increasing the ability to reverse and stop treatment. For example, use of lipoxin A4 (LXA4) may reduce neutrophil chemotaxis and facilitate resolution of inflammation [171,172]. Other cytokines, or even low exposures of IL-8, can be used to prime and stimulate neutrophils to increase chemotaxis for patients suffering from immunoparalysis. Further exploration of alternate ligands should be completed to determine potential targets that can influence leukocytes in the extracorporeal circuit, but would benefit from limited introduction into systemic circulation.

6.0 ZWITTERIONIC SURFACE TREATMENT OF POLYMETHYLPENTENE HOLLOW FIBER MEMBRANES FOR RESPIRATORY ASSIST

The following chapter includes work from a manuscript draft titled *Development of Zwitterionic Sulfobetaine Block Copolymer Conjugation Strategies for Reduced Platelet Deposition in Respiratory Assist Devices*. It has been submitted to *Langmuir* and is currently under review.

All extracorporeal devices, particularly those with large surface (e.g. artificial lungs), increase the risk of thrombotic complications. Novel surface coatings, such as zwitterionic sulfobetaine (SB) will help minimize this risk. However, functionalization of the PMP fiber surface and development of conjugation chemistry is required to implement this coating. The Medical Devices Lab and collaborators have previously developed techniques to amine functionalize materials, specifically polypropylene (PP) and polymethylpentene (PMP) oxygenator fibers, using plasma vapor deposition with allylamine [161,173]. This discusses a new method to hydroxyl functionalize materials using oxygen plasma vapor deposition and implement an SB surface coating. Zwitterionic surface coatings were evaluated on PMP fibers to determine stability of complete coatings under device flow conditions. After further development of PMP coated hollow fibers, future work may adapt these surface coatings to other blood contacting device such as the NeRD.

6.1 INTRODUCTION

Balancing required blood anticoagulation while maintaining adequate levels of hemostatic activity is a major challenge that presents with a wide variety of blood contacting medical devices. This issue is particularly challenging in extracorporeal circuits such as respiratory assist devices, which expose patient blood to large surface areas (~2 m^2) of synthetic material [174–178]. Blood contact with these artificial surfaces results in activation of the coagulation cascade, and platelet deposition onto the foreign surfaces [179,180], leading to reduced device performance and emboli formation [181–183]. Additionally, prolonged support may deplete the patient of critical coagulation factors and reduce platelet numbers, causing systemic hemostatic issues [184,185]. Physicians manage these thrombotic challenges with use of anticoagulants, most commonly systemic administration of heparin. However excess anticoagulation, particularly when administered systemically, may cause bleeding problems [186,187]. In fact bleeding issues are the most common complication in extracorporeal membrane oxygenation (ECMO), occurring in between 10-30% of cases, and the thrombotic complications that anticoagulation is meant to blunt, commonly lead to reduced device lifespan [182,187–189]. The risks associated with limited device blood biocompatibility and the pharmacologic interventions utilized to address this limitation clearly restrict the broader adoption of life saving extracorporeal therapies.

A great deal of effort has been directed at improving the hemocompatibility of extracorporeal circuits, by better pharmacologic management, more efficient circuit design and improved surfaces. These advances have led to broader use of dialysis and increasing use of ECMO and respiratory dialysis, particularly for low flow CO_2 removal [174,183,190–192]. ECMO and respiratory dialysis devices utilize gas permeable hollow fiber membranes (HFMs) to add oxygen and remove carbon dioxide from blood independent of the lung. Innovations in HFMs, such as the

introduction of polymethylpentene (PMP) HFMs in oxygenators, have facilitated extended patient support periods by preventing plasma leakage into the fiber lumen, which was common in older generation, porous wall polypropylene fibers [193]. PMP fibers greatly extended the circuit life of the oxygenator by resisting plasma leakage, but thrombotic deposition on fiber surfaces remained as a problem. Local anticoagulation using citrate is a potential solution, but it requires a more complex loop, restricted flow rates and its use is not widespread [194,195].

Surface modification of synthetic fiber materials provides a potential resolution to the coagulation dilemma. Direct coating of the fiber may allow for local inhibition of thrombotic deposition, reducing the need for systemic anticoagulation and the resulting complications for the patient. Heparin coating of blood-contacting surfaces in extracorporeal perfusion circuits is common, but it is debatable as to the how much this surface modification has resulted in clinical benefit [196]. Surface conjugation of polymers bearing zwitterionic groups (e.g. phosphorylcholine, sulfobetaine (SB), carboxybetaine) have been described and examined as anti-fouling, non-thrombogenic and anti-bacterial materials [197–200], but many of these approaches are limited by cost and stability [201–203]. Given the potential for zwitterionic surface modification to provide improved hemocompatibility in many instances, development of new surface modification strategies using this basic concept are warranted where durability and cost efficiency are design features.

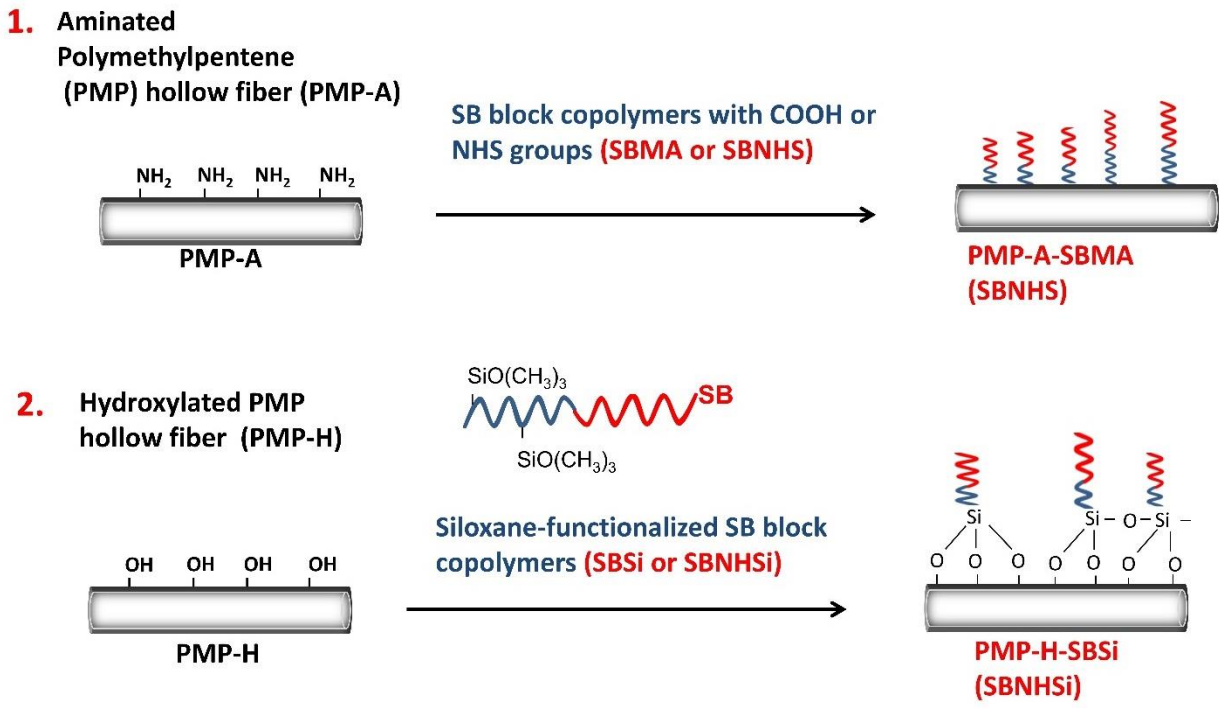

Figure 63. Approaches for pre-functionalization of PMP hollow fibers & post-conjugation of SB molecules.

In this chapter, a new SB block copolymer with *N*-hydroxysuccinimide ester groups (SBNHS) was synthesized to simplify conjugation to functionalized PMP HFMs. Two coating strategies, which pair PMP surface functionalization and zwitterionic molecule conjugation, were developed and evaluated. The first strategy employs plasma-enhanced chemical vapor deposition (PECVD) to generate amine functional groups on the PMP fiber surface that are subsequently conjugated to functional SB block copolymers, building upon our previous work with PP fibers [162]. A second strategy utilized surface hydroxylation [204] to conjugate an SB block copolymer with siloxane groups (Figure 63). The zwitterion-modified PMP surfaces were evaluated for acute thrombotic deposition, surface modification stability under anticipated shear flow conditions, and for the impact of the surface modification on gas exchange performance. These coatings address the shortcomings of currently available alternatives as they are stable under high fluid shear stress,

do not inhibit membrane transport, and employ economically attractive SB moieties as opposed to phosphorylcholine. This study evaluates the coatings for use specifically in respiratory assist devices, but the coatings are shown to be effective on several clinically relevant materials.

6.2 MATERIALS AND METHODS

6.2.1 Materials

Commercially available polymethylpentene hollow fibers (Oxyplus™; OD: 380 μm, ID: 200 μm) were obtained from Membrana GmbH (Wuppertal, Germany). N-(3-Sulfopropyl) -N-(methacryloxyethyl)-N,N-dimethylammonium betaine (SMDAB) monomer, Acrylic acid N-hydroxysuccinimide ester (AANHS), 4-Cyano-4-(phenylcarbonothioylthio) pentanoic acid (CPPA as a chain transfer agent), 4,4′-azobis(4-cyanopentanoic acid) (V-501) (ACPA, initiator), 3-aminopropyl-trimethoxysilane (APSi), N-(3-Dimethylaminopropyl)-N′-ethylcarbodiimide hydrochloride (EDC), N-Hydroxysuccinimide (NHS), 2,2,2-trifluoroethanol (TFE), and buffer reagents were purchased from Sigma-Aldrich. Methacrylic acid (MA, Sigma-Aldrich) was distilled before its use. [Sulfo-succinimidyl-4-O-(4,4´-dimethoxytrityl)-butyrate] (Sulfo-SDTB) was purchased from prochemonline. Bovine blood was freshly harvested from a local slaughterhouse and anticoagulated with heparin. Gentamycin (0.1g/mL) was added and blood was filtered (Haemonetics SQ40s 40 μm transfusion filter) to remove particulates. PBS was added to adjust hemoglobin to 12 ± 1 g/dL and glucose was adjusted to 10 mmol/dL ± 5 mmol/dL according to ISO 7199:2009.

6.2.2 Synthesis of SB block copolymers with functional groups

SB block copolymers with functional groups (COOH or NHS) were synthesized using a standard reversible addition fragmentation chain transfer (RAFT) polymerization technique previously described [162]. Briefly, after being dissolved in TFE solvent, SB prepolymer was synthesized from SMDAB monomer, CPPA chain transfer agent (CTA) and V-501 (ACPA) initiator at a determined molar ratio (SMDAB: CTA: ACPA= 10:1:0.5) to yield SB-CTA. Argon gas was bubbled into the solution for 30 min to remove oxygen, then the solution was sealed under argon for the duration of the synthesis. After stirring for 15 h at 70°C, the synthesized product was precipitated into anhydrous methanol. The obtained pink gel-like product (SB-CTA prepolymer) was further rinsed with excess methanol and dried in a vacuum oven for 24 h. Next, macro SB-CTA and MA or AANHS monomer was dissolved in TFE at a predetermined molar ratio (SB-CTA:MA=1:10 for SBMA, SB-CTA: AANHS=1:10 for SBNHS). After adding ACPA initiator and bubbling argon gas into the solution for 30 min, the reaction mixture was stirred for 15 h at 70°C. Following precipitation in anhydrous methanol, centrifugation, and rinsing to remove unreacted reagents, the synthesized SBMA or SBNHS block copolymers were obtained after vacuum drying. The siloxane functionalized SB block copolymers (SBSi or SBNHSi) were also prepared from the block copolymers after reaction with APSi via a standard EDC/NHS conjugation technique [162,205].

6.2.3 PMP fiber functionalization and characterization

6.2.3.1 Hollow fiber functionalization

Unmodified polymethylpentene (PMP) hollow fiber membranes were either amine or hydroxyl functionalized using plasma enhanced chemical vapor deposition (PECVD) with a PVA TePla Ion 40 system. Amine functionalization was completed according to a technique established by Arazawa et al [163]. Briefly, hollow fiber membrane samples, in a mat format, were cut to size (102 cm^2), washed with 0.5% Tween-20 in 100 mM phosphate buffer pH 8.5, then rinsed with deionized water. Upon adding samples, the chamber was evacuated to 50 mTorr. Allylamine was introduced to the chamber at a rate of 180 mL/min and 300 W of power at 150 Hz and a 20% duty cycle was introduced for times ranging from 1 (A1) to 5 min (A2). Samples were removed and immediately rinsed three times with 0.5% Tween-20 in 100 mM phosphate buffer pH 8.5 then thoroughly rinsed with deionized water. Hydroxyl groups were generated using oxygen plasma[204]. PMP hollow fiber samples were prepared in a similar manner to amine functionalization, but after establishing 50 mTorr in the chamber, oxygen was added to the chamber at 500 mL/min then powers ranging from 100-600 W at 150 Hz and 20% duty cycled was applied for 30-300 sec. Additional materials, including polycarbonate sheet (Makrolon®, Bayer CropScience Ltd.) and a polyvinylchloride tubing (Fisherbrand Clear PVC Tubing, Fisher Scientific Inc.), were functionalized in the same manner.

6.2.3.2 Quantification of surface amine groups using sulfo-SDTB amine assay

Surface amine density was varied by adjusting plasma exposure time. Increased time exposure raises amine density, but may adversely inhibit gas exchange performance. 4 mL of 2.4 mM Sulfo-SDTB was added to a 16 cm^2 fiber sample and incubated at room temperature for 2 hr. Fibers were

then washed with 0.5% Tween-20 in deionized water to remove unbound reagent. 35% perchloric acid was added to cleave immobilized sulfo-SDTB and induce color change. Harvested solutions were read using a spectrometer (Thermo Genysis UV-Vis) at 498nm and amine concentration was calculated using a standard curve.

6.2.3.3 SB block copolymer conjugation

To prepare an SB block copolymer conjugated surface (PMP-A-SBMA or PMP-A-SBNHS), the amine functionalized PMP fiber (PMP-A) mats were immersed in a container with 0.1 wt% of aqueous SBNHS (NHS functionalized) solution or SBMA (carboxyl functionalized) with EDC/NHS [162] and placed on a rocker at RT for 15 hr. For PMP-H-SBSi or PMP-H-SBNHSi, the hydroxyl functionalized PMP fiber (PMP-H) mats were immersed SBSi and SBNHSi solutions that were reacted with APSi in situ condition. The surface compositions were analyzed by X-ray photoelectron spectroscopy (XPS) using a Surface Instruments S-probe spectrometer with a takeoff angle 55°, performed at NESAC-BIO, University of Washington. Additional materials, including polycarbonate sheet (Makrolon®, Bayer CropScience Ltd.) and a polyvinylchloride tubing (Fisherbrand Clear PVC Tubing, Fisher Scientific Inc.), were modified and analyzed in the same manner.

6.2.3.4 In vitro blood contact test and platelet deposition characterization

Surface platelet deposition was analyzed after prolonged material contact with fresh whole ovine blood as described in previous studies [160,162,206]. In short, whole ovine blood was collected by jugular venipuncture with an 18½ gauge needle feeding directly into a syringe with a citrate solution (10mM/mL). The first 3 mL of blood were discarded to ensure sample uniformity. National Institutes of Health guidelines for the care and use of laboratory animals were observed

for all donor sheep, and all procedures were approved by the Institutional Animal Care and Use Committee (IACUC). PMP fiber swatches were cut from fiber mats into 5 cm long segments for analysis. The fiber ends were sealed using a hot glue gun to prevent blood from reaching the inner lumen. Samples were sterilized by ethanol emersion then washed with DPBS. The fibers were then placed into a vacutainer tube (BD Vacutainer, no additives) filled with 5 mL of the fresh, citrated ovine blood and rocked for 3 h at 37°C using a hematology mixer (Fisher Scientific, Pittsburgh, PA).

After removal from the tubes, samples were rinsed with DPBS at least 10 times, according to the previously described protocol, in preparation for scanning electron microscopy (SEM, JEOL USA model JSM-6330F) analysis [162]. In addition to direct visualization of the surface, a lactate dehydrogenase assay (LDH, Cytotoxicity Detection Kit, Clontech Laboratories, Inc.) was used to quantify platelet deposition [162].

The results are presented as mean ± standard deviation (SD). Data were analyzed by one-way ANOVA followed by a post hoc Neuman-Keuls testing. Significant differences were considered to exist at $p < 0.05$.

6.2.3.5 SB coated fiber stability testing

PMP hollow fibers (238 cm^2) were functionalized and coated with SBMA, SBSi, SBNHS, or SBNHSi as detailed above. Fiber mats were potted directly into polycarbonate mini-modules using 5 min epoxy (Devcon, Danvers, MA). The mini-modules have been scaled from full sized oxygenator devices and simulate flow conditions for gas exchange [21,22]

Mini-modules with open ports were sterilized using a standard ethylene oxide (EtO) sterilization cycle. Peristaltic pumps and L/S 16 Masterflex tubing were used to circulate 200 mL PBS with sodium azide through the modules at 45 mL/min for 2 wk at 37°C. The PBS solution

was replaced at one week. After recirculation was complete, samples were removed from modules and unrolled. Randomly selected 1 by 1 cm^2 fiber mats were cut and sent for XPS analysis and LDH platelet deposition testing.

6.2.3.6 Gas exchange testing of SB coated hollow fibers

Scaled polycarbonate gas exchange mini-modules were constructed from uncoated and SBNHS and SBNHSi modified fibers as described above. 5 min epoxy potting was used to separate the gas and fluid pathways. A gas exchange recirculation loop (see Figure 64) was assembled to measure CO_2 removal from freshly drawn bovine blood. The fluid side gas exchange loop contained (in series) a 1L compliant blood reservoir, peristaltic pump, Sorin Lilliput 2 D902 pediatric de-oxygenator, heat exchanger, and a mini-module before returning to the fluid reservoir. The de-oxygenator sweep gas was composed of carbon dioxide, oxygen, and nitrogen. These ratios were adjusted to set inlet blood CO_2 partial pressure at 50 mmHg ± 5 mmHg as measured by a RapidPoint 305 blood gas analyzer (Siemans, Deerfield, IL).

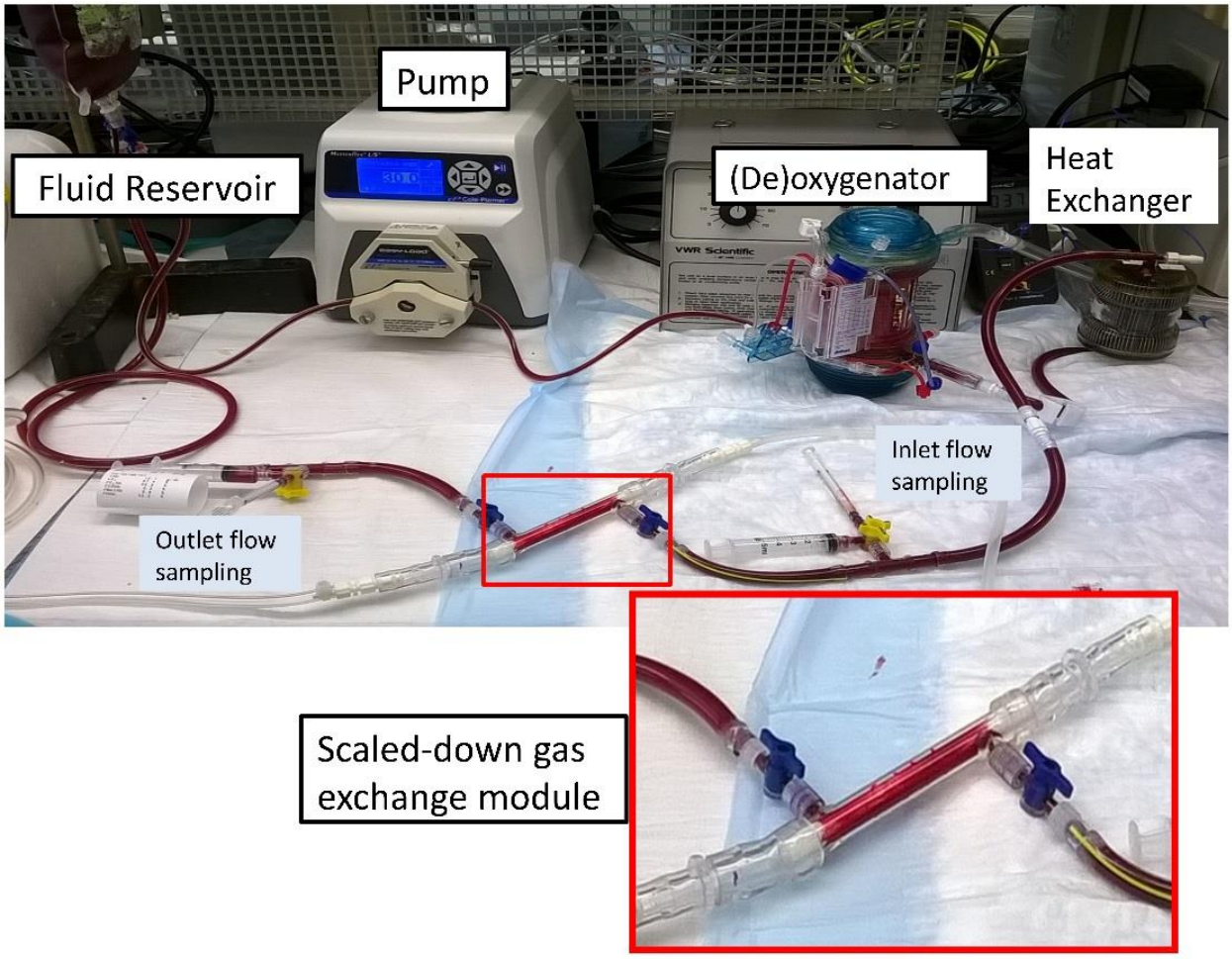

Figure 64. In vitro gas exchange analysis setup using a scaled down gas exchange module. Not shown are the CO2, N2 and O2 gas lines, the oxygen gas flow meter, condenser, and CO2 analyzer.

The oxygen sweep gas originates in a pressurized oxygen tank regulated by mass flow controller before passing through the mini-module. Sweep gas then passed through a condenser, vacuum pump, and CO_2 analyzer. Triplicates of unmodified control fibers, PMP-SBNHS, and SBNHSi were each tested in triplicate at a blood flow rate of 45 mL/min. The sweep gas flow rate was modulated to maintain a 3000 ± 100 ppm CO_2 concentration at the gas outlet. A one way ANOVA analysis was completed using SPSS 23 (IBM Analytics, Armonk, NY) with a p value<=0.05

6.3 RESULTS

6.3.1 Synthesis of SB block copolymers with functional groups

Chemical structures were confirmed using proton nuclear magnetic resonance (^{1}H NMR, BrukerBiospin Co., Billerica, MA). For the newly synthesized SBNHS in D_2O, peaks were: δ (ppm) = 0.90-1.30 (α-CH_3), 1.70-2.20 (CH_2C), 2.25-2.35 ($CH_2CH_2SO_3$), 2.80-2.85 (CH_2-CH_2), 2.90-3.00 ($CH_2CH_2SO_3$), 3.20-3.40 ($N(CH_3)_2$), 3.50-3.85 ($CH_2N(CH_3)_2CH_2$) and 4.35-4.55 (OCH_2). The peak area integration ratio of 2.80-2.85 (CH_2-CH_2, **m**) and 4.35-4.55 (OCH_2, **e**) was used to define the polymer composition. A SBNHS block copolymer, which was synthesized with a 2:1 monomer feed ratio of SBDMB and AANHS, resulted in a peak area integration ratio (e/m) of 2.7. After APSi conjugation (SBNHSi), the peak from the NHS groups, δ (ppm)=2.80-2.85 (CH_2-CH_2, **m**) was decreased and new peaks were measured at 0.65-0.75 (CH_2-Si, **n**) and 1.20-1.30 (OCH_3, **p**), indicating the presence of conjugated APSi (Figure 65).

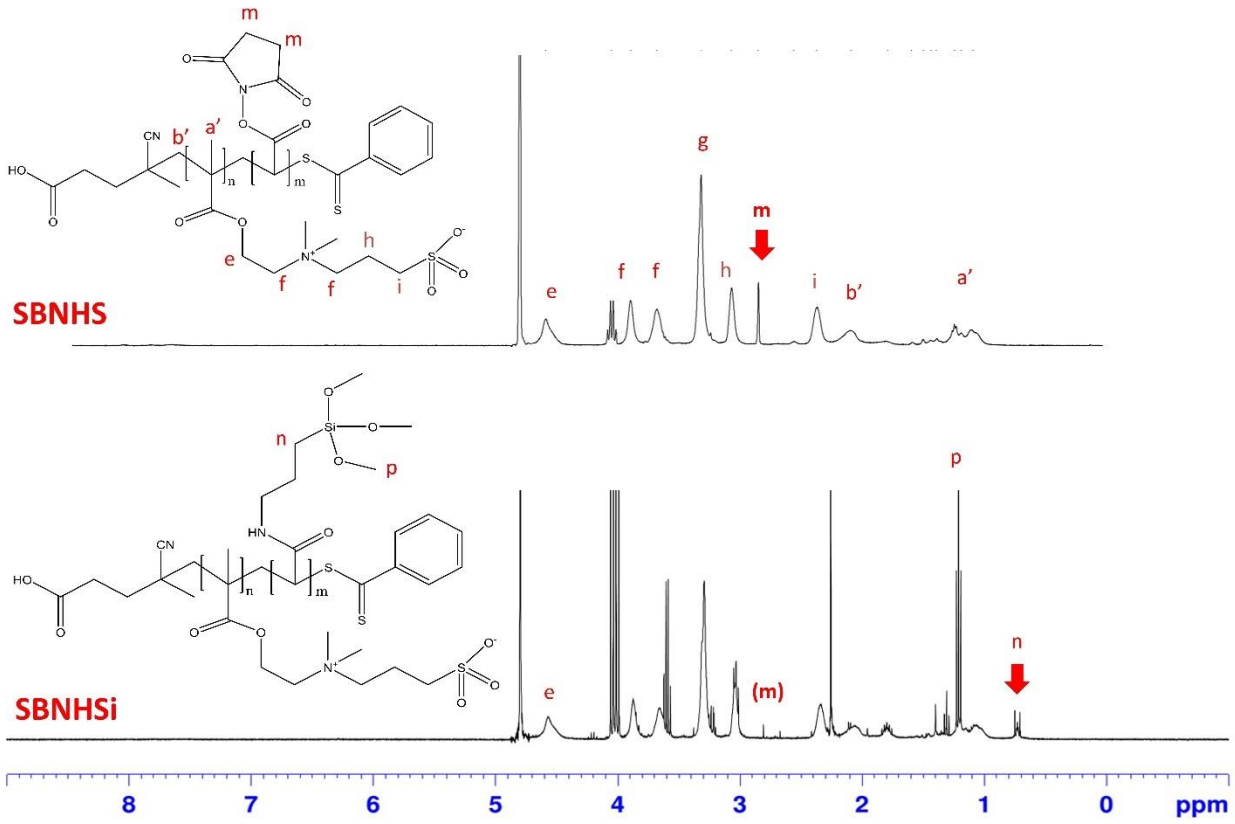

Figure 65. ^{1}H NMR spectra of functional zwitterionic block copolymers (SBNHS or SBNHSi).

6.3.2 HFM amine functionalization

PMP fibers aminated with PECVD showed that the plasma treatment time period (A1: 1 min, A2: 5 min) could be adjusted to vary HFM amine density, as measured by the sulfo-SDTB amine assay and XPS analysis (Table 5**)**. A2 showed a 3% increase in N percentage compared to A1, indicating enhanced amination. All amine functionalized HFM conjugations were completed using 5 minute time, hereby referred to as PMP-A.

Table 5. Atomic percentages for plasma treated hollow fiber surfaces as determined by X-ray photoelectron spectroscopy.

	C	O	N	Si	S
PMP-C	95.1 (±1.3)	4.9 (±1.3)	-	-	-
PMP-A1	73.0 (±1.1)	18.2 (±0.5)	5.2 (±0.5)	3.4 (±0.1)	0.2 (±0.0)
PMP-A2	68.9 (±0.6)	18.7 (±0.2)	8.2 (±0.3)	3.6 (±3.4)	0.3 (±0.0)
PMP-H (30s)	87.8 (±0.6)	9.9 (±0.8)	-	-	-
PMP-H (60s)	88.3 (±2.4)	12.0 (±0.4)	0.3 (±0.4)	0.3 (±0.4)	-
PMP-H (120s)	88.9 (±0.4)	10.9 (±0.3)	-	0.5 (±0.5)	-

PMP-C: unmodifed and cleaned HFM. **PMP-A1** = 1 min, **PMP-A2** = 5 min of plasma treatment with allyl amine. For PMP-A1 amine density was 0.09 nM/cm^2 and for PMP-A2 0.34 nM/cm^2 as measured by sulfo-SDTB assay. **PMP-H**: O_2 plasma treated by PECVD (100W) for different exposure times (n=3, mean ± st. dev.).

6.3.3 OH functionalized fiber SEMs

A new functionalization approach using hydroxyl groups (-OH) was developed. Unlike surface amine groups, hydroxyl groups are not anticipated to negatively impact biocompatibility and may increase the conjugation efficiency and loading of SB block copolymer. For hydroxylated PMP fibers (PMP-H) prepared by oxygen plasma treatment using PECVD, excessive power settings may damage the PMP fiber surface, so SEM images were taken for visual inspection (**Figure 3).** Damage to the fiber surface was observed in the 600 W, 30 sec and 5 min samples. Reduction of power to 100 W allowed for a plasma exposure time of 60 sec without visual signs of surface damage. X-ray photoelectron spectroscopy (XPS) (Table 5) was used to confirm surface

hydroxylation. The oxygen percentage peaked at 12% ± 0.4% in the 100 W, 60 sec sample. All hydroxylated PMP HFM conjugations were completed using 100W, 60 sec sample, hereby referred to as PMP-H.

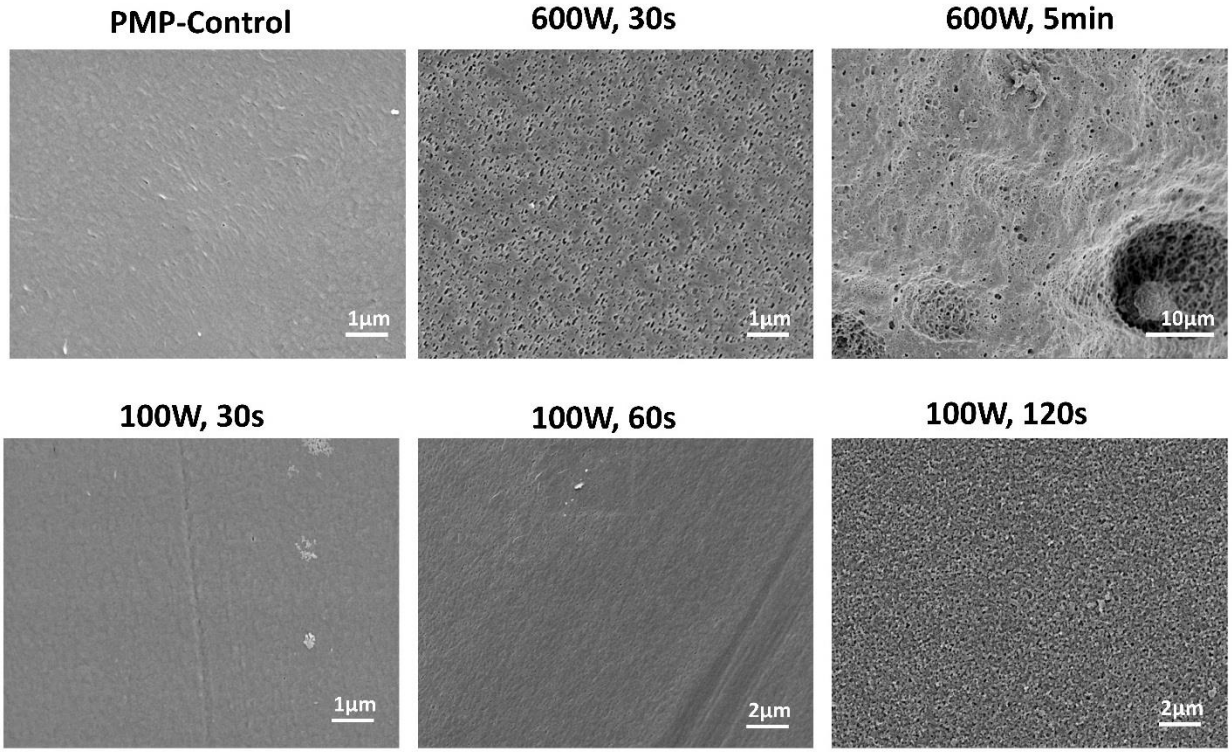

Figure 66. Surface morphology change in PMP HFMs after exposure to O_2 plasma (PECVD) at indicated power levels and exposure times.

6.3.4 SB block copolymer conjugation and platelet deposition on HFMs after ovine blood contact

SB block copolymers SBMA, SBNHS, SBSi, and SBNHSi were directly conjugated to functionalized PMP fibers (PMP-A: 5 min or PMP-H: 100 W, 60 s). The loading capacity of

SBMA onto the fibers can be measured by observing changes in the surface sulfur (S) content. XPS analysis results in Table 6 show S content ranging from 1.0± 0.1% to 1.2± 0.1%, compared to 0.3 for PMP-A and undetectable levels for PMP-C and PMP-H.

Table 6. Atomic percentages for SB block copolymers modified hollow fiber surfaces as determined by X-ray photoelectron spectroscopy.

	C	O	N	Si	S
PMP-A-SBMA	79.6 (±1.4)	11.1 (±0.8)	5.6 (±0.5)	0.3 (±0.1)	1.0 (±0.1)
PMP-H-SBSi	85.6 (±0.7)	9.8 (±2.1)	1.1 (±0.4)	0.6 (±0.1)	1.0 (±0.1)
PMP-A-SBNHS	69.3 (±0.5)	18.3 (±0.2)	7.5 (±0.2)	0.9 (±0.0)	1.1 (±0.1)
PMP-H-SBNHSi	79.8 (±1.2)	15.3 (±0.6)	1.9 (±0.1)	1.0 (±0.1)	1.2 (±0.1)

PMP-C: unmodifed and cleaned HFM. **PMP-A =** 5 min of plasma treatment with allyl amine (0.34 nM/cm^2 as measured by sulfo-SDTB assay). **PMP-H**: O_2 plasma treated by PECVD (100W) for 60 s exposure times (n=3, mean ± st. dev.).

Platelet deposition on the controls, pre-functionalized, and modified PMP hollow fibers after contact with fresh ovine blood for 3 hr is shown in Figure 67**,** Figure 68, and Figure 69.

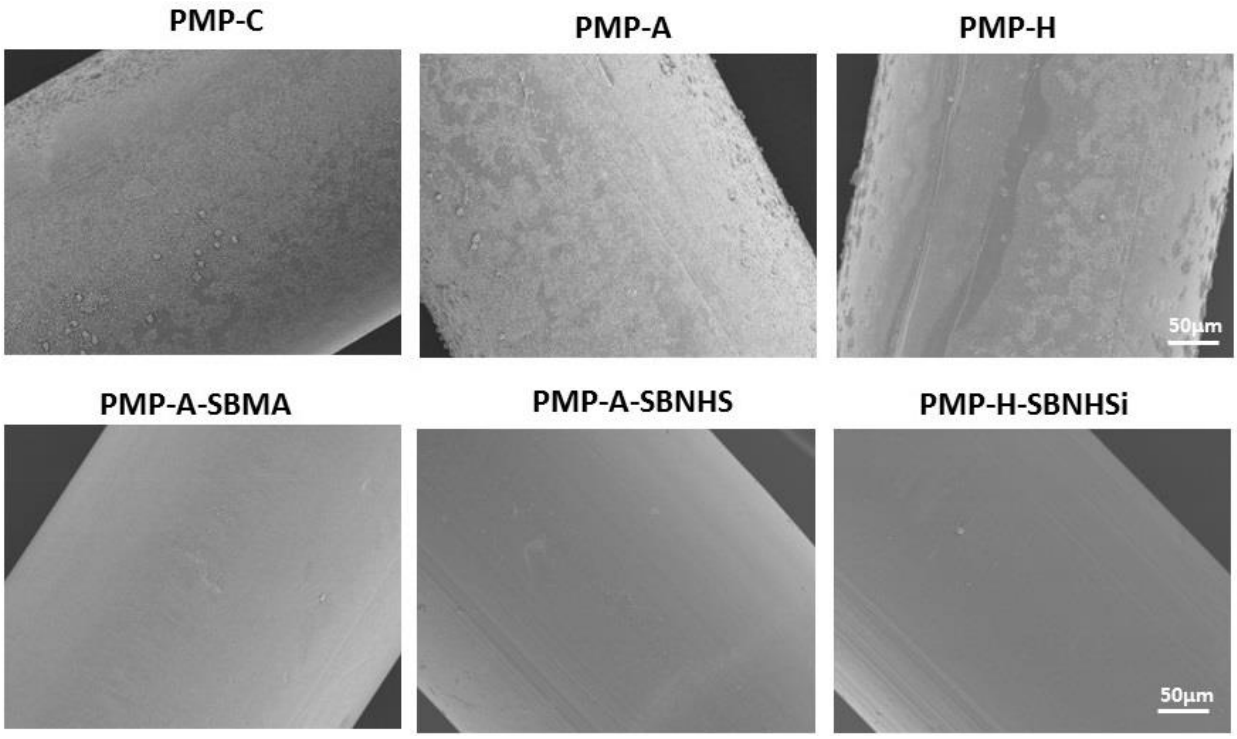

Figure 67. Scanning electron micrographs of PMP control and the modified surfaces after contact with citrated ovine whole blood for 3 h at 37°C.

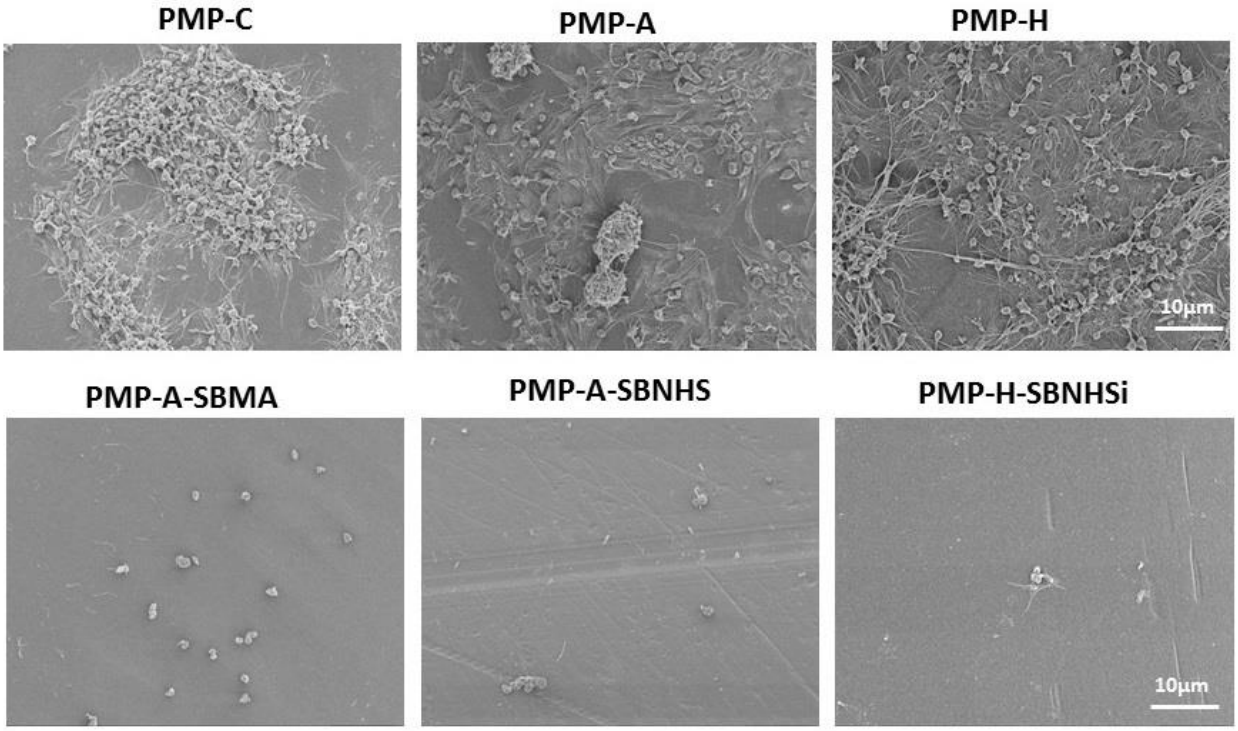

Figure 68. Scanning electron micrographs of PMP control and the modified surfaces after contact with citrated ovine whole blood for 3 h at 37°C.

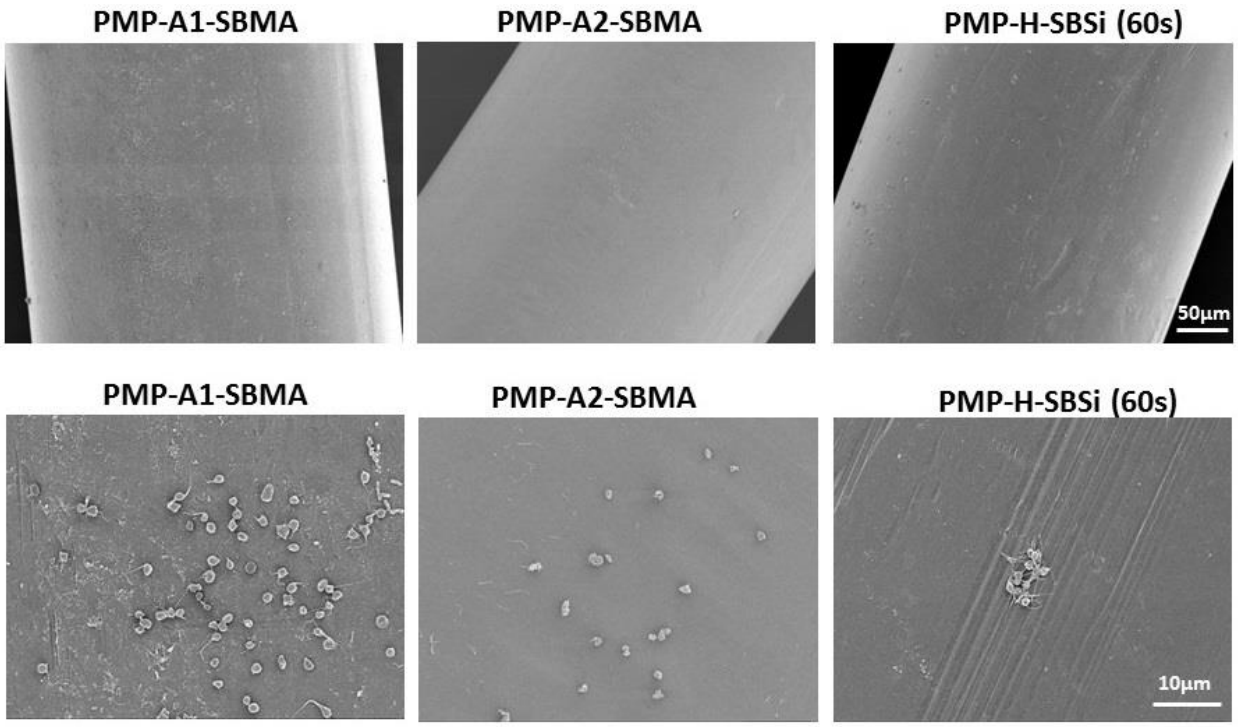

Figure 69. Scanning electron micrographs of PMP control and the modified surfaces after contact with citrated ovine whole blood for 3 h at 37°C.

The control (PMP-C) and pre-functionalized surfaces (PMP-A and PMP-H) showed large quantities of deposited platelets with aggregates spread uniformly over the entire fiber surface. The average amount of deposition on PMP-A samples showed a higher deposition than the PMP-C as well as PMP-H based on the SEM observation and LDH assay results (Figure 70). Platelet deposition and the aggregates were dramatically reduced on all of the SB block copolymer conjugated surfaces compared to control and pre-functionalized surfaces ($p<0.05$).

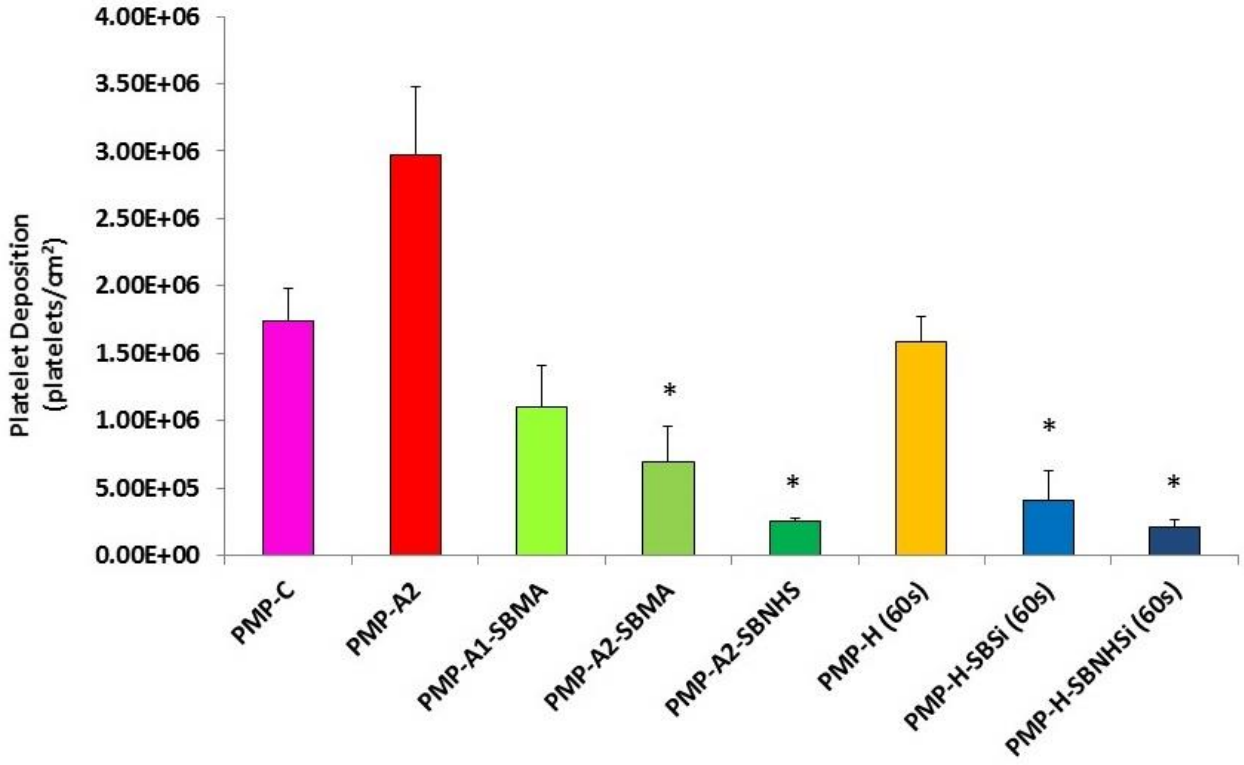

Figure 70. Platelet deposition on a fiber mat unit (1 cm2), including binding fibers, after contact with fresh ovine blood for 3 h at 37°C as determined by a lactate dehydrogenase (LDH) assay (*P<0.05 vs. PMP-C, PMP-A2 and PMP-H controls, n=3).

6.3.5 SB coating stability testing

The surface compositions of coated fibers were also measured after exposure to elevated fluid shear levels for 2 wk in PBS at 37°C (Table 7).

Table 7. Atomic percentages for the 2wk rinsed HFM surfaces as determined by X-ray photoelectron spectroscopy.

	C	O	N	Si	S
PMP-A (2 wk)	78.0 (±0.8)	14.2 (±0.4)	6.0 (±0.5)	0.5 (±0.1)	0.2 (±0.0)
PMP-A-SBMA (2 wk)	75.5 (±0.6)	19.7 (±0.5)	2.9 (±0.2)	0.4 (±0.1)	0.4 (±0.1)
PMP-H-SBSi (2 wk)	76.4 (±0.4)	19.3 (±1.3)	2.2 (±0.2)	1.8 (±0.5)	0.3 (±0.1)
PMP-A-SBNHS (2 wk)	71.8 (±1.1)	17.7 (±0.7)	6.2 (±0.1)	0.7 (±0.1)	0.9 (±0.1)
PMP-H-SBNHSi (2 wk)	81.4 (±0.2)	14.3 (±0.2)	2.0 (±0.3)	0.8 (±0.1)	1.0 (±0.1)

All rinsed samples **(2 wk)** were EtO treated then continuously rinsed with PBS (with sodium azide 0.02%) at 37°C for 2 wk (n=3, mean ± st. dev.).

Both PMP-A-SBMA (2 wk) and PMP-H-SBSi (2 wk) decreased over 50% compared to pre-flow exposure (Table 6). SBNHS and SBNHSi coated surfaces better preserved surface S, remaining above 0.9 ± 0.1% and 1.0 ± 0.1% respectively. SEM images and LDH assay results (Figure 71 and Figure 72**)** also provide evidence of coating integrity, exhibiting significantly reduced platelet deposition in both samples compared to PMP aminated controls ($p<0.05$).

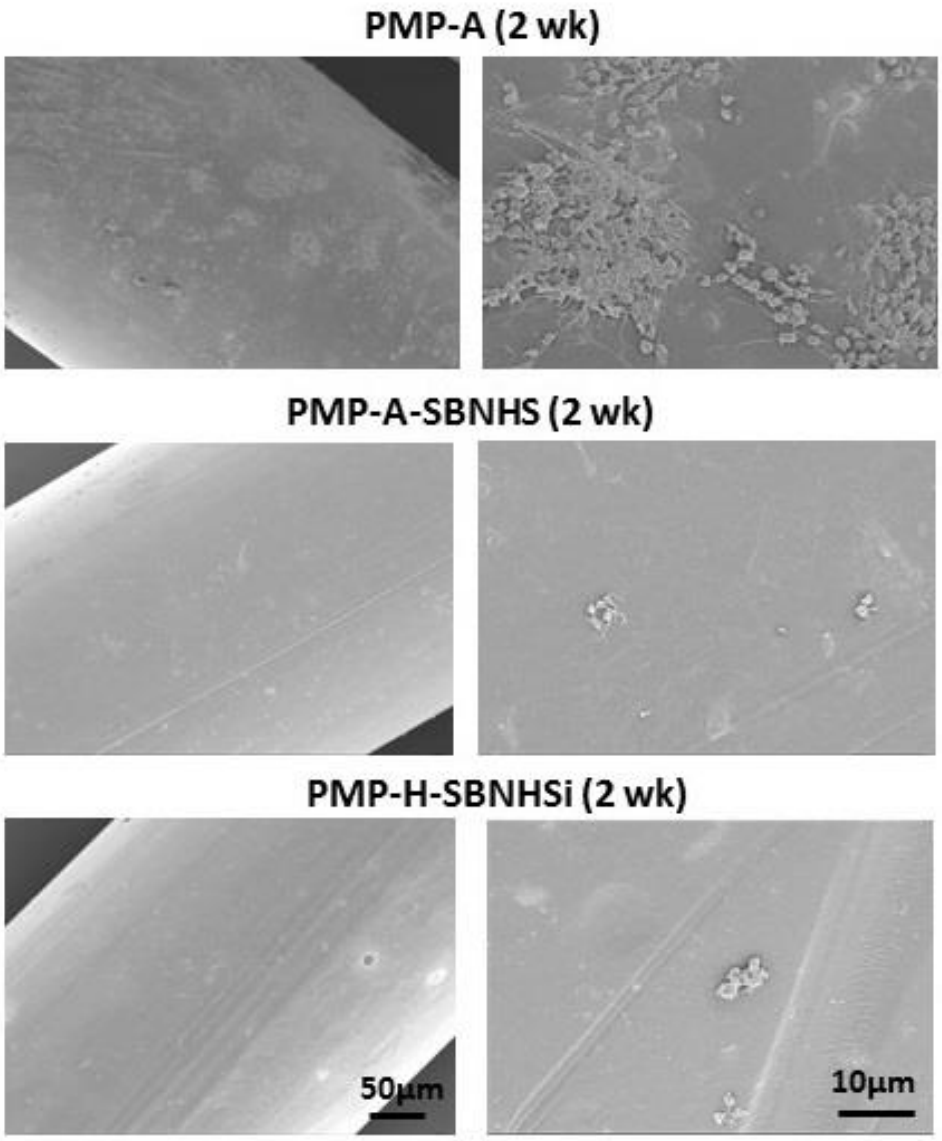

Figure 71. Scanning electron micrographs of stability tested PMP hollow fibers (PBS rinsed for 2 wk) after contact with fresh ovine blood for 3 h at 37°C.

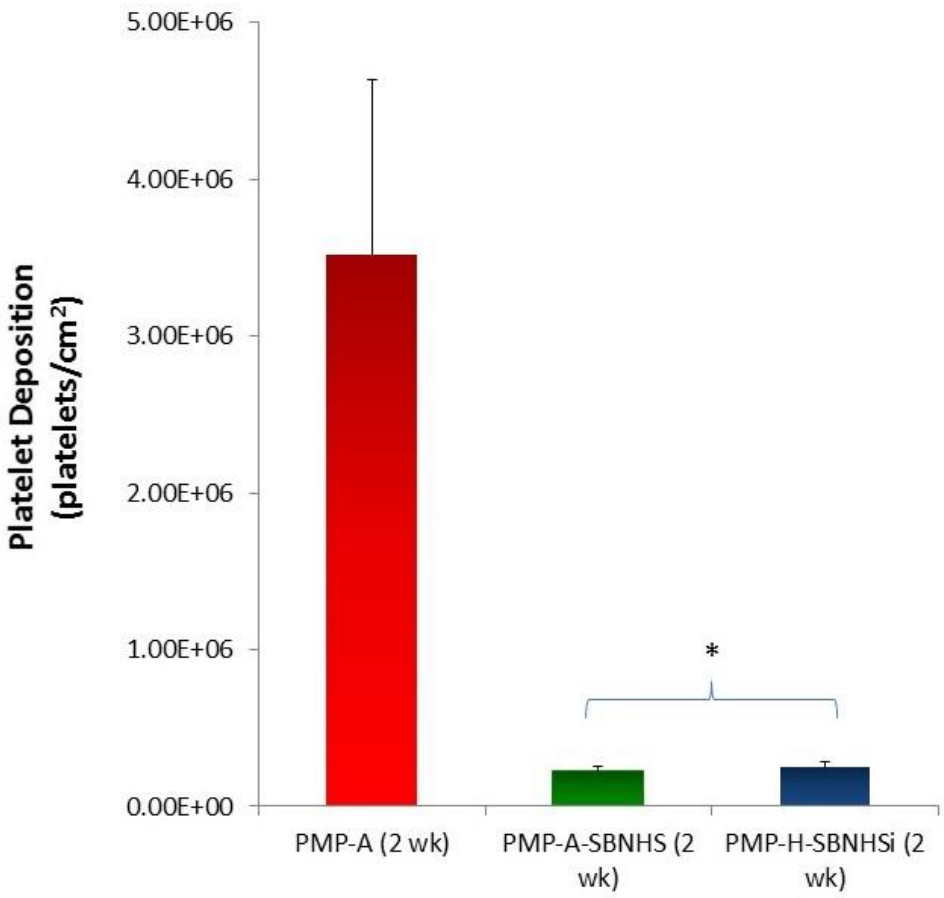

Figure 72. Platelet deposition on the stability tested PMP hollow fibers (PBS rinsed for 2 wk) after contact with fresh ovine blood for 3 h at 37°C as determined by a lactate dehydrogenase (LDH) assay (*P<0.05 vs. the controls).

6.3.6 Gas exchange testing

Gas exchange performance of hollow fibers was evaluated by examining carbon dioxide removal in a scaled experiment which simulates a clinical gas exchange setup. CO_2 removal rates were normalized using inlet CO_2 partial pressure to account for variations over the test span, then divided by fiber surface area. Only PMP-A-SBNHS and PMP-H-SBNHSi modifications were

evaluated due to their superior stability characteristics. Removal rates are shown in Figure 73. The unmodified control fiber removal rate of 248 ± 6 (mL/min/m^2) is comparable to previous testing using scaled modules [162,p.20]. Aminated SBNHS coating samples (PMP-A-SBNHS) exhibited a 6% reduction in mean CO_2 removal rate, while hydroxyl activated SBNHSi fibers (PMP-H-SBNHSi) did not vary substantially from the mean control fiber CO_2 removal rate. The statistical analysis determined a p-value of 0.08.

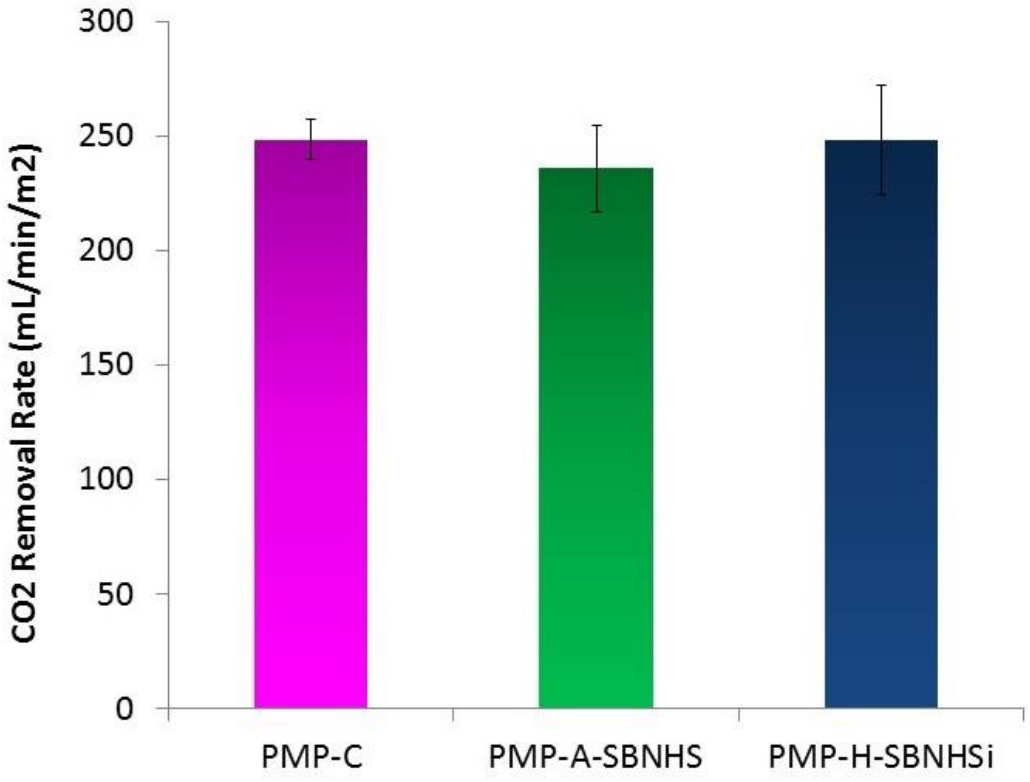

Figure 73. CO_2 removal rate by HFMs in bovine blood using a scaled down gas exchange module (n=3).

6.3.7 Polycarbonate and PVC surface modification

Both unmodified polycarbonate and polyvinylchloride (PVC) control surfaces showed widespread platelet deposition with a spread morphology and platelet aggregates after 3 h contact with fresh ovine blood contact, although polycarbonate visually exhibited less platelet deposition and aggregation than PVC, as shown in Figure 74**.**

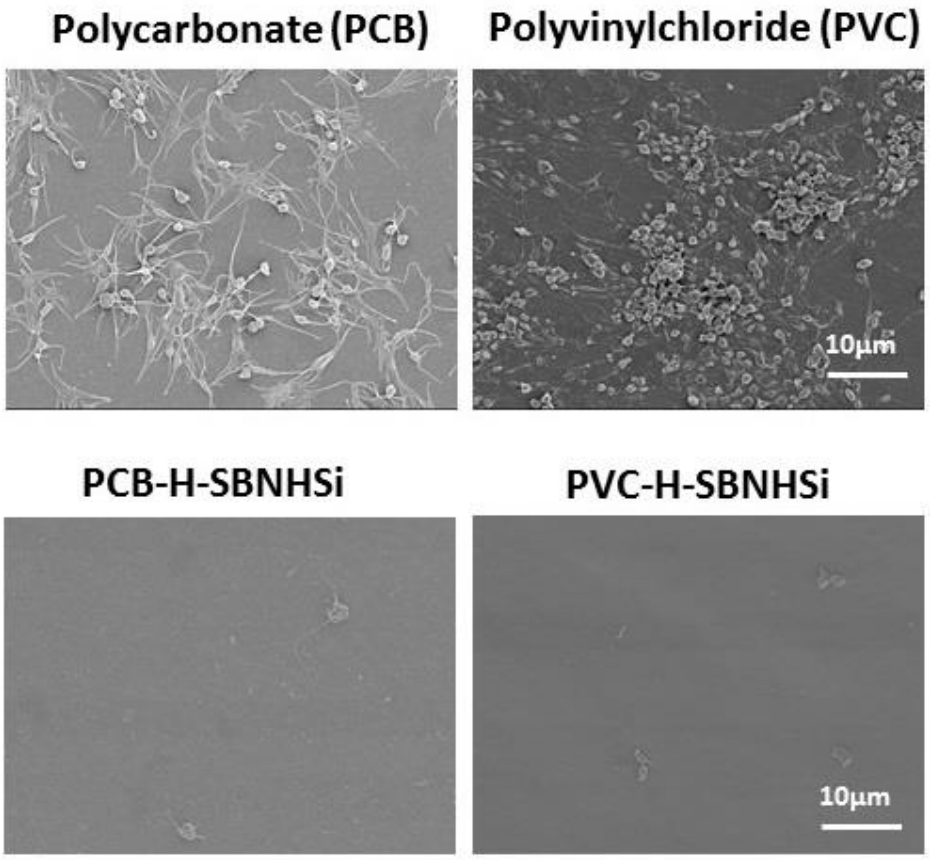

Figure 74. Scanning electron micrographs of blood-contacted polycarbonate (PCB), polyvinylchloride (PVC) and the SBNHSi modified surfaces after contact with citrated ovine whole blood for 2 h at 37°C.

After the surface modification using SBNHSi, the amount of platelet deposition was reduced on both surfaces by up to 95% as shown in the LDH assay results Figure 75.

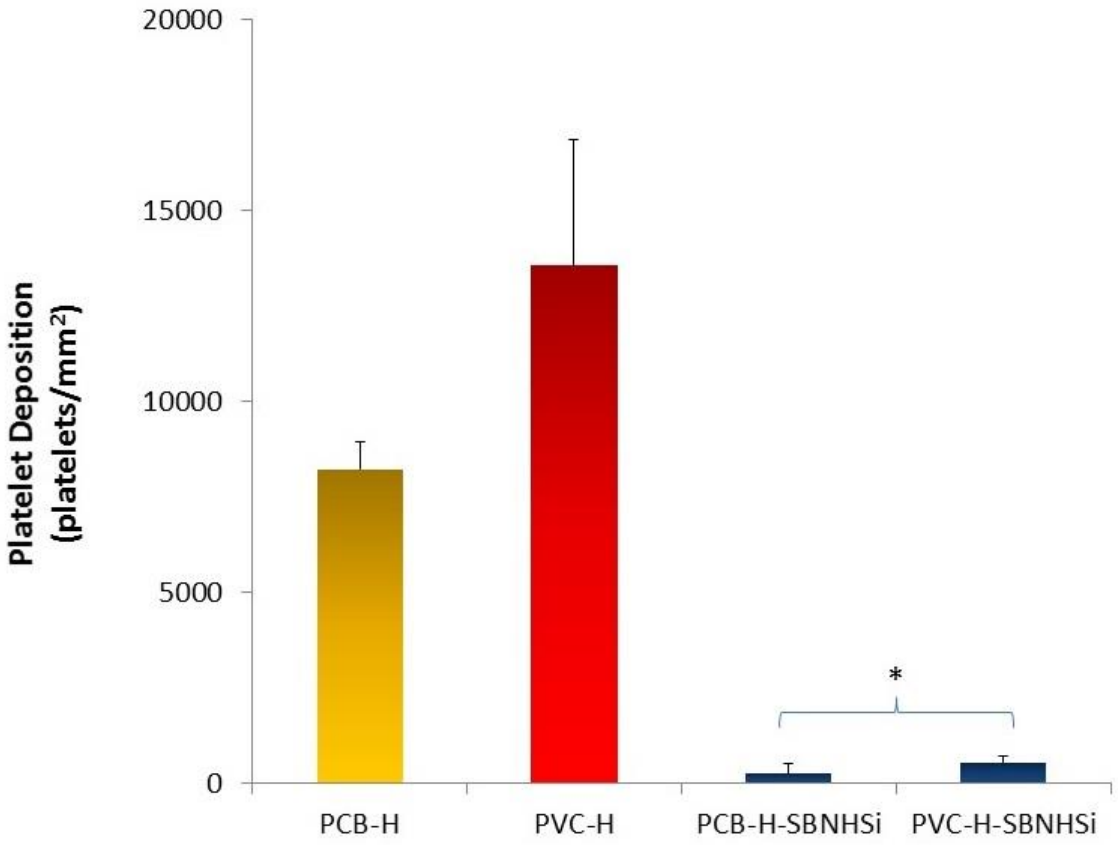

Figure 75. Platelet deposition as determined by a lactate dehydrogenase (LDH) assay after contact with citrated ovine whole blood for 2 h at 37°C (*P<0.01 vs. PCB-H and PVC-H controls).

6.4 DISCUSSION

This manuscript describes the development of zwitterionic surface modification approaches for use in extracorporeal blood-contacting medical devices such as artificial lungs. Two surface functionalization techniques, designed for amine or hydroxyl functionalized HFM surfaces respectively, were evaluated with the objective of designing a robust and simple process compatible with coating an entire extracorporeal circuit. The modified HFMs were shown to significantly reduce acute platelet deposition from whole blood, even after 2 wk exposure to continuous fluid flow. Additionally, gas exchange studies performed with the modified HFMs showed no significant reduction in gas transport, a critical feature for the application of this methodology in respiratory assist devices.

Amine functionalization of porous polypropylene hollow fibers has been studied by our group in the past [160,162]. With this approach, allylamine monomer was deposited on the fiber surface using PECVD, generating stable amine groups, but also decreasing fiber permeance [207]. Excess allylamine deposition may lead to decreased gas exchange performance, particularly if paired with a high molecular weight coating. Additionally, unreacted amines may result in increased platelet deposition. Variations of hydroxyl functionalization have been implemented in a variety of prototype extracorporeal devices [74,208]. With PMP fibers, excessive oxygen plasma runs the risk of damaging the thin outer fiber film which prevents plasma leakage [209]. This damage can be seen in SEMs of HFMs treated with elevated power and time settings (Figure 66**:** 600 W / 30 sec, 600 W / 5 min & 100 W / 120 sec), but was not present at the lower power settings (100 W / 60 sec) which were used for conjugation. The selected instrument settings did not present visible fiber damage and also exhibited the highest surface oxygen content (12.0 ± 0.4 %, Table 5), indicating these parameters balance avoidance of fiber damage and degree of functionalization.

For decades, various polymers bearing zwitterionic groups have been developed and studied as anti-fouling, non-thrombogenic and anti-inflammatory materials [197–200]. Studies by Cook [210–212], Li [208], and Gong [213] have incorporated zwitterionic coatings into prototype artificial lung devices with success on the bench. Phosphorylcholine (PC) polymer coatings have also been incorporated into CE-approved oxygenators (ALONE ECMO, EUROSETS, Italy), but there are still many potential improvements that may benefit clinical efficacy and application in the challenging extended perfusion periods associated with ECMO support. PC surface coatings may not be suitable for long term use due to the ability of the phosphoester group to be hydrolyzed [203]. Additionally, PC coatings are relatively expensive and difficult to handle compared to other zwitterionic polymers [201,202]. These limitations of PC coatings challenge widespread integration into extracorporeal devices, leading to exploration of alternative zwitterionic polymers. SB polymers in particular have shown promise, with comparable improvements in hemocompatibility and platelet deposition to PC counterparts at a lower price with higher stability. [162,199,201,214]

Our previous work developed functional zwitterionic PC macromolecules and low molecular weight (LMW <10,000) sulfobetaine (SB) block copolymer with carboxyl groups (SBMA-COOH) for polypropylene HFM surface modification [162]. These compounds are water soluble and can be conjugated onto an aminated polypropylene HFM to reduce thrombotic deposition without significantly inhibiting gas performance. Although the previous experimental coatings using the LMW SB block copolymer were promising, they have not been evaluated using PMP HFMs which are increasingly used in commercial oxygenators and are critical for the extended blood contact in chronic respiratory assist devices. The modifications have also not been tested for extended exposure to fluid flow rates commonly seen in clinical practice or on other material surfaces included in a typical extracorporeal loop (e.g. cannula, tubing and device housing material).

Given that the application of extracorporeal oxygenators is necessarily associated with continuous exposure to flowing blood and wall shear stresses, the surface modification stability is of concern, and the instability of common device coatings such as heparin and PC have been documented [214–216]. Many techniques have been developed to improve stability and these show short term improvements in thromboresistance [217–219] , but few studies have examined efficacy after long term exposure to anticipated fluid shear conditions. In this study, a 2 week perfusion with buffered saline was completed to simulate the extended operating conditions becoming more prevalent in ECMO and more recent CO_2 removal devices. Additionally, prior to the recirculation studies, the modules employed were EtO sterilized to simulate commercial devices. Results in Table 7 indicate previously developed coatings (SBMA and SBSi), which did not incorporate multiple active NHS groups, exhibited a reduction in surface sulfur groups, suggesting leaching of the conjugate from the HFM or degradation of the zwitterionic compounds. However, SBNHS and

SBNHSi coatings did not experience the same degree of reduction, indicating greater stability under the anticipated operating shear and temperature. This stability, which has not been exhibited by other coatings, would be critical to achieving prolonged reductions in systemic anticoagulation. However, it should be noted that extended perfusion with patient blood would be a more rigorous situation, given the array of protein (especially enzyme) and cellular components that could act to foul or degrade the surface activity. The resistance of the SB modified surfaces to resist such interactions would potentially act to retard this effect.

Adding any coating to HFMs raises concerns of decreased gas exchange due to increased gas transfer resistance. Higher molecular weight coatings in particular run this risk. In this study the employment of RAFT polymerization allows for generation of well-controlled, low molecular weight block copolymers with versatile functional groups. The block copolymer synthesis strategy is particularly versatile as it could be used in one approach (with SBNHS) to provide for direct conjugation to amines on the target surface, or in an alternate approach, to generate a polymer such as SBNHSi to react with surface hydroxyl groups. Gas exchange testing showed no statistical difference in CO_2 removal rates between modified and control HFMs. Comparable gas exchange evaluation on coated PMP fibers was completed by Huang [208] on PC coated PMP fibers. This testing showed a 15% reduction in mean CO_2 removal rate.

The majority of studies developing thromboresistant coatings have focused on a single material and application [162,208,213]. However, most extracorporeal circuits are composed of a variety of materials and surfaces which may contribute to thrombus formation and subsequent embolization. To evaluate the versatility of the reported surface modification approach, acute thromboresistance was evaluated for two materials commonly found in non-gas transferring surfaces included in extracorporeal devices. Polycarbonate, which is commonly used for injection

molded housings, and PVC, which is a widely used tubing material, were functionalized and modified under the same parameters as the PMP HFMs. With the effectiveness of the modification strategy shown on these surfaces, the data suggest that it may be possible to uniformly modify all blood contacting surfaces in an extracorporeal circuit, to further improve the blood biocompatibility and potentially allow for the reduction in systemic anticoagulation.

While this report has established a technique capable of reducing acute platelet deposition on a variety of materials commonly used in respiratory assist devices, without significantly reducing device performance, there are a number of limitations that should be noted. First, the surface modification strategy has only been evaluated *in vitro* and for limited contact periods with anticoagulated animal blood. *In vivo* testing would be the next step to more fully verify device gas transfer performance and thromboresistance. The notion that systemic anticoagulation might be reducible in clinical practice with such surface modifications would similarly need to first be evaluated in a large animal model. As noted previously, stability testing established modification stability at shear rates comparable to that experienced in full-sized devices, however it is unknown how the coating would perform after exposure to the proteases and high protein concentrations present in blood, not to mention with extended contact with leukocytes and platelets. While a range of functionalization and conjugation parameters were evaluated, a complete optimization was not completed and further improvements in performance and stability of the reported modifications may be possible. Finally, all testing was completed on scaled-down devices or HFM swatches. It is believed the process would scale to full sized devices, but a strategy for surface modification would need to be developed. For instance, determining whether the fibers would be modified independently of the device housing or whether an assembled oxygenator could be modified.

6.5 CONCLUSIONS

This study reports two techniques for the functionalization and subsequent conjugation of SB block copolymers to PMP HFMs with the intention of reducing thrombus formation in respiratory assist devices. Amine or hydroxyl functionalization of HFMs was accomplished using PECVD and the generated functional groups were then conjugated to newly synthesized SBNHS or SBNHSi block copolymers. The modified HFMs showed markedly reduced platelet deposition from whole ovine blood, stability under the fluid shear of anticipated operating conditions and uninhibited gas exchange performance. Additionally, the functionalization and conjugation techniques were shown to reduce platelet deposition on other materials which are common in extracorporeal circuits such as polycarbonate and PVC tubing. This flexible surface modification approach may thus allow for coating of an entire blood contacting extracorporeal circuit. Improvements in the thromboresistance of the blood-contacting surfaces in large extracorporeal devices intended for chronic support are essential to allow for the reduction of anticoagulation levels in the supported patients. Without such advancements, the implementation of these devices will be hampered since the technology will continue to be associated with limited patient mobility, a high-level of patient oversight and management, and substantial patient morbidity.

7.0 SUMMARY AND CONCLUSIONS

While research continues to improve our understanding of the biological mechanisms of sepsis, few treatments address sepsis' underlying mechanism. Similarly, advances to materials and surface coatings have improved the safety and efficacy of extracorporeal devices, but most devices still rely on formulations developed in the previous decade. While the use of respiratory dialysis, ECMO, and dialysis continues to expand, there are many other potential applications for extracorporeal devices to selectively modulate blood cell behavior. The combination of these two concepts can potentially lead to a novel range of new treatments and improvements of current devices, particularly in the area of acute inflammatory conditions. Much of the work in this dissertation focused on development of an extracorporeal device platform, which incorporates a covalently immobilized cytokine on the device surface. The specific device envisioned could "reprogram" blood cell response to improve outcomes for the target disease state.

The first goal of this dissertation was to develop a mechanistic computational model to study the role of IL-8 induced CXCR-1/2 neutrophil surface receptor downregulation and in the progression of sepsis. The model, which contains 16 ordinary differential equations and 43 parameters, was constructed based on a simplified mechanistic representation of CXCR-1/2 activation. Both neutrophil receptor level dynamics and systemic parameters were coupled with multiple activated neutrophil phenotypes which control pathogen load and adverse tissue damage. The model was calibrated using experimental data from baboons administered a two-hour infusion of *E coli* and followed for a maximum of 28 days. After model calibration, implementation of an extracorporeal device, such as the NeRD, which modulates CXCR-1/2 expression was tested *in silico*. The findings suggest that interventions aiming to modulate phenotypic composition are time

sensitive, with treatment efficacy quickly diminishing if not introduced within 15 hours of infection. Significant harm is possible with short treatments, which are predicted to reduce survival. Overall this model supports the development of a device capable of modulating CXCR-1/2 expression to treatment acute inflammatory conditions like sepsis and further development of the computation model may help guide device development and target patient populations.

The next goal of this dissertation was to develop and evaluate an extracorporeal device which uses immobilized IL-8 to reprogram neutrophils. The reprogramming would attenuate neutrophil's chemotactic response to IL-8 and reduced neutrophil induced organ damage in acute inflammatory conditions such as sepsis. A variety of device materials, immobilization methods, and wash parameters were evaluated in an attempt to find a device configuration which maximizes IL-8 activity without resulting in functionally relevant levels of IL-8 leaching from the device. While significant levels of CXCR-1 and CXCR-2 downregulation were achieved, this effect was insufficient to cause consistent migratory shutoff to IL-8 as measured by a Boyden chamber chemotaxis assay. This approach appears to be limited by the required elevated levels of active IL-8 required to induce migratory shutoff. Learnings from this set of experiments were used to develop alternate device concepts described in the next dissertation chapter.

During development of the NeRD, limitations of the current design and possibilities for alternatives were considered. These alternatives were summarized in the third dissertation chapter. In order to address challenges associated with limited activity of immobilized IL-8 and issues with IL-8 leaching, experiments were conducted with absorbent columns to remove soluble IL-8 from recirculation. An infusion adsorption device concept was conceptualized, which intentionally infused soluble IL-8 into the extracorporeal circuit, but removed the IL-8 before it could be delivered to systemic recirculation. Initial testing, with infusion rates set to minimize IL-8

leaching, was unable to achieve migratory shutoff, but further optimization of the system may allow elevated IL-8 infusion rates and a greater impact on neutrophil chemotaxis. Another concept involves utilizing either the immobilized or infusion adsorption concept with an alternate ligand which operates at lower concentrations. While further research and testing is required to find an ideal ligand for this system, there is still potential to utilize the advantages of an extracorporeal circuit.

The final goal of this dissertation was to implement a zwitterionic macromolecule coating on PMP HFMs. Two techniques of PMP HFM functionalization and subsequent conjugation of SB block copolymers were evaluated for their ability to reduce platelet deposition. Both fiber configurations resulted in 80-95% reductions in platelet deposition from whole ovine blood, stability under shear stress, and uninhibited gas exchange performance relative to unmodified HFMs. Additionally, the functionalization and SBNHSi conjugation technique was shown to reduce platelet deposition on polycarbonate and poly(vinyl chloride), two other materials commonly found in extracorporeal circuits. The observed thromboresistance and stability of the SB modified surfaces, without degradation of HFM gas transfer performance, indicate that this approach is promising for longer term pre-clinical testing in respiratory assist devices and may ultimately allow for the reduction of anticoagulation levels in patients being supported for extended periods.

7.1 FUTURE VISIONS

Sepsis remains one of the largest challenges in modern medicine. Progress has been made in sepsis treatment, but it has been incremental rather than revolutionary. The long list of failed technologies shows how difficult it is for a concept to be translated from bench to bedside. Understanding of the underlying biology and immune system's role in sepsis has led to many potential therapies, but most fail at or before reaching blinded clinical testing. The patient diversity and wide range of symptoms presented in sepsis, in addition a high frequency of elderly patients with comorbidities, is one of the largest challenges that clinicians and innovators face. This challenge will only increase as medical technology extends the life of patients and improves outcomes of other conditions.

Improved diagnosis and division of the patient population may help improve outcomes of new technologies in sepsis. Treatments must be developed to address both hyper and hypo-inflammatory aspects of sepsis and identifying the correct patient characteristics will be critical to these treatment's success. Computational modeling can help support these decisions in the clinic; considering more inputs and data than would be otherwise possible, algorithms can be powerful tools to guide treatment and inform physicians. Development of rapid diagnostics to provide personalized treatment for patients would provide data to better inform both physicians and computational model inputs. Advances in microfluidics and diagnostics makes this a possibility. Improved selection of patients may also help address the difficulties of generating evidence in clinical studies. Selecting ideal patients, from a small subset of the population, may help therapies reach the market.

Even with a history of failed therapies, modulation of the immune system offers much promise for the future of sepsis treatments. Current therapies fail to address the underlying cause of sepsis, and approaches that modulate immune response offer the possibility of returning a patient to immune homeostasis. Many available therapies run the risk of overcorrecting the immune system, therefore a treatment that is either reversible or has active feedback may be necessary for a successful treatment. A system like the NeRD, that can be halted, with its effects degrading quickly, would be a promising advancement. The concept of selectively targeting cells within an extracorporeal circulation, without the therapeutic every reaching systemic circulation could be applied to many different cell signaling pathways while minimizing risks associated with systemic drug delivery.

Use of extracorporeal devices has become increasingly safe over the last 10-20 years, but continues to be associated with significant risks. Even occasional complications associated with bleeding or thrombus formation can counteract the advantages offered by lifesavings devices. This applies not only to potential immune-modulating technologies, but the next generation of respiratory assist devices. Improvements to human factors, usability, and training has significantly reduced the incidence of these complications, but the continued use of systemic anticoagulation will always be associated with negative side effects. The use of local anticoagulation is a logical next step for extracorporeal devices. Citrate anticoagulation, while not widely used, provides an option for lower flow extracorporeal devices. However, this approach is not widely used, and the complexity and potential harm if used incorrectly, may limit its widespread adoption. Additionally, citrate prevents coagulation, but may not limit any immune or complement activation that occurs in these circuits. Novel surface coatings may provide a significant improvement over currently available options. Coatings can be applied to an entire blood contacting surface area, limiting both

thrombus formation and immune activation. Heparin coatings, which are regularly used, provide some assistance, but these are quickly overwhelmed and degraded after blood contact. A stable coating with similar or greater affects has the possibility of drastically reducing complications of extracorporeal devices by minimizing or eliminating the use of systemic anticoagulation.

BIBLIOGRAPHY

[1] Angus DC, Linde-Zwirble W, Lidicker J, et al. Epidemiology of severe sepsis in the United States: Analysis of incidence, outcome, and associated costs of care. Crit. Care Med. July 2001. 2001;29:1303–1310.

[2] Brown K, Brain S, Pearson J, et al. Neutrophils in development of multiple organ failure in sepsis. Lancet. 2006;368:157–169.

[3] Annane D, Bellissant E, Cavaillon J-M. Septic shock. The Lancet. 2005;365:63–78.

[4] Nasraway SA. Sepsis research. Crit. Care Med. 1999;27:427–430.

[5] Dellinger R, Carlet J, Masur H, et al. Surviving Sepsis Campaign guidelines for management of severe sepsis and septic shock. Intensive Care Med. 2004;30:536–555.

[6] Kaukonen K, Bailey M, Suzuki S, et al. Mortality related to severe sepsis and septic shock among critically ill patients in Australia and New Zealand, 2000-2012. JAMA. 2014;311:1308–1316.

[7] The ProCESS Investigators. A Randomized Trial of Protocol-Based Care for Early Septic Shock. N. Engl. J. Med. 2014;370:1683–1693.

[8] Lagu T, Rothberg MB, Shieh M-S, et al. Hospitalizations, costs, and outcomes of severe sepsis in the United States 2003 to 2007. Crit. Care Med. 2012;40:754–761.

[9] Angus DC, van der Poll T. Severe Sepsis and Septic Shock. N. Engl. J. Med. 2013;369:840–851.

[10] Bone RC, Sibbald WJ, Sprung CL. The ACCP-SCCM consensus conference on sepsis and organ failure. CHEST J. 1992;101:1481–1483.

[11] The Surviving Sepsis Campaign Guidelines Committee including The Pediatric Subgroup*, Dellinger RP, Levy MM, et al. Surviving Sepsis Campaign: International Guidelines for Management of Severe Sepsis and Septic Shock, 2012. Intensive Care Med. 2013;39:165–228.

[12] Warren HS. Strategies for the Treatment of Sepsis. N. Engl. J. Med. 1997;336:952–953.

[13] Hotchkiss RS, Karl IE. The pathophysiology and treatment of sepsis. N. Engl. J. Med. 2003;348:138–150.

[14] Hotchkiss RS, Monneret G, Payen D. Sepsis-induced immunosuppression: from cellular dysfunctions to immunotherapy. Nat. Rev. Immunol. 2013;13:862–874.

[15] Hotchkiss RS, Coopersmith CM, McDunn JE, et al. The sepsis seesaw: tilting toward immunosuppression. Nat. Med. 2009;15:496–497.

[16] Galli SJ, Borregaard N, Wynn TA. Phenotypic and functional plasticity of cells of innate immunity: macrophages, mast cells and neutrophils. Nat. Immunol. 2011;12:1035–1044.

[17] Bajaj MS, Kew RR, Webster RO, et al. Priming of human neutrophil functions by tumor necrosis factor: enhancement of superoxide anion generation, degranulation, and chemotaxis to chemoattractants C5a and F-Met-Leu-Phe. Inflammation. 1992;16:241–250.

[18] Hallett MB, Lloyds D. Neutrophil priming: the cellular signals that say "amber" but not "green." Immunol. Today. 1995;16:264–268.

[19] Ayala A, Chung C-S, Lomas JL, et al. Shock-Induced Neutrophil Mediated Priming for Acute Lung Injury in Mice. Am. J. Pathol. 2002;161:2283–2294.

[20] Brown K, Brain S, Pearson J, et al. Neutrophils in development of multiple organ failure in sepsis. Lancet. 2006;368:157–169.

[21] Manda A, Pruchniak MP, Araźna M, et al. Neutrophil extracellular traps in physiology and pathology. Cent.-Eur. J. Immunol. 2014;39:116–121.

[22] Summers C, Rankin SM, Condliffe AM, et al. Neutrophil kinetics in health and disease. Trends Immunol. 2010;31:318–324.

[23] Rosales C, Demaurex N, Lowell CA, et al. Neutrophils: Their Role in Innate and Adaptive Immunity. J. Immunol. Res. [Internet]. 2016 [cited 2016 Mar 29];2016. Available from: http://www.ncbi.nlm.nih.gov/pmc/articles/PMC4783580/.

[24] Mantovani A, Cassatella MA, Costantini C, et al. Neutrophils in the activation and regulation of innate and adaptive immunity. Nat. Rev. Immunol. 2011;11:519–531.

[25] Kaplan MJ, Radic M. Neutrophil Extracellular Traps: Double-Edged Swords of Innate Immunity. J. Immunol. 2012;189:2689–2695.

[26] Botha AJ, Moore FA, Moore EE, et al. Early Neutrophil Sequestration after Injury: A Pathogenic Mechanism for Multiple Organ Failure. J. Trauma Acute Care Surg. 1995;39:411–417.

[27] Mallick AA, Ishizaka A, Stephens KE, et al. MUltiple organ damage caused by tumor necrosis factor and prevented by prior neutrophil depletion. Chest. 1989;95:1114–1120.

[28] Nylén ES, Alarifi AA. Humoral markers of severity and prognosis of critical illness. Best Pract. Res. Clin. Endocrinol. Metab. 2001;15:553–573.

[29] Meng W, Paunel-Gorgulu A, Flohé S, et al. Depletion of neutrophil extracellular traps in vivo results in hypersusceptibility to polymicrobial sepsis in mice. Crit Care. 2012;16:R137.

[30] Robertson CM, Perrone EE, McConnell KW, et al. Neutrophil Depletion Causes a Fatal Defect in Murine Pulmonary Staphylococcus aureus clearance. J. Surg. Res. 2008;150:278–285.

[31] Cohen J, Vincent J-L, Adhikari NK, et al. Sepsis: a roadmap for future research. Lancet Infect. Dis. 2015;15:581–614.

[32] Rivers E, Nguyen B, Havstad S, et al. Early Goal-Directed Therapy in the Treatment of Severe Sepsis and Septic Shock. N. Engl. J. Med. 2001;345:1368–1377.

[33] Carlbom DJ, Rubenfeld GD. Barriers to implementing protocol-based sepsis resuscitation in the emergency department—Results of a national survey*: Crit. Care Med. 2007;35:2525–2532.

[34] Reade MC, Huang DT, Bell D, et al. Variability in management of early severe sepsis. Emerg. Med. J. 2010;27:110–115.

[35] Ferrer R, Artigas A, Levy MM, et al. Improvement in process of care and outcome after a multicenter severe sepsis educational program in Spain. Jama. 2008;299:2294–2303.

[36] Annane D, Bellissant E, Bollaert P-E, et al. Corticosteroids in the Treatment of Severe Sepsis and Septic Shock in Adults: A Systematic Review. JAMA. 2009;301:2362–2375.

[37] Zhang Z. Recombinant human activated protein C for the treatment of severe sepsis and septic shock: a study protocol for incorporating observational evidence using a Bayesian approach. BMJ Open. 2014;4:e005622.

[38] Christiaans SC, Wagener BM, Esmon CT, et al. Protein C and acute inflammation: a clinical and biological perspective. Am. J. Physiol. - Lung Cell. Mol. Physiol. 2013;305:L455–L466.

[39] Bernard GR, Vincent J-L, Laterre P-F, et al. Efficacy and Safety of Recombinant Human Activated Protein C for Severe Sepsis. N. Engl. J. Med. 2001;344:699–709.

[40] Ranieri VM, Thompson BT, Barie PS, et al. Drotrecogin Alfa (Activated) in Adults with Septic Shock. N. Engl. J. Med. 2012;366:2055–2064.

[41] B M, Be S, Fa M, et al. A Review of GM-CSF Therapy in Sepsis., A Review of GM-CSF Therapy in Sepsis. Med. Med. 2015;94, 94:e2044–e2044.

[42] Hotchkiss RS, Sherwood ER. Getting sepsis therapy right. Science. 2015;347:1201–1202.

[43] Hutchins NA, Unsinger J, Hotchkiss RS, et al. The new normal: immunomodulatory agents against sepsis immune suppression. Trends Mol. Med. 2014;20:224–233.

[44] Ye C, Choi J-G, Abraham S, et al. Human macrophage and dendritic cell-specific silencing of high-mobility group protein B1 ameliorates sepsis in a humanized mouse model. Proc. Natl. Acad. Sci. 2012;109:21052–21057.

[45] Angus DC, Yang L, Kong L, et al. Circulating high-mobility group box 1 (HMGB1) concentrations are elevated in both uncomplicated pneumonia and pneumonia with severe sepsis*: Crit. Care Med. 2007;35:1061–1067.

[46] Wang H, Liao H, Ochani M, et al. Cholinergic agonists inhibit HMGB1 release and improve survival in experimental sepsis. Nat. Med. 2004;10:1216–1221.

[47] Gentile LF, Moldawer LL. HMGB1 as a therapeutic target for sepsis: it's all in the timing! Expert Opin. Ther. Targets. 2014;18:243–245.

[48] Vriese ASD, Colardyn FA, Philippé JJ, et al. Cytokine Removal during Continuous Hemofiltration in Septic Patients. J. Am. Soc. Nephrol. 1999;10:846–853.

[49] Morris C, Gray L, Giovannelli M. Early report: The use of Cytosorb™ haemabsorption column as an adjunct in managing severe sepsis: initial experiences, review and recommendations. J. Intensive Care Soc. 2015;1751143715574855.

[50] Rimmelé T, Kellum JA. Clinical review: blood purification for sepsis. Crit. Care Lond. Engl. 2011;15:205.

[51] Honore PM, matson, James. Extracorporeal removal for sepsis: Acting at the tissue leve... : Critical Care Medicine [Internet]. LWW. [cited 2017 May 16]. Available from: http://journals.lww.com/ccmjournal/Fulltext/2004/03000/Extracorporeal_removal_for_sepsis__Acting_at_the.53.aspx.

[52] Kellum JA, Uchino S. International Differences in the Treatment of Sepsis: Are They Justified? JAMA. 2009;301:2496–2497.

[53] Cole L, Bellomo R, Journois D, et al. High-volume haemofiltration in human septic shock. Intensive Care Med. 2001;27:978–986.

[54] Joannes-Boyau O, Rapaport S, Bazin R, et al. Impact of High Volume Hemofiltration on Hemodynamic Disturbance and Outcome during Septic Shock: ASAIO J. 2004;50:102–109.

[55] Bellomo R, Kellum JA, Gandhi CR, et al. The Effect of Intensive Plasma Water Exchange by Hemofiltration on Hemodynamics and Soluble Mediators in Canine Endotoxemia. Am. J. Respir. Crit. Care Med. 2000;161:1429–1436.

[56] Payen D, Mateo J, Cavaillon JM, et al. Impact of continuous venovenous hemofiltration on organ failure during the early phase of severe sepsis: A randomized controlled trial*: Crit. Care Med. 2009;37:803–810.

[57] Cole L, Bellomo R, Hart G, et al. A phase II randomized, controlled trial of continuous hemofiltration in sepsis. Crit. Care Med. 2002;30:100–106.

[58] M H, R B, S M, et al. High cut-off point membranes in septic acute renal failure: a systematic review. Int. J. Artif. Organs. 2007;30:1031–1041.

[59] Haase M, Bellomo R, Baldwin I, et al. Hemodialysis Membrane With a High-Molecular-Weight Cutoff and Cytokine Levels in Sepsis Complicated by Acute Renal Failure: A Phase 1 Randomized Trial. Am. J. Kidney Dis. 2007;50:296–304.

[60] Morgera S, Klonower D, Rocktaschel J, et al. TNF- elimination with high cut-off haemofilters: a feasible clinical modality for septic patients? Nephrol. Dial. Transplant. 2003;18:1361–1369.

[61] Esteban E, Ferrer R, Alsina L, et al. Immunomodulation in Sepsis: The Role of Endotoxin Removal by Polymyxin B-Immobilized Cartridge. Mediators Inflamm. [Internet]. 2013 [cited 2014 Mar 13];2013. Available from: http://www.ncbi.nlm.nih.gov/pmc/articles/PMC3819752/.

[62] Fujii T, Ganeko R, Kataoka Y, et al. Polymyxin B-immobilised haemoperfusion and mortality in critically ill patients with sepsis/septic shock: a protocol for a systematic review and meta-analysis. BMJ Open [Internet]. 2016 [cited 2016 Dec 6];6. Available from: http://www.ncbi.nlm.nih.gov/pmc/articles/PMC5128836/.

[63] Cutuli SL, Artigas A, Fumagalli R, et al. Polymyxin-B hemoperfusion in septic patients: analysis of a multicenter registry. Ann. Intensive Care [Internet]. 2016 [cited 2016 Aug 22];6. Available from: http://www.ncbi.nlm.nih.gov/pmc/articles/PMC4977232/.

[64] Pickkers P, Payen D. What's new in the extracorporeal treatment of sepsis? Intensive Care Med. 2017;1–3.

[65] Kellum JA, Song M, Venkataraman R. Hemoadsorption removes tumor necrosis factor, interleukin-6, and interleukin-10, reduces nuclear factor-kappaB DNA binding, and improves short-term survival in lethal endotoxemia. Crit. Care Med. 2004;32:801–805.

[66] Peng Z-Y, Carter MJ, Kellum JA, et al. Effects of hemoadsorption on cytokine removal and short-term survival in septic rats. Crit. Care Med. 2008;36:1573–1577.

[67] David S, Thamm K, Schmidt BMW, et al. Effect of extracorporeal cytokine removal on vascular barrier function in a septic shock patient. J. Intensive Care [Internet]. 2017 [cited 2017 Jan 31];5. Available from: http://www.ncbi.nlm.nih.gov/pmc/articles/PMC5251288/.

[68] Bernardi MH, Rinoesl H, Dragosits K, et al. Effect of hemoadsorption during cardiopulmonary bypass surgery – a blinded, randomized, controlled pilot study using a novel adsorbent. Crit. Care. 2016;20:96.

[69] Busund R, Koukline V, Utrobin U, et al. Plasmapheresis in severe sepsis and septic shock: a prospective, randomised, controlled trial. Intensive Care Med. 2002;28:1434–1439.

[70] Eguchi Y. Plasma dia-filtration for severe sepsis. Acute Blood Purif. [Internet]. Karger Publishers; 2010 [cited 2017 May 17]. p. 142–149. Available from: http://www.karger.com/Article/Abstract/314864.

[71] Cole L, Bellomo R, Davenport P, et al. The effect of coupled haemofiltration and adsorption on inflammatory cytokines in an ex vivo model. Nephrol. Dial. Transplant. 2002;17:1950–1956.

[72] Carcillo J, Kellum J. Is there a role for plasmapheresis/plasma exchange therapy in septic shock, MODS, and thrombocytopenia-associated multiple organ failure? We still do not know - but perhaps we are closer. Intensive Care Med. 2002;28:1373–1375.

[73] Rimmele T, Assadi A, Cattenoz M, et al. High-volume haemofiltration with a new haemofiltration membrane having enhanced adsorption properties in septic pigs. Nephrol. Dial. Transplant. 2008;24:421–427.

[74] Didar TF, Cartwright MJ, Rottman M, et al. Improved treatment of systemic blood infections using antibiotics with extracorporeal opsonin hemoadsorption. Biomaterials. 2015;67:382–392.

[75] Ding F, Song JH, Jung JY, et al. A Biomimetic Membrane Device That Modulates the Excessive Inflammatory Response to Sepsis. PLoS ONE. 2011;6:e18584.

[76] Humes HD, Sobota JT, Ding F, et al. A Selective Cytopheretic Inhibitory Device to Treat the Immunological Dysregulation of Acute and Chronic Renal Failure. Blood Purif. 2010;29:183–190.

[77] Ding F, Yevzlin AS, Xu ZY, et al. The Effects of a Novel Therapeutic Device on Acute Kidney Injury Outcomes in the Intensive Care Unit: A Pilot Study: ASAIO J. 2011;57:426–432.

[78] Tumlin JA, Galphin CM, Tolwani AJ, et al. A Multi-Center, Randomized, Controlled, Pivotal Study to Assess the Safety and Efficacy of a Selective Cytopheretic Device in Patients with Acute Kidney Injury. PloS One. 2015;10:e0132482.

[79] Malkin AD, Sheehan RP, Mathew S, et al. A Neutrophil Phenotype Model for Extracorporeal Treatment of Sepsis. PLoS Comput Biol. 2015;11:e1004314.

[80] Angus DC. The search for effective therapy for sepsis: Back to the drawing board? JAMA. 2011;306:2614–2615.

[81] Iskander KN, Osuchowski MF, Stearns-Kurosawa DJ, et al. Sepsis: Multiple Abnormalities, Heterogeneous Responses, and Evolving Understanding. Physiol. Rev. 2013;93:1247–1288.

[82] Kellum JA, Kong L, Fink MP, et al. Understanding the inflammatory cytokine response in pneumonia and sepsis: Results of the genetic and inflammatory markers of sepsis (genims) study. Arch. Intern. Med. 2007;167:1655–1663.

[83] Song SO, Hogg J, Peng Z-Y, et al. Ensemble models of neutrophil trafficking in severe sepsis. PLoS Comput. Biol. 2012;8:e1002422.

[84] Angus DC, Linde-Zwirble W, Lidicker J, et al. Epidemiology of severe sepsis in the United States: Analysis of incidence, outcome, and associated costs of care. Crit. Care Med. July 2001. 2001;29:1303–1310.

[85] Dellinger R, Carlet J, Masur H, et al. Surviving Sepsis Campaign guidelines for management of severe sepsis and septic shock. Intensive Care Med. 2004;30:536–555.

[86] Yealy DM, Kellum J a, Huang DT, et al. A randomized trial of protocol-based care for early septic shock. N. Engl. J. Med. 2014;370:1683–1693.

[87] Martin GS, Mannino DM, Eaton S, et al. The epidemiology of sepsis in the United States from 1979 through 2000. N. Engl. J. Med. 2003;348:1546–1554.

[88] Lagu T, Rothberg MB, Shieh M-S, et al. Hospitalizations, costs, and outcomes of severe sepsis in the United States 2003 to 2007. Crit. Care Med. 2012;40:754–761.

[89] Angus DC. The search for effective therapy for sepsis: back to the drawing board? JAMA. 2011;306:2614–2615.

[90] Angus DC, van der Poll T. Severe sepsis and septic shock. N. Engl. J. Med. 2013;369:840–851.

[91] Iskander KN, Osuchowski MF, Stearns-Kurosawa DJ, et al. Sepsis: multiple abnormalities, heterogeneous responses, and evolving understanding. Physiol. Rev. 2013;93:1247–1288.

[92] Kellum JA, Kong L, Fink MP, et al. Understanding the inflammatory cytokine response in pneumonia and sepsis: results of the Genetic and Inflammatory Markers of Sepsis (GenIMS) Study. Arch. Intern. Med. 2007;167:1655–1663.

[93] Nylén ES, Alarifi a a. Humoral markers of severity and prognosis of critical illness. Best Pract. Res. Clin. Endocrinol. Metab. 2001;15:553–573.

[94] Simon A. Jones, Wolf M, Qin S, et al. Different Functions for the Interleukin 8 Receptors (il-8r) of Human Neutrophil Leukocytes: NADPH Oxidase and Phospholipase D are Activated through IL-8R1 but not IL-8R2. Proc. Natl. Acad. Sci. U. S. A. 1996;93:6682–6686.

[95] Nasser MW, Raghuwanshi SK, Grant DJ, et al. Differential activation and regulation of CXCR1 and CXCR2 by CXCL8 monomer and dimer. J. Immunol. Baltim. Md 1950. 2009;183:3425–3432.

[96] Alves-Filho JC, Freitas A, Souto FO, et al. Regulation of chemokine receptor by Toll-like receptor 2 is critical to neutrophil migration and resistance to polymicrobial sepsis. Proc. Natl. Acad. Sci. U. S. A. 2009;106:4018–4023.

[97] Schlag G, Redl H, Davies J, et al. Live Escherichia coli Sepsis Models in Baboons. Pathophysiol. Shock Sepsis Organ Fail. Springer Berlin Heidelberg; 1993. p. 1076–1107.

[98] Krumsiek J, Pölsterl S, Wittmann DM, et al. Odefy--from discrete to continuous models. BMC Bioinformatics. 2010;11:233.

[99] Wittmann DM, Krumsiek J, Saez-Rodriguez J, et al. Transforming Boolean models to continuous models: methodology and application to T-cell receptor signaling. BMC Syst. Biol. 2009;3:98.

[100] Baggiolini M, Walz A, Kunkel SL, et al. Neutrophil-activating peptide-1/interleukin 8, a novel cytokine that activates neutrophils. J. Clin. Invest. 1989;84:1045–1049.

[101] Lenz A, Franklin G a, Cheadle WG. Systemic inflammation after trauma. Injury. 2007;38:1336–1345.

[102] Boyle EM, Pohlman TH, Johnson MC, et al. Endothelial cell injury in cardiovascular surgery: the systemic inflammatory response. Ann. Thorac. Surg. 1997;63:277–284.

[103] Appelberg R. Neutrophils and intracellular pathogens: beyond phagocytosis and killing. Trends Microbiol. 2007;15:87–92.

[104] Badwey JA, Karnovsky ML. Active oxygen species and the functions of phagocytic leukocytes. Annu. Rev. Biochem. 1980;49:695–726.

[105] Rose JJ, Foley JF, Murphy PM, et al. On the Mechanism and Significance of Ligand-induced Internalization of Human Neutrophil Chemokine Receptors CXCR1 and CXCR2. J. Biol. Chem. 2004;279:24372–24386.

[106] Gijsbers K, Van Assche G, Joossens S, et al. CXCR1-binding chemokines in inflammatory bowel diseases: down-regulated IL-8/CXCL8 production by leukocytes in Crohn's disease and selective GCP-2/CXCL6 expression in inflamed intestinal tissue. Eur. J. Immunol. 2004;34:1992–2000.

[107] Martich BGD, Danner RL, Ceska M, et al. Detection of interleukin 8 and tumor necrosis factor in normal humans after intravenous endotoxin: the effect of antiinflammatory agents. J. Exp. Med. 1991;173:1021–1024.

[108] Feniger-Barish R, Ran M, Zaslaver a, et al. Differential modes of regulation of cxc chemokine-induced internalization and recycling of human CXCR1 and CXCR2. Cytokine. 1999;11:996–1009.

[109] Schoeberl B, Eichler-Jonsson C, Gilles ED, et al. Computational modeling of the dynamics of the MAP kinase cascade activated by surface and internalized EGF receptors. Nat. Biotechnol. 2002;20:370–375.

[110] Summers C, Rankin SM, Condliffe AM, et al. Neutrophil kinetics in health and disease. Trends Immunol. 2010;31:318–324.

[111] Cockcroft DW, Gault MH. Prediction of creatinine clearance from serum creatinine. Nephron. 1976;16:31–41.

[112] Swigon D. Ensemble Modeling of Biological Systems. In: Alexandra V. Antoniouk, Melnik RVN, editors. Math. Life Sci. Walter de Gruyter; 2012. p. 19–42.

[113] Brown K, Sethna J. Statistical mechanical approaches to models with many poorly known parameters. Phys. Rev. E. 2003;68:021904.

[114] Swendsen R, Wang J. Replica Monte Carlo simulation of spin glasses. Phys. Rev. Lett. 1986;57:2607–2609.

[115] Earl DJ, Deem MW. Parallel tempering: theory, applications, and new perspectives. Phys. Chem. Chem. Phys. PCCP. 2005;7:3910–3916.

[116] Mochan E, Swigon D, Ermentrout GB, et al. A mathematical model of intrahost pneumococcal pneumonia infection dynamics in murine strains. J. Theor. Biol. 2014;353:44–54.

[117] Fernández Slezak D, Suárez C, Cecchi GA, et al. When the optimal is not the best: Parameter estimation in complex biological models. PLoS ONE. 2010;5:e13283.

[118] Roberts G, Gelman A, Gilks W. Weak convergence and optimal scaling of random walk Metropolis algorithms. Ann. Appl. Probab. 1997;7:110–120.

[119] Gelman A, Rubin DB. lnference from Iterative Simulation Using Multiple Sequences. Stat. Sci. 1992;7:457–472.

[120] Brooks S, Gelman A. General methods for monitoring convergence of iterative simulations. J. Comput. Graph. Stat. 1998;7:434–455.

[121] Li G, Rabitz H, Yelvington PE, et al. Global sensitivity analysis for systems with independent and/or correlated inputs. J. Phys. Chem. A. 2010;114:6022–6032.

[122] Miller MA, Feng XJ, Li G, et al. Identifying biological network structure, predicting network behavior, and classifying network state with high dimensional model representation (HDMR). PLoS ONE. 2012;7:e37664.

[123] Mathew S, Bartels J, Banerjee I, et al. Global sensitivity analysis of a mathematical model of acute inflammation identifies nonlinear dependence of cumulative tissue damage on host interleukin-6 responses. J. Theor. Biol. 2014;358:132–148.

[124] Mathew S, Sundararaj S, Mamiya H, et al. Regulatory interactions maintaining self-renewal of human embryonic stem cells as revealed through a systems analysis of PI3K/AKT pathway. Bioinforma. Oxf. Engl. 2014;30:2334–2342.

[125] Hall M, Frank E, Holmes G. The WEKA data mining software: an update. ACM SIGKDD Explor. 2009;11:10–18.

[126] Gutenkunst RN, Waterfall JJ, Casey FP, et al. Universally sloppy parameter sensitivities in systems biology models. Arkin AP, editor. PLoS Comput. Biol. 2007;3:1871–1878.

[127] Haseltine EL, Rawlings JB. Approximate simulation of coupled fast and slow reactions for stochastic chemical kinetics. J. Chem. Phys. 2002;117:6959.

[128] Resat H, Petzold L, Pettigrew MF. Kinetic modeling of biological systems. Methods Mol. Biol. Clifton NJ. 2009;541:311–335.

[129] Swat MH, Thomas GL, Belmonte JM, et al. Multi-scale modeling of tissues using CompuCell3D. Methods Cell Biol. 2012;110:325–366.

[130] Lipniacki T, Paszek P, Brasier AR, et al. Stochastic regulation in early immune response. Biophys. J. 2006;90:725–742.

[131] Prokopiou S, Barbarroux L, Bernard S, et al. Multiscale Modeling of the Early CD8 T-Cell Immune Response in Lymph Nodes: An Integrative Study. Computation. 2014;2:159–181.

[132] Kiparissides A, Kucherenko SS, Mantalaris A, et al. Global Sensitivity Analysis Challenges in Biological Systems Modeling. Ind. Eng. Chem. Res. 2009;48:7168–7180.

[133] Kent E, Neumann S, Kummer U, et al. What can we learn from global sensitivity analysis of biochemical systems? PLoS ONE. 2013;8:e79244.

[134] Waydhas C, Nast-Kolb D, Jochum M, et al. Inflammatory mediators, infection, sepsis, and multiple organ failure after severe trauma. Arch. Surg. 1992;127:460–467.

[135] Ritter C, Andrades ME, Reinke A, et al. Treatment with N-acetylcysteine plus deferoxamine protects rats against oxidative stress and improves survival in sepsis. Crit. Care Med. 2004;32:342–349.

[136] Cummings CJ, Martin TR, Frevert CW, et al. Expression and function of the chemokine receptors CXCR1 and CXCR2 in sepsis. J. Immunol. 1999;162:2341–2346.

[137] Fujishima S, Aikawa N. Neutrophil-mediated tissue injury and its modulation. Intensive Care Med. 1995;21:277–285.

[138] Taneja R, Parodo J, Jia SH, et al. Delayed neutrophil apoptosis in sepsis is associated with maintenance of mitochondrial transmembrane potential and reduced caspase-9 activity. Crit. Care Med. 2004;32:1460–1469.

[139] Fialkow L, Fochesatto Filho L, Bozzetti MC, et al. Neutrophil apoptosis: a marker of disease severity in sepsis and sepsis-induced acute respiratory distress syndrome. Crit. Care Lond. Engl. 2006;10:R155.

[140] Moriconi A, Cesta MC, Cervellera MN, et al. Design of Noncompetitive Interleukin-8 Inhibitors Acting on CXCR1 and CXCR2. J. Med. Chem. 2007;50:3984–4002.

[141] Bizzarri C, Beccari AR, Bertini R, et al. ELR+ CXC chemokines and their receptors (CXC chemokine receptor 1 and CXC chemokine receptor 2) as new therapeutic targets. Pharmacol. Ther. 2006;112:139–149.

[142] Bertini R, Allegretti M, Bizzarri C, et al. Noncompetitive allosteric inhibitors of the inflammatory chemokine receptors CXCR1 and CXCR2: Prevention of reperfusion injury. Proc. Natl. Acad. Sci. U. S. A. 2004;101:11791–11796.

[143] Osuchowski MF, Remick DG, Lederer J a, et al. Abandon the mouse research ship? Not just yet! Shock Augusta Ga. 2014;41:463–475.

[144] Seok J, Warren HS, Cuenca AG, et al. Genomic responses in mouse models poorly mimic human inflammatory diseases. Proc. Natl. Acad. Sci. U. S. A. 2013;110:3507–3512.

[145] Takao K, Miyakawa T. Genomic responses in mouse models greatly mimic human inflammatory diseases. Proc. Natl. Acad. Sci. 2014;1401965111-.

[146] Fu W, Zhang Y, Zhang J, et al. Cloning and characterization of mouse homolog of the CXC chemokine receptor CXCR1. Cytokine. 2005;31:9–17.

[147] Peng Z-Y, Wang H-Z, Carter MJ, et al. Acute removal of common sepsis mediators does not explain the effects of extracorporeal blood purification in experimental sepsis. Kidney Int. 2012;81:363–369.

[148] Panagiotou A, Gaiao S, Cruz DN. Extracorporeal therapies in sepsis. J. Intensive Care Med. 2013;28:281–295.

[149] Kang JH, Super M, Yung CW, et al. An extracorporeal blood-cleansing device for sepsis therapy. Nat. Med. 2014;20:1211–1216.

[150] Rimmelé T, Kaynar AM, McLaughlin JN, et al. Leukocyte capture and modulation of cell-mediated immunity during human sepsis: an ex vivo study. Crit. Care Lond. Engl. 2013;17:R59.

[151] Gaieski DF, Mikkelsen ME, Band RA, et al. Impact of time to antibiotics on survival in patients with severe sepsis or septic shock in whom early goal-directed therapy was initiated in the emergency department. Crit. Care Med. 2010;38:1045–1053.

[152] Bozza F a, Salluh JI, Japiassu AM, et al. Cytokine profiles as markers of disease severity in sepsis: a multiplex analysis. Crit. Care. 2007;11:R49.

[153] Kibe S, Adams K, Barlow G. Diagnostic and prognostic biomarkers of sepsis in critical care. J. Antimicrob. Chemother. 2011;66 Suppl 2:ii33-40.

[154] Pierrakos C, Vincent J-L. Sepsis biomarkers: a review. Crit. Care Lond. Engl. 2010;14:R15.

[155] Pillay J, Hietbrink F, Koenderman L, et al. The systemic inflammatory response induced by trauma is reflected by multiple phenotypes of blood neutrophils. Injury. 2007;38:1365–1372.

[156] A Randomized Trial of Protocol-Based Care for Early Septic Shock. N. Engl. J. Med. 0:null.

[157] Chishti A, Shenton B, Kirby J, et al. Neutrophil chemotaxis and receptor expression in clinical septic shock. Intensive Care Med. 2004;30:605–611.

[158] Tsuchida K, Yoshimura R, Nakatani T, et al. Blood Purification for Critical Illness: Cytokines Adsorption Therapy. Ther. Apher. Dial. 2006;10:25–31.

[159] Chaudhry H, Zhou J, Zhong Y, et al. Role of Cytokines as a Double-edged Sword in Sepsis. Vivo Athens Greece. 2013;27:669–684.

[160] Kimmel JD, Arazawa DT, Ye S-H, et al. Carbonic anhydrase immobilized on hollow fiber membranes using glutaraldehyde activated chitosan for artificial lung applications. J. Mater. Sci. Mater. Med. 2013;24:2611–2621.

[161] Arazawa DT, Oh H-I, Ye S-H, et al. Immobilized carbonic anhydrase on hollow fiber membranes accelerates CO2 removal from blood. J. Membr. Sci. 2012;403–404:25–31.

[162] Ye S-H, Arazawa DT, Zhu Y, et al. Hollow Fiber Membrane Modification with Functional Zwitterionic Macromolecules for Improved Thromboresistance in Artificial Lungs. Langmuir. 2015;31:2463–2471.

[163] Arazawa DT, Kimmel JD, Finn MC, et al. Acidic sweep gas with carbonic anhydrase coated hollow fiber membranes synergistically accelerates CO2 removal from blood. Acta Biomater. 2015;25:143–149.

[164] Hermanson GT. Bioconjugate Techniques. Academic Press; 2010.

[165] Anne A, Moiroux J. Quantitative Characterization of the Flexibility of Poly(ethylene glycol) Chains Attached to a Glassy Carbon Electrode. Macromolecules. 1999;32:5829–5835.

[166] Anne A, Demaille C, Moiroux J. Terminal Attachment of Polyethylene Glycol (PEG) Chains to a Gold Electrode Surface. Cyclic Voltammetry Applied to the Quantitative Characterization of the Flexibility of the Attached PEG Chains and of Their Penetration by Mobile PEG Chains. Macromolecules. 2002;35:5578–5586.

[167] Boyden S. The Chemotactic Effect of Mixtures of Antibody and Antigen on Polymorphonuclear Leucocytes. J. Exp. Med. 1962;115:453–466.

[168] Chen H-C. Boyden Chamber Assay. In: Guan J-L, editor. Cell Migr. [Internet]. Humana Press; 2005 [cited 2014 Oct 31]. p. 15–22. Available from: http://link.springer.com/protocol/10.1385/1-59259-860-9%3A015.

[169] Thomas M, Moriyama K, Ledebo I. AN69: Evolution of the World's First High Permeability Membrane. In: Saito A, Kawanishi H, Yamashita AC, et al., editors. Contrib. Nephrol. [Internet]. Basel: KARGER; 2011 [cited 2016 Feb 4]. p. 119–129. Available from: http://www.karger.com/doi/10.1159/000328961.

[170] Feniger-Barish R, Yron I, Meshel T, et al. IL-8-Induced Migratory Responses through CXCR1 and CXCR2: Association with Phosphorylation and Cellular Redistribution of Focal Adhesion Kinase†. Biochemistry (Mosc.). 2003;42:2874–2886.

[171] Chiang N, Serhan CN, Dahlén S-E, et al. The Lipoxin Receptor ALX: Potent Ligand-Specific and Stereoselective Actions in Vivo. Pharmacol. Rev. 2006;58:463–487.

[172] Maderna P, Cottell DC, Toivonen T, et al. FPR2/ALX receptor expression and internalization are critical for lipoxin A4 and annexin-derived peptide-stimulated phagocytosis. FASEB J. 2010;24:4240–4249.

[173] Arazawa DT, Kimmel JD, Finn MC, et al. Acidic sweep gas with carbonic anhydrase coated hollow fiber membranes synergistically accelerates CO2 removal from blood. Acta Biomater. [Internet]. [cited 2015 Jul 13]; Available from: http://www.sciencedirect.com/science/article/pii/S1742706115300118.

[174] Nolan H, Wang D, Zwischenberger JB. Artificial lung basics. Organogenesis. 2011;7:23–27.

[175] Federspiel WJ, Henchir KA. Lung, artificial: basic principles and current applications. Encycl. Biomater. Biomed. Eng. 2004;9:910.

[176] Esper SA, Levy JH, Waters JH, et al. Extracorporeal Membrane Oxygenation in the Adult: A Review of Anticoagulation Monitoring and Transfusion. Anesth. Analg. 2014;118:731–743.

[177] Galbusera M, Remuzzi G, Boccardo P. Treatment of Bleeding in Dialysis Patients. Semin. Dial. 2009;22:279–286.

[178] Kaw D, Malhotra D. HEMATOLOGY: ISSUES IN THE DIALYSIS PATIENT: Platelet Dysfunction and End-Stage Renal Disease. Semin. Dial. 2006;19:317–322.

[179] Jaffer IH, Fredenburgh JC, Hirsh J, et al. Medical device-induced thrombosis: what causes it and how can we prevent it? J. Thromb. Haemost. 2015;13:S72–S81.

[180] Wendel HP, Ziemer G. Coating-techniques to improve the hemocompatibility of artificial devices used for extracorporeal circulation. Eur. J. Cardiothorac. Surg. 1999;16:342–350.

[181] Gorbet MB, Sefton MV. Biomaterial-associated thrombosis: roles of coagulation factors, complement, platelets and leukocytes. Biomaterials. 2004;25:5681–5703.

[182] Annich GM. Extracorporeal life support: the precarious balance of hemostasis. J. Thromb. Haemost. 2015;13:S336–S342.

[183] Strueber M. Artificial Lungs. Thorac. Surg. Clin. 2015;25:107–113.

[184] McManus ML, Kevy SV, Bower LK, et al. Coagulation factor deficiencies during initiation of extracorporeal membrane oxygenation. J. Pediatr. 1995;126:900–904.

[185] Despotis GJ, Avidan MS, Hogue Jr CW. Mechanisms and attenuation of hemostatic activation during extracorporeal circulation. Ann. Thorac. Surg. 2001;72:S1821–S1831.

[186] Robba C, Ortu A, Bilotta F, et al. Extracorporeal membrane oxygenation for adult respiratory distress syndrome in trauma patients: A case series and systematic literature review. J. Trauma Acute Care Surg. 2017;82:165–173.

[187] Makdisi G, Wang I. Extra Corporeal Membrane Oxygenation (ECMO) review of a lifesaving technology. J. Thorac. Dis. 2015;7:E166–E176.

[188] Andrews J, Winkler AM. Challenges with Navigating the Precarious Hemostatic Balance during Extracorporeal Life Support: Implications for Coagulation and Transfusion Management. Transfus. Med. Rev. 2016;30:223–229.

[189] Zangrillo A, Landoni G, Biondi-Zoccai G, et al. A meta-analysis of complications and mortality of extracorporeal membrane oxygenation. Crit. Care Resusc. 2013;15:172.

[190] Pesenti A, Patroniti N, Fumagalli R. Carbon dioxide dialysis will save the lung: Crit. Care Med. 2010;38:S549–S554.

[191] Lund LW, Federspiel WJ. Removing extra CO2 in COPD patients. Curr. Respir. Care Rep. 2013;2:131–138.

[192] Crotti S, Lissoni A, Tubiolo D, et al. Artificial lung as an alternative to mechanical ventilation in COPD exacerbation. Eur. Respir. J. 2012;39:212–215.

[193] Montoya JP, Shanley CJ, Merz SI, et al. Plasma Leakage through Microporous Membranes: Role of Phospholipids. ET J. 1992;38.

[194] Wu M-Y, Hsu Y-H, Bai C-H, et al. Regional Citrate Versus Heparin Anticoagulation for Continuous Renal Replacement Therapy: A Meta-Analysis of Randomized Controlled Trials. Am. J. Kidney Dis. 2012;59:810–818.

[195] Liu C, Mao Z, Kang H, et al. Regional citrate versus heparin anticoagulation for continuous renal replacement therapy in critically ill patients: a meta-analysis with trial sequential analysis of randomized controlled trials. Crit. Care [Internet]. 2016 [cited 2017 Jan 9];20. Available from: http://www.ncbi.nlm.nih.gov/pmc/articles/PMC4866420/.

[196] Silvetti S, Koster A, Pappalardo F. Do We Need Heparin Coating for Extracorporeal Membrane Oxygenation? New Concepts and Controversial Positions About Coating Surfaces of Extracorporeal Circuits. Artif. Organs. 2015;39:176–179.

[197] Ye SH, Watanabe J, Iwasaki Y, et al. Antifouling blood purification membrane composed of cellulose acetate and phospholipid polymer. Biomaterials. 2003;24:4143–4152.

[198] Sin M-C, Chen S-H, Chang Y. Hemocompatibility of zwitterionic interfaces and membranes. Polym. J. 2014;46:436–443.

[199] Schlenoff JB. Zwitteration: Coating Surfaces with Zwitterionic Functionality to Reduce Nonspecific Adsorption. Langmuir. 2014;30:9625–9636.

[200] He M, Gao K, Zhou L, et al. Zwitterionic materials for antifouling membrane surface construction. Acta Biomater. 2016;40:142–152.

[201] Zhang Z, Chen S, Chang Y, et al. Surface Grafted Sulfobetaine Polymers via Atom Transfer Radical Polymerization as Superlow Fouling Coatings. J. Phys. Chem. B. 2006;110:10799–10804.

[202] Ueda T, Oshida H, Kurita K, et al. Perparation of 2-Methacryloyloxyethyl Phosphorylcholine Copolymers with Alkyl Methacrylates and Their Blood Compatibility. Polym. J. 1992;24:1259–1269.

[203] Wang D, Williams CG, Li Q, et al. Synthesis and characterization of a novel degradable phosphate-containing hydrogel. Biomaterials. 2003;24:3969–3980.

[204] Dixit CK, Vashist SK, MacCraith BD, et al. Multisubstrate-compatible ELISA procedures for rapid and high-sensitivity immunoassays. Nat. Protoc. 2011;6:439–445.

[205] Fischer ME. Amine Coupling Through EDC/NHS: A Practical Approach. In: Mol NJ, Fischer MJE, editors. Surf. Plasmon Reson. [Internet]. Humana Press; 2010 [cited 2017 Jan 10]. p. 55–73. Available from: http://dx.doi.org/10.1007/978-1-60761-670-2_3.

[206] Arazawa DT, Oh H-I, Ye S-H, et al. Immobilized carbonic anhydrase on hollow fiber membranes accelerates CO2 removal from blood. J. Membr. Sci. 2012;403–404:25–31.

[207] Calderon JG, Harsch A, Gross GW, et al. Stability of plasma-polymerized allylamine films with sterilization by autoclaving. J. Biomed. Mater. Res. 1998;42:597–603.

[208] Huang X, Wang W, Zheng Z, et al. Surface monofunctionalized polymethyl pentene hollow fiber membranes by plasma treatment and hemocompatibility modification for membrane oxygenators. Appl. Surf. Sci. 2016;362:355–363.

[209] Toomasian JM, Schreiner RJ, Meyer DE, et al. A Polymethylpentene Fiber Gas Exchanger for Long-Term Extracorporeal Life Support: ASAIO J. 2005;51:390–397.

[210] Amoako KA, Sundaram HS, Suhaib A, et al. Multimodal, Biomaterial-Focused Anticoagulation via Superlow Fouling Zwitterionic Functional Groups Coupled with Anti-Platelet Nitric Oxide Release. Adv. Mater. Interfaces. 2016;3:1500646.

[211] Gupta S, Amoako KA, Suhaib A, et al. Multi-Modal, Surface-Focused Anticoagulation Using Poly-2-methoxyethylacrylate Polymer Grafts and Surface Nitric Oxide Release. Adv. Mater. Interfaces. 2014;1:1400012.

[212] Sundaram HS, Han X, Nowinski AK, et al. Achieving One-Step Surface Coating of Highly Hydrophilic Poly(Carboxybetaine Methacrylate) Polymers on Hydrophobic and Hydrophilic Surfaces. Adv. Mater. Interfaces. 2014;1:1400071.

[213] Wang Y-B, Gong M, Yang S, et al. Hemocompatibility and film stability improvement of crosslinkable MPC copolymer coated polypropylene hollow fiber membrane. J. Membr. Sci. 2014;452:29–36.

[214] Chen S-H, Chang Y, Lee K-R, et al. Hemocompatible Control of Sulfobetaine-Grafted Polypropylene Fibrous Membranes in Human Whole Blood via Plasma-Induced Surface Zwitterionization. Langmuir. 2012;28:17733–17742.

[215] Grode GA, Falb RD, Crowley JP. Biocompatible materials for use in the vascular system. J. Biomed. Mater. Res. 1972;6:77–84.

[216] Inauen W, Baumgartner HR, Bombeli T, et al. Dose-and shear rate-dependent effects of heparin on thrombogenesis induced by rabbit aorta subendothelium exposed to flowing human blood. Arterioscler. Thromb. Vasc. Biol. 1990;10:607–615.

[217] Olsson P, Sanchez J, Mollnes TE, et al. On the blood compatibility of end-point immobilized heparin. J. Biomater. Sci. Polym. Ed. 2000;11:1261–1273.

[218] Yang Z, Wang J, Luo R, et al. The covalent immobilization of heparin to pulsed-plasma polymeric allylamine films on 316L stainless steel and the resulting effects on hemocompatibility. Biomaterials. 2010;31:2072–2083.

[219] Kang I-K, Kwon OH, Lee YM, et al. Preparation and surface characterization of functional group-grafted and heparin-immobilized polyurethanes by plasma glow discharge. Biomaterials. 1996;17:841–847.